Renormalization-Group Approach to the Spectral Function of the Tomonaga-Luttinger Model

Dissertation
zur Erlangung des Doktorgrades
der Naturwissenschaften

vorgelegt beim Fachbereich Physik
der Johann Wolfgang Goethe-Universität
in Frankfurt am Main

von
Tom Busche
aus Hann Münden

Frankfurt 2003

vom Fachbereich Physik der
Johann Wolfgang Goethe-Universität als Dissertation angenommen.

Dekan: Prof. Dr. Horst Schmidt-Böcking
Gutachter: Prof. Dr. Peter Kopietz
Prof. Dr. Dirk Rischke

Datum der Disputation:

Contents

Chapter 1

Introduction

1.1 Overview

The physics of one-dimensional conductors has become a paradigm for the breakdown of Landau-Fermi-liquid theory. While for a Fermi liquid the low-lying excitations can be described by so-called quasi-particles this simple picture does in general not apply to non-Fermi liquids. In case of the one-dimensional electron gas (1DEG) and related models parameter regimes exist where the low-energy excitations can be described by collective charge and spin waves called holons and spinons, respectively. The two kinds of collective modes disperse with different velocities, a phenomenon which is called "spin-charge separation" or "fractionalization of the electron". Initiated by a seminal work of S. Tomonaga [1] , where a fundamental mapping of a system of interacting fermions in one spatial dimension onto a system of non-interacting bosons (bosonization) has been published, extensive research emerged in the field during the past fifty years. Once the basic concepts and ideas underlying one-dimensional physics had been pointed out clearly due to the contributions of a large number of authors [2–10], the obvious question arose if Luttinger-liquid behavior is only restricted to one-dimensional systems or if it can also be detected in higher dimensions. Especially in the context of high-T_c superconductivity an effective reduction to low dimensionality has become a candidate for explaining the phenomena in layered materials like the cuprates. Only very recently it has been shown by Kivelson et al. [11] that in the strong-coupling limit the electron-dynamics in the CuO planes of such materials is effectively one-dimensional.
Of course strictly one-dimensional models represent a theoretical idealization and cannot be expected to describe real materials at all energy scales. It is then important to find a theoretical description of quasi-one-dimensional systems, where hopping amplitudes perpendicular to the chain direction are included. Attempts

in this direction have been made within the theory of two or more coupled one-dimensional chains [12–16]. As a further simplification the generic Luttinger-liquid physics including anomalous scaling exponents and spin-charge separation have originally been calculated within the zero-temperature limit and thus represent the physical system precisely at the quantum critical point. The way in which thermal fluctuations alter the structure of correlation functions is a matter of recent research [17–19].

This question becomes particularly important when theoretical predictions are compared with experiments where the temperature is necessarily different from zero, albeit possibly very small. In the past decade considerable progress has been made in synthesizing quasi-one-dimensional materials, such that Luttinger-liquid behavior has become experimentally accessible. Non-Fermi-liquid features have been detected in various materials like the Bechgaard salts [20], the blue-bronzes $K_{0.3}Mo\,O_3$ and $Rb_{0.3}Mo\,O_3$ [21, 22] and the Lithium purple-bronze $Li_{0.9}Mo_6O_{17}$ [23, 24], as well as in other compounds [25]. Most of these experiments are based on angle resolved photo emission spectroscopy (ARPES) and related methods. Another promising class of quasi-one-dimensional systems is given by the famous carbon nanotubes [26–28] and the physics of quantum Hall edge states [29]. However, the present state of the art only allows for a more or less qualitative detection of the most striking predictions of Luttinger-liquid theory, like the suppression of spectral weight near the Fermi energy in the momentum-integrated spectral function, and only recently dispersing features like spin-charge separation [24, 30]. In Fig. 1.4 of the following section we show and example for recent measurements on quasi-one-dimensional materials.

As concerns the theoretical methods used to attack the problem of strongly correlated electrons in one spatial dimension, it has primarily been the above mentioned bosonization technique together with the exact Bethe-Ansatz solution for the one-dimensional Hubbard model [5, 31] that shed light on the nature of the elementary excitations of the electron gas in equilibrium. Unfortunately the exact solution obtained by the bosonization method relies on two basic approximations, which may well be violated in more realistic models: A strictly linear energy dispersion and the restriction to forward-scattering processes. Both premises can be relaxed and, e.g., the inclusion of backscattering processes can in principle be studied with the bosonization technique itself, see Ref. [32] for a recent review. However, there are other powerful methods which are better suited and more intuitive in this concern. One of these is the renormalization group (RG), which in a particular form will be developed and applied to the 1DEG in this thesis.

The very rich idea of the RG roots in the development of quantum electrodynamics and quantum field theory, where it has originally been a more or less empirical but sophisticated method of hiding the contributions of divergent series of Feynman diagrams within a finite number of renormalized couplings. This field

theoretic approach to the RG, leading to the Callan-Symanzik RG equations, is only applicable for theories where renormalizablility can be proven explicitly [33]. In condensed matter physics an alternative RG approach has been formulated due to the pioneering work of Wilson [34–36]. Based on Kadanoffs idea of a successive decimation of degrees of freedom and subsequent rescaling [37] Wilson put forward the idea of a continuous flow of an *infinite* number of coupling constants in a space of Hamitonians. He invented a local RG group scheme relying on three basic steps:

1. Integrating out high-energy degrees of freedom within a momentum shell of infinitesimal width,

2. rescaling of momenta (and frequencies for quantum problems) by an appropriate scale factor such that the original system size is reinstated, and

3. rescaling of the fields to ensure that the coupling flow satisfies a fixed-point condition.

The first step needs the introduction of an energy scale Λ_0 that effectively cuts off momentum integrations in the ultraviolet regime. While in the field theoretic method the analogue of this cutoff has to be sent to infinity at the end of the calculations in order to perform the continuum limit, in condensed matter physics Λ_0 has the physical interpretation of an energy scale related to the inverse lattice spacing, and consequently there is no need for taking Λ_0 to infinity.
In recent years a special implementation of the RG, which is referred to as exact renormalization group (ERG), has attracted much interest. Although the principles of this approach have already been formulated in 1972 by Wegner and Houghton [38] who included all of the above three RG steps, it was only in the past decade that a wider community payed attention to this special form of the RG. Triggered by the seminal work of Polchinski [39] a great variety of different formulations of the ERG has been developed in field theory and statistical physics [40–47] as well as in condensed-matter physics [48–52]. Among these are further developments of the Wilson-Kadanoff RG [51, 53–55], approaches using Polchinskis original version of the ERG [56–58], and a special form using Wick-ordered monomials [59–61]. The maybe most promising implementation uses one-particle irreducible (1PI) vertex functions of the Legendre effective action [44, 50, 52, 62, 63] and has been proposed independently by Wetterich [40] and Morris [42]. In all its specifications the ERG leads to an infinite and formally exact hierarchy of coupled differential equations or recurrence relations for the vertex functions. Only due to the necessity of approximations when applying these equations to physical systems the usefulness of the various approaches may differ considerably, see for instance Ref. [64] for a comparison of the different

methods. In particular the precise form in which the cutoff dependence is introduced turns out to be important in this concern. One distinguishes between smooth- and sharp-cutoff versions, depending on whether the cutoff function determining the region of momenta to be integrated is given by a smooth or by a discontinuous (sharp) step function. It turns out that the Polchinski equations are very sensitive to the actual form of the cutoff function due to tree-graph contributions which are not 1PI. They even lead to ambiguities in the sharp-cutoff version when the thermodynamic limit is performed [42]. This inconvenience can be overcome by using the Morris-Wetterich ERG where all contributions are 1PI, such that the cutoff functions always appear within integral kernels and the sharp-cutoff limit is well-defined.[1]

In this work we will develop the RG equations for the dimensionless 1PI vertex functions of the Legendre effective action, extending the Morris formalism to systems of interacting fermions. This extension is non-trivial since the shell of integrated momenta $\mathbf{k}$ must now be centered not only around the single point $\mathbf{k} = 0$, as is the case for bosons, but rather around the $D-1$ dimensional submanifold in $\mathbf{k}$-space that fixes the low-energy regime, i.e. the *interacting* Fermi surface (FS). Here D is the spatial dimension of the considered system. Furthermore we will include in our formalism the rescaling of momenta, frequencies and fields, leading to a dimensionless form of the flow equations. Although these steps belong to a complete RG program and have been pointed out early to be essential for the determination of fixed points of the RG flow [36, 65, 66], many authors abandon the rescaling [42, 49–54, 58, 61, 63]. We believe that this neglect can at best be accepted within one-loop calculations. At two-loop level a possible runaway flow of couplings obtained by using an unrescaled RG version may eventually be suppressed by the inclusion of the proper field rescaling, due to a vanishing or drastically reduced quasi-particle weight [67]. This has also been confirmed by D. Zanchi in Ref. [58] who detected such a runaway flow at one-loop level in applying an unrescaled version of Polchinskis ERG to the 2D Hubbard model on a square lattice. In the subsequent work [68] he pointed out that the divergence gets indeed suppressed when propagators dressed with the renormalized quasi-particle weight are used in the calculations. Although this approach does not correspond to a proper rescaling procedure it shows that results obtained without inclusion of the rescaling must be interpreted with care.

In regard to the great variety of available RG formalisms what could be the motivation for developing an additional version? – First of all, as we have pointed out above, there is no special implementation that works equally well for all possible physical applications. Each formalism has its own advantages and lim-

[1] Of course there is no principle need for using a sharp cutoff. However, from a technical point of view it represents a great simplification.

itations when approximations are imposed. Secondly, due to the seminal work of Shankar [69] the interest in studying *fermionic* systems by means of further developments of Wilsons momentum shell technique has greatly increased in the past decade, primarily in the context of the two-dimensional Hubbard model and high-T_c superconductivity [49, 54, 61, 70]. However, in the majority of cases the rescaling step of the RG is not included, a deficiency that has to our opinion to be remedied. Furthermore the ERG principally opens up the possibility of going beyond the usual RG task of calculating the flow of only a finite number of coupling constants. Instead, as we shall demonstrate in this work, it represents a powerful tool for studying the flow of entire correlation *functions* such as uniform susceptibilities, and even of non-perturbative spectral functions. Accept for a recent work by Ferraz [71], who calculated the spectral function of the two-dimensional electron gas with a truncated Fermi surface from the Callan-Symanzik equation, this potential of RG methods has so far not attracted much attention. It turns out that the 1PI ERG in its rescaled form is particularly well-suited for this task, and it thus traces a direct way to experimentally measurable quantities.
Finally let us stress two further advantages of the ERG compared to more conventional momentum-shell techniques [69] and the field theoretic method [33]. Firstly the ERG opens up the possibility of a systematic inclusion of the flow of irrelevant couplings into the set of flow equations. We believe that the role of couplings with a negative canonical scaling dimension is underestimated in RG theory. As we will show in this work irrelevant couplings do not only contribute to the fixed-point values of marginal or relevant couplings, but they may even give rise to new fixed points of the RG when taken into account self-consistently. The second advantage of the ERG concerns the role of the infrared flow parameter Λ which is related to the ultraviolet cutoff Λ_0 via $\Lambda = \Lambda_0 e^{-l}$. It represents the energy scale above which all degrees of freedom have been integrated out and is taken to zero at the fixed point. In the field-theoretic approach and the original Wilson RG only the most divergent contributions in Λ to the coupling flow are retained, and the flow equations thus solely determine the properties in the vicinity of the fixed-point but not the global flow towards it. On the other hand the ERG allows to follow the flow of the couplings (or even of entire correlation functions) from their initial values at scale $\Lambda = \Lambda_0$ until the fixed point at $\Lambda = 0$ is reached. At first sight this seems to be a technical point of no physical importance. But as has been proposed by D. Zanchi [72], within the ERG the low-energy scale Λ may be interpreted as an effective temperature (scale), such that decreasing the infrared cutoff Λ would effectively mean a lowering of the temperature of the physical system. This interpretation has qualitatively been confirmed by Honerkamp and Salmhofer in the context of the two-dimensional Hubbard model by means of a new formalism that explicitly uses the physical temperature as the flow parameter of the RG [73, 74]. However, we believe that a

general interpretation of Λ as an effective temperature scale is questionable and cannot replace a true finite-temperature calculation in any case.

1.2 Tomonaga-Luttinger Model

As the first part of this thesis is held very general and will mainly be concerned with the derivation of the flow equations of the 1PI vertex functions, we shall point out here some peculiarities of the physics in one spatial dimension in preparation for Part II , where the ERG formalism will be applied to the 1DEG. In particular we will sketch how the Hamiltonian of the Tomonaga-Luttinger model can be deduced from the general problem of the 1DEG.
The second-quantized Hamiltonian for a system of interacting fermions in one dimension can be written in the following form

$$\hat{H} = \hat{H}_0 + \hat{H}_{\text{int}} \,, \tag{1.1}$$

with the non-interacting or kinetic part given by

$$\hat{H}_0 = \sum_k \sum_\sigma \xi_k \, \hat{\psi}^\dagger_{k,\sigma} \hat{\psi}_{k,\sigma} \,, \tag{1.2}$$

and with the contribution related to two-body fermion-fermion interactions determined by

$$\hat{H}_{\text{int}} = \frac{1}{2L} \sum_{q,k,k'} \sum_{\sigma,\sigma'} f_q^{\sigma\sigma'} \, \hat{\psi}^\dagger_{k+q,\sigma} \hat{\psi}^\dagger_{k'-q,\sigma'} \hat{\psi}_{k',\sigma'} \hat{\psi}_{k,\sigma} \,. \tag{1.3}$$

Here the operators $\hat{\psi}^\dagger_{k,\sigma}$ and $\hat{\psi}_{k,\sigma}$ are the canonical anti-commuting creation and annihilation operators of fermions with momentum k and spin σ , and L is the spatial length of the system. We have assumed that the Landau interaction parameters $f_q^{\sigma\sigma'}$ do not depend on the momenta k and k' of the scattered fermions but exclusively on their spins and the transferred momentum q . The excitation energy ξ_k in Eq. (1.2) is defined by

$$\xi_k = \epsilon_k - \mu \,, \tag{1.4}$$

where ϵ_k is the non-interacting energy dispersion and μ is the exact chemical potential of the interacting many-body problem. In general the explicit form of the function ϵ_k depends on the band structure of the considered model, but here we shall only discuss the 1DEG for which $\epsilon_k = k^2/2m$. In this case m can be identified with the bare mass of the electrons. The crucial step towards a solution of the above problem is the linearization of the energy dispersion with respect to

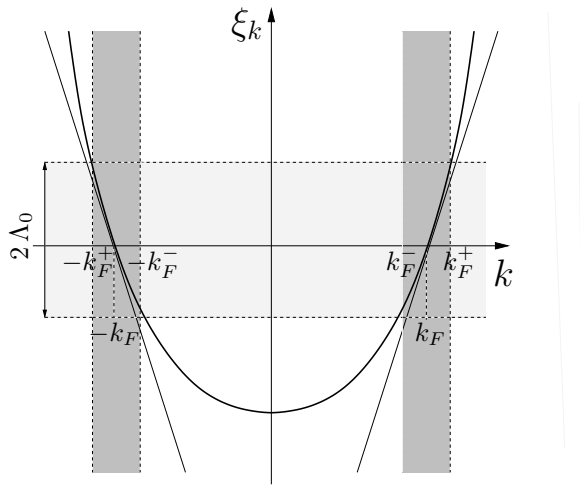

Figure 1.1: Schematical representation of the excitation energy $\xi_k = \epsilon_k - \epsilon_{k_F} = (k^2 - k_F^2)/2m$ as a function of k and its approximation by tangents with slope $\pm v_F$ at the Fermi points $\pm k_F$. The horizontal gray-shaded stripe indicates a region with excitation energies $|\xi_k| \leq \Lambda_0$. The corresponding k-values approximately lie within the vertical stripes determined by $k_F^- \leq |k| \leq k_F^+$, with $k_F^\pm = k_F \pm \Lambda_0/v_F$. If Λ_0 is sufficiently small the linearization will be a good approximation to the parabola.

the Fermi points $\pm k_F$ which represent the largest allowed momentum values of the *interacting* ground state.[2] This amounts to approximating $\xi_k \approx v_F(|k| - k_F)$ within a region of k-space that is essentially determined by the energy scales we are interested in. If Λ_0 represents the maximum value for these energy scales and if it is also small compared to the Fermi energy, the corresponding k-values will be close to the Fermi points and the linearization is justified, see Fig. 1.1. Depending on whether the initial and the final locations of scattered fermions (electrons) are close to the right or the left Fermi point, four qualitatively different scattering processes must be distinguished. The corresponding classification is called the "g-ology model" due to the fact that the Landau parameters $f_q^{\sigma\sigma'}$ usually are assigned by different g-couplings. For instance, if both k and k' in Eq. (1.3) are located near the right Fermi point k_F and the transferred momentum q is small compared to k_F the final states after a scattering process will remain close to the right Fermi point. Hence, both fermions maintain their direction of motion (forward scattering). According to the usual nomenclature we would then identify $f_q^{\sigma\sigma'} \equiv g_4^{\sigma\sigma'}(q)$. Correspondingly, we obtain a forward scattering process if q is small but the scattered fermions are located on opposite Fermi

[2] We will give a proper definition of the interacting Fermi surface in Sec. 4.1. Note that due to Luttinger's theorem [75–77] in one dimension k_F is left unchanged by interactions, such that it simply coincides with the non-interacting k_F.

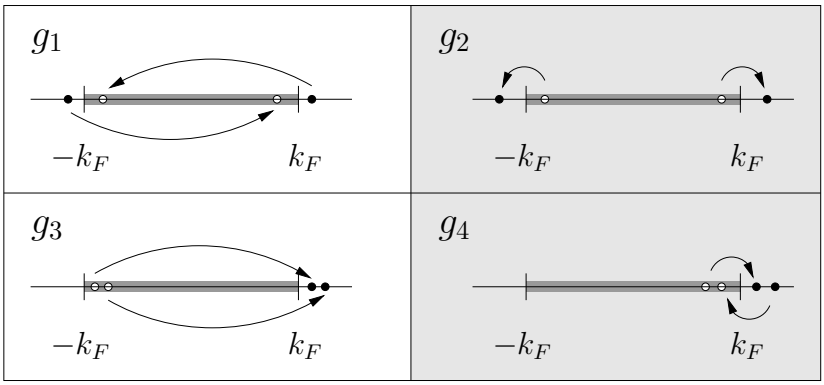

Figure 1.2: The four qualitatively different scattering processes occurring in one-dimensional conductors involving only small excitation energies. The gray-shaded regions between the Fermi points $\pm k_F$ represent the filled Fermi sea. Black dots symbolize excited fermions, while white spaces in the Fermi sea represent the corresponding holes. Further explanations see text.

points which is denoted by $f_q^{\sigma\sigma'} \equiv g_2^{\sigma\sigma'}(q)$. However, it may also happen that a scattered fermion changes its direction of motion (backward scattering), which implies a minimal momentum transfer of the order of $\sim 2k_F$. Again two cases have to be distinguished: If initially the fermions move in opposite directions we may identify $f_{2k_F+q}^{\sigma\sigma'} \equiv g_1^{\sigma\sigma'}(q)$ and otherwise $f_{2k_F+q}^{\sigma\sigma'} \equiv g_3^{\sigma\sigma'}(q)$. The situation is sketched in Fig. 1.2. In case of the 1DEG g_3-processes (which are also called "Umklapp scattering") must be excluded since they violate momentum conservation. However, in more realistic lattice models the transfered momentum of the order of $\sim 4k_F$ can be absorbed by the underlying lattice provided $4k_F$ is a multiple of a reciprocal lattice vector.
Due to the above definitions we have $g_1^{\sigma\sigma'}(q) = g_3^{\sigma\sigma'}(q)$ and $g_2^{\sigma\sigma'}(q) = g_4^{\sigma\sigma'}(q)$ in the initial Hamiltonian (1.1). This situation changes if we consider an *effective low-energy model* where high-energy degrees of freedom have already been integrated out (in the RG sense) and the effects are incorporated in appropriately defined new couplings. Then in general $\bar{g}_1^{\sigma\sigma'}(q) \neq \bar{g}_3^{\sigma\sigma'}(q)$ and $\bar{g}_2^{\sigma\sigma'}(q) \neq \bar{g}_4^{\sigma\sigma'}(q)$, where we have written $\bar{g}_i^{\sigma\sigma'}(q)$ to distinguish the renormalized from the bare couplings (subsequently we will however keep the simpler notation $g_i^{\sigma\sigma'}(q)$). In particular, as has been shown by Sólyom [9] in a careful field-theoretical RG analysis of the g-ology model, back- and Umklapp-scattering (away from half band filling) are marginally irrelevant in the RG sense and the corresponding couplings renormalize to zero at the fixed point. It is then reasonable to neglect the contribution of these processes in an effective low-energy model and to maintain only the forward-scattering part of $\hat{H}_{\rm int}$. For linearized energy dispersion the resulting *Tomonaga-*

Luttinger model is still a non-trivial many-body problem which nonetheless can be solved exactly by means of the bosonization technique. Strictly speaking, for the exact solution of the TLM an extension of the linearized energy dispersion to arbitrary momenta is necessary, see also Fig. 1.1 before. According to Eq. (1.2) this leads to a Hamiltonian which is unbounded from below, resulting in an infinite ground-state energy. This conceptual problem can be remedied by introducing an artificial Dirac sea, consisting of infinitely many fermions with negative energy. As has been shown by Gutfreud and Schick [4] the low-energy physics remain qualitatively unaffected by the Dirac sea; for a more thorough discussion of this point see also Sec. 6.4 . The resulting effective Hamiltonian for the TLM can then be written as

$$\hat{H}^{\mathrm{TLM}} = \hat{H}_0^{\mathrm{TLM}} + \hat{H}_{\mathrm{int}}^{\mathrm{TLM}} , \tag{1.5}$$

with

$$\hat{H}_0^{\mathrm{TLM}} = \sum_p \sum_{\alpha,\sigma} v_F p \; : \hat{\psi}^\dagger_{\alpha,\sigma}(p) \hat{\psi}_{\alpha,\sigma}(p) : , \tag{1.6}$$

$$\begin{aligned} \hat{H}_{\mathrm{int}}^{\mathrm{TLM}} \;=\; & \frac{1}{2L} \sum_{q,p,p'} \sum_{\alpha,\sigma,\sigma'} \Big\{ g_4^{\sigma\sigma'}(q)\, \hat{\psi}^\dagger_{\alpha,\sigma}(p+q) \hat{\psi}^\dagger_{\alpha,\sigma'}(p'-q) \hat{\psi}_{\alpha,\sigma'}(p') \hat{\psi}_{\alpha,\sigma}(p) \\ & + g_2^{\sigma\sigma'}(q)\, \hat{\psi}^\dagger_{\alpha,\sigma}(p+q) \hat{\psi}^\dagger_{\bar{\alpha},\sigma'}(p'-q) \hat{\psi}_{\bar{\alpha},\sigma'}(p') \hat{\psi}_{\alpha,\sigma}(p) \Big\} . \end{aligned} \tag{1.7}$$

Note first that we have introduced two different kinds of fermions labeled by the index $\alpha = \pm 1$, referring to the right ($\alpha = +1$) and to the left Fermi point ($\alpha = -1$). More precisely we have decomposed momenta k according to $k = \alpha(k_F + p)$, where $\alpha = \mathrm{sgn}(k)$.[3] This implies that for $|p| < k_F$ the old and the new annihilation operators are related by $\hat{\psi}_{k_F+p,\sigma} \equiv \hat{\psi}_{+,\sigma}(p)$ and $\hat{\psi}_{-k_F-p,\sigma} \equiv \hat{\psi}_{-,\sigma}(p)$ (and correspondingly for the creation operators). However, in Eqs. (1.6) and (1.7) we allow p and p' to range over all values from minus to plus infinity, such that for instance a state with $\alpha = +1$ and $p < -k_F$ has no analogue in Eqs. (1.2) and (1.3) : it belongs to the above-mentioned unphysical Dirac sea. Furthermore $:(\ldots):$ denotes normal ordering with respect to the non-interacting ground state (which is given by the completely filled Fermi and Dirac sea), and we have used $\bar{\alpha} = -\alpha$.

Now, what is so special about the physics in one compared to higher dimensions? From a semi-classical point of view it seems clear that the interaction will play a more important role than in higher dimensions since the fermions cannot avoid

[3] Here a positive p always refers to a fermion located outside the Fermi sea which is different from the usual convention in the bosonization literature.

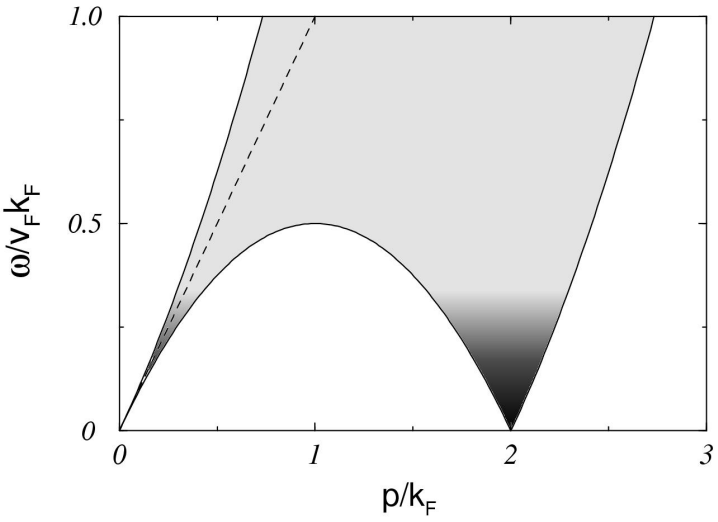

Figure 1.3: Schematical representation of the allowed region for particle-hole excitations for fermions in one dimension with excitation energies $\xi_{\alpha(k_F+p)} = v_F p + p^2/2m$. Formally, the gray-shaded region corresponds to the support of the imaginary part of the retarded polarization function $\Pi(p, \omega + i0^+)$, obtained from Eq. (8.74) by means of analytic continuation. For linear dispersion $\mathrm{Im}\,\Pi(p, \omega + i0^+) \sim \delta(\omega - v_F p)$, such that the support is just given by the dashed straight line with $\omega = v_F p$. In the white regions particle-hole excitations are excluded.

each other. Furthermore, whenever a fermion gets scattered out of the Fermi sea a particle-hole pair will be created, see Fig. 1.2, resulting in a polarization of the excited state compared to the ground state. The polarization in turn leads to dissipation if an additional fermion is injected into the system and propagates through it. In dimensions greater than one (at least in $D = 3$) the correlations with the Fermi-sea electrons are incoherent, such that the injected electron only looses parts of its energy to the background and persists as a propagating entity, described by renormalized parameters such as mass, Fermi velocity, quasi-particle residue and finite life-time. This is in brief words what is called a *quasi-particle*, the generic low-energy excitation of a Landau Fermi liquid [78, 79]. In one spatial dimension this description fails which can partially be understood by Fig. 1.3, where the allowed energies of particle-hole excitations of the non-interacting system are sketched. The gray-shaded region in this picture represents the region in the (p, ω) plane where particle-hole excitations for a system with excitation energy $\xi_{\alpha(k_F+p)} = v_F p + p^2/2m$ are possible. The dark-gray part indicates the corresponding region with small excitation energies, such that for $|p/k_F| \ll 1$ there exists an asymptotic one-to-one correspondence between ω and p. This situation is unique to one dimension and results in *coherent* particle-hole excitations.

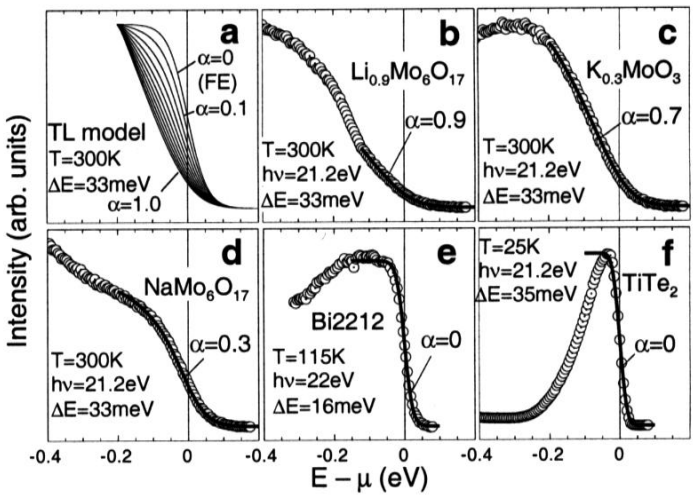

Figure 1.4: Experimental ARPES data for the momentum integrated spectral function (density of states) of various materials obtained by Gweon et al. in Ref. [24]. Here, α represents the anomalous exponent of the TLM Luttinger liquid, which we denote by η. Explanations see text.

For the strictly linear dispersion of the TLM there is even perfect coherence for all momenta, which is indicated by the dashed line in the figure. The impact on the single-particle Green function, which describes the propagation of a fermion through the interacting many-body system, is drastic: Single-particle behavior is completely suppressed and the elementary excitations are given by spinons and holons, representing collective spin and charge excitations, rather than by quasi-particles. This is typically reflected in the emergence of non-universal algebraic decay exponents, which depend on the interaction strength. For instance for the single-particle spectral function at $T = 0$, which is closely related to the experimental data of ARPES experiments, one finds

$$A(\pm k_F, \omega) \sim |\omega|^{\eta - 1}\,, \tag{1.8}$$

instead of a sharp δ-peak at $\omega = 0$, as one would expect for a Fermi liquid. Here η is the interaction-dependent anomalous dimension of the system. Correspondingly, for the momentum-integrated spectral function at $T = 0$ one obtains

$$\rho(\omega) \sim |\omega|^{\eta}\,, \tag{1.9}$$

thus predicting a suppression of the density of states near $\omega = 0$. In contrast, usual metallic Fermi liquid behavior leads to a finite value of $\rho(\omega)$ at the Fermi

edge. An example for a quite convincing measurement of such anomalous features of the function $\rho(\omega)$ is presented in Fig. 1.4 , where we show ARPES data for various quasi-one-dimensional materials recently obtained by Gweon et al. [24]. They compare the data with finite-T calculations obtained by the methods described in Ref. [17] . For the Lithium purple bronze $Li_{0.9}Mo_6O_{17}$ and the Kalium blue bronze $K_{0.3}Mo_6O_3$ the authors claim to have found strong evidence for non-Fermi-liquid behavior due to a remarkable suppression of $\rho(\omega)$ near $\omega = \mu$.[4] This can be seen from panels (a) and (b) in Fig. 1.4 if one compares with the Fermi-liquid lineshape of $TiTe_2$ in panel (f). Even for the quasi-*two*-dimensional Natrium purple bronze $NaMo_6O_{17}$ the authors find a non-vanishing anomalous exponent $\eta \approx 0.3$ which, if correct, manifests non-Fermi-liquid behavior in dimensions greater than one.

1.3 Outline

This thesis is organized as follows: In Part I we derive in detail the flow equations for the 1PI vertex functions, both in their unrescaled and rescaled form. The inclusion of the rescaling steps implies that each vertex function appears twice: one time as the physical vertex function depending on momenta and frequencies, and one time as the rescaled or dimensionless vertex function depending on dimensionless variables. As long as the infrared cutoff Λ remains finite there exists a one-to-one correspondence between each physical vertex and its dimensionless analogue given by the scaling equation (4.29). The subtle relation between the two forms at the fixed point and their rather different properties are one of the central topics of Part I . In Chap. 2 of the first part we briefly review the various types of generating functionals relevant to the ERG formalism. We introduce a notation that allows for treating fermions and bosons simultaneously. In Chap. 3 we derive the flow equations in their unrescaled version, both for bosons and fermions. Our results are basicly equivalent to the flow equations obtained independently by Salmhofer and Honerkamp [63] but more explicit and well-suited for direct applications. The implications of the sharp-cutoff limit are discussed. The important rescaling step of a full RG transformation is introduced in Chap. 4, and the flow equations for the dimensionless vertices are derived. From now on we restrict ourselves to the fermionic case, and we present an explicit construction that allows for a scaling towards the true, i.e. the interacting FS. We point out that the interacting FS should be viewed as a fixed-point manifold of the RG procedure. Finally, in Chap. 5 we discuss some of the general properties of the physical and the dimensionless vertex functions. We also show how

[4] In Ref. [24] energies are measured with respect to the origin, while we take the chemical potential μ as reference value. Eq. (1.9) then has to be replaced by $\rho(\omega) \sim |\omega - \mu|^\eta$.

our formalism can be embedded into the language of dynamic critical phenomena [19, 80, 81] and in which sense the dimensionless vertices can be interpreted as scaling functions. In particular we demonstrate that for non-Fermi liquids the vanishing radius of convergence for expansions of the physical vertex functions in powers of frequencies and momenta has important consequences on the range of validity of the scaling hypothesis. Strictly speaking the fixed-point values of the coupling constants obtained from the *dimensionless* vertices solely describe the properties of the *physical* vertex functions for momenta located directly on the interacting FS. As will be demonstrated with an explicit example in Chap. 7, it is not obvious in any case that the range of validity of the fixed-point results for the dimensionless couplings can be extended to a finite region around the FS, as is assumed by the scaling hypothesis.

In Part II we shall apply the new formalism to the 1DEG neglecting the spin degree of freedom and restricting ourselves to pure forward scattering. Our choice has the advantage that this model only involves one relevant and three marginal couplings but still displays the generic Luttinger-liquid behavior. This conceptual simplicity allows for neatly pointing out the most important subtleties inherent to our formalism and in some aspects to the RG in general. Our results are particularly important if one intends to use RG calculations for quantitative predictions, e.g. of scaling exponents, and explain the role of the ultraviolet cutoff Λ_0 within our model. Most importantly we will be able to calculate the momentum resolved spectral function of the Tomonaga-Luttinger model (TLM) at the fixed point and even the complete flow towards this point for the special case when the momentum equals the Fermi momentum.

In Chap. 6 we perform a complete self-consistent two-loop calculation including the flow of the marginal and relevant couplings related to the dimensionless two- and four-point vertex. Like in the TLM we assume a strictly linear energy dispersion. Our results display the change of the couplings as a function of the scale Λ until the fixed point is reached. As expected we find a finite anomalous dimension which corresponds to the weak-coupling result of the TLM. It is shown that the rescaling step is essential to obtain this result, as otherwise the momentum- and frequency-independent part of the unrescaled four-point vertex exhibits a runaway flow to infinity at the two-loop order. Subsequently we study the differences in using an initially finite or an infinite ultraviolet cutoff Λ_0. We show that taking Λ_0 to infinity at the beginning of the calculations basicly corresponds to introducing the Dirac sea, and it is found that the fixed-point values of the couplings indeed depend on the fact if Λ_0 is finite or not, albeit they do *not* depend on the explicit value of Λ_0. Taking the susceptibilities as the simplest example for correlation functions that can exclusively be calculated within our RG approach, we finally confirm our assertions of Chap. 5 concerning the different properties of the physical and the dimensionless vertices and the concept of universality.

In Chap. 7 we turn our attention to the calculation of the spectral function of the spinless g_2-model. Although an asymptotic result is well-known from the bosonization approach it has to the best of our knowledge never been calculated by means of RG methods. Of course the spectral function contains much more information about the physical system than the fixed-point values of only a few coupling constants, and it is consequently much harder to obtain. We start in Sec. 7.1 with considering the spectral function at second-order perturbation theory (PT) since the result can *exactly* be reproduced by means of our RG approach. This allows for a direct comparison of the flow of the coupling constants with the flow of the entire spectral function at perturbative level. In Sec. 7.2 we demonstrate that this simple toy model is a paradigm for a situation where the fixed-point results of the dimensionless couplings describe the properties of the physical spectral function exclusively at the Fermi points $\pm k_F$. While the coupling flow predicts a vanishing quasi-particle residue at the fixed-point, the fixed-point result for the perturbative spectral function exhibits a finite quasi-particle peak whenever the momentum is different from the Fermi points. The quasi-particle residue even carries most of the spectral weight down to momenta exponentially close to the Fermi points. An extension of the range of validity of the fixed-point result of the RG flow to momenta different from, albeit very close to the FS is hence misleading. This at first sight counterintuitive result can be explained by the general results of Chap. 5, and it shows that an application of the dynamic scaling hypothesis as formulated by Halperin and Hohenberg [80, 81] can fail in fermionic systems. In Sec. 7.3 we critically review some aspects of the calculation of the spectral function within the bosonization approach. By a careful analysis of the Debye-Waller factor we show that the widely accepted asymptotic result for the spectral function of the TLM is at least questionable as concerns the precise nature of the power-law singularities, even when a box-potential for the Landau interaction parameters is used.[5] In Sec. 7.4 we calculate the momentum-resolved spectral function by means of our RG approach first by making use of the scaling hypothesis. Our result coincides exactly with the weak-coupling bosonization result for momenta equal to the Fermi points and only qualitatively in the general case. Here the difference consists of a slightly different algebraic exponent for the power-law singularities. Since we have used the scaling hypothesis to obtain this result it will only be valid in the immediate vicinity of the Fermi points and for small frequencies. In Sec. 7.5 we therefore calculate the complete flow of the spectral function for the special case of momenta equal to the Fermi points without using the scaling hypothesis. For finite Λ we find a δ-peak at zero frequency

[5] The universality of the TLM result has also been questioned by Meden [82, 83] who showed that the Luttinger-liquid exponent is changed due to the momentum dependence of the Landau parameters. However, for a box potential he claimed the former results to be correct. We show that even in this case this is by no means obvious.

and a non-singular continuous part with its support starting at finite frequencies. Only in the limit $\Lambda \to 0$ the algebraic power-law singularity is recovered and the quasi-particle peak vanishes. In contrast to our former fixed-point result the sumrule for the spectral weight can be checked numerically and is shown to be satisfied during the whole flow of the spectral function. The spectral weight switches from the δ-like to the continuous part when Λ decreases. If we follow the interpretation of Λ as an effective temperature, this implies a crossover scenario from a Fermi-liquid-like spectral function to that of a Luttinger liquid with decreasing temperature. The quasi-particle weight then decays like $\sim (T_{\text{eff}})^{\eta}$, where T_{eff} is the effective temperature associated with Λ and η denotes the anomalous dimension. However, as mentioned above we believe that a direct identification of Λ with T_{eff} is questionable, such that a true finite-temperature calculation should be performed to confirm or to rebut the crossover behavior of the spectral function. In Chap. 8 we step back to the conventional RG task of calculating the flow of coupling constants, this time including in our model the non-linear correction to the energy dispersion which is related to the fermion mass and represents an irrelevant coupling. In Sec. 8.1 we first consider the spectral function at second-order perturbation theory for momenta equal to the Fermi points as a guide line for the non-perturbative approach. The line-shape of the perturbative spectral function exhibits some non-universal features at large frequencies due to the absence of perfect particle-hole symmetry. The singularity at zero frequency, characteristic of the model with strictly linear energy dispersion, is still present and shown to be of the same logarithmic nature. In preparation for the RG calculation we discuss the flow of irrelevant couplings on general grounds in Sec. 8.2, where we also justify our approximation strategy. In Sec. 8.3 we show that the fixed-point value of the coupling related to the momentum- and frequency-independent part of the four-point vertex gets renormalized by finite curvature already at one-loop level. The correction with respect to the former result for linear dispersion is found to be small. In Sec. 8.4 we study again the susceptibilities of our model. It turns out that the fixed-point results for the physical and the dimensionless susceptibilities depend very sensitively not only on the fixed-point value of the irrelevant coupling but also on its flow towards this point. Only a slight slowing down of the flow compared to the canonical exponential decay can lead to a complete suppression of the physical susceptibility at the fixed point, while on the other its dimensionless analogue approaches the finite fixed-point result of the linear model. Although we do not find such a scenario within our model it demonstrates the potentiality of irrelevant couplings to completely alter the physics. Finally we show in Sec. 8.5 within a two-loop calculation for the two-point vertex combined with the one-loop result for the four-point vertex that a self-consistent consideration of the curvature parameter does not lead to new fixed points. The Luttinger-liquid fixed point is thus found to be stable, and it is

shown that a fully consistent two-loop calculation for the four-point vertex cannot change this result. Nonetheless, the fixed-point values of the marginal couplings do depend on the initial curvature, which is partially shown analytically as well as by a numeric solution of the self-consistent flow equations. In particular we find that the anomalous dimension will only be changed in the next-to-leading order of a weak-coupling expansion, which is principally out of range of a two-loop calculation.
In appendix A we show how the flow equation for the unrescaled six-point vertex can be derived from the flow of the generating functional of the Legendre effective action. In appendix B we prove a little lemma stating that the fixed-point value of a suitably defined scale-averaged coupling coincides with the fixed-point value of the corresponding bare coupling. This is important since it is the scale-averaged anomalous dimension that enters the formal solutions of our flow equations. Finally, in appendix C we perform the analytic continuation of the dimensionless two-point vertex from imaginary to real frequencies.

Notational remarks: Throughout this work we set $\hbar = 1$ as well as $k_B = 1$, where $\hbar$ is the Planck and k_B the Boltzmann constant. Due to the fact that the inclusion of the rescaling step within our RG formalism accounts for two different versions of each vertex function and the related couplings, we have tried to consequently assign the dimensionless quantities with a tilde. For example $\Gamma_\Lambda^{(2)}(\mathbf{k}, i\omega)$ denotes the physical two-point vertex (the self-energy) while its dimensionless and rescaled analogue reads $\tilde{\Gamma}_l^{(2)}(q, i\epsilon)$. Correspondingly, the couplings related to expansions of the physical and the dimensionless vertices are for instance denoted by v_Λ and $\tilde{v}_l$, where the latter belongs to $\tilde{\Gamma}_l^{(2)}(q, i\epsilon)$. Exceptions are given by the anomalous dimension and the quasi-particle residue, which both are fundamental quantities without physical dimension. They are simply denoted by η_l and Z_l, respectively, and they simply coincide in the rescaled and the unrescaled formalism. As concerns the flow parameter of the RG itself it also appears in two versions. On the one hand we have the infrared cutoff Λ with physical dimension of an energy, and on the other hand the dimensionless logarithmic flow parameter $l = -\ln(\Lambda/\Lambda_0)$. Approaching the fixed point is hence determined by the limit $\Lambda \to 0$, or equivalently by $l \to \infty$. Depending on the context we will rather loosely switch between the two limits.

Part I

Exact Renormalization Group: Setup of the Formalism

Chapter 2

Generating Functionals

In this section we give some basic definitions and properties of the generating functionals used to derive the RG flow equations. We also explain our notations and assumptions.

We start with the definition of the $(2n)$-point disconnected Green function in its functional integral representation [84],

$$\begin{aligned} G^{(2n)}(K'_1,\ldots,K'_n;K_n,\ldots,K_1) \\ &= \frac{(-1)^n}{\mathcal{Z}_0}\int \mathcal{D}[\bar\psi,\psi]\psi_{K'_1}\cdots\psi_{K'_n}\bar\psi_{K_n}\cdots\bar\psi_{K_1}\, e^{-S[\bar\psi,\psi]} \\ &= \frac{(-1)^n}{\mathcal{Z}_0}\int \mathcal{D}[\bar\psi,\psi]\prod_{i=1}^{n}\psi_{K'_i}\bar\psi_{K_i}\, e^{-S[\bar\psi,\psi]}\,. \end{aligned} \tag{2.1}$$

The action S is given by

$$S[\bar\psi,\psi] = S_0[\bar\psi,\psi] + S_{\rm int}[\bar\psi,\psi]\,, \tag{2.2}$$

where $S_{\rm int}$ is a particle-number conserving and hence even functional of the fields ψ and $\bar\psi$, representing many-body interactions. The free part is defined by

$$S_0[\bar\psi,\psi] = -(\bar\psi, G_0^{-1}\,\psi)\,, \tag{2.3}$$

where the parantheses are short-hand for

$$(\bar\psi, G_0^{-1}\,\psi) \;=\; \sum_{K,K'}\bar\psi_K (G_0^{-1})_{K'K}\psi_{K'} \tag{2.4}$$

$$= \sum_K \bar{\psi}_K G_0^{-1}(K) \psi_K \,. \tag{2.5}$$

Here $K = (\sigma, \mathbf{k}, i\omega_n)$ is a composite label for the momenta $\mathbf{k}$, fermionic or bosonic Matsubara frequencies ω_n and a so far unspecified index σ representing additional degrees of freedom, as for instance the spin projection. We restrict ourselves to translationally invariant systems so that the free propagator is diagonal in Fourier space, i.e.

$$(G_0)_{K,K'} = \delta_{K,K'} G_0(K)\,, \tag{2.6}$$

with

$$\delta_{K,K'} = \delta_{\sigma\sigma'}\delta_{\mathbf{k}\mathbf{k}'}\delta_{\omega_n\omega_{n'}}\,, \tag{2.7}$$

in case that σ represents a conserved quantity; otherwise $\delta_{\sigma\sigma'}$ has to be replaced by unity. The sum in Eq. (2.4) is over all quantum numbers contained in K and K'. Finally let us fix the integration measure in Eq. (2.1):

$$\mathcal{D}[\bar{\psi}, \psi] = \prod_K \frac{\mathrm{d}\bar{\psi}\mathrm{d}\psi}{\mathcal{N}}\,, \tag{2.8}$$

with the normalization constant given by $\mathcal{N} = 1$ for fermions and $\mathcal{N} = 2\pi i$ for bosons.
Mathematically the fields ψ and $\bar{\psi}$ within the functional integral in Eq. (2.1) have to be interpreted as the generators of a Grassmann algebra [84, 85] in case of fermions and as complex numbers for bosons; here $\bar{\psi}$ is simply the complex conjugate of ψ.
In the following the fermionic and the bosonic cases will be distinguished by the definition

$$\zeta = \begin{cases} -1 & \text{(fermions)} \\ +1 & \text{(bosons)} \end{cases} \tag{2.9}$$

Note that our definition of the Green functions uses the free partition function $\mathcal{Z}_0$ as normalization. Explicitly,

$$\mathcal{Z}_0 = \int \mathcal{D}[\bar{\psi}, \psi]\, e^{(\bar{\psi}, (G_0)^{-1}\psi)} = [\det(-G_0)]^{\zeta}\,. \tag{2.10}$$

In the subsequent sections we will often manipulate functional integrals of Grassman numbers. The properties of Grassman algebras may be found in the textbook by Berezin [85] and we do not want to repeat them here. However, it is maybe worth to mention two peculiarities related to the differentiation defined on a

Grassman algebra. Let f be an *odd* and g be an arbitrary functional of Grassman numbers ψ_K, then the product rule reads

$$\frac{\delta}{\delta\psi_K}(f[\psi]g[\psi]) = \frac{\delta f[\psi]}{\delta\psi_K}g[\psi] + \zeta f[\psi]\frac{\delta g[\psi]}{\delta\psi_K}\,. \tag{2.11}$$

If on the other hand f is even and g arbitrary we have the usual product rule by dropping the factor ζ in front of the second term in Eq. (2.11). The chain rule holds as usual but we have to take care of the order of the outer and inner derivatives if the factors do not commute:

$$\frac{\delta}{\delta\psi_K}g[f[\psi]] = \frac{\delta f[\psi]}{\delta\psi_K}\,\frac{\delta g[\phi]}{\delta\phi}\Big|_{\phi=f[\psi]}\,. \tag{2.12}$$

Let us now define the various types of generating functionals and and point out the relations between them. The *generating functional of disconnected Green functions* is defined by

$$\mathcal{G}[\bar{J},J] = \frac{\mathcal{Z}[\bar{J},J]}{\mathcal{Z}_0}\,, \tag{2.13}$$

with the partition functional

$$\mathcal{Z}[\bar{J},J] = \int \mathcal{D}[\bar{\psi},\psi]\, e^{-S[\bar{\psi},\psi]+(\bar{\psi},J)+(\bar{J},\psi)}\,. \tag{2.14}$$

Using the fact that the exponential in Eq. (2.14) is an even functional one easily varifies that

$$\begin{aligned}\frac{\delta^{(2n)}\mathcal{G}[\bar{J},J]}{\delta\bar{J}_{K_1'}\cdots\delta\bar{J}_{K_n'}\delta J_{K_n}\cdots\delta J_{K_1}}\Bigg|_{\bar{J}=J=0} &= \frac{\zeta^n}{\mathcal{Z}_0}\int\mathcal{D}[\bar{\psi},\psi]\prod_{i=1}^{n}\psi_{K_i'}\bar{\psi}_{K_i}e^{-S[\bar{\psi},\psi]} &(2.15)\\ &= (-\zeta)^n\, G^{(2n)}(K_1',\ldots,K_n';K_n,\ldots,K_1)\,. &(2.16)\end{aligned}$$

We use the notation that ψ or J are understood as (infinite-dimensional) vectors with components ψ_K and J_K, respectively.
In contrast to Eq. (2.13) the *generating functional of connected Green functions* is determined by

$$\mathcal{G}_c[\bar{J},J] = \ln\mathcal{G}[\bar{J},J] = \ln\left(\frac{\mathcal{Z}[\bar{J},J]}{\mathcal{Z}_0}\right)\,. \tag{2.17}$$

We *define* in analogy with Eq. (2.16)

$$G_c^{(2n)}(K_1',\ldots,K_n';K_n,\ldots,K_1) = (-\zeta)^n \left.\frac{\delta^{(2n)}\mathcal{G}_c[\bar{J},J]}{\delta\bar{J}_{K_1'}\cdots\delta\bar{J}_{K_n'}\delta J_{K_n}\cdots\delta J_{K_1}}\right|_{\bar{J}=J=0} . \tag{2.18}$$

According to the linked-cluster theorem [84, 86] and in contrast to $G^{(2n)}$, perturbative expansions of the connected Green functions $G_c^{(2n)}$ only contain connected Feynman graphs; vacuum contributions and disconnected diagrams are factored out.

Let us mention another representation of $\mathcal{G}_c$ which may be useful for perturbative calculations, obtained by noting that

$$\begin{aligned} e^{-S_{\rm int}[\bar{\psi},\psi]+(\bar{\psi},J)+(\bar{J},\psi)} &= e^{-S_{\rm int}[\bar{\psi},\psi]}e^{(\bar{\psi},J)+(\bar{J},\psi)} \\ &= e^{-S_{\rm int}[\zeta\frac{\delta}{\delta J},\frac{\delta}{\delta\bar{J}}]}e^{(\bar{\psi},J)+(\bar{J},\psi)} . \end{aligned}$$

Inserting this in Eq. (2.14) and performing the remaining Gaussian integrations we get

$$e^{\mathcal{G}_c[\bar{J},J]} = e^{-S_{\rm int}[\zeta\frac{\delta}{\delta J},\frac{\delta}{\delta\bar{J}}]}e^{-(\bar{J},G_0J)} . \tag{2.19}$$

The most useful generating functional for our purposes is the *generating functional of the Legendre effective action*,

$$\mathcal{L}[\bar{\varphi},\varphi] = (\bar{\varphi},J[\bar{\varphi},\varphi]) + (\bar{J}[\bar{\varphi},\varphi],\varphi) - \mathcal{G}_c[\bar{J}[\bar{\varphi},\varphi],J[\bar{\varphi},\varphi]] . \tag{2.20}$$

Here the new fields $\bar{\varphi}$ and φ are given as functional averages of the original fermion fields, i.e.

$$\bar{\varphi} = \langle\bar{\psi}\rangle_{\bar{J}J} = \frac{\delta\mathcal{G}_c[\bar{J},J]}{\delta\bar{J}} , \tag{2.21}$$

$$\varphi = \langle\psi\rangle_{\bar{J}J} = \zeta\frac{\delta\mathcal{G}_c[\bar{J},J]}{\delta J} , \tag{2.22}$$

with

$$\langle\ldots\rangle_{\bar{J}J} = \frac{\int\mathcal{D}[\bar{\psi},\psi](\ldots)e^{-S[\bar{\psi},\psi]+(\bar{\psi},J)+(\bar{J},\psi)}}{\int\mathcal{D}[\bar{\psi},\psi]e^{-S[\bar{\psi},\psi]+(\bar{\psi},J)+(\bar{J},\psi)}} . \tag{2.23}$$

As usual for the Legendre transform $\mathcal{L}$ the functionals $\bar{J}[\bar{\varphi},\varphi]$ and $J[\bar{\varphi},\varphi]$ are obtained by inverting Eqs. (2.21) and (2.22). The corresponding vertex functions are again defined by

$$L^{(2n)}(K'_1,\ldots,K'_n;K_n,\ldots,K_1) = (-\zeta)^n \frac{\delta^{(2n)}\mathcal{L}[\bar\varphi,\varphi]}{\delta\bar\varphi_{K'_1}\cdots\delta\bar\varphi_{K'_n}\delta\varphi_{K_n}\cdots\delta\varphi_{K_1}}\Big|_{\bar\varphi=\varphi=0}, \tag{2.24}$$

and it proves useful to relate this definition to a monomial expansion of $\mathcal{L}$ given by

$$\mathcal{L}[\bar\varphi,\varphi] = \sum_{n=0}^{\infty}\frac{(-1)^n}{(n!)^2}\sum_{\substack{K'_1,\ldots,K'_n\\K_1,\ldots,K_n}} L^{(2n)}(K'_1,\ldots,K'_n;K_n,\ldots,K_1)\prod_{i=1}^{n}\bar\varphi_{K'_i}\varphi_{K_i}\,. \tag{2.25}$$

Inserting the series on the r.h.s. of Eq. (2.24) and using the fact that $L^{(2n)}$ is by definition a totally antisymmetric function (symmetric for bosons) of the first and second set of variables $\{K'_i\}$ and $\{K_i\}$, respectively, one indeed recovers the l.h.s. of Eq. (2.24). Of course, similar monomial expansions exist for $\mathcal{G}$ and $\mathcal{G}_c$. Diagrammatically in the non-symmetry broken case the vertex functions $L^{(2n)}$ are obtained from the vertices $G_c^{(2n)}$ by removing the exact external propagators [84,87], see Fig. 2.1. The remaining graphs are hence *one-particle irreducible*. The intimate relation between the two kinds of vertex functions may also be stated in terms of their generating functionals. Differentiating Eqs. (2.21) and (2.22) with respect to $\bar\varphi_K$ and φ_K and using the chain rule (2.12) one may write in rather compact form

$$\begin{pmatrix} \dfrac{\delta^2\mathcal{G}_c}{\delta\bar J\delta J} & \zeta\dfrac{\delta^2\mathcal{G}_c}{\delta\bar J\delta\bar J} \\[2ex] \zeta\dfrac{\delta^2\mathcal{G}_c}{\delta J\delta J} & \dfrac{\delta^2\mathcal{G}_c}{\delta J\delta\bar J} \end{pmatrix} = \begin{pmatrix} \dfrac{\delta^2\mathcal{L}}{\delta\bar\varphi\delta\varphi} & \dfrac{\delta^2\mathcal{L}}{\delta\bar\varphi\delta\bar\varphi} \\[2ex] \dfrac{\delta^2\mathcal{L}}{\delta\varphi\delta\varphi} & \dfrac{\delta^2\mathcal{L}}{\delta\varphi\delta\bar\varphi} \end{pmatrix}^{-1}. \tag{2.26}$$

Here, the elements of the (2×2)-matrices have to be understood as matrices with indices in K-space. Explicitly

$$\left(\frac{\delta^2\mathcal{G}_c}{\delta\bar J\delta J}\right)_{KK'} = \frac{\delta^2\mathcal{G}_c}{\delta\bar J_K\delta J_{K'}}\,, \tag{2.27}$$

and similarly for the other matrix elements. Note that setting $\bar J = J = 0$ in Eq. (2.26) (which also implies $\bar\varphi = \varphi = 0$ in the non-symmetry-broken case) only the diagonal elements are non-zero and we recover the well-known result

$$G_c^{(2)}(K;K') = [\,L^{(2)}(K;K')\,]^{-1}\,. \tag{2.28}$$

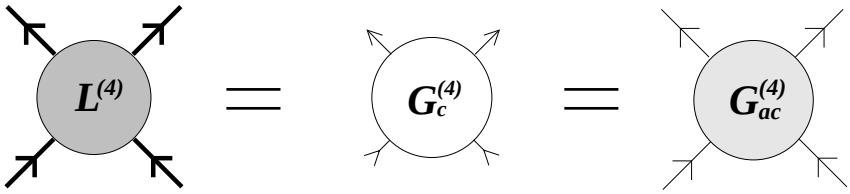

Figure 2.1: Diagrammatic relation between the four-point vertices of the Legendre effective action $L^{(4)}$, the connected Green function $G_c^{(4)}$ and the amputated connected Green function $G_{ac}^{(4)}$ in the non-symmetry broken phase. The thick line with arrow represents the full interacting propagator $G^{(2)}$ containing proper self-energy insertions and the thin line symbolizes the free propagator G_0. Lines with an arrow at the end just represent the external momenta.

Finally let us turn our attention to a kind of generating functional which has been used for the derivation of the exact flow equations in Polchinski's ERG version [39], the *generating functional of amputated connected Green functions*:

$$\mathcal{G}_{ac}[\bar{\eta},\eta] = \ln\left(\frac{1}{\mathcal{Z}_0}\int \mathcal{D}[\bar{\psi},\psi]e^{-S_0[\bar{\psi},\psi]-S_{\rm int}[\bar{\psi}-\bar{\eta},\psi-\eta]}\right). \tag{2.29}$$

By shifting the fields according to $\bar{\phi}=\bar{\psi}-\bar{\eta}$ and $\phi=\psi-\eta$ one easily finds the relation to $\mathcal{G}_c$, namely

$$\begin{aligned}\mathcal{G}_{ac}[\bar{\eta},\eta] &= \Big[(\bar{J},G_0J)+\mathcal{G}_c[\bar{J},J]\Big]_{J=G_0^{-1}\eta}^{\bar{J}=G_0^{-1}\bar{\eta}}, &(2.30)\\ &= (\bar{\eta},G_0^{-1}\eta)+\mathcal{G}_c\big[G_0^{-1}\bar{\eta},G_0^{-1}\eta\big], &(2.31)\end{aligned}$$

The vertex functions $G_{ac}^{(2n)}$ are defined in analogy with Eq. (2.18). Applying the functional derivatives to Eq. (2.31) and setting the source fields equal to zero, one obtains

$$\begin{aligned}&G_{ac}^{(2n)}(K_1',\ldots,K_n';K_n,\ldots,K_1) &(2.32)\\ &= \begin{cases} G_0^{-1}(K)G_0^{-1}(K')\big[G_c^{(2)}(K;K')-G_0(K)\delta_{K,K'}\big] & ,\ n=1\\ G_c^{(2n)}(K_1',\ldots,K_n';K_n,\ldots,K_1)\prod_{i=1}^n G_0^{-1}(K_i)G_0^{-1}(K_i') & ,\ n>1\end{cases}.\end{aligned}$$

Here we used the fact that G_0 is a diagonal matrix. Eq. (2.32) explicitly shows that for $n>1$ $G_{ac}^{(2n)}$ is obtained from the connected Green functions $G_c^{(2n)}$ by removing the external *bare* propagators G_0, see also Fig. 2.1.

Finally let us derive a representation for $\mathcal{G}_{ac}$ similar to one for $\mathcal{G}_c$ in Eq. (2.19). To this end note that the interaction part of the exponential factor in Eq. (2.29) may be written as follows,

$$e^{-S_{\rm int}[\bar\psi-\bar\eta,\psi-\eta]} = e^{-S_{\rm int}[\zeta\frac{\delta}{\delta J},\frac{\delta}{\delta\bar J}]}e^{(\bar\psi-\bar\eta,J)+(\bar J,\psi-\eta)}\big|_{\bar J=J=0}\,. \tag{2.33}$$

Inserting this on the r.h.s. of Eq. (2.29) yields

$$\begin{aligned} e^{\mathcal{G}_{ac}[\bar\eta,\eta]} &= \frac{1}{\mathcal{Z}_0}\Big[\, e^{-S_{\rm int}[\zeta\frac{\delta}{\delta J},\frac{\delta}{\delta\bar J}]}e^{-(\bar\eta,J)-(\bar J,\eta)} \\ &\qquad \times\int\mathcal{D}[\bar\psi,\psi]e^{(\bar\psi,G_0^{-1}\psi)+(\bar\psi,J)+(\bar J,\psi)}\Big]_{\bar J=J=0}\,. \end{aligned} \tag{2.34}$$

The remaining functional integration is of the Gaussian type and can be performed trivially:

$$\begin{aligned} e^{-(\bar\eta,J)-(\bar J,\eta)}&\int\mathcal{D}[\bar\psi,\psi]e^{(\bar\psi,G_0^{-1}\psi)+(\bar\psi,J)+(\bar J,\psi)} \\ &= [\det(-G_0)]^\zeta\, e^{-(\bar J,G_0J)}e^{-(\bar\eta,J)-(\bar J,\eta)} \\ &= \mathcal{Z}_0\, e^{-(\zeta\frac{\delta}{\delta\eta},G_0\frac{\delta}{\delta\bar\eta})}e^{-(\bar\eta,J)-(\bar J,\eta)}\,. \end{aligned} \tag{2.35}$$

The result in the last line can now be inserted on the r.h.s. of Eq. (2.34). Interchanging the order of the exponentials which contain the J- and the η-derivatives (this does not lead to additional ζ-factors since $S_{\rm int}$ is by assumption an even functional) and noting that

$$e^{-S_{\rm int}[\zeta\frac{\delta}{\delta J},\frac{\delta}{\delta\bar J}]}e^{-(\bar\eta,J)-(\bar J,\eta)} = e^{-S_{\rm int}[\bar\eta,\eta]}e^{-(\bar\eta,J)-(\bar J,\eta)}\,, \tag{2.36}$$

we obtain after setting $\bar J = J = 0$ as final result

$$e^{\mathcal{G}_{ac}[\bar\eta,\eta]} = e^{-(\zeta\frac{\delta}{\delta\eta},G_0\frac{\delta}{\delta\bar\eta})}e^{-S_{\rm int}[\bar\eta,\eta]}\,. \tag{2.37}$$

Chapter 3

Unrescaled Flow Equations

We now introduce a cutoff-dependent theory and derive the flow equations for the vertices of the Legendre effective action, obtained by purely integrating out high-energy degrees of freedom. Subtleties of the sharp-cutoff limit are discussed.

3.1 Sharp and Smooth Cutoff Dependence

As usual in renormalization group theory we introduce a high-energy band cutoff Λ_0 needed to regularize the theory in the ultraviolet regime. However, we emphasize again that Λ_0 in condensed matter physics has a physical significance that depends on the model under consideration. It can for instance represent an energy scale related to the inverse lattice constant, and consequently we are not forced to perform the continuum limit at the end of the calculation by taking $\Lambda_0 \to \infty$. Instead, Λ_0 should better be viewed as an irrelevant parameter of the RG incorporating non-universal features of the model at hand, a point we will discuss in more detail in Sec. 6.1. Besides Λ_0 we define a second *infrared* cutoff, related to the first by

$$\Lambda = \Lambda_0 e^{-l}\,, \tag{3.1}$$

where l is called the logarithmic flow parameter of the RG. To be more precise Λ has the dual interpretation of serving as an infrared cutoff for the flow of the amputated connected Green functions given in Eq. (2.32) and energies larger than Λ, and as an ultraviolet cutoff for the vertex functions of the Wilsonian effective action for energies smaller than Λ, see Ref. [42] for a detailed discussion of this subtle point. Since we are going to study the flow of the Legendre effective action which is closely related to the amputated connected Green functions, we are

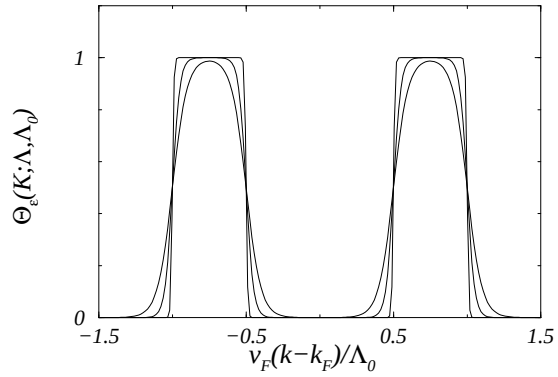

Figure 3.1: Plot of the smooth step function $\Theta_\epsilon(K;\Lambda,\Lambda_0) = \frac{1}{2}[\tanh((\Omega_K/\Lambda - 1)/\epsilon) - \tanh((\Omega_K/\Lambda_0 - 1)/\epsilon)]$, with $\Omega_K = v_F|k - k_F|$ and $\Lambda = \Lambda_0/2$ for values $\epsilon = 0.1, 0.05$ and 0.01. Obviously, $\Theta_\epsilon(K;\Lambda,\Lambda_0)$ approaches the sharp step function $\Theta(\frac{1}{2} < \Omega_K/\Lambda_0 < 1)$ when ϵ tends to zero. The origin corresponds to the right Fermi point.

interested in the first case and need both: Λ as a low-energy cutoff to regularize infrared divergences and Λ_0 as regularization of the ultraviolet regime. This is why we introduce a cutoff dependent bare propagator as follows,

$$G_0^\Lambda(K) = \Theta_\epsilon(K;\Lambda,\Lambda_0)\, G_0(K)\,, \tag{3.2}$$

where $\Theta_\epsilon(K;\Lambda,\Lambda_0)$ is by definition a smooth and non-zero function with the properties

$$\Theta_\epsilon(K;\Lambda_0,\Lambda_0) = 0\,, \tag{3.3}$$

to insure proper initial conditions, and

$$\lim_{\epsilon\to 0}\Theta_\epsilon(K;\Lambda,\Lambda_0) = \Theta(\Lambda < \Omega_K < \Lambda_0) = \begin{cases} 1 & \text{for } \Lambda < \Omega_K < \Lambda_0 \\ 0 & \text{else} \end{cases}\,. \tag{3.4}$$

In the following we shall refer to this limiting procedure as the *sharp-cutoff limit*. But even for finite ϵ we think of Θ_ϵ as a smooth function with $\Theta_\epsilon(K;\Lambda,\Lambda_0) \approx 1$ for $\Lambda < \Omega_K < \Lambda_0$ and $\Theta_\epsilon(K;\Lambda,\Lambda_0) \approx 0$ outside this interval. Here Ω_K is assumed to be a homogeneous function of $|\epsilon_{\mathbf{k}} - \epsilon_{\mathbf{k}_F}\delta_{\zeta,-1}|$ and/or $|\omega_n|$, such as $\Omega_K = |\omega_n|$, $\Omega_K = |\epsilon_{\mathbf{k}} - \epsilon_{\mathbf{k}_F}\delta_{\zeta,-1}|$ or $\Omega_K = \sqrt{\omega_n^2 + (\epsilon_{\mathbf{k}} - \epsilon_{\mathbf{k}_F}\delta_{\zeta,-1})^2}$, where $\epsilon_{\mathbf{k}}$ is the non-interacting energy dispersion. Note that in case of fermions we need to know the exact location of the interacting FS (denoted by the set of all Fermi vectors $\mathbf{k}_F$), where the process of eliminating degrees of freedom has to be stopped. This rather subtle point is discussed in detail in Sec. 4.1 where scaling variables are introduced and where we also state the precise definition of the interacting FS. In

Fig. 3.1 we give an explicit example for a smooth step function approaching the limit (3.4) for fermions in spatial dimensions $D = 1$ and for $\Omega_K = v_F|k - k_F|$.[1]
The reason for the introduction of a smooth cutoff is twofold: Mathematically, expressions involving the inverse propagator $(G_0^\Lambda)^{-1}$ are only well-defined in the smooth cutoff version. Secondly, as we will see shortly, our RG flow equations contain combinations of the form $f_\Lambda(\Theta_\epsilon(\Omega_K;\Lambda,\Lambda_0))\,\partial_\Lambda\Theta_\epsilon(\Omega_K;\Lambda,\Lambda_0)$, for some function f_Λ. If one naively performs the sharp cutoff limit this apparently leads to $f_\Lambda(\Theta(\Lambda < \Omega_K < \Lambda_0))\delta(\Omega_K - \Lambda)$, which has no precise mathematical meaning since $\Theta(\Lambda < \Omega_K < \Lambda_0)$ is not well-defined at $\Omega_K = \Lambda$. This problem is most serious when we use amputated connected Green functions for the formulation of the RG, leading to Polchinski's version of flow equations [39]. In this case tree-graph contributions exist, where terms like the above appear without being integrated over K, and one is hence restricted to the smooth-cutoff version. As has been discussed in detail by Morris in Ref. [42] , from the point of view of approximations Polchinskis equations are much less convenient than the flow equations obtained by using the 1PI vertex functions of the Legendre effective action. Here no tree-graph contributions exist and all δ-functions appear within integral kernels.
However, even if we use the Legendre effective action we still have to point out how the sharp cutoff limit of the above combination has to be interpreted. As has been shown by Morris [42], the mathematically rigorous way to perform the limit is

$$\lim_{\epsilon\to 0} f_\Lambda(\Theta_\epsilon(\Omega_K;\Lambda,\Lambda_0))\,\partial_\Lambda\Theta_\epsilon(\Omega_K;\Lambda,\Lambda_0) = -\,\delta(\Omega_K-\Lambda)\int_0^1 dt f_\Lambda(t)\,. \tag{3.5}$$

Thus, as long as we do not know the function f_Λ we have to keep ϵ finite. Note that for notational convenience we did not explicitly show the dependence of G_0^Λ on ϵ and the ultraviolet cutoff Λ_0. In the latter case we should generally keep in mind that all subsequently defined quantities implicitly depend on Λ_0 as well. As concerns the dependence on ϵ we will emphazise when we change to the sharp cutoff version.

Following this rather technical preface we may now formulate a cutoff dependent theory by replacing the action given in Eq. (2.2) as follows,

$$S^\Lambda[\bar\psi,\psi] = S_0^\Lambda[\bar\psi,\psi] + S_{\rm int}[\bar\psi,\psi]\,, \tag{3.6}$$

with

$$S_0^\Lambda[\bar\psi,\psi] = -(\bar\psi,(G_0^\Lambda)^{-1}\psi)\,. \tag{3.7}$$

[1] In one dimension we know by Luttinger's theorem [75] that the interacting Fermi vector k_F coincides with the non-interacting one.

Note that in this way the whole Λ-dependence of the model enters via the propagators G_0^Λ. Due to the property (3.3) of Θ_ϵ the initial condition is given by

$$S^{\Lambda_0}[\bar\psi,\psi] = S_{\rm int}[\bar\psi,\psi]\,, \tag{3.8}$$

and the full action with ultraviolet cutoff Λ_0 is recovered in the limit $\Lambda \to 0$.
Of course the definitions and results of Sec. 2 remain valid, and all we have to do is to replace G_0 by G_0^Λ and to add an index Λ to the various quantities to emphazise their cutoff dependence. In particular we have

$$\mathcal{G}_c^\Lambda[\bar J, J] = \ln \mathcal{G}^\Lambda[\bar J, J] = \ln\left(\frac{\mathcal{Z}^\Lambda[\bar J, J]}{\mathcal{Z}_0^\Lambda}\right)\,, \tag{3.9}$$

with

$$\mathcal{Z}_0^\Lambda = [\det(-G_0^\Lambda)]^\zeta\,. \tag{3.10}$$

3.2 Flow of $\mathcal{G}_c^\Lambda$

As a first step towards the flow equation for the Legendre effective action $\mathcal{L}^\Lambda$ have to determine the change of the generating functional $\mathcal{G}_c^\Lambda$ when the cutoff Λ is reduced. Using the "trace-log" formula [88], Eq. (3.9) may also be written as

$$\mathcal{G}_c^\Lambda[\bar J, J] = \tilde{\mathcal{G}}_c^\Lambda[\bar J, J] - \zeta {\rm Tr}\ln(-G_0^\Lambda)\,, \tag{3.11}$$

where ${\rm Tr} \equiv \sum_K$ means the trace in the K-basis and we have defined

$$e^{\tilde{\mathcal{G}}_c^\Lambda[\bar J, J]} = \mathcal{Z}^\Lambda[\bar J, J]\,. \tag{3.12}$$

From the definition of $\mathcal{Z}^\Lambda$, Eq. (2.14), we obtain

$$\begin{aligned}\partial_\Lambda \mathcal{Z}^\Lambda[\bar J, J] &= \int \mathcal{D}[\bar\psi,\psi](\bar\psi, \partial_\Lambda (G_0^\Lambda)^{-1}\psi) e^{-S^\Lambda[\bar\psi,\psi]+(\bar\psi,J)+(\bar J,\psi)} \\ &= \zeta\left(\tfrac{\delta}{\delta J}, \partial_\Lambda (G_0^\Lambda)^{-1}\tfrac{\delta}{\delta J}\right)\, \mathcal{Z}^\Lambda[\bar J, J]\,. \end{aligned} \tag{3.13}$$

Differentiating Eq. (3.12) with respect to Λ and inserting the last result yields

$$\begin{aligned}\left(\partial_\Lambda \tilde{\mathcal{G}}_c^\Lambda[\bar J, J]\right) e^{\tilde{\mathcal{G}}_c^\Lambda[\bar J, J]} &= \zeta\left(\tfrac{\delta}{\delta J}, \partial_\Lambda (G_0^\Lambda)^{-1}\tfrac{\delta}{\delta J}\right) e^{\tilde{\mathcal{G}}_c^\Lambda[\bar J, J]} \\ &= \left\{ {\rm Tr}\left[\partial_\Lambda (G_0^\Lambda)^{-1}\cdot \frac{\delta^2 \tilde{\mathcal{G}}_c^\Lambda}{\delta\bar J \delta J}\right] + \zeta\left(\tfrac{\delta \tilde{\mathcal{G}}_c^\Lambda}{\delta J}, \partial_\Lambda (G_0^\Lambda)^{-1}\tfrac{\delta \tilde{\mathcal{G}}_c^\Lambda}{\delta J}\right)\right\} \\ &\quad \times e^{\tilde{\mathcal{G}}_c^\Lambda[\bar J, J]}\,. \end{aligned} \tag{3.14}$$

Here the dot in the second line denotes the matrix product in the K-basis. The factor $\exp(\tilde{\mathcal{G}}_c^\Lambda[\bar{J},J])$ appears on both sides of Eq. (3.14) can be canceled out. Combining this result with Eq. (3.11) we obtain the flow equation for the generating functional of connected Green functions,

$$\begin{aligned}\partial_\Lambda \mathcal{G}_c^\Lambda[\bar{J},J] &= \zeta\left(\tfrac{\delta\mathcal{G}_c^\Lambda}{\delta J},\partial_\Lambda (G_0^\Lambda)^{-1}\tfrac{\delta\mathcal{G}_c^\Lambda}{\delta J}\right)\\ &+ \mathrm{Tr}\Big[\partial_\Lambda (G_0^\Lambda)^{-1}\cdot\frac{\delta^2\mathcal{G}_c^\Lambda}{\delta\bar{J}\delta J}-\zeta\partial_\Lambda\ln(-G_0^\Lambda)\Big]\,. \end{aligned}\tag{3.15}$$

It proves useful to rewrite this equation in a form that immediatly allows us to switch to an analogous equation for $\mathcal{L}^\Lambda$. To this end we define

$$\boldsymbol{\delta\mathcal{G}}_c^\Lambda[\bar{J},J]=\begin{pmatrix}\zeta\dfrac{\delta^2\mathcal{G}_c^\Lambda}{\delta\bar{J}\delta J} & \zeta\dfrac{\delta^2\mathcal{G}_c^\Lambda}{\delta\bar{J}\delta\bar{J}}\\[2ex] \dfrac{\delta^2\mathcal{G}_c^\Lambda}{\delta J\delta J} & \dfrac{\delta^2\mathcal{G}_c^\Lambda}{\delta J\delta\bar{J}}\end{pmatrix},\tag{3.16}$$

implying

$$\begin{aligned}\tilde{\mathrm{Tr}}\,\boldsymbol{\delta\mathcal{G}}_c^\Lambda[\bar{J},J] &= \mathrm{Tr}\Big(\zeta\frac{\delta^2\mathcal{G}_c^\Lambda}{\delta\bar{J}\delta J}+\frac{\delta^2\mathcal{G}_c^\Lambda}{\delta J\delta\bar{J}}\Big)\\ &= 2\,\zeta\,\mathrm{Tr}\,\frac{\delta^2\mathcal{G}_c^\Lambda}{\delta\bar{J}\delta J}\,,\end{aligned}\tag{3.17}$$

where $\tilde{\mathrm{Tr}}=\mathrm{tr}\sum_K$ and "tr" denotes the trace of the (2×2)-matrix.[2] We have used the fact that according to Eq. (2.27)

$$\zeta\frac{\delta^2\mathcal{G}_c^\Lambda}{\delta\bar{J}\delta J}={}^t\Big(\frac{\delta^2\mathcal{G}_c^\Lambda}{\delta J\delta\bar{J}}\Big)\,,\tag{3.18}$$

the index t indicating the transpose matrix. Using Eq. (3.17) and defining $\mathbf{G}_0^\Lambda = G_0^\Lambda\mathbf{1}$, where $\mathbf{1}$ is the unit (2×2)-matrix, it is easy to see that the flow equation (3.15) is equivalent with

$$\boxed{\begin{aligned}\partial_\Lambda\mathcal{G}_c^\Lambda[\bar{J},J] &= \zeta\left(\tfrac{\delta\mathcal{G}_c^\Lambda}{\delta J},\partial_\Lambda(G_0^\Lambda)^{-1}\tfrac{\delta\mathcal{G}_c^\Lambda}{\delta J}\right)\\ &+ \frac{\zeta}{2}\,\tilde{\mathrm{Tr}}\Big[\partial_\Lambda(\mathbf{G}_0^\Lambda)^{-1}\boldsymbol{\delta\mathcal{G}}_c^\Lambda[\bar{J},J]-\partial_\Lambda\ln(-\mathbf{G}_0^\Lambda)\Big]\,.\end{aligned}}\tag{3.19}$$

[2]Here and in the following bold face letters always represent (2×2)-matrices.

Here we made explicit use of the fact that G_0^Λ is by assumption diagonal in the K-basis. The initial condition for the flow of $\mathcal{G}_c^\Lambda$ is obtained from Eqs. (2.37) and (2.30). Due to the first we have $\mathcal{G}_{ac}^{\Lambda_0}[\bar\eta,\eta] = S_{\rm int}[\bar\eta,\eta]$. Inserting this in Eq. (2.30) leads to

$$\mathcal{G}_c^{\Lambda_0}[\bar J, J] = \mathcal{G}_{ac}^{\Lambda_0}[0,0] = 0\,, \tag{3.20}$$

where we have used $G_0^{\Lambda_0} = 0$. However, this boundary-value problem contains no information about the initial system and is hence of no practical use for further calculations.

3.3 Flow of Γ^Λ

To obtain the flow equation for the Legendre effective action let us define

$$\boldsymbol{\delta\mathcal{L}}^\Lambda[\bar\varphi,\varphi] = \begin{pmatrix} \zeta\,\dfrac{\delta^2\mathcal{L}^\Lambda}{\delta\bar\varphi\delta\varphi} & \zeta\,\dfrac{\delta^2\mathcal{L}^\Lambda}{\delta\bar\varphi\delta\bar\varphi} \\[2ex] \dfrac{\delta^2\mathcal{L}^\Lambda}{\delta\varphi\delta\varphi} & \dfrac{\delta^2\mathcal{L}^\Lambda}{\delta\varphi\delta\bar\varphi} \end{pmatrix}, \tag{3.21}$$

From Eq. (2.26) it is then straightforward to show that

$$\boldsymbol{\delta\mathcal{G}}_c^\Lambda[\bar J, J] = \big(\boldsymbol{\delta\mathcal{L}}^\Lambda[\bar\varphi,\varphi]\big)^{-1}. \tag{3.22}$$

Furthermore from Eq. (2.20) we get

$$\partial_\Lambda\mathcal{G}_c^\Lambda[\bar J, J] = -\,\partial_\Lambda\mathcal{L}^\Lambda[\bar\varphi,\varphi]\,, \tag{3.23}$$

so that with Eqs. (2.21) and (2.22) we may state the flow equation for the generating functional of the Legendre effective action,

$$\begin{aligned} \partial_\Lambda\mathcal{L}^\Lambda[\bar\varphi,\varphi] &= -\,(\bar\varphi, \partial_\Lambda (G_0^\Lambda)^{-1}\varphi) \\ &- \frac{\zeta}{2}\,\tilde{\rm Tr}\Big[\partial_\Lambda(\mathbf{G}_0^\Lambda)^{-1}\big(\boldsymbol{\delta\mathcal{L}}^\Lambda[\bar\varphi,\varphi]\big)^{-1} - \partial_\Lambda \ln(-\mathbf{G}_0^\Lambda)\Big]. \end{aligned} \tag{3.24}$$

We could now proceed by using this equation to derive the flow equations for the vertex functions $L_\Lambda^{(2n)}$. However, it proves useful to define another generating functional obtained from $\mathcal{L}^\Lambda$ by subtracting the free inverse propagator $(G_0^\Lambda)^{-1}$ in the following way,

$$\Gamma^\Lambda[\bar\varphi,\varphi] = \mathcal{L}^\Lambda[\bar\varphi,\varphi] + (\bar\varphi, (G_0^\Lambda)^{-1}\varphi)\,. \tag{3.25}$$

The monomial expansion of Γ^Λ is analogous to that of $\mathcal{L}^\Lambda$, namely

$$\Gamma^\Lambda[\bar\varphi,\varphi] = \sum_{n=0}^{\infty} \frac{(-1)^n}{(n!)^2} \sum_{\substack{K_1',\ldots,K_n' \\ K_1,\ldots,K_n}} \bar\Gamma_\Lambda^{(2n)}(K_1',\ldots,K_n';K_n,\ldots,K_1) \prod_{i=1}^{n} \bar\varphi_{K_i'}\varphi_{K_i}\,, \tag{3.26}$$

where for later convenience we have defined

$$\begin{aligned}\bar\Gamma_\Lambda^{(2n)}(K_1',\ldots,K_n';K_n,\ldots,K_1) &= \delta_{K_1'+\ldots+K_n',\,K_1+\ldots+K_n} \\ &\quad\times\Gamma_\Lambda^{(2n)}(K_1',\ldots,K_n';K_n,\ldots,K_1)\,,\end{aligned} \tag{3.27}$$

Due to the definitions (2.25) and (3.25) we have

$$\frac{\delta^2\Gamma^\Lambda}{\delta\varphi\delta\bar\varphi}\Big|_{\bar\varphi=\varphi=0} = (G_0^\Lambda)^{-1} - L_\Lambda^{(2)} = \Sigma_\Lambda\,, \tag{3.28}$$

where the second equality follows from Eq. (2.28) together with

$$(G_\Lambda)^{-1} = (G_0^\Lambda)^{-1} - \Sigma_\Lambda\,. \tag{3.29}$$

Here G_Λ is the exact interacting Green function and Σ_Λ the exact 1PI self-energy. Let us now define a (2×2)-matrix $\boldsymbol{\delta\Gamma}^\Lambda$ in analogy with the definition of $\boldsymbol{\delta\mathcal{L}}^\Lambda$ given in Eq. (3.21) by just replacing $\mathcal{L}^\Lambda$ with Γ^Λ. From the above considerations we then have in case of no broken symmetries

$$\boldsymbol{\delta\Gamma}^\Lambda[0,0] = \boldsymbol{\Sigma}_\Lambda = \Sigma_\Lambda\,\mathbf{1}\,. \tag{3.30}$$

Finally we subtract the self-energy part from $\boldsymbol{\delta\Gamma}^\Lambda$ and define

$$\boldsymbol{\delta\Gamma}^\Lambda_{sub}[\bar\varphi,\varphi] = \boldsymbol{\delta\Gamma}^\Lambda[\bar\varphi,\varphi] - \boldsymbol{\Sigma}_\Lambda\,, \tag{3.31}$$

such that

$$\boldsymbol{\delta\Gamma}^\Lambda_{sub}[0,0] = 0\,. \tag{3.32}$$

This property insures that only a finite number of terms will contribute to the flow of each vertex function as will be seen in the next section . The relation to $\boldsymbol{\delta\mathcal{L}}^\Lambda$ is determined by Eq. (3.25),

$$\boldsymbol{\delta\mathcal{L}}^\Lambda[\bar\varphi,\varphi] = \boldsymbol{\delta\Gamma}^\Lambda[\bar\varphi,\varphi] - (\boldsymbol{G}_0^\Lambda)^{-1} \tag{3.33}$$

$$= \boldsymbol{\delta\Gamma}^{\Lambda}_{sub}[\bar{\varphi},\varphi] - (\boldsymbol{G}_\Lambda)^{-1}\,. \tag{3.34}$$

Using the above definitions and some straightforward calculations it is now easy to show that the flow equation for $\mathcal{L}^\Lambda$ can be transformed into

$$\boxed{\begin{aligned}\partial_\Lambda \Gamma^\Lambda[\bar{\varphi},\varphi] &= \tfrac{\zeta}{2}\,\tilde{\mathrm{Tr}}\Big[\partial_\Lambda(\boldsymbol{G}_0^\Lambda)^{-1}\Big\{(\boldsymbol{G}_0^\Lambda)^2\,\boldsymbol{\Sigma}_\Lambda\big(\mathbf{1}-\boldsymbol{G}_0^\Lambda\boldsymbol{\Sigma}_\Lambda\big)^{-1}\\ &+ (\boldsymbol{G}_\Lambda)^2\,\boldsymbol{\delta\Gamma}^\Lambda_{sub}[\bar{\varphi},\varphi]\,\big(\mathbf{1}-\boldsymbol{G}_\Lambda\,\boldsymbol{\delta\Gamma}^\Lambda_{sub}[\bar{\varphi},\varphi]\big)^{-1}\Big\}\Big]\,.\end{aligned}} \tag{3.35}$$

This is the flow equation for the generating functional of the 1PI vertex functions in its smooth-cutoff form. The initial condition is fixed by [42]

$$\Gamma^{\Lambda_0}[\bar{\varphi},\varphi] = S_{\mathrm{int}}[\bar{\varphi},\varphi]\,. \tag{3.36}$$

First of all note this equation is the formal equivalent of the corresponding equation in ϕ^4 theory, see Eq. (2.16) in Ref. [46], except for the fact that all quantities on the r.h.s. now appear as (2×2)-matrices and the trace is enlarged.[3]. Furthermore Eq. (3.35) is a one-loop equation in the sense that all terms on the r.h.s. appear within a single K-trace. As a direct consequence the vertex functions $\Gamma^{(2n)}$ will be smooth functions of the flow parameter Λ even in the sharp cutoff limit, which in particular means that Σ_Λ and $\boldsymbol{\delta\Gamma}^\Lambda_{sub}[\bar{\varphi},\varphi]$ will depend smoothly on Λ. However, the exact propagator $G_\Lambda(K)$ defined in Eq. (3.29) remains discontinuous at $\Omega_K=\Lambda$, which raises the question how the sharp-cutoff limit can be performed. To see this more clearly it is useful to consider the thermodynamic limit, which formally amounts to the replacements

$$\frac{1}{\beta V}\sum_K \to \sum_\sigma \int\frac{d\mathbf{k}}{(2\pi)^D}\int_{-\infty}^{\infty}\frac{d\omega}{2\pi} \equiv \int_K\,, \tag{3.37}$$

and

$$\beta V\delta_{K,K'} \;\to\; (2\pi)^D\delta_{\sigma\sigma'}\delta(\mathbf{k}-\mathbf{k}')\delta(\omega-\omega') \tag{3.38}$$

$$\equiv\; (2\pi)^D\,\delta(K-K')\,, \tag{3.39}$$

where V is the spatial volume of the D-dimensional system and β is the inverse temperature. Together with $\partial_\Lambda(G_0^\Lambda)^{-1} = -(G_0^\Lambda)^2\partial_\Lambda G_0^\Lambda$ Eq. (3.35) turns into

[3] We use notations different from those in Ref. [46] To identify the quantities we have to replace $\Gamma^\Lambda \leftrightarrow \mathcal{G}_{\mathrm{ir}}^{\Lambda,\Lambda_0}$ and $\boldsymbol{\delta\Gamma}^\Lambda_{sub}[\bar{\varphi},\varphi] \leftrightarrow \mathcal{U}^{\Lambda,\Lambda_0}$. The different signs in the equations are due to different definitions of the self-energies.

$$\begin{aligned}\partial_\Lambda \Gamma^\Lambda[\bar\varphi,\varphi] &= -\zeta \int_K \frac{\partial_\Lambda G_0^\Lambda(K)}{[1-G_0^\Lambda(K)\Sigma_\Lambda(K)]^2} \\ &\quad \times \frac{1}{2}\mathrm{tr}\left[\boldsymbol{\delta\Gamma}^\Lambda_{sub}[\bar\varphi,\varphi]\big(\mathbf{1}-\boldsymbol{G}_\Lambda\boldsymbol{\delta\Gamma}^\Lambda_{sub}[\bar\varphi,\varphi]\big)^{-1}\right]_{KK} \\ &\quad -\zeta\,\beta V\int_K \frac{\partial_\Lambda G_0^\Lambda(K)}{1-G_0^\Lambda(K)\Sigma_\Lambda(K)}\Sigma_\Lambda(K)\,. \end{aligned} \tag{3.40}$$

Note that the term $\partial_\Lambda G_0^\Lambda$ contains the combination $\partial_\Lambda \Theta_\epsilon(K,\Lambda,\Lambda_0)$, such that performing the sharp-cutoff limit implies the knowledge of the function f_Λ introduced in Eq. (3.5). This in turn would imply having solved the many-body problem exactly, which in general is not possible. However, as Σ_Λ and $\boldsymbol{\delta\Gamma}^\Lambda_{sub}[\bar\varphi,\varphi]$ are expected to be smooth functions of Λ it is only the propagator G_Λ within the square brackets that may cause problems. At least for finite external momenta and frequencies of the vertices $\Gamma^{(2n)}_\Lambda$ it will appear in the form $G_\Lambda(K+Q)$ within the trace of Eq. (3.40), for some non-zero Q. In this case also G_Λ depends smoothly on Λ at $\Omega_K=\Lambda$. It has been emphasized by Morris [42] that even in the case $Q=0$ the physics should not be drastically altered, such that it is reasonable to assume the whole expression in the square brackets to be continuous at $\Omega_K=\Lambda$.
Of course, the safest way to proceed is to keep ϵ finite until the function f_Λ is known due to appropriate approximations, and to perform the limit $\epsilon\to 0$ at the end. However, we will choose the first way and point out when ambiguities might occur. Following the above considerations we may now identify

$$f_\Lambda(\Theta_\epsilon(K;\Lambda,\Lambda_0)) = \big(1-G_0^\Lambda(K)\,\Sigma_\Lambda(K)\big)^{-n}\,, \tag{3.41}$$

where $n=2$ for the first and $n=1$ for the second term on the r.h.s. of Eq. (3.40). The sharp-cutoff limit applied to Eq. (3.40) can then be performed with the aid of Eq. (3.5) and leads to

$$\boxed{\begin{aligned}\partial_\Lambda \Gamma^\Lambda[\bar\varphi,\varphi] &= \zeta\int_K \frac{\delta(\Omega_K-\Lambda)}{G_0^{-1}(K)-\Sigma_\Lambda(K)} \\ &\quad\times\ \frac{1}{2}\,\mathrm{tr}\Big[\boldsymbol{\delta\Gamma}^\Lambda_{sub}[\bar\varphi,\varphi]\big(\mathbf{1}-\boldsymbol{G}_\Lambda\,\boldsymbol{\delta\Gamma}^\Lambda_{sub}[\bar\varphi,\varphi]\big)^{-1}\Big]_{KK} \\ &\quad-\ \zeta\,\beta V\int_K \delta(\Omega_K-\Lambda)\,\ln\left(\frac{G_0^{-1}(K)-\Sigma_\Lambda(K)}{G_0^{-1}(K)}\right),\end{aligned}} \tag{3.42}$$

with the initial condition still given by Eq. (3.36).

3.4 Flow Equations for the Unrescaled Vertices

The flow equation for $\Gamma^\Lambda[\bar\varphi,\varphi]$ contains in very compact form the flow of all 1PI vertex functions $\Gamma^{(2n)}_\Lambda$, which we shall now derive up to the six-point vertex. To this end we expand the expression in square brackets in Eq. (3.42) in a von-Neumann series,

$$\begin{aligned}\boldsymbol{\delta\Gamma}^\Lambda_{sub}\big(\mathbf{1}-\boldsymbol{G}_\Lambda\,\boldsymbol{\delta\Gamma}^\Lambda_{sub}\big)^{-1} &= \boldsymbol{\delta\Gamma}^\Lambda_{sub}+\boldsymbol{\delta\Gamma}^\Lambda_{sub}\,\boldsymbol{G}_\Lambda\,\boldsymbol{\delta\Gamma}^\Lambda_{sub}\\ &+ \boldsymbol{\delta\Gamma}^\Lambda_{sub}\,\boldsymbol{G}_\Lambda\,\boldsymbol{\delta\Gamma}^\Lambda_{sub}\,\boldsymbol{G}_\Lambda\,\boldsymbol{\delta\Gamma}^\Lambda_{sub}\\ &+ \ldots\,,\end{aligned} \tag{3.43}$$

where we have dropped the dependence on $\bar\varphi$ and φ to unclutter the notation. What we need is the lower (or upper) diagonal element of the (2×2) product matrices, as the trace in Eq. (3.42) just yields a factor of two. Defining

$$\dot G_\Lambda(K)=\frac{\delta(\Omega_K-\Lambda)}{G_0^{-1}(K)-\Sigma_\Lambda(K)}\,, \tag{3.44}$$

evaluating the matrix product in K-space and using the cyclic invariance of the trace we obtain

$$\begin{aligned}\partial_\Lambda\Gamma^\Lambda[\bar\varphi,\varphi] =& -\zeta\,\beta V\int_K\delta(\Omega_K-\Lambda)\,\ln\left(\frac{G_0^{-1}(K)-\Sigma_\Lambda(K)}{G_0^{-1}(K)}\right)\\
&+\zeta\int_K \dot G_\Lambda(K)\,(\boldsymbol{\delta\Gamma}^\Lambda_{sub})^{22}_{KK}\\
&+\zeta\int_K\int_{K'} \dot G_\Lambda(K)\,(\boldsymbol{\delta\Gamma}^\Lambda_{sub})^{22}_{KK'}\,G_\Lambda(K')\,(\boldsymbol{\delta\Gamma}^\Lambda_{sub})^{22}_{K'K}\\
&+\zeta\int_K\int_{K'} \dot G_\Lambda(K)\,(\boldsymbol{\delta\Gamma}^\Lambda_{sub})^{21}_{KK'}\,G_\Lambda(K')\,(\boldsymbol{\delta\Gamma}^\Lambda_{sub})^{12}_{K'K}\\
&+\zeta\int_K\int_{K'}\int_{K''} \dot G_\Lambda(K)\,(\boldsymbol{\delta\Gamma}^\Lambda_{sub})^{22}_{KK'}\,G_\Lambda(K')\,(\boldsymbol{\delta\Gamma}^\Lambda_{sub})^{22}_{K'K''}\,G_\Lambda(K'')\,(\boldsymbol{\delta\Gamma}^\Lambda_{sub})^{22}_{K''K}\\
&+\zeta\int_K\int_{K'}\int_{K''} \dot G_\Lambda(K)\,(\boldsymbol{\delta\Gamma}^\Lambda_{sub})^{12}_{KK'}\,G_\Lambda(K')\,(\boldsymbol{\delta\Gamma}^\Lambda_{sub})^{22}_{K'K''}\,G_\Lambda(K'')\,(\boldsymbol{\delta\Gamma}^\Lambda_{sub})^{21}_{K''K}\\
&+\zeta\int_K\int_{K'}\int_{K''} G_\Lambda(K)\,(\boldsymbol{\delta\Gamma}^\Lambda_{sub})^{12}_{KK'}\,\dot G_\Lambda(K')\,(\boldsymbol{\delta\Gamma}^\Lambda_{sub})^{22}_{K'K''}\,G_\Lambda(K'')\,(\boldsymbol{\delta\Gamma}^\Lambda_{sub})^{21}_{K''K}\\
&+\zeta\int_K\int_{K'}\int_{K''} G_\Lambda(K)\,(\boldsymbol{\delta\Gamma}^\Lambda_{sub})^{12}_{KK'}\,G_\Lambda(K')\,(\boldsymbol{\delta\Gamma}^\Lambda_{sub})^{22}_{K'K''}\,\dot G_\Lambda(K'')\,(\boldsymbol{\delta\Gamma}^\Lambda_{sub})^{21}_{K''K}\\
&+\ldots\,,\end{aligned} \tag{3.45}$$

where the $(\boldsymbol{\delta\Gamma}^{\Lambda}_{sub})^{ij}_{KK'}$ denote the matrix elements of $\boldsymbol{\delta\Gamma}^{\Lambda}_{sub}$, which are explicitly given by

$$(\boldsymbol{\delta\Gamma}^{\Lambda}_{sub})^{11}_{KK'} = \zeta \frac{\delta^2\Gamma^{\Lambda}}{\delta\bar{\varphi}_K \delta\varphi_{K'}} - \Sigma_{\Lambda}(K)\,\delta(K-K') \tag{3.46}$$

$$(\boldsymbol{\delta\Gamma}^{\Lambda}_{sub})^{12}_{KK'} = \zeta \frac{\delta^2\Gamma^{\Lambda}}{\delta\bar{\varphi}_K \delta\bar{\varphi}_{K'}} \tag{3.47}$$

$$(\boldsymbol{\delta\Gamma}^{\Lambda}_{sub})^{21}_{KK'} = \frac{\delta^2\Gamma^{\Lambda}}{\delta\varphi_K \delta\varphi_{K'}} \tag{3.48}$$

$$(\boldsymbol{\delta\Gamma}^{\Lambda}_{sub})^{22}_{KK'} = \frac{\delta^2\Gamma^{\Lambda}}{\delta\varphi_K \delta\bar{\varphi}_{K'}} - \Sigma_{\Lambda}(K)\,\delta(K-K')\,. \tag{3.49}$$

To derive the flow equations for the free energy, the two-, the four- and the six-point vertex we use the fact that according to Eq. (3.26)

$$\bar{\Gamma}^{(2n)}_{\Lambda}(K'_1,\ldots,K'_n;K_n,\ldots,K_1) = (-\zeta)^n \frac{\delta^{(2n)}\Gamma^{\Lambda}[\bar{\varphi},\varphi]}{\delta\bar{\varphi}_{K'_1}\cdots\delta\bar{\varphi}_{K'_n}\delta\varphi_{K_n}\cdots\delta\varphi_{K_1}}\Big|_{\bar{\varphi}=\varphi=0}\,. \tag{3.50}$$

In applying the functional derivatives to both sides of Eq. (3.45), we have to use the product rule defined on a Grassman algebra, see Eq. (2.11), and we thoroughly have to keep track of all minus signs and ζ-factors. The derivation of the flow equations for the free energy, the two- and the four-point vertex is straightforward. For the six-point vertex we show in appendix A how the corresponding flow equation may be obtained from Eq. (3.45) in a rather elegant way. Here we will only display the results.
At this stage of the calculation we see the reason why it is advantageous to introduce the subtracted functional $\boldsymbol{\delta\Gamma}^{\Lambda}_{sub}[\bar{\varphi},\varphi]$: The property (3.32) guarantees that for each vertex function only a finite number of terms in the expansion Eq. (3.43) contributes.

Free energy:

The flow of the free energy is best obtained directly from Eq. (3.42) by setting $\bar{\varphi}=\varphi=0$ and using Eq. (3.32). This immediately yields

$$\boxed{\partial_{\Lambda}\Gamma^{(0)}_{\Lambda} = -\zeta\,\beta V \int_K \delta(\Omega_K-\Lambda)\,\ln\left(\frac{G_0^{-1}(K)-\Sigma_{\Lambda}(K)}{G_0^{-1}(K)}\right)\,.} \tag{3.51}$$

Two-point vertex:

Here the flow stems solely from the second term of Eq. (3.45) and is given by

$$\boxed{\partial_\Lambda \Gamma^{(2)}_\Lambda(K;K) = -\,\zeta \int_{K'} \dot{G}_\Lambda(K')\,\Gamma^{(4)}_\Lambda(K,K';K',K)\ .} \tag{3.52}$$

For a graphical representation of the flow equations we define the graphical $(2n)$-point vertex as follows:

$\Gamma^{(2n)}_\Lambda(K'_1,\ldots,K'_n;K_n,\ldots,K_1) \equiv$

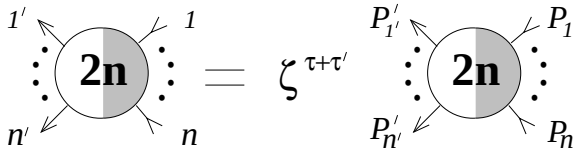

Here i and i' are short-hand for the outer labels K_i and K'_i, whereas P_i and $P'_{i'}$ are their images under arbitrary permutations P and P' acting on the n-tuples $(1,\ldots,n)$ and $(1',\ldots,n')$, respectively. Furthermore, τ and τ' are the smallest number of transpositions that generate P and P'. Thus, the exchange of any two legs on the plain or on the shaded half of the vertex yields a factor of ζ. A graphical representation of Eq. (3.52) is given in Fig. (3.2).

Four-point vertex:

Here the second, third and fourth term of Eq. (3.45) contribute and all higher orders vanish,

$$\begin{aligned}
\boxed{\partial_\Lambda \Gamma^{(4)}_\Lambda(K'_1,K'_2;K_2,K_1) &= -\,\zeta \int_K \dot{G}_\Lambda(K)\,\Gamma^{(6)}_\Lambda(K'_1,K'_2,K;K,K_2,K_1)} \\
&+ \int_K \Big[\dot{G}_\Lambda(K) G_\Lambda(K') \\
&\qquad \times \Gamma^{(4)}_\Lambda(K'_1,K'_2;K',K)\,\Gamma^{(4)}_\Lambda(K,K';K_2,K_1)\Big]_{K'=K_1+K_2-K} \\
&+ \zeta \int_K \Big[\big(\dot{G}_\Lambda(K)G_\Lambda(K') + G_\Lambda(K)\dot{G}_\Lambda(K')\big) \\
&\qquad \times \Gamma^{(4)}_\Lambda(K'_1,K';K,K_1)\,\Gamma^{(4)}_\Lambda(K'_2,K;K',K_2)\Big]_{K'=K+K_1-K'_1} \\
&+ \int_K \Big[\big(\dot{G}_\Lambda(K)G_\Lambda(K') + G_\Lambda(K)\dot{G}_\Lambda(K')\big) \\
&\qquad \times \Gamma^{(4)}_\Lambda(K'_2,K';K,K_1)\,\Gamma^{(4)}_\Lambda(K'_1,K;K',K_2)\Big]_{K'=K+K_1-K'_2}\ .
\end{aligned} \tag{3.53}$$

It is easy to check that this equation is manifestly anti-symmetric (symmetric for bosons) under the exchange of arguments within the two sets of variables, i.e. the primed and the unprimed set. The contribution of the second term is usually referred to as the BCS channel, the third term represents the zero-sound (ZS) contribution and the fourth term is called the Peierls or ZS' channel. The graphical representation of this equation is given in Fig. 3.3.

Six-point vertex:

In this case all displayed terms of Eq. (3.45) contribute and all higher orders vanish,

$$
\begin{aligned}
&\partial_\Lambda \Gamma^{(6)}_\Lambda(K_1', K_2', K_3'; K_3, K_2, K_1) = \\
&\quad -\zeta \int_K \dot{G}_\Lambda(K)\, \Gamma^{(8)}_\Lambda(K_1', K_2', K_3', K; K, K_3, K_2, K_1) \\
&\quad +3\, \mathcal{A}_{3,(2,1)} \int_K \Big[\dot{G}_\Lambda(K) G_\Lambda(K') \\
&\qquad \times \Gamma^{(6)}_\Lambda(K_1', K_2', K_3'; K_3, K', K)\, \Gamma^{(4)}_\Lambda(K, K'; K_2, K_1) \Big]_{K'=K_1+K_2-K} \\
&\quad +3\, \mathcal{A}_{(1',2'),3'} \int_K \Big[\dot{G}_\Lambda(K) G_\Lambda(K') \\
&\qquad \times \Gamma^{(4)}_\Lambda(K_1', K_2'; K', K)\, \Gamma^{(6)}_\Lambda(K, K', K_3'; K_3, K_2, K_1) \Big]_{K'=K_1'+K_2'-K} \\
&\quad +9\, \zeta\, \mathcal{A}_{(1',2'),3'} \mathcal{A}_{3,(2,1)} \int_K \Big[\Big(\dot{G}_\Lambda(K) G_\Lambda(K') + G_\Lambda(K) \dot{G}_\Lambda(K') \Big) \\
&\qquad \times \Gamma^{(4)}_\Lambda(K_3', K'; K, K_3)\, \Gamma^{(6)}_\Lambda(K_1', K_2', K; K', K_2, K_1) \Big]_{K'=K_3-K_3'+K} \\
&\quad -9\, \mathcal{A}_{(1',2'),3'} \mathcal{A}_{3,(2,1)} \int_K \Big[\Big(\dot{G}_\Lambda(K) G_\Lambda(K') G_\Lambda(K'') \\
&\qquad\quad + G_\Lambda(K) \dot{G}_\Lambda(K') G_\Lambda(K'') + G_\Lambda(K) G_\Lambda(K') \dot{G}_\Lambda(K'') \Big) \\
&\qquad\quad \times \Gamma^{(4)}_\Lambda(K_1', K_2'; K, K') \\
&\qquad\quad \times \Gamma^{(4)}_\Lambda(K_3', K'; K'', K_3)\, \Gamma^{(4)}_\Lambda(K'', K; K_2, K_1) \Big]^{K'=K_1'+K_2'-K}_{K''=K_1+K_2-K} \\
&\quad -36\, \zeta\, \mathcal{A}_{1',2',3'}\, \mathcal{A}_{3,2,1} \int_K \Big[\dot{G}_\Lambda(K) G_\Lambda(K') G_\Lambda(K'') \\
&\qquad\quad \times \Gamma^{(4)}_\Lambda(K_3', K; K'', K_3) \\
&\qquad\quad \times \Gamma^{(4)}_\Lambda(K_2', K''; K', K_2)\, \Gamma^{(4)}_\Lambda(K_1', K'; K, K_1) \Big]^{K'=K_1-K_1'+K}_{K''=K_3'-K_3+K} .
\end{aligned}
\tag{3.54}
$$

The (anti-)symmetrization operators $\mathcal{A}_{(\ldots)}$ are defined by the requirement that

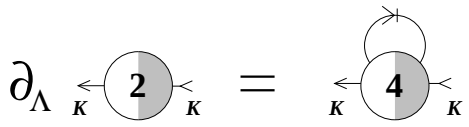

Figure 3.2: Graphical representation of the flow equation for the two-point vertex, Eq. (3.52). The solid directed line with a slash symbolizes the propagator $\dot{G}_\Lambda$ defined in Eq. (3.44).

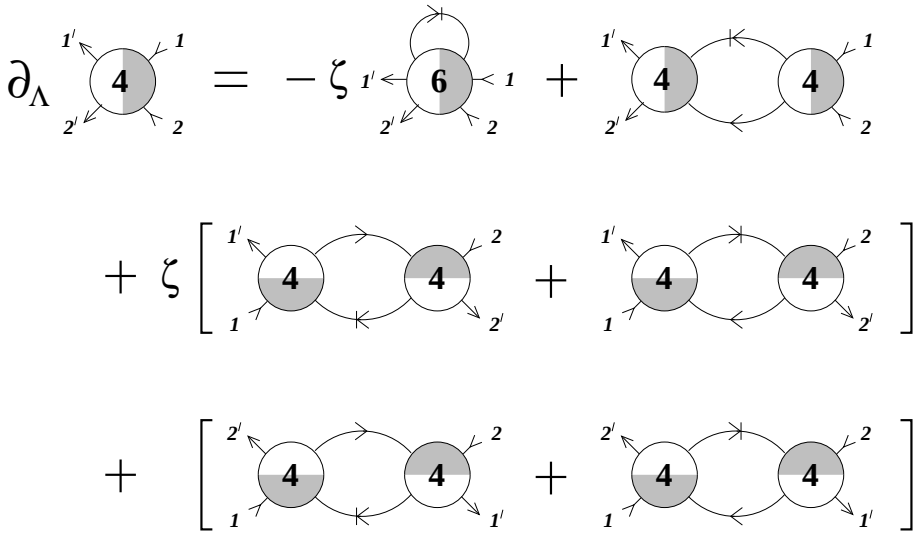

Figure 3.3: Graphical representation of the flow equation for the four-point vertex, Eq. (3.53). Again, solid lines with a slash are symbolic for $\dot{G}_\Lambda$, whereas a pure directed line represents the full cutoff-dependent propagator G_Λ given in Eq. (3.29). Note that due to our definition of the graphical vertices the correct labeling of the external legs is important. Our choice is in agreement with the flow equation (3.53).

the r.h.s. of Eq. (3.54) has to be antisymmetric with respect to the exchange of any two labels within the primed or the unprimed variable set. As every single term corresponds to a topologically different Feynman diagram this can only be true if each term itself is antisymmetric. Explicitly, we have defined for an arbitrary function $f(1,2,3)$

$$\begin{aligned}\mathcal{A}_{1,2,3} f(1,2,3) &= \frac{1}{6}\big[f(1,2,3) + f(2,3,1) + f(3,1,2) \\ &+ \zeta\, f(2,1,3) + \zeta\, f(1,3,2) + \zeta\, f(3,2,1)\big]\,. \end{aligned} \tag{3.55}$$

In case that f is already antisymmetric with respect to the first two arguments 1 and 2, the function

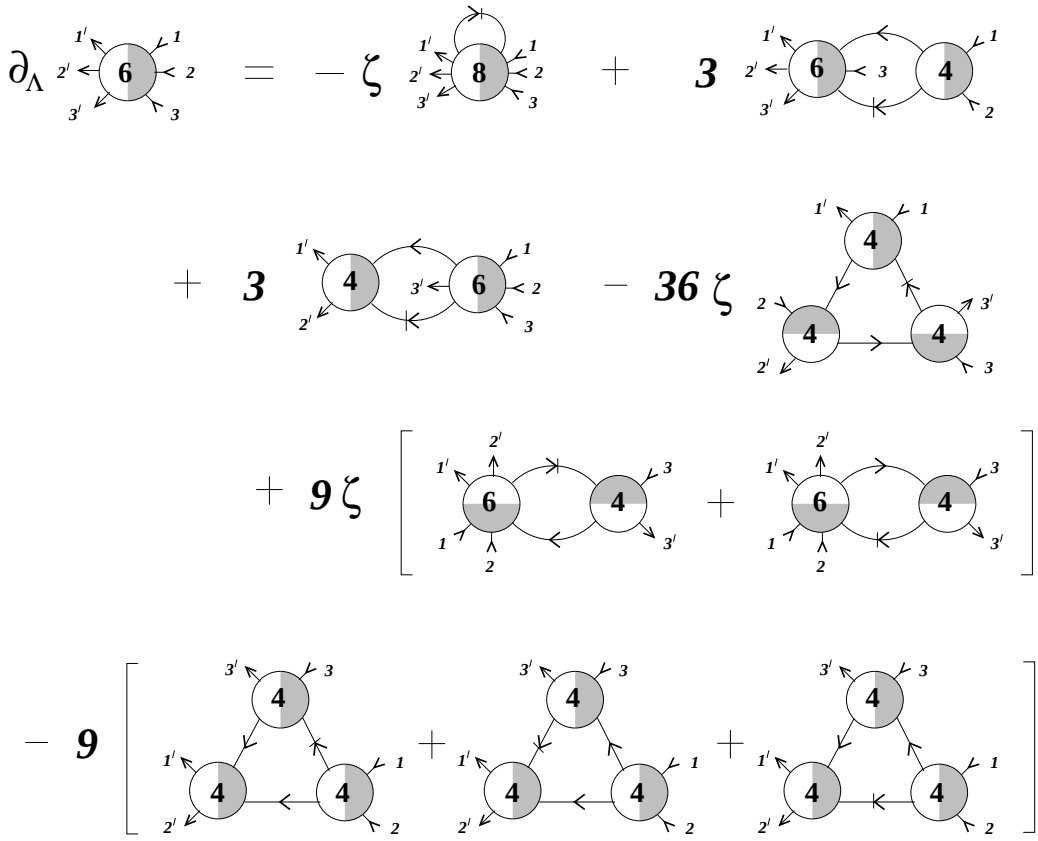

Figure 3.4: Graphical representation of the flow equation for the six-point vertex, Eq. (3.54). Again, the labeling of the external legs correctly reproduces the flow equation (3.54). For convenience we dropped the antisymmetrization operators $\mathcal{A}_{(\ldots)}$; it is understood that graphs with combinatorial prefactors larger than one have to be antisymmetrized with respect to the primed and the unprimed variable set.

$$\mathcal{A}_{(1,2),3} f(1,2,3) = \frac{1}{3}\big[f(1,2,3) + \zeta\, f(1,3,2) + \zeta\, f(3,2,1)\big] \tag{3.56}$$

is totally antisymmetric. Finally

$$\mathcal{A}_{3,(2,1)} f(3,2,1) = \frac{1}{3}\big[f(3,2,1) + \zeta\, f(2,3,1) + \zeta\, f(1,2,3)\big]\,, \tag{3.57}$$

yields a totally antisymmetric function in case that f is already antisymmetric with respect to the last two arguments 2 and 1. Of course, Eqs. (3.56) and (3.57) may be combined into a single equation, but we find it clearer to give the definitions seperately in the form they appear in Eq. (3.54). For a better

understanding of Eq. (3.54) see also appendix A .
Below Eq. (3.35) we have already emphazised the formal equivalence of the flow equation for the generating functional $\Gamma^\Lambda[\bar{\varphi}, \varphi]$ to its counterpart in ϕ^4 theory. Of course this analogy should also be reflected in the flow equations. Let us take for instance take the flow of the six-point vertex. If we remove all the arrows from the propagators and external legs in Fig. 3.4 we are left with three kinds of topologically different diagrams: One diagram involving the eight-point vertex, 15 diagrams composed of one four- and one six-point vertex and 45 diagrams made up of three four-point vertices. These are indeed the diagrams that also appear in ϕ^4 theory, with the same factorials (see Ref. [46]).

Chapter 4

Inclusion of the Rescaling Step

In this section we derive the flow equations including the rescaling of frequencies, momenta and the fermionic fields. For a proper description of the fixed-point properties of the model beyond the one-loop approximation it will be necessary to take the possibility of a reduced or even vanishing quasi-particle weight into account. An appropriately defined rescaling factor has to be included in the field rescaling for the vertex functions to approach finite fixed-point expressions. We discuss two decompositions of the momenta in **k***-space that allow for a scaling towards the true FS of the interacting system.*

4.1 Scaling Variables

In the following we shall restrict our considerations to fermions[1] for which the rescaling step of the RG involves conceptional difficulties. This is due to the fact that the mode elimination has to be stopped at the true interacting FS, which is not known at the beginning. For rotationally invariant systems with a spherical FS this problem does not arise, as by Luttinger's theorem [75] we know that at fixed density the volume enclosed by the FS is invariant, implying that $k_F = |\mathbf{k}_F|$ is left unchanged by interactions. However, in general the shape of the FS will change. Expressed in terms of RG language this implies that the mode elimination leads to a deformation of the FS. When all degrees of freedom are integrated out we expect the FS to assume the shape of a $D-1$ dimensional fixed-point manifold in $\mathbf{k}$-space, which corresponds to the true interacting FS provided the RG has been set up appropriately. In the next section, where we define the relevant and marginal couplings for interacting fermions, we will present an

[1] We hence explicitly set $\zeta = -1$ from now on.

explicit construction that allows for a self-consistent calculation of the FS by imposing a fixed-point condition on the chemical-potential parameter of the RG. Here let us just assume that the true FS is fully determined by the bare energy dispersion, the chemical potential and the exact self-energy of the interacting system, which is equivalent to the self-energy Σ_Λ at the fixed point. For a proper scaling towards the true FS we decompose all momenta $\mathbf{k} = \mathbf{n}\, k$, where $\mathbf{n} = \mathbf{k}/k$ is a unit vector in the direction of $\mathbf{k}$ and $k = |\mathbf{k}|$, in a component $\mathbf{k}_F(\mathbf{n})$ located on the FS and a second component $\mathbf{p}(\mathbf{n})$ such that $\mathbf{k} = \mathbf{k}_F(\mathbf{n}) + \mathbf{p}(\mathbf{n})$. The construction must be chosen such that the decomposition is unique for each $\mathbf{k}$. Of course various choices for $\mathbf{k}_F(\mathbf{n})$ and $\mathbf{p}(\mathbf{n})$ are possible depending on the actual form of the FS. We will discuss two constructions, the one given in Ref. [89] and a second one which turns out to be simpler in many cases of interest. First let us define the true FS by the set of momenta satisfying the equation [75]

$$\epsilon_{\mathbf{k}_F} = \mu - \Sigma(\mathbf{k}_F, 0)\,, \tag{4.1}$$

where μ is the chemical potential and Σ the 1PI self-energy of the interacting system. Note that μ is an adjustable parameter being independent of the direction $\hat{\mathbf{k}}_F$ of $\mathbf{k}_F$. On the other hand the counter-term $\Sigma(\mathbf{k}_F, 0)$ will in general depend on $\hat{\mathbf{k}}_F$. We define the local Fermi velocity by

$$\mathbf{v}_F = \boldsymbol{\nabla}_{\mathbf{k}} \epsilon_{\mathbf{k}}|_{\mathbf{k}=\mathbf{k}_F}\,. \tag{4.2}$$

According to this definition $\mathbf{v}_F$ is defined as the gradient of the *bare* energy-dispersion $\epsilon_{\mathbf{k}}$ evaluated at the *interacting* FS. In the following we will suppress the dependence of $\mathbf{v}_F$ and $\mathbf{k}_F$ on the direction $\mathbf{n}$ of $\mathbf{k}$ in our notations. As a next step we expand the excitation energy for each given $\mathbf{k}$ with respect to the corresponding $\mathbf{k}_F$, i.e.

$$\xi(\mathbf{k}) = \epsilon_{\mathbf{k}} - \epsilon_{\mathbf{k}_F} = \mathbf{v}_F \cdot (\mathbf{k} - \mathbf{k}_F) + \frac{(\mathbf{k} - \mathbf{k}_F)^2}{2m} + \cdots\,, \tag{4.3}$$

where m is the bare mass of the model in the sense that it is not renormalized by interactions, while it may differ from the mass of free fermions due to some kind of band structure. The two decompositions of $\mathbf{k}$ we are going to discuss are

$$\boldsymbol{a)} \quad \mathbf{k} = \mathbf{k}_F + \hat{\mathbf{v}}_F p\,, \tag{4.4}$$

$$\boldsymbol{b)} \quad \mathbf{k} = \mathbf{n}(k_F + p)\,, \tag{4.5}$$

with $\hat{\mathbf{v}}_F = \mathbf{v}_F/|\mathbf{v}_F|$ and $\mathbf{v}_F$ given by Eq. (4.2). Let us start with the decomposition (4.4) used in Ref. [89], where we introduced dimensionless scaling variables according to[2]

[2]Note that we have changed our notations. The infrared cutoff ξ in Ref. [89] is now denoted by Λ while the logarithmic flow parameter t corresponds to l.

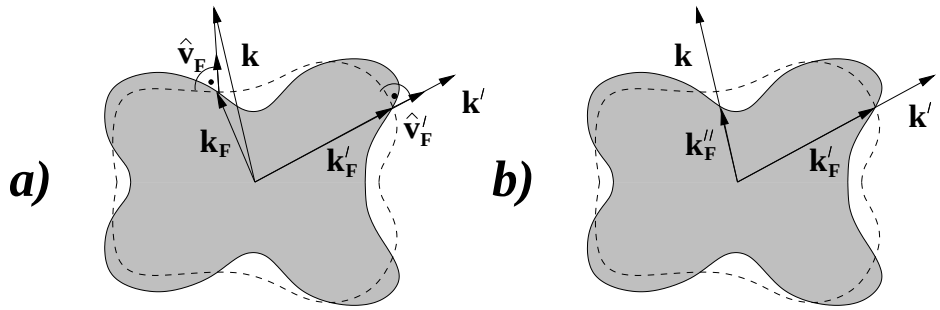

Figure 4.1: Illustration of the decompositions of $\mathbf{k}$ according to Eqs. (4.4) and (4.5) for some kind of irregular shaped FS in $D = 2$ and for two different points $\mathbf{k}$ and $\mathbf{k}'$. The gray-shaded region corresponds to the interacting Fermi-sea with its boundary line being the interacting FS. The dashed line shows the non-interacting FS corresponding to the same particle density. **a**) Decomposition of $\mathbf{k}$ according to Eq. (4.4). Note that $\hat{\mathbf{v}}_F$ is perpendicular to the *non*-interacting FS at the interacting $\mathbf{k}_F$. **b**) Decomposition of $\mathbf{k}$ according to Eq. (4.5), being unique for any starlike Fermi-sea region. For the point $\mathbf{k}'$ we have $\hat{\mathbf{v}}_F = \mathbf{n}$ and the two constructions coincide.

$$q = \frac{v_F p}{\Lambda} = \frac{\mathbf{v}_F \cdot (\mathbf{k} - \mathbf{k}_F)}{\Lambda}\,, \quad \epsilon = \frac{\omega}{\Lambda}\,, \tag{4.6}$$

where v_F is the absolute value of $\mathbf{v}_F$. The dimensionless dispersion obtained from Eq. (4.3) is then given by

$$\xi_l(q) = \frac{\xi(\mathbf{k})}{\Lambda} = q + \frac{c_l^\mathbf{n}}{2} q^2 + \mathcal{O}(q^3)\,, \tag{4.7}$$

with

$$c_l^\mathbf{n} = \frac{\Lambda}{m v_F^2} = \frac{\Lambda_0}{m v_F^2}\, e^{-l}\,. \tag{4.8}$$

The problem with this construction is that to determine the vector $\mathbf{v}_F$ we need to fix D initially unknown quantities, namely the D components of $\mathbf{k}_F$ yielding $\mathbf{v}_F$ via Eq. (4.2). The Jacobian associated with the variable transformation $q \leftrightarrow \mathbf{k}$ will in general, i.e. for non-spherical Fermi surfaces, be rather complicated. Furthermore we cannot give a general statement for which kind of Fermi surfaces this construction is useful: The decomposition is only unique when $|\mathbf{k} - \mathbf{k}_F|$ does not exceed a limiting value that is determined by the point of maximum curvature of the non-interacting FS at the interacting FS, see also Fig. 4.1. The reason why we originally used this construction is the property (4.7) insuring that points with equal q correspond to leading order to excitations with the same excitation energy $\xi(\mathbf{k}) \approx q\,\Lambda$. Furthermore, if the non-interacting FS is only slightly altered by the interactions, $\hat{\mathbf{v}}_F$ will approximately be perpendicular to the interacting FS. However, in general this is not the case as indicated in Fig. 4.1 **a**).

Let us now turn our attention to the second decomposition given by Eq. (4.5). The property that equal values of q lead to the same excitation-energy is particularly important if the flow of Λ will be stopped at a finite scale $\Lambda^\star > 0$, a feature we would like to retain. This is indeed easily implemented by defining the scaling variable q slightly different from Eq. (4.6),

$$q = \frac{v_\parallel^{\mathbf{n}}\, p}{\Lambda} = \frac{\mathbf{v}_F \cdot (\mathbf{k} - \mathbf{k}_F)}{\Lambda}\,, \quad \epsilon = \frac{\omega}{\Lambda}\,, \tag{4.9}$$

with

$$v_\parallel^{\mathbf{n}} = \mathbf{v}_F \cdot \mathbf{n} \tag{4.10}$$

being the component of $\mathbf{v}_F$ parallel to $\mathbf{k}$. It is straightforward to show that in this case expression (4.7) remains valid but with $c_l^{\mathbf{n}}$ now given by

$$c_l^{\mathbf{n}} = \frac{\Lambda}{2m(v_\parallel^{\mathbf{n}})^2} = \frac{\Lambda_0}{2m(v_\parallel^{\mathbf{n}})^2} e^{-l}\,. \tag{4.11}$$

This construction has various advantages. First of all we can immediately state for which kind of physical systems our decomposition is unique. This is the case whenever the region occupied by the interacting Fermi sea is *starlike* with respect to the origin.[3] To determine the decomposition (4.5) for a given $\mathbf{k}$ we only need to find one initially unknown quantity instead of D, namely the magnitude of $\mathbf{k}_F$. Furthermore, the dimensionless Jacobian introduced in Eq. (3.7) of Ref. [89] may now be chosen to be that of spherical coordinates with an $\mathbf{n}$-dependent radial coordinate for any starlike Fermi-sea region. If we define

$$\int_Q = \sum_\sigma \int_{-\infty}^{\infty} \frac{d\epsilon}{2\pi} \int \frac{d\Omega_{\mathbf{n}}}{\Omega_D} \int_{-v_\parallel^{\mathbf{n}} k_F/\Lambda}^{\infty} dq \left(1 + \frac{q\,\Lambda}{v_\parallel^{\mathbf{n}} k_F}\right)^{D-1}\,, \tag{4.12}$$

where $d\Omega_{\mathbf{n}}$ is a surface element and Ω_D is the surface area of the D-dimensional unit sphere, it is easy to show that the K-integration introduced in Eq. (3.37) may be written as

$$\int_K = \int_Q \Lambda^2\, \nu_0^{\mathbf{n}}\,. \tag{4.13}$$

Here we have defined

[3] A region $\mathcal{V}$ is called starlike with respect to a point $p \in \mathcal{V}$ if for any other point $p' \in \mathcal{V}$ the straight line from p to p' completely lies within $\mathcal{V}$.

$$\nu_0^{\mathbf{n}} = \frac{\Omega_D}{(2\pi)^D} \frac{k_F^{D-1}}{v_\parallel^{\mathbf{n}}} \,. \tag{4.14}$$

Note that $\nu_0^{\mathbf{n}}$ corresponds to the density of states at the FS of a system with a spherical FS of radius $k_F = k_F(\mathbf{n})$ and reduced Fermi-velocity $v_\parallel^{\mathbf{n}} = \mathbf{v}_F \cdot \mathbf{n}$. Note further that the angular and the q-integration in Eq. (4.12) must not be interchanged as k_F and $v_\parallel^{\mathbf{n}}$ in the integration boundary depend on $\mathbf{n}$. In Eq. (4.12) we have introduced a dimensionless composite variable Q defined by

$$Q = (\sigma, \mathbf{n}, q, i\epsilon) = (\sigma, \mathbf{v}_F \cdot (\mathbf{k} - \mathbf{k}_F)/\Lambda, i\omega/\Lambda) \,. \tag{4.15}$$

For notational convenience we will denote the connection between K and Q rather sloppily by $K = \Lambda\, Q$ or $Q = K/\Lambda$. This has of course to be understood in the sense given by Eq. (4.15).

4.2 Scaling Form of the Irreducible Vertices

To ensure that our RG transformation will satisfy a fixed-point condition we do not only have to rescale momenta and frequencies according to Eq. (4.9) , but we have to rescale the fermionic fields as well. The correct field rescaling is obtained from the requirement that the bare part of the action $S_0^{\Lambda_0}[\bar{\psi}, \psi]$ has to retain its form after integrating out fields with K satisfying $\Lambda < \Omega_K < \Lambda_0$ and subsequent rescaling of momenta and frequencies. However, we must be aware of the fact that in general the propagator will pick up a multiplicative factor due to a reduced or even vanishing quasi-particle weight when degrees of freedom are eliminated. Without the field rescaling the irreducible vertex functions will in general fail to approach fixed-point values in the limit $\Lambda \to 0$, see Ref. [65]. Defining a scale-dependent quasi-particle weight in the usual way by

$$Z_l^{\mathbf{n}} = \frac{1}{1 - \partial_{i\omega} \Sigma_\Lambda(\mathbf{k}_F, i\omega)|_{\omega=0}} \,, \tag{4.16}$$

the correct field rescaling is given by

$$\varphi_K = \left(\frac{Z_l^{\mathbf{n}}}{\Lambda^3 \nu_0^{\mathbf{n}}} \right)^{\frac{1}{2}} \varphi'_Q \,, \tag{4.17}$$

Here φ'_Q are the new fields as functions of the dimensionless scaling variables Q. Of course, this choice is not unique and depends explicitly on our decomposition of $\mathbf{k}$, Eq. (4.5). However, the explicit dependence on the logarithmic flow-parameter l is determined by the fixed-point condition.

Using Eqs. (4.9), (4.13) and (4.17) we may now introduce the rescaled and dimensionless vertex functions which we denote by $\tilde{\Gamma}_l^{(2n)}(Q'_1,\ldots,Q'_n;Q_n,\ldots,Q_1)$. Let us develop the relation between these vertices and the physical vertex functions $\Gamma_\Lambda^{(2n)}$, starting with the

Free energy:

Due to the field rescaling the free energy picks up an additive term. This is best understood by using the functional integral representation of the partition functional given in Eq. (2.14) together with the definition of $\mathcal{G}_c^\Lambda$. Noting that the fields ψ must scale in the same way as the fields φ the integration measure of the partition functional $\mathcal{Z}^\Lambda$ changes according to

$$\mathcal{D}[\bar{\psi},\psi] = \prod_{\tilde{\Omega}_Q<1} \Big(\frac{Z_l^{\mathbf{n}}}{\Lambda^3 \nu_0^{\mathbf{n}}}\Big)^{-1} \mathcal{D}[\bar{\psi}',\psi']\,, \tag{4.18}$$

where

$$\tilde{\Omega}_Q = \frac{\Omega_K}{\Lambda}\,, \tag{4.19}$$

Note that for variable transformations of Grassman numbers the inverse Jacobian appears on the r.h.s. of Eq. (4.18). For the free partition functional $\mathcal{Z}_0^\Lambda$ in the expression for $\mathcal{G}_c^\Lambda$ the integration measure transforms similarly to Eq. (4.18) but without the factor $Z_l^{\mathbf{n}}$ as here no interactions are involved. Putting both together and following the way from $\mathcal{Z}^\Lambda$ via $\mathcal{G}_c^\Lambda$ to Γ^Λ we obtain in the thermodynamic limit

$$\tilde{\Gamma}_l^{(0)} = \Gamma_\Lambda^{(0)} + \beta V \int_K \Theta(\Lambda-\Omega_K)\ln Z_l^{\mathbf{n}}\,. \tag{4.20}$$

Here Θ is the usual Heavyside function related to our previous definition in Eq. (3.4) by $\Theta(x)\equiv\Theta(0<x<\infty)$.

Two-point vertex:

The scaling of the exact Green function may directly be obtained by dimensional analysis including the $Z_l^{\mathbf{n}}$-factor,

$$\tilde{G}_l(Q) = \frac{\Lambda}{Z_l^{\mathbf{n}}} G_\Lambda\big(\sigma, \mathbf{n}(k_F + \tfrac{\Lambda}{v_\parallel^{\mathbf{n}}} q), i\Lambda\epsilon\big)\,. \tag{4.21}$$

It is now useful to state a more explicit form of the inverse Green function which follows from Eqs. (3.29) and (4.1). To this end we define the inverse rescaled propagator by

$$\tilde{r}_l(Q) = \frac{Z_l^{\mathbf{n}}}{\Lambda}[i\omega - \epsilon_{\mathbf{k}} + \mu - \Sigma_\Lambda(\mathbf{k}, i\omega)] \tag{4.22}$$

$$= Z_l^{\mathbf{n}}[i\epsilon - \xi_l(q)] + \tilde{\Gamma}_l^{(2)}(Q)\,, \tag{4.23}$$

with

$$\boxed{\tilde{\Gamma}_l^{(2)}(Q) = \tfrac{Z_l^{\mathbf{n}}}{\Lambda}\Gamma_\Lambda^{(2)}(K) = -\tfrac{Z_l^{\mathbf{n}}}{\Lambda}[\Sigma_\Lambda(K) - \Sigma(\mathbf{k}_F, 0)]\,.} \tag{4.24}$$

The argument K on the r.h.s. of this and the above equation has to be understood as a function of Q, namely $K = (\sigma, \mathbf{n}(k_F + q\Lambda/v_\parallel^{\mathbf{n}}), i\Lambda\epsilon)$. We also define the rescaled inverse free propagator by

$$\tilde{r}_l^0(Q) = i\epsilon - \xi_l(q) = G_0^{-1}(K)/\Lambda\,. \tag{4.25}$$

Note that $\tilde{r}_l^0$ explicitly depends on the logarithmic flow-parameter l while G_0 does not. The rescaled Green function may now be written as

$$\tilde{G}_l(Q) = \frac{\Theta(1 < \tilde{\Omega}_Q < e^l)}{\tilde{r}_l(Q)}\,. \tag{4.26}$$

Finally let us define

$$\dot{G}_l(Q) = \frac{\delta(\tilde{\Omega}_Q - 1)}{\tilde{r}_l(Q)} = \Lambda^2 (Z_l^{\mathbf{n}})^{-1} \dot{G}_\Lambda(K)\,, \tag{4.27}$$

where the second equality follows from Eq. (3.44).

Higher-order vertices ($\mathbf{n \geq 2}$):

The scaling equations for the higher-order irreducible vertices may be obtained recursively from the flow equations by using the fact that for all n $\tilde{\Gamma}_l^{(2n)}$ depends on $\tilde{\Gamma}_l^{(2n+2)}$ via the second term of the expansion (3.45). Explicitly

$$\partial_\Lambda \Gamma_\Lambda^{(2n)}(K_1', \ldots, K_n'; K_n, \ldots, K_1) = \int_K \dot{G}_\Lambda(K)\, \Gamma_\Lambda^{(2n+2)}(K_1', \ldots, K_{n+1}'; K_{n+1}, \ldots, K_1) \pm \ldots\,, \tag{4.28}$$

while all other terms of the expansion exclusively depend on vertices $\Gamma_\Lambda^{(2m)}$ with $m \leq n$. The scaling of the two-point vertex, Eq. (4.24), together with Eq. (4.12) and $\Lambda\partial_\Lambda = -\partial_l$ can now be used to transform the flow equation for the two-point

vertex into its dimensionless equivalent. From the first term on the r.h.s. of Eq. (4.28) (for $n = 1$) we may then read off the scaling of the dimensionless four-point vertex. In the same way we proceed from $2n$ to $2(n+1)$. It is then straightforward to show by induction that the scaling of the higher-order vertices is given by

$$\begin{aligned}\tilde{\Gamma}_l^{(2n)}(Q_1', \ldots, Q_n'; Q_n, \ldots, Q_1) &= \Big(\prod_{i=2}^{n} \nu_0^{\mathbf{n}_i'} \nu_0^{\mathbf{n}_i}\Big)^{\frac{1}{2}} \Big(\prod_{i=1}^{n} Z_l^{\mathbf{n}_i'} Z_l^{\mathbf{n}_i}\Big)^{\frac{1}{2}} \Lambda^{n-2} \\ &\times \Gamma_\Lambda^{(2n)}(K_1', \ldots, K_n'; K_n, \ldots, K_1)\,.\end{aligned} \tag{4.29}$$

Note that the index i for the first product only starts at $i = 2$. For a spherical FS $\nu_0^{\mathbf{n}} = \nu_0$ is independent of $\mathbf{n}$ and the first factor on the r.h.s. then simply yields ν_0^{n-1}, reproducing the scaling equations (3.21) of Ref. [89]. In this special case the two decompositions of $\mathbf{k}$ given in Eqs. (4.4) and (4.5) coincide.

4.3 Flow Equations for the Rescaled Vertices

Given the above relations between the vertices $\Gamma_\Lambda^{(2n)}$ and their corresponding scaling functions $\tilde{\Gamma}_l^{(2n)}$ it is now easy to derive the flow equations in their rescaled form.

Free energy:

Let us define the interaction correction to the free energy per Fourier component by

$$f_l = \tilde{\Gamma}_l^{(0)}/N_l\,, \tag{4.30}$$

where N_l is the number of Fourier components contained in a shell corresponding to excitations with excitation energies smaller than Λ, i.e.

$$N_l = \beta V \int_K \Theta(\Lambda - \Omega_K)\,. \tag{4.31}$$

In this way we get rid of unphysical infinities in the expression for $\tilde{\Gamma}_l^{(0)}$ related to the factor βV in the thermodynamic limit. The flow equation for f_l is now obtained from Eqs. (3.51) and (4.20),

$$\boxed{\partial_l f_l = n_l\, f_l + \dot{\Gamma}_l^{(0)}\,,} \tag{4.32}$$

with the inhomogeneity given by

$$\dot{\Gamma}_l^{(0)} = -\frac{\int_Q \Theta(1-\tilde{\Omega}_l)\,\nu_0^{\mathbf{n}}\eta_l^{\mathbf{n}}}{\int_Q \Theta(1-\tilde{\Omega}_l)\,\nu_0^{\mathbf{n}}} - \frac{\int_Q \delta(1-\tilde{\Omega}_l)\,\nu_0^{\mathbf{n}} \ln\left(\frac{\tilde{r}_l(Q)}{\tilde{r}_l^0(Q)}\right)}{\int_Q \Theta(1-\tilde{\Omega}_l)\,\nu_0^{\mathbf{n}}}\,, \tag{4.33}$$

and where

$$n_l = -\frac{\partial_l N_l}{N_l} = -\partial_l \ln N_l \tag{4.34}$$

is the relative change of the number of Fourier components when the cutoff is reduced. Furthermore

$$\eta_l^{\mathbf{n}} = -\frac{\partial_l Z_l^{\mathbf{n}}}{Z_l^{\mathbf{n}}} = -\partial_l \ln Z_l^{\mathbf{n}} \tag{4.35}$$

is the relative change of the quasi-particle weight, i.e. the anomalous dimension associated with the direction $\mathbf{n}$.
If we choose $\Omega_K = |\mathbf{v}_F \cdot (\mathbf{k} - \mathbf{k}_F)|$, which implies $\tilde{\Omega}_Q = |q|$, the q-integration in Eq. (4.33) may be performed trivially. However, the resulting equation does not simplify very much, but it is worth to give the explicit expression for n_l for this choice,

$$\begin{aligned} n_l &= \frac{\int_Q \delta(1-|q|)\,\nu_0^{\mathbf{n}}}{\int_Q \Theta(1-|q|)\,\nu_0^{\mathbf{n}}} \\ &= \frac{\int d\Omega_{\mathbf{n}}\,\nu_0^{\mathbf{n}}\left[(1+\frac{\Lambda}{v_\parallel^{\mathbf{n}}k_F})^{D-1} + (1-\frac{\Lambda}{v_\parallel^{\mathbf{n}}k_F})^{D-1}\right]}{\int d\Omega_{\mathbf{n}}\,\nu_0^{\mathbf{n}}\,\frac{v_\parallel^{\mathbf{n}}k_F}{D\Lambda}\left[(1+\frac{\Lambda}{v_\parallel^{\mathbf{n}}k_F})^{D} - (1-\frac{\Lambda}{v_\parallel^{\mathbf{n}}k_F})^{D}\right]}\,. \end{aligned} \tag{4.36}$$

From Eq. (4.36) it is now easy to show that

$$\lim_{l\to\infty} n_l = 1\,. \tag{4.37}$$

This property means that f_l is a relevant parameter of the RG with asymptotic scaling-dimension $+1$. Consequently for f_l to reach a finite fixed-point value in the limit $l \to \infty$, the initial value $f_{l=0}$ has to be fine-tuned. This is best seen if we switch to the integral representation of f_l obtained from the flow equation (4.32),

$$\boxed{f_l = \left[f_0 + \int_0^l dt\, e^{-t\,\bar{n}_t}\dot{\Gamma}_l^{(0)}\right] e^{l\,\bar{n}_l}\,,} \tag{4.38}$$

where $\bar{n}_l$ denotes a scale average of n_l given by

$$\bar{n}_l = \frac{1}{l} \int_0^l dt\, n_t \,. \tag{4.39}$$

In App. C we show that for any bounded n_l satisfying $\lim_{l\to\infty} n_l = n_\infty < \infty$

$$\lim_{l\to\infty} \bar{n}_l = n_\infty \,. \tag{4.40}$$

According to Eq. (4.37) we have $\bar{n}_\infty = 1$ so that for f_l approaching a fixed point, i.e. $f_\infty < \infty$, we find as critical condition

$$f_0 = -\int_0^\infty dt\, e^{-t\,\bar{n}_t}\, \dot{\Gamma}_t^{(0)} \,. \tag{4.41}$$

For the rescaled flow equations of the higher-order vertices we use the following identity obtained from the scaling equation (4.29),

$$\begin{aligned} \Lambda\, \partial_\Lambda \Gamma_\Lambda^{(2n)}(K_1', \ldots, K_n'; K_n, \ldots, K_1) \;&=\; \Lambda^{2-n} \Big(\prod_{i=2}^n \nu_0^{\mathbf{n}_i'} \nu_0^{\mathbf{n}_i} \Big)^{-\frac{1}{2}} \Big(\prod_{i=1}^n Z_l^{\mathbf{n}_i'} Z_l^{\mathbf{n}_i} \Big)^{-\frac{1}{2}} \\ &\times \Big[2 - n - n\, \langle \eta_l \rangle_{2n} - \partial_l - \sum_{i=1}^n \Big(Q_i' \cdot \partial_{Q_i'} + Q_i \cdot \partial_{Q_i} \Big) \Big] \\ &\times \tilde{\Gamma}_l^{(2n)}(Q_1', \ldots, Q_n'; Q_n, \ldots, Q_1) \,, \end{aligned} \tag{4.42}$$

where we have defined

$$Q \cdot \partial_Q = q\, \partial_q + \epsilon\, \partial_\epsilon \,, \tag{4.43}$$

and an average anomalous dimension

$$\langle \eta_l \rangle_{2n} = \frac{1}{2n} \sum_{i=1}^n \big(\eta_l^{\mathbf{n}_i} + \eta_l^{\mathbf{n}_i'} \big) \,. \tag{4.44}$$

Two-point vertex:

Using the above formula together with Eqs. (4.13) and (4.29) it is easy to derive the flow equation for the two-point vertex,

$$\boxed{\partial_l \tilde{\Gamma}_l^{(2)}(Q) = (1 - \eta_l^{\mathbf{n}} - Q \cdot \partial_Q)\, \tilde{\Gamma}_l^{(2)}(Q) + \dot{\Gamma}_l^{(2)}(Q) \,,} \tag{4.45}$$

with

$$\dot{\Gamma}_l^{(2)}(Q) = -\int_{Q'} \dot{G}_l(Q')\, \tilde{\Gamma}_l^{(4)}(Q, Q'; Q', Q) \,. \tag{4.46}$$

It is also convenient to give an integral representation of Eq. (4.45), which is obtained by methods similar to those described in Ref. [46],

$$\boxed{\tilde{\Gamma}^{(2)}_l(Q) = e^{(1-\bar{\eta}^{\mathbf{n}}_l)l}\Big[\,\tilde{\Gamma}^{(2)}_{l=0}(e^{-l}Q) + \textstyle\int_0^l dt\, e^{(\bar{\eta}^{\mathbf{n}}_t-1)t}\,\dot{\Gamma}^{(2)}_t(e^{t-l}Q)\,\Big]\,,} \tag{4.47}$$

where $e^tQ \equiv (\sigma, \mathbf{n}, e^tq, e^ti\epsilon)$ and $\bar{\eta}^{\mathbf{n}}_l$ is defined in analogy with Eq. (4.39),

$$\bar{\eta}^{\mathbf{n}}_l = \frac{1}{l}\int_0^l dt\,\eta^{\mathbf{n}}_t\,, \tag{4.48}$$

and hence represents a scale-averaged anomalous dimension for the direction $\mathbf{n}$.

Higher-order vertices ($n \geq 2$):

The flow equations for the irreducible vertices with $n \geq 2$ have the common form

$$\boxed{\begin{aligned}&\partial_l\tilde{\Gamma}^{(2n)}_l(Q'_1,\ldots,Q'_n;Q_n,\ldots,Q_1) = \\ &\qquad\Big[\,2-n-n\,\langle\eta_l\rangle_{2n} - \sum_{i=1}^{n}\Big(Q'_i\cdot\partial_{Q'_i} + Q_i\cdot\partial_{Q_i}\Big)\Big] \\ &\qquad\qquad\times\tilde{\Gamma}^{(2n)}_l(Q'_1,\ldots,Q'_n;Q_n,\ldots,Q_1) \\ &\qquad+\dot{\Gamma}^{(2n)}_l(Q'_1,\ldots,Q'_n;Q_n,\ldots,Q_1)\,,\end{aligned}} \tag{4.49}$$

where the inhomogeneities $\dot{\Gamma}^{(2n)}_l$ are due to the mode-elimination step and given as dimensionless versions of the right-hand sides of the unrescaled flow equations (3.53) and (3.54). For $n \geq 4$ we did not calculate explicit expressions for $\dot{\Gamma}^{(2n)}_l$ since eight-point and higher-order vertices are only involved in approximations beyond the two-loop order. For convenience let us display the two special cases $n = 2$ and $n = 3$ seperately.

Four-point vertex:
Setting $n = 2$ in Eq. (4.49) we obtain For convenience let us display the two

special cases $n = 2$ and $n = 3$ seperately.

$$\boxed{\begin{aligned}&\partial_l \tilde{\Gamma}_l^{(4)}(Q_1', Q_2'; Q_2, Q_1) = \\ &\Big[-2\,\langle \eta_l \rangle_4 - \textstyle\sum_{i=1}^{2} \Big(Q_i' \cdot \partial_{Q_i'} + Q_i \cdot \partial_{Q_i} \Big) \Big]\, \tilde{\Gamma}_l^{(4)}(Q_1', Q_2'; Q_2, Q_1) \\ &+ \dot{\Gamma}_l^{(4)}(Q_1', Q_2'; Q_2, Q_1)\,,\end{aligned}} \tag{4.50}$$

with

$$\begin{aligned}\dot{\Gamma}_l^{(4)}(Q_1', Q_2'; Q_2, Q_1) = &- \int_Q \dot{G}_l(Q)\, \tilde{\Gamma}_l^{(6)}(Q_1', Q_2', Q; Q, Q_2, Q_1) \\ -\frac{1}{2} \int_Q &\Big[\big(\dot{G}_l(Q) G_l(Q') + G_l(Q) \dot{G}_l(Q') \big) \\ &\qquad \times \tilde{\Gamma}_l^{(4)}(Q_1', Q_2'; Q', Q)\, \tilde{\Gamma}_l^{(4)}(Q, Q'; Q_2, Q_1) \Big]_{K' = K_1 + K_2 - K} \\ + \int_Q &\Big[\big(\dot{G}_l(Q) G_l(Q') + G_l(Q) \dot{G}_l(Q') \big) \\ &\qquad \times \tilde{\Gamma}_l^{(4)}(Q_1', Q'; Q, Q_1)\, \tilde{\Gamma}_l^{(4)}(Q_2', Q; Q', Q_2) \Big]_{K' = K + K_1 - K_1'} \\ - \int_Q &\Big[\big(\dot{G}_l(Q) G_l(Q') + G_l(Q) \dot{G}_l(Q') \big) \\ &\qquad \times \tilde{\Gamma}_l^{(4)}(Q_2', Q'; Q, Q_1)\, \tilde{\Gamma}_l^{(4)}(Q_1', Q; Q', Q_2) \Big]_{K' = K + K_1 - K_2'}\,.\end{aligned} \tag{4.51}$$

Six-point vertex:
Here we have to insert $n = 3$ in Eq. (4.49), yielding

$$\boxed{\begin{aligned}&\partial_l \tilde{\Gamma}_l^{(6)}(Q_1', Q_2', Q_3'; Q_3, Q_2, Q_1) = \Big[-1 - 3\,\langle \eta_l \rangle_6 \\ &\quad - \textstyle\sum_{i=1}^{3} \Big(Q_i' \cdot \partial_{Q_i'} + Q_i \cdot \partial_{Q_i} \Big) \Big]\, \tilde{\Gamma}_l^{(6)}(Q_1', Q_2', Q_3'; Q_3, Q_2, Q_1) \\ &\quad + \dot{\Gamma}_l^{(6)}(Q_1', Q_2', Q_3'; Q_3, Q_2, Q_1)\,,\end{aligned}} \tag{4.52}$$

with

$$
\begin{aligned}
&\dot{\Gamma}_l^{(6)}(Q_1', Q_2', Q_3'; Q_3, Q_2, Q_1) = \\
&\qquad - \int_Q \dot{G}_l(Q)\, \tilde{\Gamma}_l^{(8)}(Q_1', Q_2', Q_3', Q; Q, Q_3, Q_2, Q_1) \\
&- 3\, \mathcal{A}_{3,(2,1)} \int_Q \Big[\dot{G}_l(Q) G_l(Q') \\
&\qquad \times \tilde{\Gamma}_l^{(6)}(Q_1', Q_2', Q_3'; Q_3, Q', Q)\, \tilde{\Gamma}_l^{(4)}(Q, Q'; Q_2, Q_1) \Big]_{K'=K_1+K_2-K} \\
&- 3\, \mathcal{A}_{(1',2'),3'} \int_Q \Big[\dot{G}_l(Q) G_l(Q') \\
&\qquad \times \tilde{\Gamma}_l^{(4)}(Q_1', Q_2'; Q', Q)\, \tilde{\Gamma}_l^{(6)}(Q, Q', Q_3'; Q_3, Q_2, Q_1) \Big]_{K'=K_1'+K_2'-K} \\
&+ 9\, \mathcal{A}_{(1',2'),3'} \mathcal{A}_{3,(2,1)} \int_Q \Big[\Big(\dot{G}_l(Q) G_l(Q') + G_l(Q) \dot{G}_l(Q') \Big) \\
&\qquad \times \tilde{\Gamma}_l^{(4)}(Q_3', Q'; Q, Q_3)\, \tilde{\Gamma}_l^{(6)}(Q_1', Q_2', Q; Q', Q_2, Q_1) \Big]_{K'=K_3-K_3'+K} \\
&+ 9\, \mathcal{A}_{(1',2'),3'} \mathcal{A}_{3,(2,1)} \int_Q \Big[\Big(\dot{G}_l(Q) G_l(Q') G_l(Q'') + G_l(Q) \dot{G}_l(Q') G_l(Q'') \\
&\qquad\qquad + G_l(Q) G_l(Q') \dot{G}_l(Q'') \Big) \\
&\qquad \times \tilde{\Gamma}_l^{(4)}(Q_1', Q_2'; Q, Q') \\
&\qquad \times \tilde{\Gamma}_l^{(4)}(Q_3', Q'; Q'', Q_3)\, \tilde{\Gamma}_l^{(4)}(Q'', Q; Q_2, Q_1) \Big]_{K''=K_1+K_2-K}^{K'=K_1'+K_2'-K} \\
&- 36\, \mathcal{A}_{1',2',3'}\, \mathcal{A}_{3,2,1} \int_Q \Big[\dot{G}_l(Q) G_l(Q') G_l(Q'') \\
&\qquad \times \tilde{\Gamma}_l^{(4)}(Q_3', Q; Q'', Q_3) \\
&\qquad \times \tilde{\Gamma}_l^{(4)}(Q_2', Q''; Q', Q_2)\, \tilde{\Gamma}_l^{(4)}(Q_1', Q'; Q, Q_1) \Big]_{K''=K_3'-K_3+K}^{K'=K_1-K_1'+K} .
\end{aligned}
\tag{4.53}
$$

In Eqs. (4.51) and (4.53) K' has to be expressed in terms of the rescaled variables. This rather complicated non-linear transformation follows from our definition of the scaling variables, Eqs. (4.5) and (4.9). For the four-point vertex we give the

explicit result for the zero sound contribution involving the combination $K' = K + K_1 - K_1'$. The other cases can be obtained by appropriate substitution of the external labels. For the energy and spin component we simply have $\epsilon' = \epsilon + \epsilon_1 - \epsilon_1'$ and $\sigma' = \sigma + \sigma_1 - \sigma_1'$ but the expressions for $\mathbf{n}'$ and q' are non-trivial,

$$\mathbf{n}' = \frac{\mathbf{n}(1+q\,c_l^{\mathbf{n}}) + \mathbf{n}_1(1+q_1\,c_l^{\mathbf{n}_1})\,r_F^{\mathbf{n}_1,\mathbf{n}} - \mathbf{n}_1'(1+q_1'\,c_l^{\mathbf{n}_1'})\,r_F^{\mathbf{n}_1',\mathbf{n}}}{\left|\,\mathbf{n}(1+q\,c_l^{\mathbf{n}}) + \mathbf{n}_1(1+q_1\,c_l^{\mathbf{n}_1})\,r_F^{\mathbf{n}_1,\mathbf{n}} - \mathbf{n}_1'(1+q_1'\,c_l^{\mathbf{n}_1'})\,r_F^{\mathbf{n}_1',\mathbf{n}}\,\right|}\,, \tag{4.54}$$

and

$$\begin{aligned} q' = \frac{1}{c_l^{\mathbf{n}'}}\Big[\,\Big|\mathbf{n}(1+q\,c_l^{\mathbf{n}})\,r_F^{\mathbf{n},\mathbf{n}'} + \mathbf{n}_1(1+q_1\,c_l^{\mathbf{n}_1})\,r_F^{\mathbf{n}_1,\mathbf{n}'} \\ - \mathbf{n}_1'(1+q_1'\,c_l^{\mathbf{n}_1'})\,r_F^{\mathbf{n}_1',\mathbf{n}'}\,\Big| - 1\,\Big]\,, \end{aligned} \tag{4.55}$$

where $\mathbf{n}'$ in the last equation has to be substituted by Eq. (4.54). We have defined the ratio of Fermi vectors $k_F(\mathbf{n})$ for the two directions $\mathbf{n}$ and $\mathbf{n}'$ by

$$r_F^{\mathbf{n},\mathbf{n}'} = \frac{k_F(\mathbf{n})}{k_F(\mathbf{n}')}\,. \tag{4.56}$$

For a spherical FS we simply have $c_l^{\mathbf{n}} = \Lambda/mv_F^2 = c_l$ and $k_F(\mathbf{n}) = k_F$, being independent of $\mathbf{n}$ and hence $r_F^{\mathbf{n},\mathbf{n}'} = 1$. Let us finally state the integral representation corresponding to the flow equation (4.49),

$$\begin{aligned} &\tilde{\Gamma}_l^{(2n)}(Q_1',\ldots,Q_n';Q_n,\ldots,Q_1) = \\ &\qquad e^{(2-n-n\langle\bar{\eta}_l\rangle_{2n})l}\Big[\,\tilde{\Gamma}_{l=0}^{(2n)}(e^{-l}Q_1',\ldots,e^{-l}Q_n'\,;\,e^{-l}Q_n,\ldots,e^{-l}Q_1) \\ &+\int_0^l dt\,e^{(n\langle\bar{\eta}_t\rangle_{2n}+n-2)t}\,\dot{\Gamma}_t^{(2n)}(e^{t-l}Q_1'\ldots,e^{t-l}Q_n'\,;\,e^{t-l}Q_n,\ldots,e^{t-l}Q_1)\Big]\,, \end{aligned} \tag{4.57}$$

where $\langle\bar{\eta}_l\rangle_{2n}$ is a combined average over the logarithmic flow parameter l and the directions given by the external labels,

$$\langle\bar{\eta}_l\rangle_{2n} = \frac{1}{2n}\sum_{i=1}^{n}(\bar{\eta}_l^{\mathbf{n}_i} + \bar{\eta}_l^{\mathbf{n}_i'}) = \frac{1}{2n}\sum_{i=1}^{n}\frac{1}{l}\int_0^l dt\,(\eta_t^{\mathbf{n}_i} + \eta_t^{\mathbf{n}_i'})\,. \tag{4.58}$$

The second equality is due to the definition of $\bar{\eta}_l^{\mathbf{n}}$ in Eq. (4.48). For practical calculations Eq. (4.57) is very useful if we find a reasonable approximation for the inhomogeneity $\dot{\Gamma}_t^{(2n)}$. However, by closer observation we recognize that the limit $l \to \infty$ can not be performed directly in Eq. (4.57). In fact we still have to point out more precisely what the physical meaning of this limit applied to the scaling functions actually is. This will be the subject of the next section. Here we still want to present another useful integral representation which can be obtained from Eq. (4.57), relevant for the *physical* vertex functions $\Gamma_\Lambda^{(2n)}$.
Note that as long as we keep the flow parameter l finite we have a one-to-one correspondence between the $2n$-point vertex $\Gamma_\Lambda^{(2n)}$ and its associated dimensionless vertex $\tilde{\Gamma}_l^{(2n)}$ given by the scaling equation (4.29). Due to the definition of the anomalous dimension $\eta_l^{\mathbf{n}}$ in Eq. (4.35) we may express the quasi-particle residue as follows,

$$Z_l^{\mathbf{n}} = e^{-\bar{\eta}_l^{\mathbf{n}}\, l}\,. \tag{4.59}$$

Using this it is easy to show that the scaling equation (4.29) may also be written as

$$\begin{aligned}
&\Gamma_\Lambda^{(2n)}(K_1', \ldots, K_n'; K_n, \ldots, K_1) = \\
&\Big(\prod_{i=2}^{n} \nu_0^{\mathbf{n}_i'} \nu_0^{\mathbf{n}_i}\Big)^{-\frac{1}{2}} \Lambda_0^{2-n}\, e^{-[2-n-n\langle\bar{\eta}_l\rangle_{2n}]\, l}\; \tilde{\Gamma}_l^{(2n)}(Q_1', \ldots, Q_n'; Q_n, \ldots, Q_1)\,.
\end{aligned} \tag{4.60}$$

Inserting Eq. (4.57) on the r.h.s. we see that the exponential prefactor is canceled exactly, and it is then straightforward to show that

$$\begin{aligned}
\Gamma_\Lambda^{(2n)}(K_1', \ldots, K_n'; K_n, \ldots, K_1) = \\
&\Gamma_{\Lambda_0}^{(2n)}(K_1', \ldots, K_n'; K_n, \ldots, K_1) + \Lambda_0^{2-n} \Big(\prod_{i=2}^{n} \nu_0^{\mathbf{n}_i'} \nu_0^{\mathbf{n}_i}\Big)^{-\frac{1}{2}} \\
&\times \int_0^l dt\, e^{[n\langle\bar{\eta}_t\rangle_{2n}+n-2]\, t}\; \dot{\Gamma}_t^{(2n)}(e^t\, \bar{K}_1', \ldots, e^t\, \bar{K}_n'; e^t\, \bar{K}_n, \ldots, e^t\, \bar{K}_1)\,,
\end{aligned} \tag{4.61}$$

with

$$e^t\, \bar{K}_j \;=\; e^t \left(\sigma_j, \mathbf{n}_j, \frac{\mathbf{v}_F \cdot [\mathbf{k}_j - \mathbf{k}_F]}{\Lambda_0}, \frac{i\omega_j}{\Lambda_0}\right) \tag{4.62}$$

$$= \left(\sigma_j, \mathbf{n}_j, e^t \frac{v_\parallel^{\mathbf{n}_j} p_j}{\Lambda_0}, e^t \frac{i\omega_j}{\Lambda_0}\right). \tag{4.63}$$

Provided that the integral in Eq. (4.61) converges we may now directly take the limit $l \to \infty$, i.e. $\Lambda \to 0$, and we obtain an integral represention of the physical $2n$-point vertex at the fixed point,

$$\begin{aligned}\lim_{\Lambda\to 0} \Gamma_\Lambda^{(2n)}(K_1', \ldots, K_n'; K_n, \ldots, K_1) = \\ \Gamma_{\Lambda_0}^{(2n)}(K_1', \ldots, K_n'; K_n, \ldots, K_1) + \Lambda_0^{2-n} \left(\prod_{i=2}^{n} \nu_0^{\mathbf{n}_i'} \nu_0^{\mathbf{n}_i}\right)^{-\frac{1}{2}} \\ \times \int_0^\infty dt\, e^{[n\langle \bar{\eta}_t\rangle_{2n} + n - 2]\, t}\, \dot{\Gamma}_t^{(2n)}(e^t\, \bar{K}_1', \ldots, e^t\, \bar{K}_n'; e^t\, \bar{K}_n, \ldots, e^t\, \bar{K}_1),\end{aligned} \tag{4.64}$$

Chapter 5

General Properties of the Vertex Functions

We discuss the analytic properties of the physical vertex functions and their dimensionless analogues for vanishing momenta and frequencies. First we show how our formalism can be embedded in the framework of dynamic critical phenomena in the way it has been formulated by Halperin and Hohenberg [81]. We follow these authors and define a hydrodynamic and a scaling regime, the first being restricted to the description of the flow of coupling constants while the second is relevant to describe the flow of entire vertex functions. We show that in the limit $l \to \infty$ the hydrodynamic regime only represents a single physical point given by $p = \omega = 0$. In addition we define the circle of convergence (COC) for expansions of the physical and the dimensionless vertices in powers of their variables at the origin. It will be shown that the COC of the dimensionless vertices covers the whole (q, ϵ) plane when the system represents a Fermi liquid, while for non-Fermi liquids it is basically identical with the hydrodynamic regime. From a mathematical point of view this implies that fixed-point results obtained by an expansion of the dimensionless vertices in powers of q and ϵ only represent the physics at $\mathbf{k} = \mathbf{k}_F$ and $\omega = 0$. We discuss subtleties related to the scaling hypothesis in this context. Finally we classify the couplings defined within the COC in the usual RG categories "relevant", "marginal" and "irrelevant" to the RG flow.

5.1 Hydrodynamic and Scaling Regimes

The rescaled flow equations constitute an infinite hierarchy of nonlinear integro-differential equations that will in general only be solvable due to appropriate approximations. In the majority of applications the RG has been used to study the behavior of so-called *coupling constants* when the cutoff is reduced. These

coupling constants will undergo a flow in parameter space and possibly run into a fixed point, where the theory becomes scale independent and may be associated with a critical state of the system [66]. The determination of such fixed points is the central task of conventional RG approaches. In this way one may for instance find critical exponents for various types of susceptibilities or simply study the flow of the couplings related to the momentum- and frequency-independent part of the two-body interaction. But the detailed shape of the correlation functions, e.g. of the single-particle Green function at criticality, remains unknown. In this context it is important to recognize that our flow equations (4.45) and (4.49), which are so far formally exact, principally open up the possibility to go beyond the usual task and to follow the flow of entire correlation *functions*. It is then advantageous to embed our RG formalism in the framework and language of dynamic critical phenomena, especially in the way it has been introduced by Halperin and Hohenberg [81]. To this end we define a length scale ξ and a time scale τ related to the infrared energy-band cutoff by

$$\xi = \bar{v}_F/\Lambda\,, \qquad \tau = 1/\Lambda\,, \tag{5.1}$$

where $\bar{v}_F$ can for instance be chosen to be the average Fermi velocity at the interacting FS,

$$\bar{v}_F = \frac{1}{S_{FS}} \int_{FS} dS_{\mathbf{n}}\, v_F(\mathbf{n})\,, \tag{5.2}$$

with S_{FS} being the surface area of the FS.[1] The scaling variables introduced in Eq. (4.9) may then be reexpressed in terms of ξ and τ,

$$q = \frac{v_\parallel^{\mathbf{n}} p}{\Lambda} = \lambda_F^{\mathbf{n}}\, p\xi\,, \qquad \epsilon = \frac{\omega}{\Lambda} = \omega\tau\,, \tag{5.3}$$

where $\lambda_F^{\mathbf{n}} = v_\parallel^{\mathbf{n}}/\bar{v}_F$ is the ratio of the parallel component of the local Fermi velocity $v_F(\mathbf{n})$ and the average Fermi velocity. In general $\lambda_F^{\mathbf{n}}$ will be of the order of unity. Let us restrict our considerations to the two-point vertex and denote the corresponding scaling function by $\Phi_l^{(2)}$ in analogy with the theory of dynamic critical phenomena [19]. Explicitly, we define

$$\Phi_l^{(2)}(\sigma, \mathbf{n}, p\xi, i\omega\tau) = \tilde{G}_l(\sigma, \mathbf{n}, \lambda_F^{\mathbf{n}}\, p\xi, i\omega\tau)\,. \tag{5.4}$$

Note that $\Phi_l^{(2)}$ and $\tilde{G}_l$ only differ by the less important factor $\lambda_F^{\mathbf{n}}$ in front of $p\xi$. For spherical Fermi surfaces they even coincide as in this case $\lambda_F^{\mathbf{n}} = 1$. We may now reexpress the scaling equation (4.21) using Eq. (5.1) and obtain

[1] Note that if we simply had chosen $v_\parallel^{\mathbf{n}}$ instead of $\bar{v}_F$ the length ξ would depend on the direction $\mathbf{n}$ of $\mathbf{k}$, which is not convenient for our present purposes.

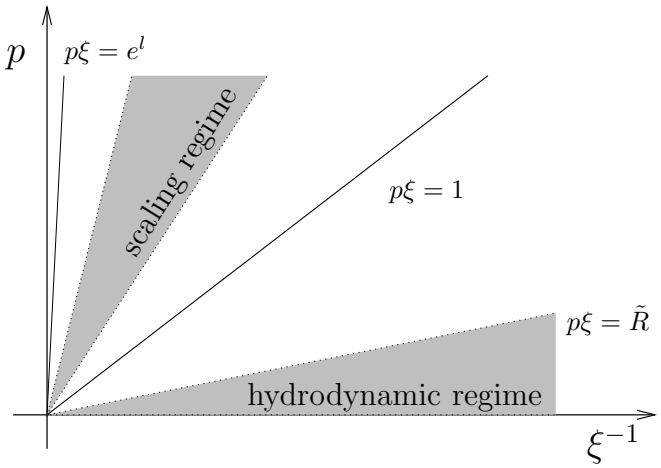

Figure 5.1: Schematical representation of the hydrodynamic and the scaling regime for a spherical FS in the (ξ^{-1}, p) plane. The line of criticality is given by the ordinate where $\xi^{-1} = 0$, i.e. $l = \infty$. An equivalent picture may be drawn with p replaced by ω. The line $q = p\xi = \tilde{R}$ corresponds to a constant radius of convergence with respect to q but to a vanishing radius of convergence for the physical momenta p when $l \to \infty$, i.e. $\xi^{-1} \to 0$.

$$G_\Lambda(\sigma, \mathbf{n}(k_F + p), i\omega) = \tau\, Z_l^{\mathbf{n}}\, \Phi_l^{(2)}(\sigma, \mathbf{n}, p\xi, i\omega\tau)\,. \tag{5.5}$$

This is the dynamic-scaling form common in the theory of critical phenomena [19, 81]. Similar relations can be obtained for the higher-order vertices. In the following we will not further distinguish between $\Phi_l^{(2)}$ and $\tilde{G}_l$ and speak like before of $\tilde{G}_l$ as the scaling function. Due to this formal resemblance to the theory of dynamic critical phenomena it makes sense to view ξ as a *correlation length*. Following the nomenclature of Halperin and Hohenberg we may then specify two regions depending on whether the characteristic length scales (time scales) are much larger or much smaller than the correlation length ξ (than τ). In Fourier space we introduce two different regions, determind by

$$\left.\begin{array}{r} |p\xi| \ll 1 \\ |\omega\tau| \ll 1 \end{array}\right\} \quad \equiv \quad \text{hydrodynamic regime}\,, \tag{5.6}$$

$$\left.\begin{array}{r} 1 \ll |p\xi| \ll e^l \\ 1 \ll |\omega\tau| \ll e^l \end{array}\right\} \quad \equiv \quad \text{scaling regime}\,. \tag{5.7}$$

In the scaling regime we have kept track of the fact that within our formalism we also have a minimal length scale, e.g. the lattice constant, that should be much smaller then all lengths of interest. In Fig. 5.1 the two regions are shown in the

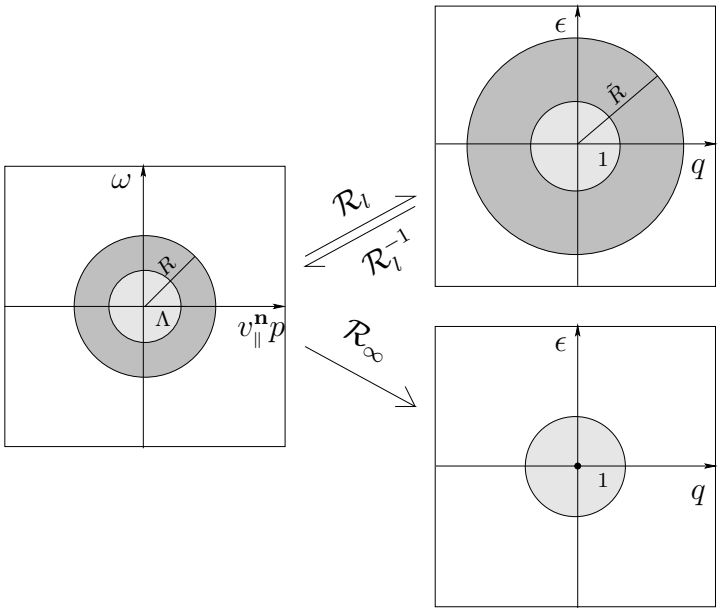

Figure 5.2: Schematical representation of the variable transformation $\mathcal{R}_l[(v_\parallel^{\mathbf{n}} p, \omega)] = (v_\parallel^{\mathbf{n}} p\, e^l/\Lambda_0, \omega\, e^l/\Lambda_0) \equiv (q, \epsilon)$. The mapping of two circles, one with constant radius R and one with radius $R_\Lambda = \Lambda = \Lambda_0\, e^{-l}$, is shown. As long as l is finite the first is mapped to another circle with radius $\tilde{R} = \Lambda^{-1} R$ while the image of the second is the unit circle. In this case the inverse mapping $\mathcal{R}_l^{-1}$ exists, which is simply the multiplication with Λ. On the other hand for $l = \infty$ the whole circle with radius R is mapped to infinity except for the origin $p = \omega = 0$. The inverse image of the unit circle is now given by the "circle" with radius $\Lambda = 0$, hence the point $p = \omega = 0$. An inverse mapping $\mathcal{R}_\infty^{-1}$ does clearly not exist.

(ξ^{-1}, p) plane.

Now let us express the two regimes in terms of our scaling variables q and ϵ. The whole subsequent discussion and even the next section will deal with subtleties related to the variable transformation given by Eq. (4.9). At first sight the transformation $q = v_\parallel^{\mathbf{n}} p/\Lambda$ and $\epsilon = \omega/\Lambda$ is trivial. This is true provided Λ remains finite. In this case there is a unique relation between q and p as well as ϵ and ω. However, when $\Lambda \to 0$ the transformation becomes singular and the whole (p, ω) plane is mapped to infinity except for the single point $p = \omega = 0$ which remains unchanged, see Fig. 5.2. The uniqueness of the transformation is hence lost at the fixed point. Note that the same will then be true for the corresponding vertices related by the scaling equation (4.29). This is nothing but the well-known fact that the RG transformation has no inverse element at the fixed point anymore and thus only constitutes a semi-group [33].

For simplicity we again restrict the discussion to a spherical FS such that $\lambda_F^{\mathbf{n}} = 1$ and $v_\parallel^{\mathbf{n}} = v_F$ in Eq. (5.3). The scaling regime is then characterized by $1 \ll |q| \ll e^l$

and $1 \ll |\epsilon| \ll e^l$. To which physical momenta and frequencies do these conditions correspond? Due to Eqs. (5.1) and (5.3) we have $q = p\xi = p\xi_0 e^l$ as well as $\epsilon = \omega\tau = \omega\tau_0 e^l$, such that for each finite $|p| \ll \xi_0^{-1}$ and $|\omega| \ll \tau_0^{-1}$ the conditions will be satisfied if l becomes large enough. *Thus the physics on all energy scales with $|p| \ll \xi_0^{-1}$ and $|\omega| \ll \tau_0^{-1}$ will finally be described by the scaling regime.*[2] In other words: If for instance we succeeded to calculate $\tilde{G}_l(q, i\epsilon)$ in the scaling regime and we transformed back to the physical Green function $G_\Lambda(p, i\omega)$ before the limit $l \to \infty$ is taken, our result would a priori not be restricted to the asymptotic regime $p, \omega \to 0$.

On the other hand the usual RG task of calculating the flow of coupling constants relies on an expansion of the scaling functions $\tilde{\Gamma}_l^{(2n)}$ in powers of q and ϵ, associating with each power of the Taylor expansion a certain coupling constant. Of course, such an expansion will in general only be justified in the hydrodynamic regime[3] where $|q| = |p|\xi_0 e^l \ll 1$ and $|\epsilon| = |\omega|\tau_0 e^l \ll 1$. Here the values of physical momenta and frequencies satisfying this condition when $l \to \infty$ must shrink to zero, i.e. $p \to 0$ and $\omega \to 0$. This can also be seen from Fig. 5.1. Consequently *the fixed-point values of the couplings evaluated in the hydrodynamic regime solely represent the point $p = \omega = 0$, i.e. asymptotic low-energy physics.*

This in turn implies that when we step from the singular point $p = \omega = 0$ to a point with arbitrarily small but finite p and ω this is equivalent to a change from the hydrodynamic into the scaling regime in terms of the dimensionless variables q and ϵ. However, in general we do not expect that the physics at $p = \omega = 0$ will be drastically different from its closest neighborhood. It is then reasonable to assume the scaling functions to vary smoothly from the hydrodynamic into the scaling regime, which is the essence of the *dynamic scaling hypothesis* [81]. Applied to the dimensionless fermionic Green function this may also be expressed by an eqution of the form

$$\tilde{G}_l(Q) \approx \tilde{G}_\infty(Q) \qquad \text{for } 1 \ll |q|, |\epsilon| \ll e^l\,, \tag{5.8}$$

and similarly for higher-order correlation functions. In Eq. (5.8) it is assumed that in the scaling regime the explicit scale-dependence of $\tilde{G}_l$ vanishes (which amounts to the replacement $\tilde{G}_l \to \tilde{G}_\infty$) and the only scale dependence left is given implicitly via $q = p\xi = p\xi_0 e^l$ and $\epsilon = \omega\tau = \omega\tau_0 e^l$. A necessary condition for the applicability of the scaling hypothesis is that the fixed-point function $\tilde{G}_\infty$ is a homogeneous function in the scaling regime. More precisely it must satisfy the property

[2] The only exception is the point $p = \omega = 0$ which is mapped to $q = \epsilon = 0$. This special point we will find to be the only one characterized by the hydrodynamic regime.

[3] In the next section we will be more precise and define the COC where the expansions of the vertex functions really are justified.

$$\tilde{G}_\infty(sq, si\epsilon) = s^{\eta^{\mathbf{n}}-1}\,\tilde{G}_\infty(q, i\epsilon) \qquad \text{for } 1 \ll |q|, |\epsilon| \ll e^l\,, \tag{5.9}$$

where $\eta^{\mathbf{n}}$ is the fixed-point value of the anomalous dimension. Only under this condition the physical Green function $G_\Lambda(\sigma, \mathbf{k}, i\omega)$ will approach a finite result, which will become evident in a moment. In the following we shall describe two different ways for obtaining G_Λ from its dimensionless analogue:

1. We first calculate the fixed point scaling function $\tilde{G}_\infty$ and use the scaling hypothesis together with Eq. (4.21) to transform back to the physical variables. Explicitly we set

$$\begin{aligned} G_\Lambda(\sigma, \mathbf{k}, i\omega) &\approx \Lambda^{-1} Z_l^{\mathbf{n}}\, \tilde{G}_\infty\big(\sigma, \tfrac{\mathbf{v}_F\cdot(\mathbf{k}-\mathbf{k}_F)}{\Lambda}, \tfrac{i\omega}{\Lambda}\big) \\ &= \Lambda_0^{-1}\left(\tfrac{\Lambda}{\Lambda_0}\right)^{\bar{\eta}_l^{\mathbf{n}}-1} \tilde{G}_\infty\big(\sigma, \tfrac{\mathbf{v}_F\cdot(\mathbf{k}-\mathbf{k}_F)}{\Lambda}, \tfrac{i\omega}{\Lambda}\big)\,, \end{aligned} \tag{5.10}$$

where for the second equality we have used that according to Eq. (4.59) we may write $Z_l = (\Lambda/\Lambda_0)^{\bar{\eta}_l}$. Now, for Eq. (5.10) to reach a finite limit when $\Lambda \to 0$ the scaling function $\tilde{G}_\infty(\sigma, q, i\epsilon)$ has to be a homogeneous function of degree $\eta^{\mathbf{n}} - 1$ in the variables q and ϵ in the scaling regime. Assuming this property we get

$$\boxed{\lim_{\Lambda\to 0} G_\Lambda(\sigma, \mathbf{k}, i\omega) \approx (\Lambda_0)^{-\eta^{\mathbf{n}}}\, \tilde{G}_\infty(\sigma, \mathbf{v}_F\cdot(\mathbf{k}-\mathbf{k}_F), i\omega)\,.} \tag{5.11}$$

What is the region of validity of this approximation? At first sight one is tempted to say that this must be the scaling region (5.7) translated to the physical variables. In the limit $\Lambda \to 0$ this would imply $|\mathbf{v}_F\cdot(\mathbf{k}-\mathbf{k}_F)| \ll \Lambda_0$ and $|\omega| \ll \Lambda_0$. However, due to the scaling hypothesis (5.8) we used the fixed point scaling function $\tilde{G}_\infty(Q)$, where the argument Q is left finite, while on the other hand we already performed the limit $l \to \infty$ to remove the explicit l-dependence. But for Q remaining finite when $l \to \infty$ we must again have $p \to 0$ and $\omega \to 0$, just for the same reasons we have seen for the expansions in the hydrodynamic regime. We conclude that *all correlation functions calculated by means of the scaling hypothesis represent the asymptotic regime* $p, \omega \to 0$.[4] We then expect the correlation functions to assume a certain generic low-energy form representative for a whole class of initial Hamiltonians ("universality").

[4] Of course, so far this is just a mathematical statement while the scaling hypothesis assumes that the region of validity extends to finite values of p and ω. However, for a Luttinger liquid or, more generally, for a non-Fermi liquid this region might be extremely small. We will discuss this important point in the context of the spinless g_2-model in Part II of this thesis.

2. While the feature of universality is important from a theoretical point of view providing us with the concept of universality classes [33] it however leads to a loss of information about the physical system at consideration. For instance it might be instructive to know at which energy scale the Green function switches to its asymptotic scaling form, which cannot be derived as a result of the above procedure in a straightforward way. In this case we need $G_{\Lambda\to 0}$ without making use of the scaling hypothesis, we thus have to transform back to the physical variables as long as l is finite, without completely removing the rescaling step. The limit $l \to \infty$ will then be performed at the very end. We have already derived an expression for the physical correlation functions satisfying these criteria, given by Eq. (4.61). For a direct comparison with Eq. (5.11) let us display the explicit result for the Green function[5],

$$\lim_{\Lambda\to 0} G_\Lambda(\sigma,\mathbf{k},i\omega) = \frac{\Theta(\Lambda_0-\Omega_K)}{i\omega-\xi(\mathbf{k})-\Sigma(\sigma,\mathbf{k},i\omega)+\Sigma(\mathbf{k}_F,0)}\,, \tag{5.12}$$

where the self-energy at the fixed point is determined by

$$\boxed{\begin{aligned}&\Sigma(\sigma,\mathbf{k},i\omega) = \\ &\quad \Sigma_{\Lambda_0}(\sigma,\mathbf{k},i\omega) - \Lambda_0 \textstyle\int_0^\infty dt\, e^{(\bar\eta_t^{\mathbf{n}}-1)\,t}\, \dot\Gamma_t^{(2)}\big(\sigma, \frac{\mathbf{v}_F\cdot(\mathbf{k}-\mathbf{k}_F)}{\Lambda_0 e^{-t}}, \frac{i\omega}{\Lambda_0 e^{-t}}\big)\,.\end{aligned}} \tag{5.13}$$

In deriving Eq. (5.13) no approximation has been made and it is principally valid for all momenta and frequencies with $\Omega_K \le \Lambda_0$.

5.2 Fermi and Non-Fermi Liquids

There is still a subtlety hidden in the above statements about expansions in the hydrodynamic regime that becomes an important difference depending on whether we consider Fermi or non-Fermi liquids. In Eq. (5.6) we have defined the hydrodynamic regime by $|q| = |p\xi| \ll 1$ as well as $|\epsilon| = |\omega\tau| \ll 1$ and stated that expansions of the scaling functions in powers of q and ϵ will in general only be justified in this regime. Note however that the definition of the hydrodynamic regime is physically motivated rather than mathematically. As concernes expansions in the variables q and ϵ we should better define the corresponding circle of convergence (COC). In the following we will restrict our conciderations to the two-point vertex, but similar reflections will apply to higher order vertices as well.

[5] Eq. (4.61) has only been derived for $n \ge 2$ but the formula for $n = 1$ is similar with the product over $\nu_0^{\mathbf{n}_i}$ replaced by unity.

We define the COC of the *retarded* two-point vertex $\tilde{\Gamma}_l^{(2)}(q, \epsilon + i0^+)$ for expansions in powers of q and ϵ by the region in the (q, ϵ) plane determined by[6]

$$q^2 + \epsilon^2 < \tilde{R}_l^2 \,. \tag{5.14}$$

Here $\tilde{R}_l$ is the radius of convergence, which will in general depend on the logarithmic scale factor l. In most applications the magnitude of $\tilde{R}_l$ will be determined by the low-energy ends of branch cuts of the self-energy located on the real-frequency axis. A special case is given when $\tilde{R}_l = \tilde{R}$ is independant of the scale l. Setting $\epsilon = 0$ in Eq. (5.14) we get back to the situation sketched in Fig. 5.1 where $|q| = |p\xi| = \tilde{R}$ is the border line of the hydrodynamic regime. The COC for an expansion of the *physical* two-point vertex $\Gamma_\Lambda^{(2)}$ in powers of the variables p and ω, which is then given by $(v_F p)^2 + \omega^2 < \tilde{R}^2 \Lambda_0^2 e^{-2l}$, will exponentially shrink to zero when $l \to \infty$. But by physical reasons we do not generally expect such a behavior. In fact for Fermi liquids the irreducible self-energy is expected to have a finite radius of convergence as this is one of the basic properties of a Fermi liquid [75]. More generally, if we multiply Eq. (5.14) with Λ^2 we get

$$(v_F p)^2 + \omega^2 < (\Lambda_0 e^{-l}\, \tilde{R}_l)^2 = (\Lambda\, \tilde{R}_l)^2 \equiv R_\Lambda^2 \,, \tag{5.15}$$

which is now the Λ-dependent COC of the physical vertex $\Gamma_\Lambda^{(2)}$, since for finite l there is a one-to-one correspondence between $\tilde{\Gamma}_l^{(2)}$ and $\Gamma_\Lambda^{(2)}$ given by Eq. (4.29). For R_Λ to reach a non-zero limit $0 < \lim_{\Lambda \to 0} R_\Lambda \leq \infty$, i.e. for Fermi liquids, the radius of convergence in Q-space has to diverge at least as $\tilde{R}_l \sim e^l$. Consequently the two-point scaling function $\tilde{\Gamma}_l^{(2)}(Q)$ at the fixed point will in this case be analytic in the whole (q, ϵ) plane.

On the other hand non-Fermi liquid behavior implies a breakdown of the quasiparticle picture, which is expressed by a vanishing or drastically reduced quasiparticle weight. Note that due to our definition of Z_l in Eq. (4.16) this implies that $\partial_{i\omega} \Sigma_\Lambda\ (\mathbf{k}_F, i\omega)|_{\omega=0}$ must diverge in the limit $\Lambda \to 0$. In other words: The fixed-point self-energy $\Sigma(\mathbf{k}, i\omega)$ will be non-analytic at $\mathbf{k} = \mathbf{k}_F$ and $\omega = 0$. Consequently we expect $R_\Lambda \to 0$ when the fixed point is approached. From Eq. (5.15) we see that this will be the case when $\tilde{R}_l$ diverges slower than $\sim e^l$. However, in the setup of our RG formalism we have imposed a low-energy cutoff Λ to regularize infrared divergences. In the Q-variables the cutoff Λ turns into the scale-independent number $\Lambda/\Lambda = 1$, such that we also expect $\tilde{R}_l$ to be a constant

[6] We could equally well define the COC of the analytically continued two-point vertex $\tilde{\Gamma}_l^{(2)}(q, z)$, where z is an arbitrary complex number. In this case a proper definition of the COC for an expansion both in z and q is more difficult, see also Sec. 7.5. However, for our present purposes it is only important to notice that if the COC of the retarded two-point vertex $\tilde{\Gamma}_l^{(2)}(q, \epsilon + i0^+)$ vanishes this will also be true for $\tilde{\Gamma}_l^{(2)}(q, z)$.

of the order of unity. This implies that the scaling functions $\tilde{\Gamma}_l^{(2n)}$ will be analytic at $q = \epsilon = 0$ with a finite radius of convergence *even when the critical limit* $l \to \infty$ *is performed*, see also Fig. 5.2.
Although the above considerations are rather formal they show what is implicitly assumed by the scaling hypothesis concerning the analytical properties of the vertex functions. On pure mathematical grounds the applicability of the scaling hypothesis is not obvious at all, and it may well happen that the validity of the fixed-point results of the dimensionless couplings cannot be extended to a finite region around the FS. An example for such a scenario will be given in Sec. 7.2 .
Let us now turn our attention to the question wether it is allowed to use the unrescaled flow equations instead of their rescaled analogues. We again restrict our considerations to the irreducible self-energy.

Fermi liquids: Here we assume the physical self-energy to be an analytic function at $p = \omega = 0$ with some finite radius of convergence, and this will then also be true for $\Gamma_\Lambda^{(2)}$, see Eq. (4.24). An expansion

$$\Gamma_\Lambda^{(2)}(\sigma, \mathbf{n}(k_F + p), i\omega) \;=\; \mu_\Lambda^{\mathbf{n}} + b_\Lambda^{\mathbf{n}}\, p + c_\Lambda^{\mathbf{n}}\, i\omega + \mathcal{O}(p^2, \omega^2, p\omega) \qquad (5.16)$$

will hence be justified even in the limit $\Lambda \to 0$ and have finite radius of convergence. Consequently the couplings $\mu_\Lambda^{\mathbf{n}} = \Gamma_\Lambda^{(2)}(\mathbf{k}_F, 0)$, $b_\Lambda^{\mathbf{n}} = \partial_p \Gamma_\Lambda^{(2)}(\sigma, \mathbf{n}(k_F + p), 0)\big|_{p=0}$ and $c_\Lambda^{\mathbf{n}} = \partial_\omega \Gamma_\Lambda^{(2)}(\sigma, \mathbf{k}_F, i\omega)\big|_{\omega=0}$ are expected to approach finite and well-defined fixed-point values when $\Lambda \to 0$. The same will be true for the dimensionless couplings related to an expansion of the scaling function $\tilde{\Gamma}_l^{(2)}(Q)$ in powers of q and ϵ , since we have shown that for Fermi liquids the COC of $\tilde{\Gamma}_l^{(2)}(Q)$ at the fixed point is given by the whole (q, ϵ) plane.

Non-Fermi liquids: The physical self-energy $\Gamma_\Lambda^{(2)}(K)$ is assumed to exhibit some kind of non-analyticity at $p = \omega = 0$. In this case the expansion given in Eq. (5.16) has a vanishing radius of convergence when $\Lambda \to 0$. At least for the coupling $c_\Lambda^{\mathbf{n}}$ defined above this means that it will diverge at the fixed point, and this might also be true for $b_\Lambda^{\mathbf{n}}$. Such a runaway-flow of the unrescaled couplings has been interpreted as an indication of non-Fermi-liquid behavior by several authors in the context of the two-dimensional Hubbard model [61, 70, 72]. However, within loop approximations such an interpretation is less obvious and also depends on the loop order where the non-analyticities occur. We will return to this point in the next section.
On the other hand, as we have shown above, an expansion of $\tilde{\Gamma}_l^{(2)}(Q)$ in powers of q and ϵ is expected to be well-defined even in the limit $l \to \infty$, and the related

couplings will then approach finite fixed-point values.[7] What we have shown below Eq. (5.7) is that the values of these couplings at the fixed point characterize the physical system only in the asymptotic regime $p, \omega \to 0$.

In summary we have seen that for non-Fermi liquids the determination of the fixed-point values for the coupling constants of the unrescaled vertices must fail, while the couplings of the rescaled vertices are expected to approach well-defined fixed-point values. In contrast, for Fermi liquids, from our present point of view there should be no principal difference between using the rescaled or the unrescaled versions of the flow equations. However, as we will see in the next section this is only true within one-loop approximations. At two-loop order differences related to the field rescaling will appear, and the predictions of the unrescaled flow equations turn out to be incorrect.
Finally, what about calculating entire correlation functions using the unrescaled version? Here we cannot give a general statement, but in light of the above discussion it seems clear that we will run into severe problems at least when anomalous scaling is involved. In this case the unrescaled vertices will fail to reach finite fixed point functions, as a proper field-rescaling within the RG transformation turns out to be crucial then. But even if we just try to calculate uniform susceptibilities related to a perturbative expansion of the four-point vertex we get ambiguous results, as has been shown in Ref. [89]. No such problems arise when we use the rescaled equations and the correct results are recovered. As we will show in Chap. 7 for the spinless g_2-model it is even possible to calculate a non-perturbative expression for the spectral function using Eq. (4.45).

5.3 Classification of Couplings

Let us now follow the usual RG task and expand the scaling functions in powers of q and ϵ in their domains of analyticity. For simplicity we will again restrict our considerations to the case of rotationally invariant systems with a spherical FS. As long as no symmetry breaking sets in the irreducible two-point vertex $\tilde{\Gamma}_l^{(2)}(\sigma, \mathbf{n}, q, i\epsilon)$ will then be independent of the direction $\mathbf{n}$ and so will the couplings obtained from a Taylor expansion. Inserting this expansion in the flow equation (4.45) we will find the corresponding exact flow equations for the couplings by comparing the powers of the Taylor series. Here we will only give the definitions of the relevant and the marginal couplings obtained from the scaling functions. Following the usual nomenclature we shall call a coupling *relevant* if its canonical

[7] For relevant couplings this needs a fine-tuning of the initial conditions as we have already seen for the free energy, Eq. (4.41).

scaling dimension[8] d_s is positive, *marginal* if d_s is zero and *irrelevant* when d_s is negative. We start with the momentum- and frequency-independent part of $\tilde{\Gamma}_l^{(2)}$, which is related to renormalizations of the chemical potential,

$$\tilde{\mu}_l = \tilde{\Gamma}_l^{(2)}(\sigma, \mathbf{n}, 0)\,, \tag{5.17}$$

where we have used the notation $\tilde{\Gamma}_l^{(2)}(\sigma, \mathbf{n}, 0) \equiv \tilde{\Gamma}_l^{(2)}(\sigma, \mathbf{n}, q = 0, i\epsilon = 0)$. The flow of $\tilde{\mu}_l$ is then easily obtained from Eq. (4.45),

$$\boxed{\partial_l \tilde{\mu}_l = (1 - \eta_l)\,\tilde{\mu}_l + \dot{\Gamma}_l^{(2)}(\sigma, \mathbf{n}, 0)\,.} \tag{5.18}$$

Provided that $\eta \equiv \eta_\infty < 1$ we see from this equation that $\tilde{\mu}_l$ is a *relevant* coupling with $d_s = 1$ but with an interaction-dependent scaling dimension $1 - \eta_l$. Consequently, for $\tilde{\mu}_l$ to reach a finite fixed-point value we must fine-tune the initial value $\tilde{\mu}_0$ at $l = 0$, just in the same way we have seen for the free energy, Eq. (4.41). This is best understood by the integral representation of Eq. (5.18), which is simply obtained from Eq. (4.47) by setting $q = \epsilon = 0$,

$$\tilde{\mu}_l = e^{(1-\bar{\eta}_l)l}\Big[\,\tilde{\mu}_0 + \int_0^l dt\, e^{(\bar{\eta}_t - 1)t}\,\dot{\Gamma}_t^{(2)}(\sigma, \mathbf{n}, 0)\,\Big]\,. \tag{5.19}$$

From the requirement $\tilde{\mu} < \infty$ we then find the critical initial-value to be

$$\tilde{\mu}_0 = -\int_0^\infty dt\, e^{(\bar{\eta}_t - 1)t}\,\dot{\Gamma}_t^{(2)}(\sigma, \mathbf{n}, 0)\,, \tag{5.20}$$

provided that $\eta < 1$. Remember that according to the lemma in appendix B we have $\bar{\eta} = \eta$. In case that $\eta \geq 1$ we see from Eq. (5.18) that the asymptotic scaling-dimension $1 - \eta$ equals to zero or becomes even negative, turning $\tilde{\mu}_l$ into a marginal or an irrelevant coupling, respectively. A fine-tuning of the initial value is then not necessary.

In Ref. [90] it has been shown, that Eq. (5.20) may be reduced to the self-consistent Hartree-Fock equation, when the momentum and frequency dependence of the four-point vertex in the definition (4.46) of $\dot{\Gamma}_l^{(2)}$ is neglected. Furthermore let us define

$$\tilde{v}_l = Z_l - \partial_q \tilde{\Gamma}_l^{(2)}(Q)|_{Q=0}\,, \tag{5.21}$$

where $Q = 0$ means $Q = (\sigma, \mathbf{n}, 0, i0)$. As we will point out shortly for Fermi liquids $\tilde{v}_l$ is equivalent with the renormalization factor of the Fermi velocity while for non-Fermi liquids no such obvious interpretation exists. The quasi-particle

[8] By *canonical* or *engineering* scaling dimension we mean the scaling dimension resulting exclusively from the rescaling of frequencies and momenta, which is typically an integer. The contribution of the field rescaling depends on the interaction and is considered separately.

weight Z_l defined in Eq. (4.16) may also be expressed in terms of $\tilde{\Gamma}_l^{(2)}$ using Eq. (4.24),

$$Z_l = 1 + \partial_{i\epsilon} \tilde{\Gamma}_l^{(2)}(Q)|_{Q=0} \,. \tag{5.22}$$

With these definitions the Taylor expansion of the dimensionless two-point vertex may be written as

$$\tilde{\Gamma}_l^{(2)}(Q) = \tilde{\mu}_l + (1 - Z_l)\, i\epsilon + (Z_l - \tilde{v}_l)\, q + \mathcal{O}(q^2, \epsilon^2, q\epsilon) \,, \tag{5.23}$$

so that for small q and ϵ the dimensionless inverse propagator defined in Eq. (4.23) is given by

$$\tilde{r}_l(Q) = Z_l\,(i\epsilon - q) + \tilde{\Gamma}_l^{(2)}(Q) = i\epsilon - \tilde{v}_l q + \tilde{\mu}_l + \mathcal{O}(q^2, \epsilon^2, q\epsilon) \,. \tag{5.24}$$

The exact flow equations for the couplings Z_l and $\tilde{v}_l$ may now easily be derived using Eqs. (4.45), (4.35) and (5.21),

$$\boxed{\begin{aligned} \partial_l Z_l &= -\,\eta_l Z_l \\ \partial_l \tilde{v}_l &= -\,\eta_l \tilde{v}_l - \partial_q \dot{\Gamma}_l^{(2)}(Q)|_{Q=0} \,. \end{aligned}} \tag{5.25}$$

From these equations we see explicitly that Z_l and $\tilde{v}_l$ are marginal couplings with canonical scaling dimension $d_s = 0$. It is also useful and straithforward to give an explicit equation for the anomalous dimension. This can be achieved by differentiating the flow equation (4.45) with respect to $i\epsilon$, setting $\epsilon = 0$ and using Eq. (5.22),

$$\boxed{\begin{aligned} \eta_l &= \partial_{i\epsilon} \dot{\Gamma}_l^{(2)}(Q)|_{Q=0} \\ &= -\tfrac{1}{2} \textstyle\int_{Q'} \dot{G}_l(Q')\, \partial_{i\epsilon} \tilde{\Gamma}_l^{(4)}(Q, Q'; Q', Q)\big|_{Q=0} \,, \end{aligned}} \tag{5.26}$$

where for the second equality we used Eq. (4.46). Note that all couplings associated with higher orders in the expansion (5.23) of the two-point scaling function are irrelevant with canonical scaling dimensions $d_s \leq -1$. Further marginal couplings are given by the momentum- and frequency-independent part of the dimensionless four-point vertex which we denote by

$$\tilde{g}_l(\sigma_1' \mathbf{n}_1', \sigma_2' \mathbf{n}_2'; \sigma_2 \mathbf{n}_2, \sigma_1 \mathbf{n}_1) = \tilde{\Gamma}_l^{(4)}(\sigma_1', \mathbf{n}_1', 0, \sigma_2', \mathbf{n}_2', 0; \sigma_2, \mathbf{n}_2, 0, \sigma_1, \mathbf{n}_1, 0) \,. \tag{5.27}$$

As $\tilde{\Gamma}_l^{(4)}$ is antisymmetric with respect to the exchange of the incoming or the outgoing fermions this must also be true for $\tilde{g}_l$ under exchange of $\sigma_1'\mathbf{n}_1'$ and $\sigma_2'\mathbf{n}_2'$ as well as $\sigma_1\mathbf{n}_1$ and $\sigma_2\mathbf{n}_2$. Note that Eq. (5.27) defines an infinite number of couplings[9], one for each of the infinitely-many directions of the $\mathbf{n}_i$. However, as has been pointed out by Shankar [69], due to the restriction of momentum conservation the number of marginal couplings below those given by Eq. (5.27) is drastically reduced, while the majority is rendered irrelevant by this constraint. Within our formalism this property is inherent to the flow equation (4.50) from which we derive the exact flow equation for the couplings $\tilde{g}_l$,

$$\boxed{\begin{aligned}\partial_l \tilde{g}_l(\sigma_1'\mathbf{n}_1', \sigma_2'\mathbf{n}_2'; \sigma_2\mathbf{n}_2, \sigma_1\mathbf{n}_1) &= -2\eta_l\, \tilde{g}_l(\sigma_1'\mathbf{n}_1', \sigma_2'\mathbf{n}_2'; \sigma_2\mathbf{n}_2, \sigma_1\mathbf{n}_1) \\ &\quad + B_l(\sigma_1'\mathbf{n}_1', \sigma_2'\mathbf{n}_2'; \sigma_2\mathbf{n}_2, \sigma_1\mathbf{n}_1)\,,\end{aligned}} \tag{5.28}$$

where B_l is usually called the *β-function*, here defined by

$$B_l(\sigma_1'\mathbf{n}_1', \sigma_2'\mathbf{n}_2'; \sigma_2\mathbf{n}_2, \sigma_1\mathbf{n}_1) = \dot{\Gamma}_l^{(4)}(\sigma_1', \mathbf{n}_1', 0, \sigma_2', \mathbf{n}_2', 0; \sigma_2, \mathbf{n}_2, 0, \sigma_1, \mathbf{n}_1, 0)\,, \tag{5.29}$$

with $\dot{\Gamma}_l^{(4)}$ given by Eq. (4.51).

Finally let us turn our attention to the relation between the couplings of the rescaled and the unrescaled vertex functions. To this end we also expand the physical inverse Green function in powers of p and ω in its COC characterized by the radius of convergence R_Λ, see Eq. (5.15). Hence, as long as Λ is finite the expansion is expected to be well-defined, both for Fermi and non-Fermi liquids. Using Eqs. (4.1) and (4.24) we may write

$$\begin{aligned} &i\omega - \epsilon_{\mathbf{k}} + \mu - \Sigma_\Lambda(\mathbf{k}, i\omega) \\ &\quad = i\omega - \epsilon_{\mathbf{k}} + \epsilon_{\mathbf{k}_F} + \Gamma_\Lambda^{(2)}(\mathbf{k}, i\omega) &(5.30)\\ &\quad = Z_l^{-1}\left[i\omega - v_\Lambda p + \mu_\Lambda\right] + \mathcal{O}(p^2, \omega^2, p\omega)\,, &(5.31)\end{aligned}$$

where the velocity v_Λ is given by

$$v_\Lambda = v_F\, Z_l\Big[1 - \frac{|\boldsymbol{\nabla}_{\mathbf{k}}\, \Gamma_\Lambda^{(2)}(\mathbf{k}, i0)|_{\mathbf{k}=\mathbf{k}_F}}{v_F}\Big]\,, \tag{5.32}$$

[9] In $D = 1$ the number of couplings is finite since in this case there are just two possible directions for the $\mathbf{n}_i$.

and the chemical-potential parameter has been defined by

$$\mu_\Lambda = Z_l\,\Gamma^{(2)}_\Lambda(\mathbf{k}_F, i0) = -\,Z_l\,[\Sigma_\Lambda(\mathbf{k}_F, i0) - \Sigma(\mathbf{k}_F, i0)]\,. \tag{5.33}$$

For Fermi liquids we have $R_{\Lambda\to 0} > 0$ such that $v_{\Lambda\to 0}$ remains finite and coincides with the usual definition of the renormalized Fermi velocity. Due to $\Sigma_\Lambda(\mathbf{k}_F, i0) \to \Sigma(\mathbf{k}_F, i0)$ we also see that $\mu_\Lambda \to 0$; hence the chemical-potential parameter vanishes. This expresses the fact that we have expanded the energy dispersion at the true interacting FS, see Eq. (4.3).
In contrast, for non-Fermi liquids $R_\Lambda \to 0$ and we expect $|\boldsymbol{\nabla}_\mathbf{k}\,\Gamma^{(2)}_\Lambda(\mathbf{k}, i0)|_{\mathbf{k}=\mathbf{k}_F} \to \infty$ when $\Lambda \to 0$. On the other hand $|\partial_{i\omega}\Gamma^{(2)}_\Lambda(\mathbf{k}_F, i\omega)|_{\omega=0} \to \infty$ such that according to Eq. (4.16) $Z_l \to 0$, resulting in two competing effects in Eq. (5.32). Provided that $\partial_{i\omega}\Gamma^{(2)}_\Lambda(\mathbf{k}_F, i\omega)|_{\omega=0} \to +\infty$ this implies

$$v_\Lambda \;\stackrel{\Lambda\to 0}{\longrightarrow}\; \frac{|\boldsymbol{\nabla}_\mathbf{k}\,\Gamma^{(2)}_\Lambda(\mathbf{k}, i0)|_{\mathbf{k}=\mathbf{k}_F}}{\partial_{i\omega}\Gamma^{(2)}_\Lambda(\mathbf{k}_F, i\omega)|_{\omega=0}} = \frac{|\boldsymbol{\nabla}_\mathbf{k}\,\Sigma_\Lambda(\mathbf{k}, i0)|_{\mathbf{k}=\mathbf{k}_F}}{\partial_{i\omega}\Sigma_\Lambda(\mathbf{k}_F, i\omega)|_{\omega=0}}\,, \tag{5.34}$$

which may well be finite if the numerator and the denominator have the same degree of divergence. But it is also clear that we should no longer interpret v_Λ as a Fermi velocity since the expansion (5.31) and hence the quasi-particle picture breaks down when Λ reduces to zero. On the other hand we still have $\mu_{\Lambda\to 0} = 0$ like for Fermi liquids. It is important to notice that even if the couplings related to an expansion of $\Gamma^{(2)}_\Lambda$ diverge due to a vanishing radius of convergence their physically relevant combinations, like for instance the velocity v_Λ, may remain finite.
Let us now stress the relation to the dimensionless couplings. This is easily done using Eqs. (4.9), (4.22) and (5.24) to give

$$\tilde{v}_l = \frac{v_\Lambda}{v_F} = Z_l\Big[1 - \frac{|\boldsymbol{\nabla}_\mathbf{k}\,\Gamma^{(2)}_\Lambda(\mathbf{k}, i0)|_{\mathbf{k}=\mathbf{k}_F}}{v_F}\Big]\,, \tag{5.35}$$

and

$$\tilde{\mu}_l = \Lambda^{-1}\mu_\Lambda = -\,\Lambda^{-1}Z_l\,[\Sigma_\Lambda(\mathbf{k}_F, i0) - \Sigma(\mathbf{k}_F, i0)]\,. \tag{5.36}$$

For the marginal part of the four-point vertex we just have to set $q = \epsilon = 0$ in Eq. (4.29) for $n = 2$, yielding

$$\begin{aligned}\tilde{g}_l(\sigma_1'\mathbf{n}_1', \sigma_2'\mathbf{n}_2; \sigma_2\mathbf{n}_2, \sigma_1\mathbf{n}_1) &= \nu_0\, Z_l^2 \\ &\times\Gamma^{(4)}_\Lambda(\sigma_1', \mathbf{k}_{F,1}', 0, \sigma_2', \mathbf{k}_{F,2}', 0; \sigma_2, \mathbf{k}_{F,2}, 0, \sigma_1, \mathbf{k}_{F,1}, 0)\,.\end{aligned} \tag{5.37}$$

From Eq. (5.35) we see that the couplings $\tilde{v}_l$ and v_Λ only differ by the constant prefactor $1/v_F$ so that for Fermi liquids $\tilde{v}_l$ is indeed identical with the renormalization factor of the Fermi velocity. For the couplings $\tilde{\mu}_l$ and μ_Λ we see that they behave quite differently when $l \to \infty$. We have already seen that $\mu_\Lambda \to 0$, but $\tilde{\mu}_l$ may reach a finite fixed-point value or even diverge. The physical meaning of $\tilde{\mu}_l$ is best understood if we consider the second equality in Eq. (5.36) at $l = 0$,

$$\tilde{\mu}_0 = - Z_0 \, \Lambda_0^{-1} \left[\Sigma_{\Lambda_0}(\mathbf{k}_F, i0) - \Sigma(\mathbf{k}_F, i0) \right], \tag{5.38}$$

As Σ is by definition the self-energy at the fixed point and Σ_{Λ_0} the self-energy at the initial scale Λ_0 (which is often set equal to zero) we see that $\tilde{\mu}_0$ is proportional to the interaction contribution to the chemical potential between the scales $l = 0$ and $l = \infty$. To lowest order in perturbation theory it is given by the usual Hartree and Fock contributions. Note that this enables us to determine the initially unknown counter term $\Sigma(\mathbf{k}_F, i0)$ from the fixed-point condition for the chemical potential parameter $\tilde{\mu}_l$ in Eq. (5.20). In Ref. [90] this fact is used to derive an exact integral equation that allows for a self-consistent calculation of the interacting FS.
Finally, from Eq. (5.38) we see that the couplings $\tilde{g}_l(\sigma_1' \mathbf{n}_1', \sigma_2' \mathbf{n}_2; \sigma_2 \mathbf{n}_2, \sigma_1 \mathbf{n}_1)$ are essentially the dimensionless versions of the momentum- and frequency-independent part of the four-point vertex $\Gamma_\Lambda^{(4)}$. However, the field-rescaling factor Z_l, which may be different from one or even vanish when $l \to \infty$, appears as a prefactor in Eq. (5.38). As we have emphasized above for non-Fermi liquids the physical self-energy is expected to be a non-analytic function at $p = \omega = 0$. This will in general also be true for $\Gamma_\Lambda^{(4)}$, and like for $\Gamma_\Lambda^{(2)}$ this can result in a runaway-flow of the couplings $\Gamma_\Lambda^{(4)}(\sigma_1', \mathbf{k}_{F,1}', 0, \sigma_2', \mathbf{k}_{F,2}', 0; \sigma_2, \mathbf{k}_{F,2}, 0, \sigma_1, \mathbf{k}_{F,1}, 0)$.[10] If these divergeancies only appear at the two-loop level it is important to notice that they may be compensated by a vanishing Z_l-factor such that $\tilde{g}_l(\sigma_1' \mathbf{n}_1', \sigma_2' \mathbf{n}_2; \sigma_2 \mathbf{n}_2, \sigma_1 \mathbf{n}_1)$ in Eq. (5.38) remains finite. We shall give an explicit example for such a scenario in Sec. 6.3 when we calculate the two-loop β-function of the spinless g_2-model. But even for Fermi liquids where both kinds of couplings are expected to approach finite fixed-point values the quasi-particle residue will in general be different from one at the fixed point, i.e. $0 < Z < 1$, implying that the unrescaled couplings will in general approach the wrong fixed-point values.

[10] The non-analyticity of the four-point vertex at vanishing momenta and frequencies is the actual reason for the breakdown of perturbation theory in non-Fermi liquids. Typically, expansions of $\Gamma_\Lambda^{(4)}$ in powers of its momentum- and frequency-independent part yield logarithmically divergent contributions that indecate the non-analyticity at $p = \omega = 0$.

5.4 Flow Equations for the Subtracted Vertices

Following the determination of the relevant and marginal couplings let us now focus on yet another conceptional subtlety originally pointed out by Polchinski [39]. Note that even if we restrict ourselves to the classical RG task of determining the flow of coupling constants, we need for instance to calculate the susceptibilities obtained from a weak-coupling expansion of the four-point vertex within our formalism. In fact we have to calculate their full dependence on momenta, frequencies and the logarithmic flow parameter l. Consequently, we have to resum an infite number of irrelevant couplings to obtain these functions. To ensure that they approach finite fixed-point expressions it is necessary to subtract off their marginal and relevant parts, since only the subtracted vertices will become local functions of the relevant and marginal couplings when the fixed-point manifold is approached [39]. The way we have to implement this important feature of the RG within our formalism has already been described in the context of ϕ^4 theory in Ref. [46]. This is why we shall be rather brief here.
As we have seen in the previous section there are just one relevant ($\tilde{\mu}_l$) and two marginal couplings (Z_l and $\tilde{v}_l$) related to the two-point vertex of rotationally invariant systems. In addition for the four-point vertex only the momentum and frequency independent part is marginal. This gives rise to the subsequent definitions, starting with the two-point vertex,

$$\begin{aligned}\tilde{\Gamma}_l^{(2,sub)}(Q) &= \tilde{\Gamma}_l^{(2)}(Q) - \tilde{\Gamma}_l^{(2)}(\sigma, \mathbf{n}, 0, i0) \\ &\quad -i\epsilon\, \partial_{i\epsilon} \tilde{\Gamma}_l^{(2)}(Q)\big|_{Q=0} - q\, \partial_q \tilde{\Gamma}_l^{(2)}(Q)\big|_{Q=0} \\ &= \tilde{\Gamma}_l^{(2)}(Q) - \tilde{\mu}_l - i\epsilon(1 - Z_l) - q(Z_l - \tilde{v}_l)\,. \end{aligned} \tag{5.39}$$

The rescaled inverse propagator defined in Eq. (5.24) can then be written as

$$\tilde{r}_l(Q) = i\epsilon - \tilde{v}_l q + \tilde{\mu}_l + \tilde{\Gamma}_l^{(2,sub)}(Q)\,. \tag{5.40}$$

The irrelevant part of the four-point vertex is obtained by subtracting its marginal part,

$$\begin{aligned}&\tilde{\Gamma}_l^{(4,sub)}(Q_1', Q_2'; Q_2, Q_1) \\ &= \tilde{\Gamma}_l^{(4)}(Q_1', Q_2'; Q_2, Q_1) - \tilde{\Gamma}_l^{(4)}(Q_1', Q_2'; Q_2, Q_1)\big|_{Q_i'=Q_i=0} \\ &= \tilde{\Gamma}_l^{(4)}(Q_1', Q_2'; Q_2, Q_1) - \tilde{g}_l(\sigma_1' \mathbf{n}_1', \sigma_2' \mathbf{n}_2'; \sigma_2 \mathbf{n}_2, \sigma_1 \mathbf{n}_1)\,. \end{aligned} \tag{5.41}$$

For the higher-order vertices no subtraction is needed as their momentum- and frequency-independent parts are already irrelevant.

The flow equations for $\tilde{\Gamma}_l^{(2,sub)}$ and $\tilde{\Gamma}_l^{(4,sub)}$ can now easily be derived by differentiating Eqs. (5.39) and (5.41) with respect to the flow parameter l and using the original flow equations (4.45) and (4.50). This yields

$$\boxed{\partial_l \tilde{\Gamma}_l^{(2,sub)}(Q) = (1 - \eta_l - Q \cdot \partial_Q)\tilde{\Gamma}_l^{(2,sub)}(Q) + \dot{\Gamma}_l^{(2,sub)}(Q)} \tag{5.42}$$

for the subtracted two-point vertex, where we have defined

$$\begin{aligned} \dot{\Gamma}_l^{(2,sub)}(Q) &= \dot{\Gamma}_l^{(2)}(Q) - \dot{\Gamma}_l^{(2)}(\sigma, \mathbf{n}, 0, i0) - i\epsilon\, \partial_{i\epsilon} \dot{\Gamma}_l^{(2)}(Q)\big|_{Q=0} \\ &\quad -q\, \partial_q \dot{\Gamma}_l^{(2)}(Q)\big|_{Q=0}\,, \end{aligned} \tag{5.43}$$

and

$$\boxed{\begin{aligned} &\partial_l \tilde{\Gamma}_l^{(4,sub)}(Q_1', Q_2'; Q_2, Q_1) = \\ &\Big[-2\,\langle \eta_l \rangle_4 - \textstyle\sum_{i=1}^{2} \Big(Q_i' \cdot \partial_{Q_i'} + Q_i \cdot \partial_{Q_i} \Big) \Big]\, \tilde{\Gamma}_l^{(4,sub)}(Q_1', Q_2'; Q_2, Q_1) \\ &+ \dot{\Gamma}_l^{(4,sub)}(Q_1', Q_2'; Q_2, Q_1) \end{aligned}} \tag{5.44}$$

for the subtracted four-point vertex. Here we have

$$\begin{aligned} &\dot{\Gamma}_l^{(4,sub)}(Q_1', Q_2'; Q_2, Q_1) = \\ &\dot{\Gamma}_l^{(4)}(Q_1', Q_2'; Q_2, Q_1) - \dot{\Gamma}_l^{(4)}(\sigma_1', \mathbf{n}_1', 0, \sigma_2', \mathbf{n}_2', 0; \sigma_2, \mathbf{n}_2, 0, \sigma_1, \mathbf{n}_1, 0)\,. \end{aligned} \tag{5.45}$$

Eqs. (5.42) and (5.44) are formally identical with their unsubtracted analogues in Eqs. (4.45) and (4.50) , and obviously the integral representation (4.57) is then still valid if we replace $\tilde{\Gamma}_l^{(2n)}$ and $\dot{\Gamma}_l^{(2n)}$ with $\tilde{\Gamma}_l^{(2n,sub)}$ and $\dot{\Gamma}_l^{(2n,sub)}$, respectively.

Part II

Application to the Spinless g_2-Model

Chapter 6

Self-Consistent Two-Loop Calculation

In this chapter we define the initial action of the basic model considered throughout the rest of this work. We show how the infinite hierarchy of flow equations may be truncated systematically by a weak-coupling expansion and determine the flow of the relevant and marginal couplings up to the two-loop order. In particular we demonstrate that the two-loop β-function, which determines the flow of the momentum- and frequency independent part of the four-point vertex $\tilde{g}_l$, only vanishes if (1) we use the rescaled instead of the unrescaled flow equations and (2) if we introduce the Dirac sea. Without Dirac sea the coupling $\tilde{g}_l$ exhibits a small flow to a non-vanishing fixed-point value different from its initial value $\tilde{g}_0$.

6.1 Initial Conditions and Cutoff Dependence

In Sec. 1.2 we have motivated and introduced the Hamiltonian of the Tomonaga-Luttinger model (TLM), which we shall study now by means of the ERG formalism developed in the first part of this work. In particular we will take explicit care of the role of the ultraviolet band cutoff Λ_0 of the RG. As we are going to perform a complete two-loop calculation for the two- and the four-point vertex, which involves very lengthy calculations, we shall further simplify the Hamiltonian $\hat{H}$ in Eq. (1.5). Firstly, we will neglect the spin degree of freedom, although it accounts for interesting features like spin-charge separation. However, the resulting spinless TLM is still an interesting and non-trivial many-body problem which exhibits non-Fermi liquid features. Secondly, we shall neglect the initial momentum dependence of the Landau parameters and replace them by coupling constants. According to Sec. 5.3 this amounts to the neglect of infinitely-many irrelevant couplings, which is consistent with the usual procedure in RG calcu-

lations. It will then essentially be the band cutoff Λ_0 that mimics the effects of a finite interaction range. Hence, our initial Hamiltonian will be given by Eqs. (1.5)–(1.7) without the spin summations and with the replacements $g_2^{\sigma\sigma'}(q) \to g_2$ and $g_4^{\sigma\sigma'}(q) \to g_4$. However, since we shall keep the ultraviolet cutoff Λ_0 finite the problem of an infinite ground-state energy does not occur, such that principally we do not need the normal ordering of the creation and annihilation operators in Eq. (1.6). Furthermore, due to the fact that the field operators anti-commute g_4-processes are excluded from the initial Hamiltonian when coupling *constants* are used, since g_4-scattering exclusively involves fermions located on the same energy branch, see Sec. 1.2. Consequently, the model we are going to study we shall call the *spinless g_2-model*.

Let us now turn our attention to the role of Λ_0. For the construction of the RG one essentially needs an energy-band cutoff that truncates excitations with energies larger than some maximum value Λ_0. We have already emphasized that this energy scale may be chosen to be proportional to the inverse lattice constant and thus has a physical significance. The way in which RG calculations are usually implemented opens up yet another interpretation. As has been emphasized above Λ_0 may also be viewed as simulating the range of the interaction in Fourier space due to the neglect of the momentum dependence of the initial Landau interaction parameters. We may then identify $\Lambda_0 \equiv v_F p_c$, where p_c is the characteristic momentum range of the interaction. Of course this will at best be a crude approximation if one intends to study the effects of the interaction range, since the detailed dependence on p_c will actually be different. However, due to the fact that the momentum- and frequency-dependent part of the four-point vertex is related to irrelevant couplings we conclude that Λ_0 *should be considered as an effective irrelevant parameter of the model reflecting some of the non-universal features of physical system.* [1] The situation is thus rather different from quantum field theory where physically meaningful results must not depend on the actual value of Λ_0 and the limit $\Lambda_0 \to \infty$ has to be performed at the end of the calculation to recover the continuous structure of space-time.

Subsequently we will study is the spinless g_2-model with *finite* Λ_0 and assume $\Lambda_0 \ll v_F k_F/2$, reflecting the fact that the linearization of the energy dispersion is only justified for momenta small compared to k_F, see Fig. 1.1. This is why our model should better be compared to the original Tomonaga model where the artificial Dirac sea (introduced in favor of the exact solubility of the TLM) is absent. However, just like in the TLM we will introduce right- and left-movers with assigned creation and annihilation operators to maintain the possibility of

[1] This interpretation is also supported by the "flow equation" of $\Lambda = \Lambda_0 e^{-l}$ which reads $\partial_l \Lambda = -\Lambda$. This implies that Λ has the scaling dimension $d_s = -1$ and is hence irrelevant by construction.

performing the limit $\Lambda_0 \to \infty$. This limit turns out to be basically equivalent to the introduction of the Dirac sea if Λ is treated as an independent parameter, a point which will be discussed in detail in Sec. 6.4 . According to this we will be able to study the consequences if the Dirac sea is introduced.
Let us now express the assumptions about the initial Hamiltonian in the form we need it within our ERG formalism. Due to the initial condition for the flow of the generating functional $\Gamma^{\Lambda}[\bar{\varphi}, \varphi]$ given in Eq. (3.36) we need to fix the Grassman representation $S_{\rm int}[\bar{\varphi}, \varphi]$ of the action related to the interaction part $\hat{H}_{\rm int}$ of the Hamiltonian (1.7). Furthermore we have to determine the structure of the function $\xi(k)$ within the exact Green function $G_{\Lambda}(K)$ which follows from the non-interacting part $\hat{H}_0$.
First of all in one dimension we know by Luttinger's theorem [75], which also holds in one-dimensional systems [76], that the interacting Fermi vector coincides with the non-interacting k_F. With respect to this k_F we linearize the energy dispersion which amounts to approximate Eq. (4.3) by

$$\xi(k) \approx v_F(k - k_F) \,. \tag{6.1}$$

This is assumed to be justified in the momentum interval $k_F - \Lambda_0/v_F < |k| < k_F + \Lambda_0/v_F$, see Fig. 1.1. If we decompose $k = \alpha(k_F + p)$ and introduce $K \equiv (k, i\omega) = (\alpha(k_F + p), i\omega)$, where $\alpha = +1$ labels the right and $\alpha = -1$ labels the left Fermi point, the cutoff-dependent exact propagator explicitly reads

$$G_{\Lambda}(K) = \frac{\Theta(\Lambda < |v_F p| < \Lambda_0)}{i\omega - v_F p + \Gamma^{(2)}_{\Lambda}(K)} \,, \tag{6.2}$$

where we have set $\Omega_K = v_F|k - k_F| = |v_F p|$ in Eq. (3.4). Furthermore let us write the initial condition (3.36) for the generating functional $\Gamma^{\Lambda_0}[\bar{\varphi}, \varphi]$ as follows,

$$\begin{aligned} \Gamma^{\Lambda_0}[\bar{\varphi}, \varphi] &= S_{\rm int}[\bar{\varphi}, \varphi] \\ &= \frac{1}{(2!)^2} \int_{K_1'} \int_{K_2'} \int_{K_2} \int_{K_1} \delta(K_1' + K_2' - K_2 - K_1) \\ &\quad \times \Gamma^{(4)}_{\Lambda_0}(K_1', K_2'; K_2, K_1)\, \bar{\varphi}_{K_1'} \bar{\varphi}_{K_2'} \varphi_{K_2} \varphi_{K_1} \,. \end{aligned} \tag{6.3}$$

Here the integrations are given by

$$\int_K = \sum_{\alpha} \int_{-k_F}^{\infty} \frac{dp}{2\pi} \int_{-\infty}^{\infty} \frac{d\omega}{2\pi} \,, \tag{6.4}$$

which can formally be obtained from Eq. (3.37) by introducing spherical coordinates and shifting the radial integration according to $k = k_F + p$. The angular

integration in $D = 1$ then turns into the summation over the branch index α. Set up in this way a positive p always refers to a point that is located outside the Fermi sea which is different from the corresponding definitions commonly used in the bosonization literature. The δ-function in Eq. (6.3) is given by Eq. (3.39) with σ replaced by α. Finally and most importantly the initial antisymmetrized four-point vertex is defined as follows,

$$\Gamma^{(4)}_{\Lambda_0}(K_1', K_2'; K_2, K_1) = A_{\alpha_1'\alpha_2';\,\alpha_2\alpha_1}\, g_0\,, \tag{6.5}$$

which means that only a single interaction constant g_0 is present in the initial action. The antisymmetry with respect to the exchanges $K_1' \leftrightarrow K_2'$ or $K_1 \leftrightarrow K_2$ on the l.h.s. is reflected on the r.h.s. by the definition

$$A_{\alpha_1'\alpha_2';\,\alpha_2\alpha_1} = D_{\alpha_1'\alpha_2';\alpha_2\alpha_1} - E_{\alpha_1'\alpha_2';\alpha_2\alpha_1}\,, \tag{6.6}$$

with

$$D_{\alpha_1'\alpha_2';\alpha_2\alpha_1} = \delta_{\alpha_1'\alpha_1}\delta_{\alpha_2'\alpha_2} \qquad \text{(direct term)} \tag{6.7}$$

$$E_{\alpha_1'\alpha_2';\alpha_2\alpha_1} = \delta_{\alpha_1'\alpha_2}\delta_{\alpha_2'\alpha_1} \qquad \text{(exchange term)}\,. \tag{6.8}$$

It is then easy to verify that

$$A_{\alpha_1'\alpha_2';\,\alpha_2\alpha_1} = -A_{\alpha_1'\alpha_2';\,\alpha_1\alpha_2} = -A_{\alpha_2'\alpha_1';\,\alpha_2\alpha_1}\,. \tag{6.9}$$

As a direct consequence $A_{\alpha\alpha;\alpha\alpha} = 0$ which means that forward scattering between spinless fermions located on the same energy branch is excluded, i.e. g_4-processes do not occur in the initial action. As emphasized above this exclusion is due to the fact that we have neglected the initial momentum (and frequency) dependence of $\Gamma^{(4)}_{\Lambda_0}$. Note, however, that g_4-processes will indeed be generated by the interaction given in Eq. (6.3) in higher orders of perturbation theory. This is illustrated in Fig. 6.1 **a)** and **b)**. Hence, the coupling g_0 itself represents an initial g_2-process. Finally let us fix the initial condition for the *rescaled* four-point vertex, which can directly be obtained from Eq. (6.5) together with the scaling relation (4.29),

$$\tilde{\Gamma}^{(4)}_{l=0}(Q_1', Q_2'; Q_2, Q_1) = A_{\alpha_1'\alpha_2';\,\alpha_2\alpha_1}\tilde{g}_0\,, \tag{6.10}$$

with

$$\tilde{g}_0 = \nu_0 g_0 = \frac{g_0}{\pi v_F}\,, \tag{6.11}$$

denoting the dimensionless interaction constant. We have used $Z_{l=0} = 1$ and the fact that the non-interacting density of states in one dimension is given by $\nu_0 = 1/(\pi v_F)$. For arbitrary values of the flow parameter l we define

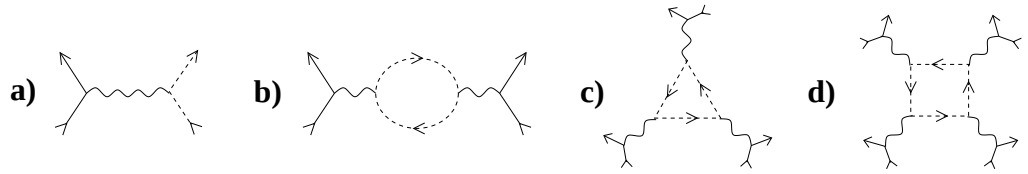

Figure 6.1: **a)** Graphical representation of the vertex g_0 in Eq. (6.5). The solid arrows correspond to the right Fermi point $+k_F$ while the dashed arrows belong to the left Fermi point $-k_F$. In this way g_0 represents a g_2-scattering amplitude. **b)** Second-order Feynman diagram representing an effective g_4-type interaction composed of two g_2-vertices. The external legs all correspond to the right Fermi point. **c)** Simplest one-loop Feynman graph that contributes to the six-point vertex. **d)** Simplest one-loop Feynman graph that contributes to the eight-point vertex. The corresponding analytical expression is of order $\sim \tilde{g}_l^4$ and can be neglected within a two-loop calculation for the four-point vertex.

$$\tilde{\Gamma}_l^{(4)}(\alpha_1', 0, \alpha_2', 0; \alpha_2, 0, \alpha_1, 0) = A_{\alpha_1'\alpha_2';\alpha_2\alpha_1}\tilde{g}_l \;, \tag{6.12}$$

and the dimensionless analogy of Eq. (6.2) reads

$$\tilde{G}_l(Q) = \frac{\Theta(1 < |q| < e^l)}{Z_l[i\epsilon - q] + \tilde{\Gamma}_l^{(2)}(Q)} = \frac{\Theta(1 < |q| < e^l)}{i\epsilon - \tilde{v}_l q + \tilde{\mu}_l + \tilde{\Gamma}_l^{(2,sub)}(Q)} \,, \tag{6.13}$$

where we have set $Q = (\alpha, q, i\epsilon)$ and used Eq. (5.40) for the second equality.

6.2 One-Loop Flow

Before we turn our attention to explicit calculations we have to clarify the general approximation strategy used to truncate the infinite hierarchy of flow-equations determined by Eq. (4.49). We have already pointed out that the flow of $\tilde{\Gamma}_l^{(2n)}$ couples to the higher-order vertex $\tilde{\Gamma}_l^{(2n+2)}$ via the inhomogeneity $\dot{\Gamma}_l^{(2n)}$. A systematic truncation is then given by a *weak-coupling loop-expansion* of $\dot{\Gamma}_l^{(2n)}$. This can be seen by noting that in each connected Feynman graph a fixed relation between the number V of bare vertices, the number E of external legs and the number L of loops exists, which is given by $V = L - 1 + E/2$. From this follows

$$V = E/2 \qquad \text{(one-loop calculation)}\,, \tag{6.14}$$

$$V = E/2 + 1 \qquad \text{(two-loop calculation)}\,. \tag{6.15}$$

Eqs. (6.14) and (6.15) imply that if we want to perform one-loop calculations for the two-point vertex ($E = 2$) and the four-point vertex ($E = 4$) we have to retain

all terms of order $\sim \tilde{g}_l$ in the first and all terms of order $\sim \tilde{g}_l^2$ in the second case. Equivalently, for a two-loop calculation we need all terms of order $\sim \tilde{g}_l^2$ for the two-point vertex and all terms of order $\sim \tilde{g}_l^3$ for the four-point vertex. We may thus identify the loop order by simply counting the powers of the coupling $\tilde{g}_l$.[2] Now, for a one-loop calculation of the β-function we can thus neglect the contribution of the six-point vertex in Eq. (4.50), as the simplest connected diagram with six external legs is, according to Eq. (6.14), of order $\sim \tilde{g}_l^3$. However, for a two-loop calculation of the β-function we need to retain $\tilde{\Gamma}_l^{(6)}$ but we can neglect the contribution of $\tilde{\Gamma}_l^{(8)}$ as it gives rise to terms of order $\sim \tilde{g}_l^4$ (see Fig. 6.1 **d)**). Having found a systematic way for truncating the hierarchy of flow equations we still have to clarify by what the exact propagators $\dot{G}_l$ and $\tilde{G}_l$ in the flow equations should be approximated? – A first answer could be to replace them by their non-interacting versions if we otherwise expand in powers of $\tilde{g}_l$. But remember that we have linearized the energy dispersion with respect to the interacting FS, which is indeed essential. Although in one-dimensional systems the interacting and the non-interacting k_F coincide, in general they do not. Thus we have to keep interaction effects in the zeroth order Green function anyway. Furthermore we know that the parameters $\tilde{v}_l$ and $\tilde{\mu}_l$ within the inverse propagator $\tilde{r}_l(q, i\epsilon)$ in Eq. (5.40) are marginal or rather relevant. It is then more careful to take them self-consistently into account, *as long as we do not know their destinations at the fixed point.* We will thus proceed as follows: In a first step we approximate the propagator in Eq. (6.13) by

$$\tilde{G}_l(Q) \approx \frac{\Theta(1 < |q| < e^l)}{i\epsilon - \tilde{v}_l q + \tilde{\mu}_l}, \tag{6.16}$$

which amounts to setting $\tilde{\Gamma}_l^{(2,sub)} = 0$. Using Eq. (5.18) we will then determine the destination of $\tilde{\mu}_l$ self-consistently. According to Eq. (5.20) this implies a fine-tuning of the initial condition to keep the density of the system fixed. We will find $\tilde{\mu}_l$ to be proportional to $\tilde{g}_l$ and it is then consequent to further approximate the denominator of Eq. (6.16) by $\tilde{r}_l(Q) \approx i\epsilon - \tilde{v}_l q$ within a weak-coupling expansion, as keeping $\tilde{\mu}_l$ would give rise to higher orders in $\tilde{g}_l$. For the Green functions $\dot{G}_l$ and $\tilde{G}_l$ this means that we will replace them by

$$\dot{G}_l^0(Q) = \frac{\delta(|q| - 1)}{i\epsilon - \tilde{v}_l q} \quad \text{and} \quad \tilde{G}_l^0(Q) = \frac{\Theta(1 < |q| < e^l)}{i\epsilon - \tilde{v}_l q}, \tag{6.17}$$

respectively. Note that we still keep $\tilde{v}_l$ self-consistently. When it seems convenient we will switch between the notations $\tilde{G}_l(Q)$ and $\tilde{G}_l(q, i\epsilon)$ keeping in mind that

[2] Remember that the flow equations (4.49) formally are one-loop equations. The higher loop-orders are generated by iteration of the flow equations.

due to time-reversal symmetry the Green function is independent of the branch index α. Note as well that we have

$$\dot{G}_l^0(-q,-i\epsilon) = -\dot{G}_l^0(q,i\epsilon)\,, \tag{6.18}$$

and analogous for $\tilde{G}_l^0$, reflecting the perfect symmetry between particle and hole excitations within our model. Let us now calculate the flow of the couplings $\tilde{\mu}_l$, Z_l and $\tilde{v}_l$ at one-loop order, which implies that we have to retain all contributions of order $\tilde{g}_l$ to the inhomogeneity $\dot{\Gamma}_l^{(2)}$ in the flow equation (4.45). We start with $\tilde{\mu}_l$ using Eqs. (5.18) and (4.46) and get

$$\begin{aligned} \partial_l\tilde{\mu}_l &= (1-\eta_l)\tilde{\mu}_l - \int_{Q'} \dot{G}_l(Q')\,\tilde{\Gamma}_l^{(4)}(Q,Q';Q',Q) && (6.19)\\ &= \tilde{\mu}_l - \tilde{g}_l \int_Q \frac{\delta(|q|-1)\,e^{i\epsilon 0^+}}{i\epsilon - \tilde{v}_l q + \tilde{\mu}_l} A_{\alpha\alpha';\alpha'\alpha} + \mathcal{O}(\tilde{g}_l^2)\,. && (6.20) \end{aligned}$$

In the second line we have used the fact that $\eta_l \sim \tilde{g}_l^2$ which is obvious from simple perturbation theory and we have inserted the convergence factor $e^{i\epsilon 0^+}$ to regularize the integration. The dimensionless integration is given by Eq. (4.12) for $D=1$ without the spin summation and with the angular integration replaced by a sum over the branch index α. Note that $\Omega_{D=1}=2$ which explicitly yields

$$\int_Q = \sum_\alpha \int_{-\infty}^{\infty} \frac{dq}{2} \int_{-\infty}^{\infty} \frac{d\omega}{2\pi} = \sum_\alpha \int_Q{}' \,. \tag{6.21}$$

Observe that we have replaced the lower boundary $-v_F k_F/\Lambda$ of the q-integration by $-\infty$. This is justified by our assumption that $\Lambda_0 \ll v_F k_F/2$ and hence $-v_F k_F/\Lambda = -v_F k_F e^l/\Lambda_0 \ll -2e^l$, combined with the fact that the q-integration always appears in combination with $\delta(|q|-1)$ or $\Theta(1<|q|<e^l)$. The integrations in Eq. (6.20) may then easily be performed and we obtain

$$\partial_l\tilde{\mu}_l = \tilde{\mu}_l - \frac{\tilde{g}_l}{2}[\Theta(\tilde{\mu}_l+\tilde{v}_l) + \Theta(\tilde{\mu}_l-\tilde{v}_l)] + \mathcal{O}(\tilde{g}_l^2)\,. \tag{6.22}$$

If nothing drastical happens $\tilde{v}_l$ will remain of the order of unity as $\tilde{v}_0=1$. By a self-consistency argument we may then assume $\tilde{\mu}_l < \tilde{v}_l$ and obtain at one-loop order

$$\boxed{\partial_l\tilde{\mu}_l = \tilde{\mu}_l - \frac{\tilde{g}_l}{2}\,.} \tag{6.23}$$

From this equation it is obvious that if we set $\tilde{\mu}_l = \tilde{g}_l/2$ for all values of l, which also implies that the initial condition is given by

$$\tilde{\mu}_0 = \frac{\tilde{g}_0}{2}\,, \tag{6.24}$$

$\tilde{\mu}_l$ will reach a finite fixed-point value whenever $\tilde{g}_l$ does. We will see shortly that $\tilde{g}_l$ and $\tilde{v}_l$ do not flow at all at one-loop level, such that our assumption $\tilde{\mu}_l < \tilde{v}_l$ is justified a posteriori and Eq. (6.23) is indeed the correct flow equation for $\tilde{\mu}_l$ if we keep the density fixed.
Now, to determine the flow of Z_l and $\tilde{v}_l$ we just have to notice that a momentum and frequency dependence of the four-point vertex is only generated at the order $\tilde{g}_l^2$ as the initial value is a constant, see Eq. (6.11). From Eqs. (5.25) and (4.46) we then immediately get

$$\boxed{\begin{aligned} \partial_l Z_l &= 0\,, \\ \partial_l \tilde{v}_l &= 0\,, \end{aligned}} \tag{6.25}$$

implying

$$Z_l = \tilde{v}_l = 1\,, \tag{6.26}$$

which follows from the initial conditions $Z_{l=0} = \tilde{v}_{l=0} = 1$. As a direct consequence we see that at this level the anomalous dimension defined in Eq. (4.35) must vanish

$$\boxed{\eta_l = -\tfrac{\partial_l Z_l}{Z_l} = 0\,.} \tag{6.27}$$

Finally let us turn our attention to the one-loop β-function. Here some more work is necessary. First of all from Eq. (5.28) we get

$$\partial_l \tilde{g}_l = -2\eta_l \tilde{g}_l + B_l\,, \tag{6.28}$$

where we have identified $\tilde{g}_l(\mathbf{n}_1', \mathbf{n}_2'; \mathbf{n}_2, \mathbf{n}_1)$ with $\tilde{g}_l A_{\alpha_1'\alpha_2';\,\alpha_2\alpha_1}$ as well as $B_l(\mathbf{n}_1', \mathbf{n}_2'; \mathbf{n}_2, \mathbf{n}_1)$ with $A_{\alpha_1'\alpha_2';\,\alpha_2\alpha_1} B_l$. Furthermore we have set $\alpha_1' = \alpha_1 = \alpha$ and $\alpha_2' = \alpha_2 = -\alpha \equiv \bar{\alpha}$ and used that due to Eq. (6.6) we have $A_{\alpha,\bar{\alpha};\bar{\alpha},\alpha} = 1$. The β-function B_l is then explicitly given by

$$B_l = \dot{\Gamma}_l^{(4)}(\alpha, 0, \bar{\alpha}, 0\,; \bar{\alpha}, 0, \alpha, 0)\,. \tag{6.29}$$

We could now proceed by directly calculating $\dot{\Gamma}_l^{(4)}$ for vanishing momenta and frequencies as it is needed in Eq. (6.29). For later purposes it is however convenient to draw some more general results and to calculate the full momentum- and frequency-dependent function $\dot{\Gamma}_l^{(4)}(Q_1', Q_2'; Q_2, Q_1)$ up to the perturbative order $\sim \tilde{g}_l^2$. To this end we have to replace $\tilde{\Gamma}_l^{(4)}(Q_1', Q_2'; Q_2, Q_1)$ on the r.h.s. of Eq. (4.51) by $\tilde{g}_l\, A_{\alpha_1'\alpha_2';\,\alpha_2\alpha_1}$ as well as $\tilde{G}_l$ and $\dot{G}_l$ by $\tilde{G}_l^0$ and $\dot{G}_l^0$. This yields

$$\begin{aligned}
\dot{\Gamma}_l^{(4)}(Q_1', Q_2'; Q_2, Q_1) &= \tilde{g}_l^2 \sum_\alpha \Big\{ -\frac{1}{2} A_{\alpha_1'\alpha_2';\alpha'\alpha} A_{\alpha\alpha';\alpha_2\alpha_1} \\
&\quad \times \int_Q{}' \left[\dot{G}_l^0(Q)\tilde{G}_l^0(Q') + \dot{G}_l^0(Q')\tilde{G}_l^0(Q)\right]_{K'=K_1+K_2-K} \\
&\qquad + A_{\alpha_1'\alpha';\alpha\alpha_1} A_{\alpha_2'\alpha;\alpha'\alpha_2} \\
&\quad \times \int_Q{}' \left[\dot{G}_l^0(Q)\tilde{G}_l^0(Q') + \dot{G}_l^0(Q')\tilde{G}_l^0(Q)\right]_{K'=K_1-K_1'+K} \\
&\qquad - A_{\alpha_2'\alpha';\alpha\alpha_1} A_{\alpha_1'\alpha;\alpha'\alpha_2} \\
&\quad \times \int_Q{}' \left[\dot{G}_l^0(Q)\tilde{G}_l^0(Q') + \dot{G}_l^0(Q')\tilde{G}_l^0(Q)\right]_{K'=K_1-K_2'+K} \Big\} \\
&\qquad + \mathcal{O}(\tilde{g}_l^3)\,. \qquad (6.30)
\end{aligned}$$

In a next step we are going to perform the α-sum and define the following three auxiliary functions,

$$\begin{aligned}
\dot{\Pi}_l(Q) &= \frac{1}{2}\int_{Q'}{}' \Big[\dot{G}_l^0(q', i\epsilon')\,\tilde{G}_l^0(q'+q, i\epsilon'+i\epsilon) \\
&\qquad + \tilde{G}_l^0(q', i\epsilon')\,\dot{G}_l^0(q'+q, i\epsilon'+i\epsilon)\Big]\,, \qquad (6.31) \\
\dot{\chi}_l(Q) &= \frac{1}{2}\int_{Q'}{}' \Big[\dot{G}_l^0(-q', i\epsilon')\,\tilde{G}_l^0(q'+q, i\epsilon'+i\epsilon) \\
&\qquad + \tilde{G}_l^0(-q', i\epsilon')\,\dot{G}_l^0(q'+q, i\epsilon'+i\epsilon)\Big]\,, \qquad (6.32) \\
\dot{\chi}_l'(Q) &= -\frac{1}{2}\int_{Q'}{}' \Big[\dot{G}_l^0(q', -i\epsilon')\,\tilde{G}_l^0(q'+q, i\epsilon'+i\epsilon) \\
&\qquad + \tilde{G}_l^0(q', -i\epsilon')\,\dot{G}_l^0(q'+q, i\epsilon'+i\epsilon)\Big]\,, \qquad (6.33)
\end{aligned}$$

which physically represent susceptibilities after being integrated over the flow parameter l. The function $\dot{\Pi}_l$ corresponds to a particle-hole pair of fermions located on the same and $\dot{\chi}_l$ to fermions located on different branches of the energy dispersion. On the other hand $\dot{\chi}_l'$ describes a particle-particle (hole-hole) pair of fermions on different energy branches. In the usual nomenclature they correspond to the zero sound (ZS), the Peierls (ZS') and the BCS channel, see also Fig. 6.3. If $\dot{G}_l^0$ satisfies the particle-hole symmetry given by Eq. (6.18) the functions $\dot{\chi}_l$ and $\dot{\chi}_l'$ coincide. However, for later convenience when we are going to study the effects of a non-linear energy dispersion, we will now derive an explicit expression for $\tilde{\Gamma}_l^{(4)}$ without referring to the explicit form of the excitation energy

$\xi_l(q)$. So let $\dot{G}_l^0$ and $\tilde{G}_l^0$ be some arbitrary functions such that the integrals in Eqs. (6.31) – (6.33) are absolutely convergent. It is then easy to show that the auxiliary functions have the following symmetries,

$$\dot{\Pi}_l(-q,-i\epsilon) = \dot{\Pi}_l(q,i\epsilon)\,, \tag{6.34}$$

$$\dot{\chi}_l(q,-i\epsilon) = \dot{\chi}_l(q,i\epsilon)\,, \tag{6.35}$$

$$\dot{\chi}_l'(-q,i\epsilon) = \dot{\chi}_l'(q,i\epsilon)\,. \tag{6.36}$$

Performing the α-sum in Eq. (6.30) it is then possible to express $\tilde{\Gamma}_l^{(4)}$ in terms of these functions. Note that K' in Eq. (6.30) still has to be expressed as a function of the rescaled variables. The procedure has been described below Eq. (4.53) and after some straightforward algebra we obtain as final result

$$\begin{aligned}\dot{\Gamma}_l^{(4)}(Q_1',Q_2';Q_2,Q_1) &= \tilde{g}_l^2 \Big\{ A_{\alpha_1'\alpha_2';\alpha_2\alpha_1}\, \dot{\chi}_l'(q_1-q_2,i\epsilon_1+i\epsilon_2) \\ &\quad + E_{\alpha_1'\alpha_2';\alpha_2\alpha_1}\big[\,\delta_{\alpha_1\alpha_2}\dot{\Pi}_l(q_1'-q_1,i\epsilon_1-\epsilon_1') \\ &\qquad + \delta_{\alpha_1\bar{\alpha}_2}\dot{\chi}_l(q_1'+q_1,i\epsilon_1-\epsilon_1')\,\big] \\ &\quad - D_{\alpha_1'\alpha_2';\alpha_2\alpha_1}\big[\,\delta_{\alpha_1\alpha_2}\dot{\Pi}_l(q_2'-q_1,i\epsilon_1-\epsilon_2') \\ &\qquad + \delta_{\alpha_1\bar{\alpha}_2}\dot{\chi}_l(q_2'+q_1,i\epsilon_1-\epsilon_2')\,\big]\Big\} \\ &\quad + \mathcal{O}(\tilde{g}_l^3)\,,\end{aligned} \tag{6.37}$$

where we made explicit use of the symmetries (6.34)-(6.36). We emphasize again that this equation is valid irrespective of the explicit form of the energy dispersion. Note that the overall sign of Eq. (6.37) is different from Eq. (B.3) in Ref. [67], where we used different definitions for the auxiliary functions. In case of linear energy dispersion the integrations in Eqs. (6.31) and (6.32) may easily be performed and we get

$$\dot{\chi}_l(q,i\epsilon) = \dot{\chi}_l'(q,i\epsilon) = -\Theta(e^l-1>|q|)\frac{\tilde{v}_l(2+|q|)}{\epsilon^2+\tilde{v}_l^2(2+|q|)^2}\,, \tag{6.38}$$

$$\dot{\Pi}_l(q,i\epsilon) = \Theta(e^l+1>|q|>2)\frac{s_q}{i\epsilon-\tilde{v}_l q}\,, \tag{6.39}$$

Actually to prove the vanishing of the β-function at one-loop level we do not even need the explicit expressions for $\dot{\chi}_l$ and $\dot{\Pi}_l$. *This result follows whenever the*

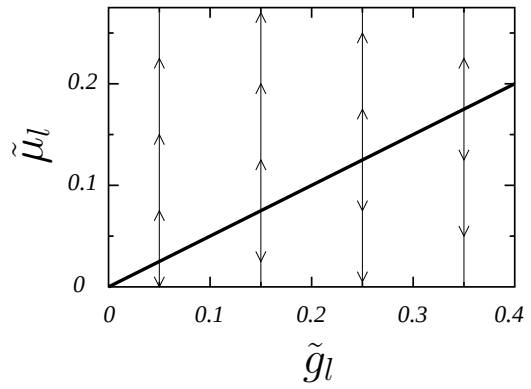

Figure 6.2: One-loop flow in the $(\tilde{g}_l, \tilde{\mu}_l)$ plane according to Eq. (6.44). The thick solid line is a line of fixed points, given by $\tilde{\mu}_l = \tilde{g}_l/2$. Any small deviation from this line leads to a runaway flow to plus or minus infinity.

propagator $\tilde{G}_l^0$ *satisfies the particle-hole symmetry* $\tilde{G}_l^0(-q, -i\epsilon) = -\tilde{G}_l^0(q, i\epsilon)$. To prove this just note that from Eqs. (6.29) and (6.37) we immediately get

$$\boxed{B_l = \tilde{g}_l^2 \left[\dot{\chi}_l'(0, i0) - \dot{\chi}_l(0, i0) \right].} \tag{6.40}$$

Given the symmetry of $\tilde{G}_l^0$ we have $\dot{\chi}_l' = \dot{\chi}_l$ and the r.h.s. indeed vanishes. For the flow equation of $\tilde{g}_l$ this means

$$\boxed{\partial_l \tilde{g}_l = 0\,,} \tag{6.41}$$

which implies that $\tilde{g}_l$ does not flow at all and hence

$$\tilde{g}_l = \tilde{g}_0\,. \tag{6.42}$$

The flow of the couplings $Z_l, \tilde{v}_l$ and $\tilde{g}_l$ thus turns out to be trivial while the chemical potential parameter $\tilde{\mu}_l$ needs a well adjusted initial condition to avoid a runaway flow to infinity. To make this completely clear consider Eq. (5.19) with $\bar{\eta}_l = 0$ taking on the form

$$\tilde{\mu}_l = e^l \left[\tilde{\mu}_0 - \int_0^l dt\, e^{-t}\, \frac{\tilde{g}_t}{2} \right] + \mathcal{O}(\tilde{g}_l^2)\,, \tag{6.43}$$

where we have used our one-loop result $\dot{\Gamma}_l^{(2)}(\alpha, 0) = -\tilde{g}_l/2$. Note that $\tilde{\mu}_l$ depends non-locally on $\tilde{g}_l$ but due to $\tilde{g}_l = \tilde{g}_0$ the integration can immediately be performed to give

$$\tilde{\mu}_l = \frac{\tilde{g}_l}{2} + e^l \left[\tilde{\mu}_0 - \frac{\tilde{g}_l}{2} \right] + \mathcal{O}(\tilde{g}_l^2) \,. \tag{6.44}$$

In Fig. 6.2 the implications of this equation are shown in the $(\tilde{\mu}_l, \tilde{g}_l)$ plane.

6.3 Two-Loop Flow

Let us now proceed and see how the couplings change at the two-loop order. For the two-point vertex this means that we have to retain all contributions up to the order $\sim \tilde{g}_l^2$ while for the four-point vertex we need all terms including the order $\sim \tilde{g}_l^3$.

Two-point vertex:

To calculate the flow of the couplings Z_l,η_l, $\tilde{v}_l$ and $\tilde{\mu}_l$ determined by Eqs. (5.18) and (5.25) at this level we need to know the full momentum and frequency dependence of the four-point vertex at the order $\sim \tilde{g}_l^2$. We define

$$\tilde{\Gamma}_l^{(4)}(Q_1', Q_2'; Q_2, Q_1) = \tilde{g}_l \, A_{\alpha_1'\alpha_2';\,\alpha_2\alpha_1} + \tilde{g}_l^2 \, \tilde{\gamma}_l^{(4)}(Q_1', Q_2'; Q_2, Q_1) + \mathcal{O}(\tilde{g}_l^3) \,, \tag{6.45}$$

where the dimensionless function $\tilde{\gamma}_l^{(4)}$ is by definition antisymmetric with respect to the exchanges $Q_1' \leftrightarrow Q_2'$ and $Q_1 \leftrightarrow Q_2$. To determine $\tilde{\gamma}_l^{(4)}$ we have to use the *subtracted* flow equation (5.44) for the reasons described in Sec. 5.4. From the corresponding integral representation we get

$$\begin{aligned} \tilde{\Gamma}_l^{(4,sub)}(Q_1', Q_2'; Q_2, Q_1) \;&\approx\; \int_0^l dt \, \dot{\Gamma}_t^{(4,sub)}(e^{t-l}Q_1', e^{t-l}Q_2'; e^{t-l}Q_2, e^{t-l}Q_1) \\ &=\; \int_0^l dt \, \dot{\Gamma}_{l-t}^{(4,sub)}(e^{-t}Q_1', e^{-t}Q_2'; e^{-t}Q_2, e^{-t}Q_1) \,, \end{aligned} \tag{6.46}$$

where we have set $\eta_l = 0$ since Eq. (6.45) is still a one-loop equation. Note that the function $\tilde{\Gamma}_l^{(4,sub)}$ coincides with $\tilde{\gamma}_l^{(4)}$ at one-loop level up to the prefactor $\tilde{g}_l^2$. Note as well that according to Eq. (6.46) $\tilde{\Gamma}_l^{(4,sub)}$ depends non-locally on the flow parameter l. This is indeed a general feature of the integral representations given by Eq. (4.57), and the question arises, how this difficulty can be overcome? – First of all there are two different kinds of l-dependencies in $\tilde{\Gamma}_l^{(4,sub)}$: One is given implicitly due to the couplings we take into account self-consistently, and the second is given by an explicit l-dependence related to the ultraviolet cutoff

Λ_0. If for instance we consider the explicit expression for $\dot{\Gamma}_l^{(4)}$ given in Eq. (6.37) combined with Eqs. (6.38) and (6.39) we recognize the implicit dependence via the couplings $\tilde{v}_l$ and $\tilde{g}_l$ as well as an explicit dependence due to the factor e^l within the Θ-functions. As concerns the first we can approximate $\tilde{v}_{l-t} \approx \tilde{v}_l$ and $\tilde{g}_{l-t} \approx \tilde{g}_l$ since $\tilde{v}_l$ and $\tilde{g}_l$ both are *marginal* couplings, such that the non-localities give rise to higher orders in $\tilde{g}_l$ which can be neglected within a weak-coupling expansion.[3] On the other hand the factor e^l turns into e^{l-t} and should of course be kept entirely.
Let us now state an explicit equation for $\tilde{\gamma}_l^{(4)}$ using the subtracted version of Eq. (6.37) together with Eq. (6.46). We obtain

$$\begin{aligned}\tilde{\gamma}_l^{(4)}(Q_1', Q_2'; Q_2, Q_1) &= A_{\alpha_1'\alpha_2';\,\alpha_2\alpha_1}\,\tilde{\chi}_l'(q_1 - q_2, i\epsilon_1 + i\epsilon_2) \\ &+ E_{\alpha_1'\alpha_2';\alpha_2\alpha_1}\big[\,\delta_{\alpha_1\alpha_2}\tilde{\Pi}_l(q_1' - q_1, i\epsilon_1 - \epsilon_1') \\ &\qquad + \delta_{\alpha_1\bar{\alpha}_2}\tilde{\chi}_l(q_1' + q_1, i\epsilon_1 - \epsilon_1')\,\big] \\ &- D_{\alpha_1'\alpha_2';\alpha_2\alpha_1}\big[\,\delta_{\alpha_1\alpha_2}\tilde{\Pi}_l(q_2' - q_1, i\epsilon_1 - \epsilon_2') \\ &\qquad + \delta_{\alpha_1\bar{\alpha}_2}\tilde{\chi}_l(q_2' + q_1, i\epsilon_1 - \epsilon_2')\,\big]\,, \end{aligned} \tag{6.47}$$

where we have defined

$$\tilde{\Pi}_l(q, i\epsilon) = \int_0^l dt\,[\,\dot{\Pi}_{l-t}(e^{-t}q, e^{-t}i\epsilon) - \dot{\Pi}_{l-t}(0, i0)\,]\,, \tag{6.48}$$

$$\tilde{\chi}_l(q, i\epsilon) = \int_0^l dt\,[\,\dot{\chi}_{l-t}(e^{-t}q, e^{-t}i\epsilon) - \dot{\chi}_{l-t}(0, i0)\,]\,, \tag{6.49}$$

and equivalently for $\tilde{\chi}_l'$. Again it is our aim to derive an expression for the β-function at two-loop order without referring to the explicit form of the energy dispersion as long as we do not need it. This is why we still have distinguished between $\tilde{\chi}_l$ and $\tilde{\chi}_l'$ for later purposes. Physically the functions $\tilde{\Pi}_l$ and $\tilde{\chi}_l$ are the (subtracted) susceptibilities appearing in a perturbative expansion of the four-point vertex.
To obtain explicit results for the susceptibilities in case of linear dispersion we have to use the expressions for $\dot{\Pi}_l$ and $\dot{\chi}_l$ given in Eqs. (6.38) and (6.39) and to perform the t-integration Eqs. (6.48) and (6.49) . Approximating $\tilde{v}_{l-t} \approx \tilde{v}_l$ as discussed above we get

$$\tilde{\Pi}_l(q, i\epsilon) = \frac{1}{2}\,\frac{s_q}{i\epsilon - \tilde{v}_l q}\Big\{\Theta(2 < |q| < e^l + 1)\,(|q| - 2)$$

[3] If relevant or irrelevant couplings are considered we must proceed differently. For irrelevant couplings this will be shown in Chap. 8 when a non-linear term of the energy dispersion is included.

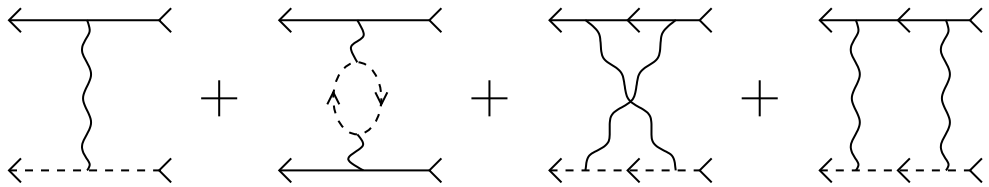

Figure 6.3: Feynman diagrams contributing to the effective interaction within the one-loop approximation, see Eqs. (6.45) and (6.47). The solid (dashed) lines represent the fermion propagators with momenta close to the right (left) Fermi point, and the wavy lines represent the flowing coupling constant $\tilde{g}_l$. As the outer legs of the second diagram both correspond to fermions propagating in the same direction, it represents an effective g_4-type interaction.

$$+\,\Theta(e^l+1<|q|<2e^l)\,(2e^l-|q|)\Big\}\,, \qquad (6.50)$$

and

$$\begin{aligned}\tilde{\chi}_l(q,i\epsilon) &= \tilde{\chi}_l'(q,i\epsilon)=\Theta(e^l-1<|q|)\,\frac{l}{2\tilde{v}_l}\\ &+ \Theta(|q|<e^l-1)\,\frac{1}{4\tilde{v}_l}\ln\left[\frac{\epsilon^2+\tilde{v}_l^2(2+|q|)^2}{\epsilon^2e^{-2l}+\tilde{v}_l^2(2-e^{-l}|q|)^2}\right]\,. \qquad (6.51)\end{aligned}$$

Notice that the limit $l\to\infty$ is well defined for both functions - for $\tilde{\chi}_l$ this would not be true without the subtraction term in Eq. (6.49). The subtleties related to this limit and an eventual transformation back to the physical variables p and ω will be discussed in detail in Sec. 6.5.
To evaluate the flow of the couplings Z_l, η_l, $\tilde{v}_l$ and $\tilde{\mu}_l$ we need the following expression for the four-point vertex,

$$\tilde{\Gamma}_l^{(4)}(Q,Q';Q',Q)=\delta_{\alpha,\bar{\alpha}'}\tilde{g}_l+\tilde{g}_l^2\,\tilde{\gamma}_l^{(4)}(Q,Q';Q',Q)+\mathcal{O}(\tilde{g}_l^3)\,, \qquad (6.52)$$

which follows from Eq. (4.46). Here

$$\begin{aligned}\tilde{\gamma}_l^{(4)}(Q,Q';Q',Q) &= -\delta_{\alpha,\alpha'}\,\tilde{\Pi}_l(q'-q,i\epsilon-i\epsilon')\\ &+\delta_{\alpha,\bar{\alpha}'}\left[\tilde{\chi}_l(q-q',i\epsilon+i\epsilon')-\tilde{\chi}_l(q+q',i\epsilon-i\epsilon')\right]. \qquad (6.53)\end{aligned}$$

In Fig. 6.3 we show a graphical representation of Eq. (6.52). From Eq. (6.19) we now directly obtain for the flow of the coupling $\tilde{\mu}_l$ at two-loop order

$$\begin{aligned}\partial_l\tilde{\mu}_l &= \tilde{\mu}_l - \frac{\tilde{g}_l}{2} + \frac{\tilde{g}_l^2}{2}\int_Q \frac{\delta(|q|-1)}{[i\epsilon - \tilde{v}_l q]^2} \\ &\quad - \tilde{g}_l^2 \int_{Q'} \dot{G}_l^0(Q')\,\tilde{\gamma}_l^{(4)}(\alpha 0, Q'; Q', \alpha 0) + \mathcal{O}(\tilde{g}_l^3)\,. \end{aligned} \tag{6.54}$$

The first integral on the r.h.s. of this equation is easily shown to vanish while the second involves the α'-sum over $\tilde{\gamma}_l^{(4)}(\alpha 0, Q'; Q', \alpha 0)$ which is obtained from Eq. (6.53),

$$\sum_{\alpha'=\pm\alpha} \tilde{\gamma}_l^{(4)}(\alpha 0, Q'; Q', \alpha 0) = -\,\tilde{\Pi}_l(q', i\epsilon')\,. \tag{6.55}$$

Note that due to Eq. (6.50) $\tilde{\Pi}_l(q, i\epsilon)$ only contributes if $|q| > 2$ such that the second integral in Eq. (6.54) also vanishes due to the δ-function within $\dot{G}_l^0$. Consequently

$$\boxed{\partial_l\tilde{\mu}_l = \tilde{\mu}_l - \frac{\tilde{g}_l}{2} + \mathcal{O}(\tilde{g}_l^3)\,,} \tag{6.56}$$

and the one-loop result for $\tilde{\mu}_l$ remains unchanged at the two-loop level. For the flow of the other couplings we need to calculate the inhomogeneity $\dot{\Gamma}_l^{(2)}(Q)$ on the right-hand side of the flow equation for the two-point vertex. To this end we substitute our approximate expression for $\tilde{\Gamma}_l^{(4)}(Q, Q'; Q', Q)$ into Eq. (4.46). Separating the contributions due to the zero sound (ZS) and the Peierls-BCS (PB) channels, we have

$$\dot{\Gamma}_l^{(2)}(q, i\epsilon) = -\frac{\tilde{g}_l}{2} + \dot{\Gamma}_l^{(2,\mathrm{ZS})}(q, i\epsilon) + \dot{\Gamma}_l^{(2,\mathrm{PB})}(q, i\epsilon) + \mathcal{O}(\tilde{g}_l^3)\,, \tag{6.57}$$

where

$$\begin{aligned}\dot{\Gamma}_l^{(2,\mathrm{ZS})}(q, i\epsilon) &= -\tilde{g}_l^2 \int \frac{dq'}{2} \int \frac{d\epsilon'}{2\pi} \frac{\delta(|q'|-1)}{i\epsilon' - \tilde{v}_l q'}\,\tilde{\Pi}_l(q'-q, i\epsilon - i\epsilon') \\ &= -\frac{\tilde{g}_l^2}{4} s_q \Big[\Theta(1 < |q| < e^l)\,\frac{|q|-1}{i\epsilon s_q + \tilde{v}_l(2+|q|)} \\ &\quad + \Theta(e^l < |q| < 2e^l - 1)\,\frac{2e^l - 1 - |q|}{i\epsilon s_q + \tilde{v}_l(2+|q|)}\Big]\,, \end{aligned} \tag{6.58}$$

and

$$\dot{\Gamma}_l^{(2,\mathrm{PB})}(q, i\epsilon) = -\tilde{g}_l^2 \int \frac{dq'}{2} \int \frac{d\epsilon'}{2\pi} \frac{\delta(|q'|-1)}{i\epsilon' - \tilde{v}_l q'}$$

$$\times\Big[\tilde{\chi}_l(q-q',i\epsilon+i\epsilon')-\tilde{\chi}_l(q+q',i\epsilon-i\epsilon')\Big]$$

$$\begin{aligned}=\;&\frac{\tilde{g}_l^2}{4\tilde{v}_l}s_q\Bigg[\Theta(2-e^l<|q|<1)\ln\left(\frac{i\epsilon s_q+\tilde{v}_l(4-|q|)}{i\epsilon s_q+\tilde{v}_l(2e^l+|q|)}\right)\\&+\Theta(1<|q|<e^l)\ln\left(\frac{i\epsilon s_q+\tilde{v}_l(2+|q|)}{i\epsilon s_q+\tilde{v}_l(2e^l+2-|q|)}\right)\\&-\Theta(|q|<e^l-2)\ln\left(\frac{i\epsilon s_q-\tilde{v}_l(4+|q|)}{i\epsilon s_q-\tilde{v}_l(2e^l-|q|)}\right)\Bigg]\;.\end{aligned}\tag{6.59}$$

Here, we have introduced the short-hand notation

$$s_q=\mathrm{sgn}(q)\;.\tag{6.60}$$

Expanding to first order in q and ϵ, we obtain

$$\begin{aligned}&\dot{\Gamma}_l^{(2,\mathrm{PB})}(q,i\epsilon)\\&\quad=\;\frac{\tilde{g}_l^2}{8\tilde{v}_l^2}\Theta(e^l-2)\Big[(1-2e^{-l})i\epsilon-(1+2e^{-l})\tilde{v}_l q\Big]+\mathcal{O}(\epsilon^2,q^2,\epsilon q)\;.\end{aligned}\tag{6.61}$$

Because $\dot{\Gamma}_l^{(2,\mathrm{ZS})}(q,i\epsilon)$ vanishes for $|q|<1$, it does not contribute to the flow of the marginal couplings Z_l and $\tilde{v}_l$. From Eq. (5.26) we obtain for the anomalous dimension at scale l,

$$\boxed{\eta_l=\frac{\tilde{g}_l^2}{8\tilde{v}_l^2}\Theta(e^l-2)(1-2e^{-l})\;,}\tag{6.62}$$

and from Eq. (5.25) we find

$$\boxed{\partial_l\tilde{v}_l=\frac{\tilde{g}_l^2}{2\tilde{v}_l}\Theta(e^l-2)e^{-l}\;.}\tag{6.63}$$

Finally the flow of the quasi-particle residue is given by

$$\boxed{\partial_l Z_l=\frac{\tilde{g}_l^2}{8\tilde{v}_l^2}\Theta(e^l-2)(1-2e^{-l})\,Z_l\,.}\tag{6.64}$$

For a proper integration of these equations we still need to know the flow of $\tilde{g}_l$ at two-loop order.

Four-point vertex:

Let us now state the equation determining the β-function at two-loop order. Due to our one-loop result for B_l we already know that all terms of order $\sim \tilde{g}_l^2$ vanish. From the flow equation (6.28) and the definition of B_l, Eq. (6.29), together with the explicit expression for $\dot{\Gamma}_l^{(4)}$ in Eq. (4.51) we get

$$\begin{aligned} B_l \;=\; -\tilde{g}_l^3 \Big\{ & \int_Q \dot{G}_l^0(Q)\, \tilde{\gamma}_l^{(6)}(\beta 0, \bar{\beta} 0, Q; Q, \bar{\beta} 0, \beta 0) \\ & + \int_Q \big[\, \dot{G}_l^0(Q)\, \tilde{G}_l^0(Q') + \tilde{G}_l^0(Q)\, \dot{G}_l^0(Q') \,\big] \\ & \times \Big\{ \frac{1}{2} \Big[\, A_{\beta\bar{\beta};\bar{\alpha}\alpha}\, \tilde{\gamma}_l^{(4)}(Q, Q'; \bar{\beta} 0, \beta 0) \Big]_{Q'=(q,-i\epsilon)} \\ & \quad + \frac{1}{2} \Big[\, \tilde{\gamma}_l^{(4)}(\beta 0, \bar{\beta} 0; Q', Q)\, A_{\alpha\bar{\alpha};\bar{\beta}\beta} \Big]_{Q'=(q,-i\epsilon)} \\ & \quad - \Big[\, A_{\beta\alpha;\alpha\beta}\, \tilde{\gamma}_l^{(4)}(\bar{\beta} 0, Q; Q', \bar{\beta} 0) \Big]_{Q'=(q,i\epsilon)} \\ & \quad - \Big[\, \tilde{\gamma}_l^{(4)}(\beta 0, Q'; Q, \beta 0)\, A_{\bar{\beta}\alpha;\alpha\bar{\beta}} \Big]_{Q'=(q,i\epsilon)} \\ & \quad + \Big[\, A_{\bar{\beta}\bar{\alpha};\alpha\beta}\, \tilde{\gamma}_l^{(4)}(\beta 0, Q; Q', \bar{\beta} 0) \Big]_{Q'=(-q,i\epsilon)} \\ & \quad + \Big[\, \tilde{\gamma}_l^{(4)}(\bar{\beta} 0, Q'; Q, \beta 0)\, A_{\beta\alpha;\bar{\alpha}\bar{\beta}} \Big]_{Q'=(-q,i\epsilon)} \Big\} \Big\} \\ & + \mathcal{O}(\tilde{g}_l^4)\,. \end{aligned} \tag{6.65}$$

Here we have denoted the external branch index by β to avoid notational confusion and again we have set $\bar{\beta} = -\beta$. Note that at two-loop order we must retain the momentum- and frequency-dependent part of the six-point vertex $\tilde{\gamma}_l^{(6)}$ which is generated at order $\sim \tilde{g}_l^3$. Explicitly we have defined

$$\tilde{\Gamma}_l^{(6)}(Q_1', Q_2', Q_3'; Q_3, Q_2, Q_1) = \tilde{g}_l^3\, \tilde{\gamma}_l^{(6)}(Q_1', Q_2', Q_3'; Q_3, Q_2, Q_1) + \mathcal{O}(\tilde{g}_l^4)\,, \tag{6.66}$$

in analogy with $\tilde{\gamma}_l^{(4)}$ in Eq. (6.66). Again our next step of the calculation is to perform the α-sum in Eq. (6.65). To this end we first need to identify the functions $\tilde{\gamma}_l^{(4)}$ in Eq. (6.65) with the susceptibilities via Eq. (6.47). After some tedious algebra we find

$$B_l = B_l^{(4)} + B_l^{(6)}\,, \tag{6.67}$$

where $B_l^{(4)}$ denotes the contribution of the four-point vertex to the β-function, explicitly given by

$$\boxed{\begin{aligned} B_l^{(4)} \;=\; & -4\,\tilde{g}_l^3 \int_Q{}' \Big[\dot{G}_l^0(q,i\epsilon)\,\tilde{G}_l^0(q,i\epsilon)\,\tilde{\Pi}_l(q,-i\epsilon) \\ & \qquad + \dot{G}_l^0(q,i\epsilon)\,\tilde{G}_l^0(-q,i\epsilon)\,\tilde{\chi}_l'(q,i\epsilon) \\ & \qquad - \dot{G}_l^0(q,i\epsilon)\,\tilde{G}_l^0(q,-i\epsilon)\,\tilde{\chi}_l(q,i\epsilon) \Big] . \end{aligned}} \tag{6.68}$$

and

$$B_l^{(6)} = -\,\tilde{g}_l^3 \int_Q \dot{G}_l^0(Q)\,\tilde{\gamma}_l^{(6)}(\beta 0,\bar{\beta}0,Q;Q,\bar{\beta}0,\beta 0)\,, \tag{6.69}$$

denoting the contribution of the six-point vertex. Eq. (6.68) is again valid for an arbitrary form of the energy dispersion. In Eq. (6.69) we did not yet perform the α-sum and we would like to find an expression of the form of Eq. (6.68). However, in case of $B_l^{(6)}$ a corresponding expression is very hard to obtain. What we need is the function $\tilde{\gamma}_l^{(6)}$ defined via Eq. (6.66). Using the integral representation (4.49) for $n=3$ with the initial condition $\Gamma_{l=0}^{(6)}=0$ and $\eta_l=\bar{\eta}_l=0$ we get

$$\begin{aligned} & \tilde{\Gamma}_l^{(6)}(Q_1',Q_2',Q_3';Q_3,Q_2,Q_1) \\ & \approx \int_0^l dt\, e^{-t}\,\dot{\Gamma}_{l-t}^{(6)}(e^{-t}Q_1',e^{-t}Q_2',e^{-t}Q_3';e^{-t}Q_3,e^{-t}Q_2,e^{-t}Q_1)\,. \end{aligned} \tag{6.70}$$

Remember that for the six-point vertex it is not necessary to introduce a subtracted version, see also Sec. 5.4. To determine the function $\tilde{\gamma}_l^{(6)}$, which equals $\tilde{\Gamma}_l^{(6)}$ up to the prefactor $\tilde{g}_l^3$ at two-loop order, we need to fix all contributions to $\dot{\Gamma}_l^{(6)}$ in Eq. (4.53) of order $\sim \tilde{g}_l^3$. It is easy to see that the lowest order contributions in this equation are due to the last two terms on the r.h.s. involving a product of three four-point vertices. This is also evident from Fig. 6.1 **c)**. By iteration it is then obvious that those terms involving a product of a four- and a six-point vertex are at least of order $\sim \tilde{g}_l^4$ and can be neglected within a two-loop calculation. The same is true for the eight-point vertex which is only generated at order $\tilde{g}_l^4$, see Fig. 6.1 **d)**. This means that the relevant approximation turns out to be

$$\begin{aligned} & \dot{\Gamma}_l^{(6)}(Q_1',Q_2',Q_3';Q_3,Q_2,Q_1) \\ & \quad = \tilde{g}_l^3 \Big\{ 9\,\mathcal{A}_{(1',2'),3'}\,\mathcal{A}_{3,(2,1)} \Big[A_{\alpha_1'\alpha_2';\alpha\alpha'}\,A_{\alpha_3'\alpha';\alpha''\alpha_3}\,A_{\alpha''\alpha;\alpha_2\alpha_1} \end{aligned}$$

$$\times \int_Q \dot{G}_l^0(Q)\,\tilde{G}_l^0(Q')\,\tilde{G}_l^0(Q'')\,\Big]_{K''=K_1+K_2-K}^{K'=K_1'+K_2'-K}$$
$$-\,36\,\mathcal{A}_{1',2',3'}\,\mathcal{A}_{3,2,1}\Big[\,A_{\alpha_1'\alpha';\alpha\alpha_1}\,A_{\alpha_2'\alpha'';\alpha'\alpha_2}\,A_{\alpha_3'\alpha;\alpha''\alpha_3}$$
$$\times \int_Q \Big(\dot{G}_l^0(Q)\,\tilde{G}_l^0(Q')\,\tilde{G}_l^0(Q'') + \tilde{G}_l^0(Q)\,\dot{G}_l^0(Q')\,\tilde{G}_l^0(Q'')$$
$$+\,\tilde{G}_l^0(Q)\,\tilde{G}_l^0(Q')\,\dot{G}_l^0(Q'')\Big)\,\Big]_{K''=K_3'-K_3+K}^{K'=K_1-K_1'+K}\Big\}$$
$$+\,\mathcal{O}(\tilde{g}_l^4)\,. \tag{6.71}$$

The analysis of this equation involves very lengthy and tedious combinatorics. This is why we do not display the details of the calculation, but it is worth to give some remarks on the procedure. What we actually need for the β-function is the above expression for $Q_1' = Q_1 = (\beta, 0, i0)$, $Q_2' = Q_2 = (\bar{\beta}, 0, i0)$ and $Q_3' = Q_3 = (\alpha, q, i\epsilon)$, see Eq. (6.69). This drastically reduces the number of non-zero terms on the r.h.s. of Eq. (6.71). From the nine terms of the first expression only four and from the 36 terms of the second expression only twelve terms survive for fixed α, the rest is excluded by the property $A_{\alpha_1'\alpha_2';\alpha\alpha} = A_{\alpha\alpha;\alpha_2\alpha_1} = 0$. Note, however, that we cannot just insert the explicit values for the external Q's on the r.h.s. but we *first* have to apply the antisymmetrization operators $\mathcal{A}_{(\ldots)}$ to determine the 45 permutations and only then it is allowed to set the external Q's equal to the values needed for the two-loop β-function. It is also possible to start with performing the α-sum in Eq. (6.71) and to derive an expression analogous to Eq. (6.37) for $\dot{\Gamma}_l^{(4)}$ valid for arbitrary external momenta. But the result is rather lengthy and represents all possible connected Feynman graphs which may be drawn from a product of three antisymmetrized bare vertices with three propagators, which may alternatively correspond to left- and to right-movers. As we do not need the general result for our present purposes let us just stress the fact that for arbitrary energy dispersion it is possible to express $\dot{\Gamma}_l^{(6)}(Q_1', Q_2', Q_3'; Q_3, Q_2, Q_1)$ in terms of five auxiliary functions defined by

$$\dot{\Delta}_l((q, i\epsilon); (q', i\epsilon')) =$$
$$\int_{Q''}{}' \dot{G}_l^0(q'', i\epsilon'')\,\tilde{G}_l^0(-q''+q, i\epsilon''+i\epsilon)\,\tilde{G}_l(-q''+q', i\epsilon''+i\epsilon')\,, \tag{6.72}$$
$$\dot{\Delta}_l'((q, i\epsilon); (q', i\epsilon')) =$$
$$\int_{Q''}{}' \dot{G}_l^0(q'', i\epsilon'')\,\tilde{G}_l^0(q''-q, -i\epsilon''-i\epsilon)\,\tilde{G}_l(q''-q', -i\epsilon''-i\epsilon')\,, \tag{6.73}$$

$$\dot{\Lambda}_l((q,i\epsilon);(q',i\epsilon')) = \int_{Q''}{}' \dot{G}_l^0(q'',i\epsilon'')\,\tilde{G}_l^0(-q''+q,i\epsilon''+i\epsilon)\,\tilde{G}_l(q''+q',i\epsilon''+i\epsilon')\,, \tag{6.74}$$

$$\dot{\Lambda}'_l((q,i\epsilon);(q',i\epsilon')) = -\int_{Q''}{}' \dot{G}_l^0(q'',i\epsilon'')\,\tilde{G}_l^0(q''-q,-i\epsilon''-i\epsilon)\,\tilde{G}_l(q''+q',i\epsilon''+i\epsilon')\,, \tag{6.75}$$

and

$$\dot{\Omega}_l((q,i\epsilon);(q',i\epsilon')) = \int_{Q''}{}' \dot{G}_l^0(q'',i\epsilon'')\,\tilde{G}_l^0(q''+q,i\epsilon''+i\epsilon)\,\tilde{G}_l(q''+q',i\epsilon''+i\epsilon')\,. \tag{6.76}$$

Except for

$$\dot{\Delta}_l((q,i\epsilon);(q',i\epsilon')) = \dot{\Delta}_l((q',i\epsilon');(q,i\epsilon))\,, \tag{6.77}$$

$$\dot{\Delta}'_l((q,i\epsilon);(q',i\epsilon')) = \dot{\Delta}'_l((q',i\epsilon');(q,i\epsilon))\,, \tag{6.78}$$

$$\dot{\Omega}_l((q,i\epsilon);(q',i\epsilon')) = \dot{\Omega}_l((q',i\epsilon');(q,i\epsilon))\,, \tag{6.79}$$

these functions have no obvious symmetries which can be stated without referring to the explicit form of the energy dispersion. For linear dispersion with the propagator symmetries (6.18) we have $\dot{\Lambda}_l = \dot{\Lambda}'_l$ as well as $\dot{\Delta}_l = \dot{\Delta}'_l$ such that only three different functions appear. This is due to the fact that from the six possible combinations for a product of three propagators, where each of them may correspond to a right- or a left-moving fermion, only three combinations lead to qualitatively different results. This assertion is easily checked by replacing $\dot{G}_l(q,i\epsilon)$ with $\dot{G}_l(-q,i\epsilon)$ and $\tilde{G}_l(q,i\epsilon)$ with $\tilde{G}_l(-q,i\epsilon)$ in the definitions (6.74), (6.72) and (6.76). Subsequent change of the q''-integration from q'' to $-q''$ leaves us with the functions $\dot{\Lambda}_l((-q,i\epsilon);(-q',i\epsilon))$, $\dot{\Delta}_l((-q,i\epsilon);(-q',i\epsilon))$ and $\dot{\Omega}_l((-q,i\epsilon);(-q',i\epsilon))$. Note that $\dot{\Omega}_l$ involves the product of three propagators of the same type. Diagrammatically the contribution of this term to the six-point vertex is represented by the Feynman graph shown in Fig. 6.1 **c)**. For a two-loop calculation of the β-function this term is excluded for the same reasons that applied to the function $\dot{\Pi}_l$ within our one-loop result, see Eq. (6.40). This is not surprising as the contribution of $\dot{\Pi}_l$ to the four-point vertex is graphically represented by the Feynman graph shown in Fig. 6.1 **b)**, which is just the lower order version of the graph shown in Fig. 6.1 **c)**.

So far the prologue, let us now state the explicit result for $\dot{\Gamma}_l^{(6)}$ in the form it is needed for a two-loop calculation. After a lengthy and tedious calculation we obtain for an arbitrary energy dispersion

$$\begin{aligned}
&\dot{\Gamma}_l^{(6)}(\alpha 0, \bar{\alpha} 0, (\pm\alpha, q, i\epsilon); (\pm\alpha, q, i\epsilon); \bar{\alpha} 0, \alpha 0) \\
&\quad = \tilde{g}_l^3 \Big\{ \ \tfrac{1}{2} \big[\, \dot{\Delta}_l((0,i0);(0,i0)) + \dot{\Delta}'_l((0,i0);(0,i0)) \, \big] \\
&\qquad + \tfrac{1}{2} \big[\, \dot{\Delta}_l((q,-i\epsilon);(q,-i\epsilon)) + \dot{\Delta}'_l((q,-i\epsilon);(q,-i\epsilon)) \, \big] \\
&\qquad - \ \big[\, \dot{\Delta}_l((0,i0);(q,-i\epsilon)) + \dot{\Delta}'_l((0,i0);(q,-i\epsilon)) \, \big] \\
&\qquad + \ \big[\, \dot{\Lambda}_l((q,i\epsilon);(0,i0)) - \dot{\Lambda}'_l((-q,-i\epsilon);(0,i0)) \, \big] \\
&\qquad + \ \big[\, \dot{\Lambda}_l((0,i0);(0,i0)) - \dot{\Lambda}'_l((0,i0);(0,i0)) \, \big] \\
&\qquad - \ \big[\, \dot{\Lambda}_l((q,i\epsilon);(-q,i\epsilon)) - \dot{\Lambda}'_l((-q,-i\epsilon);(q,-i\epsilon)) \, \big] \\
&\qquad - \ \big[\, \dot{\Lambda}_l((0,i0);(q,-i\epsilon)) - \dot{\Lambda}'_l((0,i0);(-q,i\epsilon)) \, \big] \Big\} \\
&\qquad + \ \mathcal{O}(\tilde{g}_l^4) \, .
\end{aligned} \tag{6.80}$$

For linear energy dispersion where $\dot{\Lambda}_l = \dot{\Lambda}'_l$ and $\dot{\Delta}_l = \dot{\Delta}'_l$ this equation simplifies to

$$\begin{aligned}
&\dot{\Gamma}_l^{(6)}(\alpha 0, \bar{\alpha} 0, (\pm\alpha, q, i\epsilon); (\pm\alpha, q, i\epsilon); \bar{\alpha} 0, \alpha 0) \\
&\quad = \ \tilde{g}_l^3 \Big\{ \dot{\Delta}_l((0,i0);(0,i0)) + \dot{\Delta}_l((q,-i\epsilon);(q,-i\epsilon)) - 2\,\dot{\Delta}_l((0,i0);(q,-i\epsilon)) \\
&\qquad + \dot{\Lambda}_l((q,i\epsilon);(0,i0)) - \dot{\Lambda}_l((-q,-i\epsilon);(0,i0)) \\
&\qquad - \dot{\Lambda}_l((q,i\epsilon);(-q,i\epsilon)) + \dot{\Lambda}_l((-q,-i\epsilon);(q,-i\epsilon)) \\
&\qquad - \dot{\Lambda}_l((0,i0);(q,-i\epsilon)) + \dot{\Lambda}_l((0,i0);(-q,i\epsilon)) \Big\} + \mathcal{O}(\tilde{g}_l^4) \, ,
\end{aligned} \tag{6.81}$$

In Fig. 6.4 **a)** we show the topologically different Feynman diagrams that contribute to the six-point vertex at order $\sim \tilde{g}_l^3$. Due to momentum conservation for the spinless g_2-model only two diagrams give a non-zero contribution, which are shown in Fig. 6.4 **b)**. The analytical expression corresponding to the first diagram involves the function $\dot{\Delta}_l$ while the second diagram involves $\dot{\Lambda}_l$. Using Eq. (6.81) together with Eqs. (6.66) and (6.70) we may now state an explicit expression for the momentum- and frequency-dependent part of the six-point vertex at order $\sim \tilde{g}_l^3$,

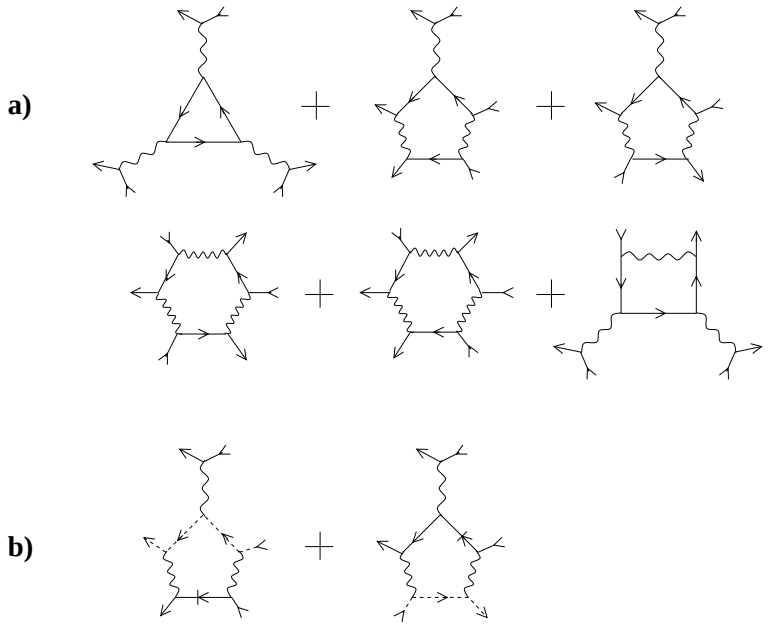

Figure 6.4: **a)** Topologically different Feynman graphs contributing to the six-point vertex at third order in the bare coupling. **b)** The two graphs contributing within our model. The solid (dashed) directed lines correspond to the propagators of right (left) moving fermions. The slashed line symbolizes the propagator $\dot{G}_l$.

$$\begin{aligned}
&\tilde{\gamma}_l^{(6)}(\alpha 0, \bar{\alpha} 0, (\pm\alpha, q, i\epsilon); (\pm\alpha, q, i\epsilon); \bar{\alpha} 0, \alpha 0) \\
&\quad = \quad \Delta_l((0, i0); (0, i0)) + \Delta_l((q, -i\epsilon); (q, -i\epsilon)) \\
&\qquad -2\,\Delta_l((0, i0); (q, -i\epsilon)) + 2\,\Lambda_l((q, i\epsilon); (0, i0)) \\
&\qquad -2\,\Lambda_l((q, i\epsilon); (-q, i\epsilon)) - 2\,\Lambda_l((0, i0); (q, -i\epsilon))
\end{aligned} \tag{6.82}$$

where we have defined

$$\Delta_l((q, i\epsilon); (q', i\epsilon')) = \int_0^l dt\, e^{-t}\, \dot{\Delta}_{l-t}((e^{-t}q, e^{-t}i\epsilon); (e^{-t}q', e^{-t}i\epsilon'))\,, \tag{6.83}$$

$$\begin{aligned}
\Lambda_l((q, i\epsilon); (q', i\epsilon')) &= \frac{1}{2}\int_0^l dt\, e^{-t} \big[\dot{\Lambda}_{l-t}((e^{-t}q, e^{-t}i\epsilon); (e^{-t}q', e^{-t}i\epsilon')) \\
&\quad -\dot{\Lambda}_{l-t}((-e^{-t}q, -e^{-t}i\epsilon); (-e^{-t}q', -e^{-t}i\epsilon'))\big]\,.
\end{aligned} \tag{6.84}$$

For the explicit calculation of the functions Δ_l and Λ_l we first need to determine the auxiliary functions $\dot{\Delta}_l$ and $\dot{\Lambda}_l$ from their definitions in Eqs. (6.72) and (6.74). It is possible to state a closed expression for these two functions, but many cases have to be distinguished depending on the actual values of the arguments. In particular at this stage of the calculation we meet again the problem outlined in Sec. 3.1 where we discussed the subtleties of the sharp-cutoff limit. Note for instance that the first term on the r.h.s. of Eq. (6.81) involves the combination $\delta(|q|-1)\Theta^2(1<|q|<e^l)$ due to the fact that $q=q'=\epsilon=\epsilon'=0$ in the definition (6.72) of $\dot{\Delta}_l$. This has to be interpreted in the sense of Eq. (3.5), such that $\delta_\epsilon(|q|-1)\Theta_\epsilon^2(1<|q|<e^l)\to 1/3\,\delta(|q|-1)$ when the smoothness parameter ϵ is sent to zero. In the same way we obtain $\delta_\epsilon(|q|-1)\Theta_\epsilon(1<|q|<e^l)\to 1/2\,\delta(|q|-1)$. Keeping this in mind the integrations in Eqs. (6.72) and (6.74) may be performed straightforwardly and we get the following results,

$$\dot{\Delta}_l((0,i0);(0,i0)) = 0\,, \tag{6.85}$$

$$\dot{\Delta}_l((q,-i\epsilon);(q,-i\epsilon)) = \frac{s_q}{2}\,\frac{\Theta(|q|<e^l-1)}{[i\epsilon s_q+\tilde{v}_l(|q|+2)]^2}\,, \tag{6.86}$$

$$\dot{\Lambda}_l((q,i\epsilon);(0,i0)) = -\frac{s_q}{4}\,\frac{\Theta(|q|<e^l-1)}{[i\epsilon s_q-\tilde{v}_l(|q|+2)]^2}\,, \tag{6.87}$$

$$\begin{aligned}\dot{\Lambda}_l((0,i0);(q,-i\epsilon)) &= \dot{\Delta}_l((0,i0);(q,-i\epsilon))\\ &= \frac{s_q}{8\tilde{v}_l}\left\{\frac{\Theta(|q|<e^l-1)}{i\epsilon s_q+\tilde{v}_l(|q|+2)}+\frac{\Theta(2<|q|<e^l+1)}{i\epsilon s_q+\tilde{v}_l|q|}\right\},\end{aligned} \tag{6.88}$$

$$\begin{aligned}&\dot{\Lambda}_l((q,i\epsilon);(-q,\epsilon))\\ &= \frac{s_q}{4\tilde{v}_l}\left\{\frac{\Theta(|q|<e^l-1)}{[|q|+1]\,[i\epsilon s_q-\tilde{v}_l(|q|+2)]}+\frac{\Theta(2<|q|<e^l+1)}{[|q|-1]\,[i\epsilon s_q+\tilde{v}_l|q|]}\right\},\end{aligned} \tag{6.89}$$

In a next step we have to calculate the corresponding equations for the functions Δ_l and Λ_l using Eqs. (6.83) and (6.84). This yields

$$\Delta_l((0,i0);(0,i0)) = 0\,, \tag{6.90}$$

$$\Delta_l((q,-i\epsilon);(q,-i\epsilon)) = \frac{s_q}{2}\,\frac{\Theta(|q|<e^l-1)\,(e^l-1-|q|)}{[i\epsilon s_q+\tilde{v}_l(|q|+2)]\,[i\epsilon s_q+\tilde{v}_l(2e^l-|q|)]}\,, \tag{6.91}$$

$$\Lambda_l((q,i\epsilon);(0,i0)) = -\frac{s_q}{4}\,\frac{\Theta(|q|<e^l-1)\,(e^l-1-|q|)}{[i\epsilon s_q-\tilde{v}_l(|q|+2)]\,[i\epsilon s_q-\tilde{v}_l(2e^l-|q|)]}\,, \tag{6.92}$$

$$\begin{aligned}
&\Lambda_l((0,i0);(q,-i\epsilon)) = \Delta_l((0,i0);(q,-i\epsilon)) \\
&= \frac{s_q}{8\tilde{v}_l\,(i\epsilon s_q+\tilde{v}_l|q|)}\Bigg\{\Theta(2<|q|<e^l+1)\,\ln\left|\frac{q}{2}\right| \\
&\quad+\Theta(e^l+1<|q|<2e^l)\,\ln\left|\frac{q}{2(|q|-e^l)}\right| \\
&\quad+\Theta(|q|<e^l-1)\,\left[\ln\left|e^l-|q|\right|+\ln\left(\frac{i\epsilon s_q+\tilde{v}_l(|q|+2)}{i\epsilon s_q+\tilde{v}_l(2e^l-|q|)}\right)\right]\Bigg\}\,,
\end{aligned} \tag{6.93}$$

$$\begin{aligned}
&\Lambda_l((q,i\epsilon);(-q,i\epsilon)) \\
&= \frac{s_q}{4\tilde{v}_l\,(i\epsilon s_q+\tilde{v}_l|q|)}\Bigg\{-\Theta(2<|q|<e^l+1)\,\ln\left|\frac{q}{2(|q|-1)}\right| \\
&\quad-\Theta(e^l+1<|q|<2e^l)\,\ln\left|\frac{q}{2e^l}\right| \\
&\quad-\Theta(|q|<e^l-1)\,\left[\ln\left(\frac{i\epsilon s_q-\tilde{v}_l(|q|+2)}{i\epsilon s_q-\tilde{v}_l(2e^l-|q|)}\right)+\ln\left|\frac{e^l}{|q|+1}\right|\right]\Bigg\}\,,
\end{aligned} \tag{6.94}$$

Now, combining the results (6.90) – (6.94) in Eq. (6.82) yields the final result for the momentum- and frequency-dependent part of the six-point vertex at order $\sim \tilde{g}_l^3$,

$$\begin{aligned}
&\tilde{\gamma}_l^{(6)}(\alpha 0,\bar{\alpha}0,(\pm\alpha,q,i\epsilon);(\pm\alpha,q,i\epsilon);\bar{\alpha}0,\alpha 0) \\
&= -s_q\,\Theta(|q|<e^l-1)\Bigg\{\frac{i\epsilon s_q\,4\tilde{v}_l\,(1+e^{-l})(1+|q|e^{-l}-e^{-l})}{[\epsilon^2+\tilde{v}_l^2(2+|q|)^2]\,[\epsilon^2e^{-2l}+\tilde{v}_l^2(2-|q|e^{-l})^2]} \\
&\quad+\frac{1}{\tilde{v}_l[i\epsilon s_q+\tilde{v}_l|q|]}\,\left[\ln\left(\frac{\epsilon^2+\tilde{v}_l^2(2+|q|)^2}{\epsilon^2e^{-2l}+\tilde{v}_l^2(2-|q|e^{-l})^2}\right)+\ln\left|\frac{1-|q|e^{-l}}{1+|q|}\right|\right]\Bigg\} \\
&\quad-s_q\,\Theta(2<|q|<e^l+1)\,\frac{\ln|1-|q||}{\tilde{v}_l[i\epsilon s_q+\tilde{v}_l|q|]}
\end{aligned}$$

$$+ s_q\,\Theta(1+e^l<|q|<2e^l)\,\frac{\ln|1-|q|e^{-l}|}{\tilde{v}_l[i\epsilon s_q+\tilde{v}_l|q|]}\,. \tag{6.95}$$

Note that this expression approaches a finite limit when $l\to\infty$. All that remains for the calculation of B_l is to perform the final Q-integrations in Eqs. (6.68) and (6.69). First of all note that for linear dispersion Eq. (6.68) simplifies to

$$B_l^{(4)} = -\,8\,\tilde{g}_l^3\int_Q{}' \dot{G}_l^0(q,i\epsilon)\,\tilde{G}_l(-q,i\epsilon)\,\tilde{\chi}_l(q,i\epsilon)\,. \tag{6.96}$$

Again the $\tilde{\Pi}_l$-term vanishes due to the fact that $\tilde{\Pi}_l$ is only non-zero for $|q|>2$. Inserting the explicit expression for the susceptibility $\tilde{\chi}_l$ given in Eq. (6.51) into Eq. (6.96) the remaining integrations may be performed and we obtain

$$B_l^{(4)} = \frac{\tilde{g}_l^3}{\tilde{v}_l^2}\left[\,l\,\Theta(2-e^l)+\ln 2\,\Theta(e^l-2)\,\right]. \tag{6.97}$$

In the same way we proceed for $B_l^{(6)}$. From Eqs. (6.69) and (6.95) we get

$$B_l^{(6)} = \frac{\tilde{g}_l^3}{4\tilde{v}_l^2}\left[\,1-2e^{-l}-4\ln(2-2e^{-l})\,\right]\Theta(e^l-2)\,. \tag{6.98}$$

Finally, let us rewrite the flow equation for $\tilde{g}_l$ given in Eq. (6.28) in the following way,

$$\partial_l\tilde{g}_l = B_l^{(r)} + B_l\,, \tag{6.99}$$

where $B_l^{(r)}$ denotes the rescaling contribution to the flow of $\tilde{g}_l$ explicitly given by

$$B_l^{(r)} = -2\eta_l\tilde{g}_l = -\,\frac{\tilde{g}_l^3}{4\tilde{v}_l^2}\,(1-2e^{-l})\,\Theta(e^l-2)+\mathcal{O}(\tilde{g}_l^4)\,, \tag{6.100}$$

where for the second equality we have used Eq. (6.62). The final two-loop result is then given by

$$\boxed{\begin{aligned}\partial_l\tilde{g}_l &= B_l^{(r)}+B_l^{(4)}+B_l^{(6)}\\ &= \frac{\tilde{g}_l^3}{\tilde{v}_l^2}\left[\,l\,\Theta(2-e^l)-\ln(1-e^{-l})\,\Theta(e^l-2)\right].\end{aligned}} \tag{6.101}$$

Our first observation is that

$$\lim_{l\to\infty}\partial_l\tilde{g}_l = 0\,. \tag{6.102}$$

In contrast to the one-loop result (6.41) at two-loop order this is only an asymptotic result and it is instructive to see how it comes about. Note that according to Eqs. (6.97), (6.98) and (6.100) for $l \gg 1$ we have

$$B_l^{(r)} \simeq -\frac{\tilde{g}_l^3}{4\tilde{v}_l^2}\,, \tag{6.103}$$

$$B_l^{(4)} \simeq \frac{\tilde{g}_l^3}{\tilde{v}_l^2}\ln 2\,, \tag{6.104}$$

$$B_l^{(6)} \simeq \frac{\tilde{g}_l^3}{4\tilde{v}_l^2} - \frac{\tilde{g}_l^3}{\tilde{v}_l^2}\ln 2\,, \tag{6.105}$$

where "$\simeq$" means "asymptotically equal". From Eqs. (6.103) – (6.105) it is easy to sea that the first term of $B_l^{(6)}$ cancels the field-rescaling contribution $B_l^{(r)}$ and the second term cancels the contribution of $B_l^{(4)}$. This in turn means that *if we had used the unrescaled flow equations, i.e. if we had neglected $B_l^{(r)}$, the momentum- and frequency-independent part of the four-point vertex would have exhibited a runaway flow.* To see this clearer we shall now integrate the flow equations. First of all notice that the expression on the r.h.s. of Eq. (6.101) is continuous for all $l \geq 0$. This is obvious except for the point $l = \ln 2$, where the assertion is easily checked by approaching $l = \ln 2$ from the left and from the right separately. Note that this implies that $\tilde{g}_l$ varies smoothly at this point. However, we cannot directly integrate Eq. (6.101) as it couples to the flow of $\tilde{v}_l$, which is determined by the flow equation (6.63). From this equation follows

$$\tilde{v}_l = \sqrt{\tilde{v}_0 + \frac{\tilde{g}_l^2}{2}(1-2e^{-l})\Theta(e^l-2)}\,, \tag{6.106}$$

where we have again neglected non-localities in the dependence of $\tilde{v}_l$ on l, leading to corrections beyond the two-loop order. For small values of $\tilde{g}_l$ Eq. (6.106) can be expanded in powers of $\tilde{g}_l$, leading to

$$\boxed{\tilde{v}_l = 1 + \frac{\tilde{g}_l^2}{4}(1-2e^{-l})\Theta(e^l-2) + \mathcal{O}(\tilde{g}_l^3)\,,} \tag{6.107}$$

where we have used that $\tilde{v}_0 = 1$. Note that $\tilde{v}_l$ is continuous but not differentiable at the point $l = \ln 2$, which can also be seen in Fig. 6.7, where the flow of $\tilde{v}_l$ is shown for several initial values of $\tilde{g}_l$.[4] In Sec. 7.1 we will see explicitly that $\tilde{v}_l$ does not correspond to the renormalization factor of the charge velocity of the

[4]For the line-shapes in Fig. 6.7 we have replaced $\tilde{g}_l$ with $\tilde{g}_0$ since keeping $\tilde{g}_l$ gives rise to terms of order $\sim \tilde{g}_0^4$, see Eq. (6.111).

g_2-model. This is indeed not surprising if we keep in mind that the flow equation for $\tilde{v}_l$ has been derived by expanding the logarithms in Eq. (6.59) in powers of q and ϵ. As we have shown in Sec. 5 such an expansion is only justified in the hydrodynamic regime but not in the scaling regime where $|q| \gg 1$ and $|\epsilon| \gg 1$ and where we expect to recover the results of perturbation theory.
Now, if we insert our result for $\tilde{v}_l$ in the flow equation (6.101) for $\tilde{g}_l$ we see that keeping $\tilde{v}_l$ gives rise to higher orders in the coupling $\tilde{g}_l$. Hence, within a two-loop expansion we should better insert $\tilde{v}_l = 1$ such that Eq. (6.101) can be integrated to

$$\tilde{g}_l = \frac{\tilde{g}_0}{\sqrt{1 - 2\tilde{g}_0^2 K_l}}\,, \tag{6.108}$$

where the function K_l is given by

$$K_l = \Theta(2 - e^l)\,\frac{l^2}{2} + \Theta(e^l - 2)\left[\,\frac{\pi^2}{12} - \mathrm{Li}_2(e^{-l})\,\right]. \tag{6.109}$$

Here Li_2 is the Dilogarithm function defined by [91]

$$\mathrm{Li}_2(z) = -\int_0^z dt\,\frac{\ln(1-t)}{t}\,. \tag{6.110}$$

At two-loop order we should expand the result for $\tilde{g}_l$ in powers of the initial value $\tilde{g}_0$ which leads to

$$\boxed{\tilde{g}_l = \tilde{g}_0\,(1 + \tilde{g}_0^2\,K_l) + \mathcal{O}(\tilde{g}_0^4)\,.} \tag{6.111}$$

Just like we expect it from the properties of the flow equation of $\tilde{g}_l$ this result can be shown to have a continuous derivative even at the point $l = \ln 2$ such that K_l is a smooth function of the flow parameter l. To prove this it is advantageous to use functional relationships of the Dilogarithm function [91] implying

$$\mathrm{Li}_2\big(\tfrac{1}{2}\big) = \frac{\pi^2}{12} - \frac{(\ln 2)^2}{2}\,. \tag{6.112}$$

By closer observation of Eqs. (6.108) and (6.109) we recognize that for large enough initial values $\tilde{g}_0$ the r.h.s. of Eq. (6.108) diverges or is even ill-defined. These problems, however, only arise for values of $\tilde{g}_0$ beyond a weak coupling expansion. It can be shown that the function K_l defined in Eq. (6.109) grows strictly monotonically. On the other hand from Eq. (6.110) follows $\lim_{l\to\infty} \mathrm{Li}_2(e^{-l}) = 0$ such that

$$\lim_{l\to\infty} K_l = \frac{\pi^2}{12} \tag{6.113}$$

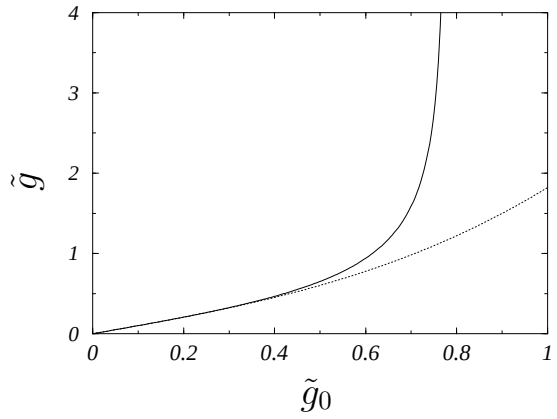

Figure 6.5: The solid line represents the function $\tilde{g}(\tilde{g}_0) = \tilde{g}_0/\sqrt{1-\tilde{g}_0^2\pi^2/6}$ determined by Eq. (6.108) in the limit $l \to \infty$. The expression becomes singular at $\tilde{g}_0 = \sqrt{6}/\pi \approx 0.78$. The dotted line shows the approximating function at two-loop order given by Eq. (6.111) in the limit $l \to \infty$. In the range $0 \leq \tilde{g}_0 \lesssim 0.4$ the fixed-point value $\tilde{g}$ remains small such that our weak-coupling expansion in $\tilde{g}_l$ is justified even at the fixed point.

appears to be the maximum value of K_l. This implies that Eq. (6.108) is only well defined for initial values satisfying

$$\tilde{g}_0 < \frac{\sqrt{6}}{\pi} \approx 0.78\,. \tag{6.114}$$

In Fig. 6.5 the fixed-point value $\tilde{g}$ is shown as a function of the initial value $\tilde{g}_0$ as predicted by Eq. (6.108) in the limit $l \to \infty$. From this plot we may draw the conclusion that our weak-coupling expansion can be trusted for initial values $\tilde{g}_0 \lesssim 0.4$.[5] For this range of allowed initial values we should replace Eq. (6.108) by Eq. (6.111).
The two-loop flow of the couplings Z_l and η_l is now obtained from Eqs. (6.62) and (6.64) by setting $\tilde{v}_l = 1$ and $\tilde{g}_l = \tilde{g}_0$,

$$\boxed{\begin{aligned} \eta_l &= \frac{\tilde{g}_0^2}{8}\,(1-2e^{-l})\,\Theta(e^l-2) \\ Z_l &= e^{-\bar{\eta}_l l}\,. \end{aligned}} \tag{6.115}$$

[5]The singular behavior of the function $\tilde{g}(\tilde{g}_0)$ is also reflected in the exact solution of the TLM when the g_4-coupling is set equal to zero. In this case the anomalous dimension diverges at $\tilde{g}_0 = 1$, which is an artifact of the pure g_2-model.

The scale-averaged anomalous dimension defined in Eq. (4.48) is at two-loop level given by

$$\bar{\eta}_l = \frac{\tilde{g}_0^2}{8}\left[1 - \frac{1+\ln 2 - 2e^{-l}}{l}\right]\Theta(e^l - 2) + \mathcal{O}(\tilde{g}_0^3)\,. \tag{6.116}$$

In contrast to $\tilde{v}_l$ and η_l for the couplings Z_l and $\bar{\eta}_l$ it can be shown that they are smooth functions of the logarithmic scale parameter l. However, the bare anomalous dimension η_l is continuous but not differentiable at $l = \ln 2$ and its slope jumps from zero to $\tilde{g}_0^2/8$ at this point. It is now easy to find the two-loop fixed-point values of the four couplings if we send $l \to \infty$ in Eqs. (6.107), (6.111) and (6.115),

$$\boxed{\begin{gathered}\tilde{\mu} = \frac{\tilde{g}}{2} \quad , \quad \tilde{v} = 1 + \frac{\tilde{g}^2}{4} \quad , \quad \tilde{g} = \tilde{g}_0\left(1 + \frac{\pi^2}{12}\,\tilde{g}_0^2\right), \\ Z = 0 \quad , \quad \eta = \frac{\tilde{g}^2}{8}\,.\end{gathered}} \tag{6.117}$$

For the fixed-point value $\tilde{g}$ we have used Eq. (6.113), and for completeness we have added the two-loop result for the chemical-potential parameter $\tilde{\mu}_l$, obtained from Eqs. (6.44) and (6.56). Note that in contrast to the one-loop results the set of fixed-point values at two-loop order describe a Luttinger rather than a Fermi liquid. The finite anomalous dimension is proportional to the interaction strength and hence non-universal in nature. In Figs. 6.6 – 6.8 we show the flow of the couplings $\tilde{g}_l$, $\tilde{v}_l$ and Z_l as functions of the flow parameter l for different initial values $\tilde{g}_0$. In Fig. 6.9 we compare the flow of the bare anomalous dimension η_l with that of the scale-averaged anomalous dimension $\bar{\eta}_l$. We see that the latter approaches the common fixed-point value much slower than η_l which is also obvious from Eqs. (6.115) and (6.116).

So far we have finished the two-loop calculation. A new aspect of our formalism is that it enables us to precisely follow the flow of the couplings over the whole energy regime from $\Lambda = \Lambda_0$ to $\Lambda = 0$ and we will draw some important conclusions upon this fact in the next section when we discuss the role of the Dirac sea.

Let us now discuss the consequences related to the field rescaling contribution $B_l^{(r)}$ on the flow of $\tilde{g}_l$. To this end we denote the momentum- and frequency-independent part of the *unrescaled* four-point vertex at the scale $\Lambda = \Lambda_0 e^{-l}$ by g_l, i.e.

$$\Gamma^{(4)}_{\Lambda_0 e^{-l}}(\alpha_1' k_F, 0, \alpha_2' k_F, 0; \alpha_2 k_F, 0, \alpha_1 k_F, 0) = A_{\alpha_1'\alpha_2';\,\alpha_2\alpha_1}\, g_l\,. \tag{6.118}$$

The flow equation for g_l is simply obtained from Eq. (6.101) by dropping the contribution of $B_l^{(r)}$ and inserting the correct physical dimensions according to

the initial condition (6.11). Explicitly we have

$$\partial_l g_l = \nu_0^2\, g_l^3 \Big[l\,\Theta(2-e^l) + \big[\tfrac{1}{4}(1-2e^{-l}) - \ln(1-e^{-l})\big]\Theta(e^l-2) \Big]\,, \qquad (6.119)$$

which integrates to

$$g_l = \frac{g_0}{\sqrt{1-2(\nu_0 g_0)^2 M_l}}\,. \qquad (6.120)$$

The function M_l is given by

$$\begin{aligned} M_l &= \frac{l^2}{2}\Theta(2-e^l) \\ &+ \Big[\frac{1}{4}(\,l - \ln 2 + 2e^{-l} - 1) + \frac{\pi^2}{12} - \mathrm{Li}_2(e^{-l})\Big]\Theta(e^l-2)\,, \end{aligned} \qquad (6.121)$$

which is still a smooth and strictly monotonically increasing function. But in contrast to K_l defined in Eq. (6.109) it is unbounded and grows linearly with l for $l \gg 1$. This implies that for *any* initial value g_0 there exists a finite scale $l^\star$ for which $g_{l^\star}$ becomes singular. For $|\nu_0 g_0| \ll 1$ this scale is approximately given by $l^\star \approx 2/(\nu_0 g_0)^2$. Hence the unrescaled flow equations predict an unphysical flow to strong coupling at a finite energy scale, while no such runaway flow exists for the properly rescaled coupling $\tilde{g}_0$. We have already pointed out that the TLM is an effective model where the g_2-and g_4-couplings have to be identified with the RG fixed-point values for the corresponding scattering processes. This is why we should identify

$$\nu_0 g_2 = \lim_{l\to\infty} \tilde{g}_l = \nu_0 \lim_{l\to\infty} [Z_l^2 g_l]\,. \qquad (6.122)$$

The second equality follows from Eq. (5.38) in one dimension, which is in turn a consequence of the scaling equation (4.29). Eq. (6.122) shows that the runaway flow of the unrescaled coupling g_l is exactly compensated by the vanishing quasi-particle residue Z_l such that the rescaled coupling $\tilde{g}_l$ remains finite at all scales.

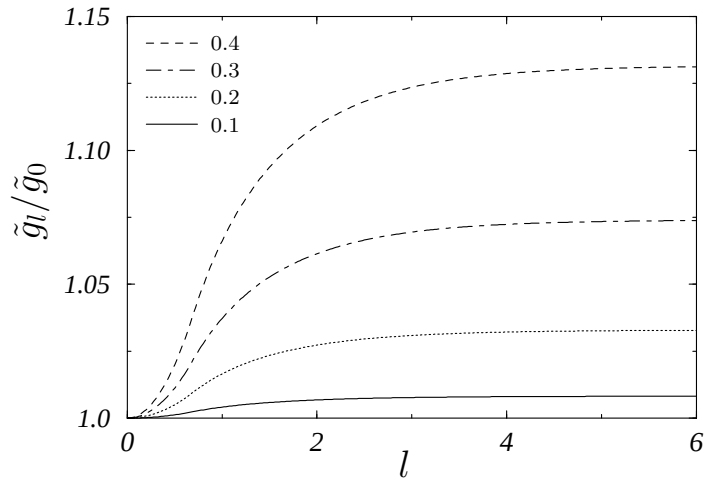

Figure 6.6: Relative change of the the dimensionless interaction coupling $\tilde{g}_l$ as a function of the flow parameter l as determined by Eq. (6.111). The flow is shown for the initial values $\tilde{g}_0$ depicted in the legend. Note that $\tilde{g}_l/\tilde{g}_0$ rapidly approaches its fixed-point value $\tilde{g}/\tilde{g}_0 = 1 + \tilde{g}_0^2\pi^2/12$.

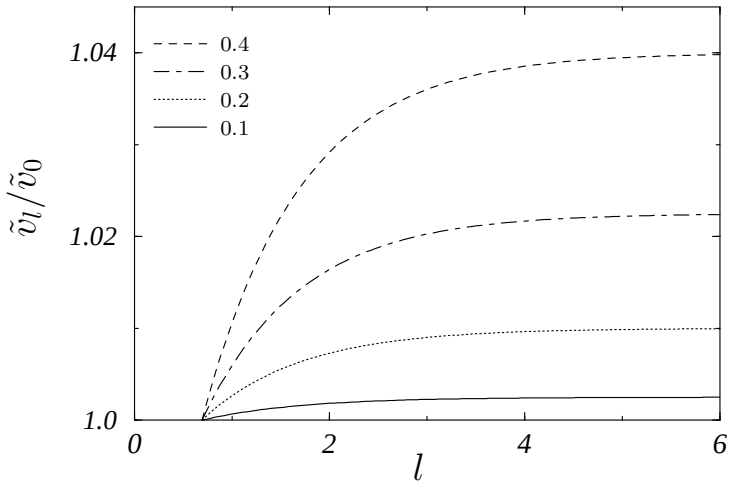

Figure 6.7: Relative change of the velocity renormalization factor $\tilde{v}_l$ as a function of the flow parameter for four different values of $\tilde{g}_0$, see Eq. (6.107). Note that $\tilde{v}_l$ is continuous but not differentiable at $l = \ln 2$.

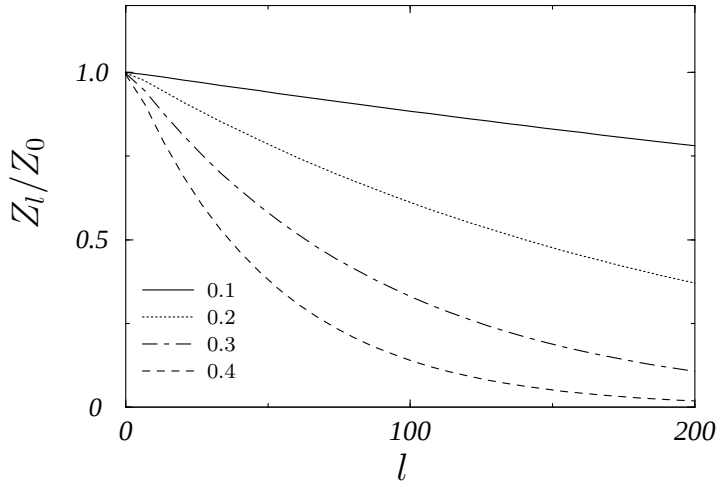

Figure 6.8: Decay of the quasi-particle residue Z_l as a function of the flow parameter determined by Eq. (6.115). Note that Z_l decays very slowly with l, such that only at very small energy scales it may be set equal to zero. The flow is shown for the initial values $\tilde{g}_0$ depicted in the legend.

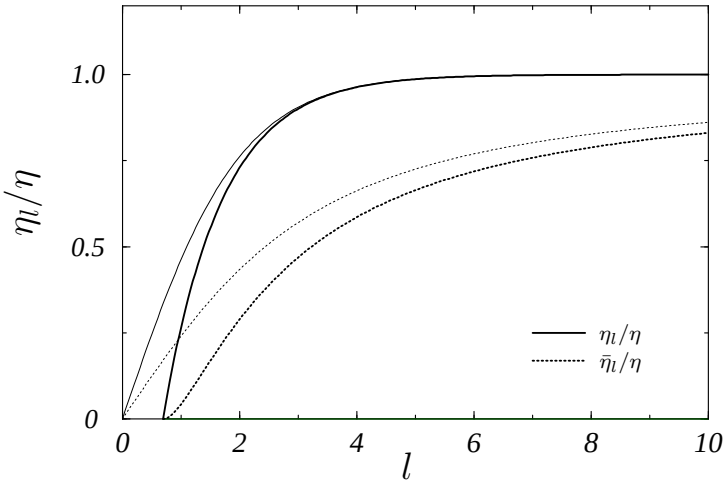

Figure 6.9: Comparison of the flow of the bare anomalous dimension η_l with the flow of the scale-averaged anomalous dimension $\bar{\eta}_l$. The thick lines represent the results given by Eqs. (6.115) and (6.116) while the light curves show the corresponding results obtained for the model with infinite Dirac sea, see Eqs. (6.128) and (6.134). In both cases $\bar{\eta}_l$ approaches the common fixed point $\eta = \tilde{g}_0^2/8$ only as $\sim 1/l$ while η_l approaches it exponentially.

6.4 Dirac Sea and Energy Scales

In this section we wish to discuss the consequences resulting from the introduction of the Dirac sea. In our context the Dirac sea is related to a mathematical construction extending the range of validity of the linearized energy dispersion to all momenta p. This only possible in a unique way if we introduce two different types of Fermions which we have called right- and left-movers. Originally introduced by Luttinger [2] this was the first and crucial step towards the exact solubility of the TLM. However, such a construction is also associated with conceptional problems, in particular with an infinite ground state energy which can be compensated by introducing the "Dirac sea" consisting of infinitely many Fermions of negative energy. As has been shown by Gutfreud and Schick [4] the low-energy physics is *qualitatively* unaffected by the unphysical Dirac sea. On the other hand Schulz and Shastry [92] argued that the Dirac sea leads to corrections of the anomalous dimension in the next-to-leading orders in a weak-coupling expansion. We will now explicitly verify this assertion using our RG method.
The first question we have to answer is how the Dirac sea can be introduced within our model? This is not as obvious as it might seem at first sight. Of course, extending the range of the linearized energy dispersion to infinity is achieved by the limit $\Lambda_0 \to \infty$, see Fig. 1.1. However, for the infrared cutoff Λ this leads to an ill-defined initial condition: Note that for $l = 0$ we have $\Lambda = \Lambda_0$. This conceptional problem cannot be avoided within our formalism as we cannot send $\Lambda = \Lambda_0 e^{-l}$ to infinity as well. We will hence proceed in considering Λ as an independent parameter and demand that physically meaningful results must not depend on its initial value Λ_0.
Within our formalism the limit $\Lambda_0 \to \infty$ formally amounts to dropping the condition $|q| < e^l = \Lambda_0/\Lambda$ within the Θ-functions of the dimensionless Green functions defined in Eq. (6.12). It is then easy to check that for the auxiliary functions $\dot{\Pi}_l$, $\dot{\chi}_l$, $\dot{\Delta}_l$ and $\dot{\Lambda}_l$ defined in the previous section this simply means that we have to send the factors e^l to infinity. This is *not* true anymore for their l-integrated versions like for instance the susceptibilities $\tilde{\Pi}_l$ and $\tilde{\chi}_l$. Note that the upper integration boundaries in Eqs. (6.48) and (6.49) give rise to additional factors e^l in the explicit results, which have nothing to do with the ultraviolet cutoff Λ_0. We thus cannot just send $e^l \to \infty$ in our previous final results for the flow of the couplings $Z_l, \tilde{v}_l, \tilde{g}_l$ and η_l. We have to repeat the whole calculations, this time using

$$\tilde{G}_l^0(Q) = \frac{\Theta(1 < |q|)}{i\epsilon - \tilde{v}_l q}\,, \tag{6.123}$$

instead of Eq. (6.17). Since the calculations are principally the same like before we will only state the most important results and assign all relevant quantities with

an index D for "Dirac sea" in favor of a clear distinction. The inhomogeneities of the two-point vertex given in Eqs. (6.58) and (6.59) now turn into

$$\begin{aligned}\dot{\Gamma}^{(2,\mathrm{ZS})}_{D,l}(q,i\epsilon) &= \frac{(\tilde{g}_l^D)^2}{4}\, s_q \Big[\Theta(1<|q|<2e^l-1)\, \frac{1-|q|}{i\epsilon s_q + \tilde{v}_l^D(|q|+2)} \\ &\qquad + \Theta(2e^l-1<|q|)\, \frac{2(e^l-1)}{i\epsilon s_q + \tilde{v}_l^D(|q|+2)} \Big] \\ &\quad + \mathcal{O}((\tilde{g}_l^D)^3)\,, \end{aligned} \tag{6.124}$$

and

$$\begin{aligned}\dot{\Gamma}^{(2,\mathrm{PB})}_{D,l}(q,i\epsilon) &= \frac{(\tilde{g}_l^D)^2}{4\tilde{v}_l^D}\, s_q \Big[\Theta(|q|<1)\, \ln\left(\frac{i\epsilon s_q + \tilde{v}_l^D(4-|q|)}{i\epsilon s_q + \tilde{v}_l^D(2e^l+2-|q|)}\right) \\ &\qquad + \Theta(1<|q|)\, \ln\left(\frac{i\epsilon s_q + \tilde{v}_l^D(2+|q|)}{i\epsilon s_q + \tilde{v}_l^D(2e^l+|q|)}\right) \\ &\qquad - \ln\left(\frac{i\epsilon s_q - \tilde{v}_l^D(4+|q|)}{i\epsilon s_q - \tilde{v}_l^D(2e^l+2+|q|)}\right) \Big] \\ &\quad + \mathcal{O}((\tilde{g}_l^D)^3)\,. \end{aligned} \tag{6.125}$$

Like before $\dot{\Gamma}^{(2,\mathrm{ZS})}_{D,l}$ does not contribute to the flow of $\tilde{v}_l^D$ and η_l^D. Expanding $\dot{\Gamma}^{(2,\mathrm{PB})}_{D,l}$ in powers of q and ϵ we get

$$\dot{\Gamma}^{(2,\mathrm{PB})}_{D,l}(q,i\epsilon) = \frac{(\tilde{g}_l^D)^2}{8(\tilde{v}_l^D)^2}\left(1-\frac{2}{e^l+1}\right)(i\epsilon - \tilde{v}_l^D q) + \mathcal{O}(q^2,\epsilon^2,q\epsilon)\,, \tag{6.126}$$

leading to

$$\boxed{\partial_l \tilde{v}_l^D = 0\,,} \tag{6.127}$$

and

$$\boxed{\eta_l^D = \frac{(\tilde{g}_l^D)^2}{8(\tilde{v}_l^D)^2}\left(1-\frac{2}{e^l+1}\right).} \tag{6.128}$$

For the flow of the coupling $\tilde{g}_l^D$ we find the contributions

$$B_l^{(D,r)} = \frac{(\tilde{g}_l^D)^3}{4(\tilde{v}_l^D)^2}\left(\frac{2}{e^l+2}-1\right) + \mathcal{O}((\tilde{g}_l^D)^4)\,, \tag{6.129}$$

$$B_l^{(D,4)} = \frac{(\tilde{g}_l^D)^3}{(\tilde{v}_l^D)^2} \ln\left(\frac{2}{1+e^{-l}}\right) + \mathcal{O}((\tilde{g}_l^D)^4)\,, \tag{6.130}$$

and

$$B_l^{(D,6)} = \frac{(\tilde{g}_l^D)^3}{4(\tilde{v}_l^D)^2}\left[1 - \frac{2}{e^l+1} - 4\ln\left(\frac{2}{1+e^{-l}}\right)\right] + \mathcal{O}((\tilde{g}_l^D)^4)\,, \tag{6.131}$$

such that

$$\boxed{\partial_l \tilde{g}_l^D = B_l^{(D,r)} + B_l^{(D,4)} + B_l^{(D,6)} = 0\,.} \tag{6.132}$$

Hence the couplings $\tilde{v}_l^D$ and $\tilde{g}_l^D$ do not flow at all even at two-loop level, implying

$$\tilde{v}_l^D = \tilde{v}_0^D = 1 + \mathcal{O}(\tilde{g}_0^3)\,, \qquad \text{and} \qquad \tilde{g}_l^D = \tilde{g}_0^D = \tilde{g}_0 + \mathcal{O}(\tilde{g}_0^4)\,. \tag{6.133}$$

In contrast the anomalous dimension η_l^D undergoes a flow from zero to its fixed-point value, this time already starting at $l = 0$ instead of $l = \ln 2$ for finite Λ_0, see also Fig. 6.9. The scale averaged anomalous dimension determining the flow of Z_l^D is easily obtained to be

$$\bar{\eta}_l^D = \frac{\tilde{g}_0^2}{8}\left[1 + \frac{2}{l}\ln\left(\frac{1+e^{-l}}{2}\right)\right], \tag{6.134}$$

where we have already used Eq. (6.133). The quasi-particle residue is then given by

$$Z_l^D = \exp[-\bar{\eta}_l^D l]\,. \tag{6.135}$$

Hence, for the fixed-point values at the two-loop order we find

$$\boxed{\begin{aligned} \tilde{v}^D &= 1 \quad , \quad \tilde{g}^D = \tilde{g}_0\,, \\ Z^D &= 0 \quad , \quad \eta^D = \frac{\tilde{g}_0^2}{8}\,. \end{aligned}} \tag{6.136}$$

Keeping in mind that to leading order in the initial value $\tilde{g}_0$ according to Eq. (6.117) we have $\eta = \tilde{g}_0^2/8$ such that

$$Z^D = Z \quad \text{and} \quad \eta^D = \eta\,, \tag{6.137}$$

but

$$\tilde{v}^D \neq \tilde{v} \quad \text{and} \quad \tilde{g}^D \neq \tilde{g}\,. \tag{6.138}$$

Note that $Z^D = Z = 0$ expresses the fact that the spinless g_2-model describes a Luttinger liquid instead of a Fermi liquid. This result is well-known and we do not expect it to change if higher orders in a weak-coupling expansion are retained. However, although $\eta^D = \eta$ at two-loop level we expect $\eta^D \neq \eta$ at higher loop orders due to the fact that $\tilde{g}^D \neq \tilde{g}$. We may thus confirm the statement of Schulz and Shastry that the Dirac sea will lead to finite renormalizations of the anomalous dimension beyond the leading order. It is important to recognize that our results for the fixed-point values given in Eqs. (6.117) and (6.136) do not explicitly depend on the initial value Λ_0 *but exclusively on the fact wether* Λ_0 *is finite or not.*

Note also that within our model the introduction of the Dirac sea removes the only energy scale which is left when the fixed-point is approached. On the one hand this is just a general feature of the critical limit $\Lambda \to 0$ since we have shown in Sec. 5.1 that the fixed-point properties of non-Fermi liquids only represent *asymptotic* low-energy physics where all finite energy scales appear infinitely large. On the other hand we have just shown that the limits $\Lambda \to 0$ and $\Lambda_0 \to \infty$ do not commute and that the fixed-point properties thus have a "memory" for the fact if initially there was an energy scale other than the infrared cutoff Λ or not. Remember as well that in our case the ultraviolet cutoff Λ_0 also simulates the range of the interaction in Fourier space as we have neglected the momentum dependence of the initial interaction parameter. Hence, in introducing the Dirac sea we have also extended the range of the interaction to infinity, which is clearly unphysical but nevertheless a frequently used approximation, for instance in the on-site Hubbard model. We will return to this point when we discuss some results of the bosonization approach in Sec. 7.3. However, in more realistic models there will be an interaction cutoff p_c in momentum space defining an independent energy scale besides Λ_0. This energy scale will of course remain finite even if we introduce the Dirac sea, and the question arises in how far this cutoff leaves traces in the fixed-point results? – If we identify $\Lambda_0 = v_F p_c$ from the results of this and the previous section we conclude that in general a finite p_c will lead to finite renormalizations of the couplings and of the anomalous dimension at least beyond the leading order. Keeping in mind that p_c effectively replaces an infinite number of *irrelevant* couplings which determine the detailed momentum dependence of the initial interaction, this implies that the fixed-point results for the marginal and relevant couplings are less universal than widely believed.[6] This

[6] We have already pointed out below Eq. (6.117) that the anomalous dimension of the one-dimensional electron gas is non-universal since it explicitly depends on the initial value $\tilde{g}_0$.

statement is also supported by results drawn with the aid of the bosonization technique, see Ref. [82]. In Chap. 8 we will for instance show how the initial curvature, which is represented by an irrelevant coupling, alters the fixed-point values of the couplings $\tilde{g}_l$ and $\tilde{v}_l$.

Finally let us draw some results upon the flow we have found for the anomalous dimension η_l and the quasi-particle residue Z_l. First of all note that η_l approaches its fixed-point value exponentially fast, both with and without Dirac sea. This is also true for Z_l but the exponent is not an integer but proportional to $\bar{\eta}_l$, which is in general small compared to one even beyond weak-coupling. Consequently the quasi-particle residue decays only slowly. As we are free to stop the flow at any finite scale l, say $l = 6$ in Figs. 6.8 and 6.9 , providing us with an effective theory at the energy scale $\Lambda = \Lambda_0 e^{-6} \approx 0.002\Lambda_0$, we see that $\eta_{l=6} \approx \eta$ but still $Z_{l=6} \approx 1$. Taking this picture for serious this implies that down to a very small energy scale (actually depending on the initial value Λ_0) we find already the fully developed anomalous dimension η but a persisting quasi-particle residue of the order of one. Now, from the "exact" solution for the spectral function of the TLM we know that the anomalous dimension is assigned to collective mode excitations while in Fermi liquids Z_l measures the weight of quasi-particle excitations. It is widely accepted that the low-energy excitations of one-dimensional conductors are dominated by plasmon modes rather than quasi-particles. But it has never been quantified what "low-energy" actually means, since the spectral function of the TLM is only obtained from an asymptotic analysis, see Ref. [93, 94]. This picture may be drastically altered by our results for the flow of η_l and Z_l: If we accept Z_l to be a measure for the spectral weight of quasi-particle excitations it predicts that down to very low energy scales the quasi-particle excitations dominate and that the spectral weight of plasmon excitations remains thus negligible.[7] The energy scale where this behavior changes depends crucially on the value of η and can be determined at least for the model with finite Λ_0 using the *exact* relation

$$Z_l = e^{-\bar{\eta}_l\, l} = \left(\tfrac{\Lambda}{\Lambda_0}\right)^{\bar{\eta}_l} . \tag{6.139}$$

Here we should insert $l = -\ln(\Lambda/\Lambda_0)$ in the exponent on the r.h.s. of the equation. Keeping in mind that $\bar{\eta}_l \to \eta$ for $\Lambda \to 0$, we asymptotically have $Z_l \simeq (\Lambda/\Lambda_0)^{\eta}$, and with $x = \Lambda/\Lambda_0$ we find $\partial_x Z_l \sim \eta\, x^{\eta-1}$. Consequently for $\eta < 1$ the quasi-particle residue drops down to zero with infinite slope at $\Lambda/\Lambda_0 = 0$. In Fig. 6.10

However, it is a wide-spread belief that η must only depend on the initial values of marginal but not on those of irrelevant couplings.

[7] The latter conclusion follows from a sum rule for the spectral function: The spectral weights of all physical excitations together with a possible incoherent background must add up to one.

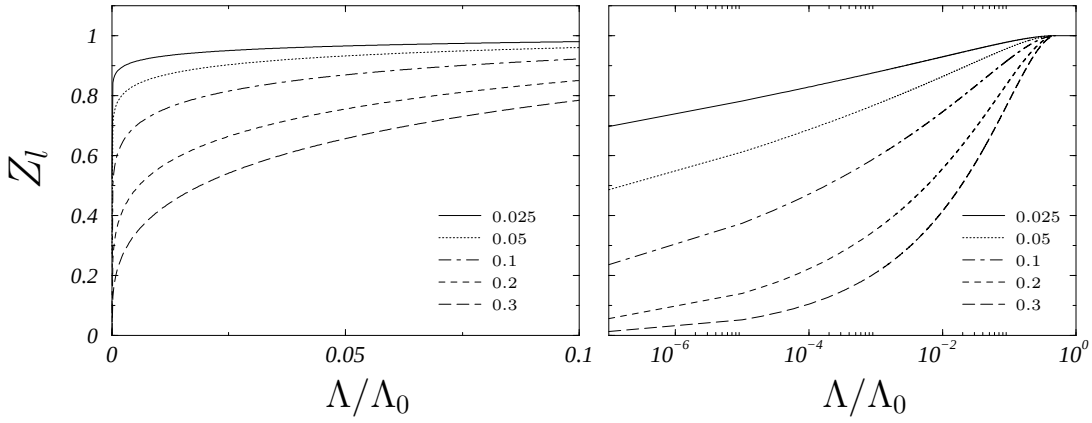

Figure 6.10: The quasi-particle residue Z_l as a function of the relative energy scale Λ/Λ_0 on a linear (left plot) and on a logarithmic scale (right plot) as predicted by Eq. (6.139). We have inserted our two-loop result for $\bar{\eta}_l$ in Eq. (6.116) for the values of η indicated in the legend.

this is shown for various values of η using our two-loop result for $\bar{\eta}_l$ given in Eq. (6.116).

Asymptotically we can invert Eq. (6.139) and determine the energy scale where $Z_l = Z \ll 1$,

$$\boxed{\frac{\Lambda}{\Lambda_0} \approx Z^{1/\eta}\,.} \tag{6.140}$$

Note that the above reasoning is independent of our weak-coupling result for $\bar{\eta}_l$ and would still be valid if we were able to resolve the flow equations exactly. In our present discussion we may hence choose arbitrary values for η. This is what we have done in Fig. 6.10, as according to our result $\eta = \tilde{g}_0^2/8$ the value $\eta = 0.1$ would already correspond to $\tilde{g}_0 \approx 0.9$, which is of course out of range of a weak-coupling expansion.

Now, imagine that there exists a low-energy scale $\Lambda^* > 0$ where the RG flow has to be stopped. This energy scale might for instance be given by a hopping amplitude to neighboring chains, thus representing a crossover scale to higher dimensionality, a finite temperature or a scale where backscattering becomes important. Let us estimate the magnitude of Λ^* in units of Λ_0 that would be sufficient to reinstate a quasi-particle weight of $Z = 1/2$ when $\eta = 0.1$. We identify Λ_0 with $v_F p_c \ll v_F k_F/2$, where p_c is the range of the interaction in momentum space. Due to Eq. (6.140) we get $\Lambda^* \approx 2^{-10} v_F p_c$. Note that this implies that already an extremely small Λ^* leads to a measurable or even dominating quasi-particle weight. In terms of our RG language this means that a finite low-energy cutoff Λ^* appears to be a

relevant perturbation of the Luttinger liquid state.
In sections 7.2 and 7.5 where we calculate the complete flow of the perturbative and the non-perturbative spectral function of the spinless g_2-model at Fermi momentum, it will become completely clear how the results of this section have to be interpreted.
What we should *not* do is taking the limit $\Lambda_0 \to \infty$ in the second equality of Eq. (6.139) while keeping Λ fixed, which corresponds to the procedure we have introduced the Dirac sea before. This would imply an abruptly vanishing quasi-particle weight for arbitrarily weak interaction and $Z_l = 1$ for the non-interacting system where $\bar{\eta}_l = 0$. However, note that for the second equality in Eq. (6.139) we made explicit use of the relation $\Lambda = \Lambda_0 e^{-l}$ which becomes ill-defined in the limit $\Lambda_0 \to \infty$ if on the other hand we keep Λ finite. Note as well that our Dirac sea result for η_l^D in Eq. (6.128) does not predict an abrupt inset of the anomalous dimension but a continuous flow from $\eta_l^D = 0$ to its fixed-point value.

6.5 Susceptibilities and Universality

In this section we will check some of the assertions stated in Sec. 5 concerning the analytic properties of the dimensionless and the corresponding physical correlation functions. As well we will be concerned with the feature of universality. We will use our results for the susceptibilities $\tilde{\chi}_l$ and $\tilde{\Pi}_l$ given in Eqs. (6.50) and (6.51) since they represent the simplest nontrivial correlation *functions* that can be calculated purely within our RG formalism. Furthermore the results can directly be compared with perturbation theory.
We will thus start by calculating the corresponding expressions obtained within conventional perturbation theory. Diagrammatically the function Π_{PT} is related to the particle-hole bubble constituted of two fermions of the same type, i.e. of two right- or two left-movers. On the other hand the function χ_{PT} corresponds to a particle-hole pair of a right- and a left-moving fermion. It is well-known that the latter leads to the $2k_F$ instability that is responsible for the Luttinger-liquid behavior in one-dimensional metals dominated by forward scattering. For a proper comparison of our RG results with perturbation theory we should keep in mind that different cutoff procedures incorporate non-universal features of the model. It is then important to use the same non-interacting propagators within the perturbative expressions as those defined within our RG approach. In our case we should use the zeroth order Green function

$$G_0(\alpha(k_F \pm p), i\omega) = \frac{\Theta(|v_F p| < \Lambda_0)}{i\omega \mp v_F p}\,, \tag{6.141}$$

obtained from Eq. (3.2) in the sharp-cutoff limit and for $\Lambda = 0$. The susceptibilities we should compare with are then determined by

$$\begin{aligned}\Pi_{\rm PT}(p,i\omega) &= \int_{-\infty}^{\infty}\frac{dp'}{2\pi}\int_{-\infty}^{\infty}\frac{d\omega'}{2\pi}\,G_0(k_F+p',i\omega')\,G_0(k_F+p'+p,i\omega'+i\omega)\\ &= \frac{\nu_0}{2}\,\frac{s_p}{i\omega - v_F p}\Big\{|v_F p|\Theta(|v_F p|<\Lambda_0)\\ &\quad + [2\Lambda_0 - |v_F p|]\,\Theta(\Lambda_0<|v_F p|<2\Lambda_0)\Big\}, \qquad (6.142)\end{aligned}$$

where $s_p = \mathrm{sgn}(p)$ and $\nu_0 = 1/\pi v_F$, and

$$\begin{aligned}\chi_{\rm PT}(p,i\omega) &= \int_{-\infty}^{\infty}\frac{dp'}{2\pi}\int_{-\infty}^{\infty}\frac{d\omega'}{2\pi}\,G_0(k_F-p',i\omega')\,G_0(k_F+p'+p,i\omega'+i\omega)\\ &= \Theta(|v_F p|<\Lambda_0)\,\frac{\nu_0}{4}\,\ln\left(\frac{\omega^2+(v_F p)^2}{\omega^2+(2\Lambda_0-|v_F p|)^2}\right). \qquad (6.143)\end{aligned}$$

Trying to recover these results from our explicit expressions for $\tilde{\Pi}_l$ and $\tilde{\chi}_l$ by directly using equation (4.29) for $n = 2$ and $Z_l = 1$, we get the correct result only in case of $\tilde{\Pi}_l$. The expression obtained from $\tilde{\chi}_l$ diverges when the limit $\Lambda \to 0$ is taken. The reason for this divergence is that we had to subtract the momentum- and frequency-independent parts of $\tilde{\Pi}_l$ and $\tilde{\chi}_l$ for the fixed-point functions $\tilde{\Pi}_\infty$ and $\tilde{\chi}_\infty$ to remain finite, see the defining equations (6.48) and (6.48).[8] But if we scale back to the physical variables p and ω, we have to use the un-subtracted versions. Here this makes only a difference for $\tilde{\chi}_l$ as the subtraction term $\dot{\Pi}_l(0,i0)$ in Eq. (6.48) is zero, while $\dot{\chi}_l(0,i0) = -1/2\tilde{v}_l \neq 0$. Hence, to recover the correct perturbative results we have to use the functions

$$\begin{aligned}\tilde{\Pi}_l(q,i\epsilon) &= \frac{1}{2}\,\frac{s_q}{i\epsilon - q}\Big\{\Theta(2<|q|<e^l+1)\,(|q|-2)\\ &\quad + \Theta(e^l+1<|q|<2e^l)\,(2e^l-|q|)\Big\}, \qquad (6.144)\end{aligned}$$

and

$$\tilde{\chi}_l(q,i\epsilon) = \Theta(|q|<e^l-1)\,\frac{1}{4}\ln\left(\frac{\epsilon^2+(2+|q|)^2}{\epsilon^2+(2e^l-|q|)^2}\right), \qquad (6.145)$$

[8] We did not emphasize this fact in our notations of $\tilde{\Pi}_l$ and $\tilde{\chi}_l$, i.e. we wrote $\tilde{\Pi}_l$ instead of $\tilde{\Pi}_l^{(sub)}$ and equivalently for $\tilde{\chi}_l$.

where we have replaced $\tilde{v}_l$ by $\tilde{v}_0 = 1$ and removed the term $l/2\tilde{v}_l$ in the expression for $\tilde{\chi}_l$. Now we can use the scaling relation (4.29) to transform back to the physical susceptibilities,

$$\begin{aligned}\Pi_\Lambda(p, i\omega) &= \nu_0 \, \tilde{\Pi}_l \left(\tfrac{v_F p}{\Lambda}, \tfrac{i\omega}{\Lambda}\right) \\ &= \frac{\nu_0}{2} \, \frac{s_p}{i\omega - v_F p} \Big\{ [|v_F p| - 2\Lambda] \, \Theta(2\Lambda < |v_F p| < \Lambda_0 + \Lambda) \\ &\quad + [2\Lambda_0 - |v_F p|] \, \Theta(\Lambda_0 + \Lambda < |v_F p| < 2\Lambda_0) \Big\} , \end{aligned} \tag{6.146}$$

and

$$\begin{aligned}\chi_\Lambda(p, i\omega) &= \nu_0 \, \tilde{\chi}_l \left(\tfrac{v_F p}{\Lambda}, \tfrac{i\omega}{\Lambda}\right) \\ &= \Theta(|v_F p| < \Lambda_0 - \Lambda) \, \frac{\nu_0}{4} \, \ln \left(\frac{\omega^2 + (2\Lambda + |v_F p|)^2}{\omega^2 + (2\Lambda_0 - |v_F p|)^2} \right) . \end{aligned} \tag{6.147}$$

It is then easy to see that

$$\lim_{\Lambda \to 0} \Pi_\Lambda(p, i\omega) = \Pi_{\mathrm{PT}}(p, i\omega) , \tag{6.148}$$

and

$$\lim_{\Lambda \to 0} \chi_\Lambda(p, i\omega) = \chi_{\mathrm{PT}}(p, i\omega) . \tag{6.149}$$

We hence precisely recover the perturbative result given in Eqs. (6.142) and (6.143), including the full dependence on the ultraviolet cutoff Λ_0. Now let us try to get the same results by means of the first method described at the end of Sec. 5.1 which explicitly uses the scaling hypothesis. We start with Π_l. In this case we need the fixed-point expression for Π_l obtained from Eq. (6.144) in the limit $l \to \infty$,

$$\tilde{\Pi}_\infty(q, i\epsilon) = \frac{1}{2} \, \frac{s_q}{i\epsilon - q} \, [|q| - 2] \, \Theta(2 < |q|) . \tag{6.150}$$

According to the scaling hypothesis we then approximate

$$\begin{aligned}\tilde{\Pi}_l(q, i\epsilon) &\approx \tilde{\Pi}_\infty(q, i\epsilon) \quad \text{for} \quad |q|, |\epsilon| \gg 1 , \\ &\approx \frac{1}{2} \, \frac{q}{i\epsilon - q} , \end{aligned} \tag{6.151}$$

and finally scale back,

$$\begin{aligned}\Pi(p,i\omega) &\approx \nu_0\,\tilde{\Pi}_\infty\left(\tfrac{v_F p}{\Lambda},\tfrac{i\omega}{\Lambda}\right)\\ &= \frac{\nu_0}{2}\,\frac{v_F p}{i\omega - v_F p}\,.\end{aligned} \tag{6.152}$$

In contrast to Eq. (6.146) this result is independent of the cutoff Λ_0 and corresponds to the asymptotic low-energy form of the perturbative expression (6.142) or, more precisely, to $\Pi_{\rm PT}(p,i\omega)$ for $|v_F p| \ll \Lambda_0$. In this way the result (6.152) may be considered as the generic low-energy form or the universal structure of the susceptibility $\Pi(p,i\omega)$, in the sense that it is independent of the value of the irrelevant parameter Λ_0. This viewpoint will also be supported by the results of Sec. 8.4 when the non-linearity of the energy dispersion is included in our calculations. Using the scaling hypothesis we will recover Eq. (6.152) irrespective of the initial curvature of the energy dispersion. On the other hand, transforming back to the physical susceptibility $\Pi_\Lambda(p,i\omega)$ *before* the limit $\Lambda \to 0$ is taken, and approaching the fixed point only then we shall recover the full PT result, including its dependence on the initial curvature (which is characterized by an irrelevant coupling).

Trying to proceed in the same way with $\tilde{\chi}_l$, we immediately see that using the scaling hypothesis is bound to fail. Note that in the limit $l \to \infty$ we have to use the subtracted version of $\tilde{\chi}_l$ given in Eq. (6.51) instead of Eq. (6.145), as only the first approaches a finite limit. In the scaling regime $|q|, |\epsilon| \gg 1$ the fixed-point expression reads

$$\tilde{\chi}_\infty(q,i\epsilon) \approx \frac{1}{4}\,\ln\left(\frac{\epsilon^2+q^2}{4}\right)\,. \tag{6.153}$$

Note that in contrast to $\tilde{\Pi}_\infty(q,i\epsilon)$ the function $\tilde{\chi}_\infty(q,i\epsilon)$ is *not* homogenous in the variables q and ϵ, which has been emphasized to be a premise for the applicability of the scaling hypothesis. Consequently, if we set $\chi(p,i\omega) \approx \nu_0\,\tilde{\chi}_\infty(v_F p/\Lambda, i\omega/\Lambda)$ this leads to a logarithmic divergence in the limit $\Lambda \to 0$.

In summary we have seen that calculations relying on the scaling hypothesis must be handled with care and we have to check explicitly if the fixed-point expressions fulfill the property of homogeneity. On the other hand, as long as l is left finite there is a one-to-one correspondence between the dimensionless and the physical vertices (susceptibilities) provided by Eq. (4.29). Transforming back to the physical expressions at finite l we may even follow the complete flow of the physical correlation functions to their fixed-point expressions. Results obtained in this way also incorporate the non-universal features of the vertex function. In case that the application of the scaling hypothesis is justified the fixed-point results assume a generic low-energy form, representative for a larger class of initial

Hamiltonians. In the following section where we calculate the spectral function of the spinless g_2-model, we will give further examples to substantiate these assertions.

Let us finally turn our attention to the question of analyticity of the dimensionless and the physical susceptibilities as discussed in a more general context in Chap. 5. We restrict ourselves to the functions $\tilde{\chi}_l$ and χ_Λ determined by Eqs. (6.51) and (6.147). First of all note that

$$\tilde{\chi}_\infty(q, i\epsilon) = \frac{1}{4} \ln\left(\frac{\epsilon^2 + (2 + |q|)^2}{4}\right) , \tag{6.154}$$

while χ_Λ at the fixed point is identical with $\chi_{\rm PT}$, see Eqs. (6.143) and (6.149). From Eq. (6.154) it is evident that an expansion of $\tilde{\chi}_l(q, i\epsilon)$ in powers of q and ϵ is justified even at the fixed point, with a radius of convergence of the order of unity. On the other hand the radius of convergence of an expansion of χ_Λ in powers of p and ω vanishes when the fixed point is approached, which clearly follows from the fact that $\chi_{\rm PT}$ is non-analytic at $p = \omega = 0$ while for finite Λ the expansion is justified. As predicted in Chap. 5 we would then expect that the couplings related to a Taylor expansion at finite Λ exhibit a runaway flow when $\Lambda \to 0$. This assertion is easily checked if we write

$$\chi_\Lambda(p, i\omega) = a_\Lambda + v_F p\, b_\Lambda + i\omega\, c_\Lambda + \mathcal{O}(p^2, \omega^2, p\omega) , \tag{6.155}$$

where the explicit values $a_\Lambda = \nu_0 \ln(\Lambda/\Lambda_0)/2$, $b_\Lambda = \nu_0(\Lambda^{-1} + \Lambda_0^{-1})/4$ and $c_\Lambda = 0$ are easily obtained by expanding χ_Λ in Eq. (6.147). We hence indeed have $a_\Lambda, b_\Lambda \to \infty$ in the limit $\Lambda \to 0$. Note that this runaway flow appears already at one-loop level for the unrescaled susceptibilities and may correctly be interpreted as an indication of Luttinger-liquid behavior.

Chapter 7

Results for the Spectral Function

We will now go beyond the usual task of RG theory and try to recover the momentum-resolved spectral function of our model as it has been derived in the context of bosonization [93]. To this end we will first study in detail the spectral function obtained from the self-energy at second-order perturbation theory (PT) for two reasons. (1) We show that different renormalizations of the Fermi velocity due to different cutoff procedures are already evident at the perturbative level and (2) the result for the perturbative spectral function can exactly be reproduced by means of our RG methods, in a way that we may even follow the complete flow from $\Lambda = \Lambda_0$ to the fixed point at $\Lambda = 0$. The sum rule for the spectral weight is found to be satisfied independently of the scale. In the following we will propose a simple procedure providing us with a non-perturbative expression for the spectral function. The result correctly reproduces the weak-coupling form of the spectral function at Fermi momentum. For momenta different from k_F we get an expression with power-law singularities at the plasmon modes, but with an exponent that slightly differs from the predicted behavior of bosonization.

7.1 Second-Order Perturbation Theory as a Toy Model

For the spinless g_2-model the self-energy at second-order perturbation theory is determined by the Feynman diagram shown in Fig. 7.1 . The corresponding analytical expression depends on the definition of the zeroth-order Green function $G_0(\alpha(k_F + p), i\omega)$ and the interaction parameter.[1] We will derive two results: First we use the Dirac-sea expression for the propagator, i.e. $G_0^{-1}(k_F + p, i\omega) =$

[1] In the following we will always refer to the right Fermi point ($\alpha = +1$) . Due to time-reversal symmetry the results for $\alpha = -1$ are identical with those for $\alpha = +1$.

$i\omega - v_F p$, together with a momentum-dependent g_2-interaction, defined by $g_2(p) = g_0\,\Theta(p_c - |p|)$. For the second expression, which is the one to be compared with our RG result, we use a finite band cutoff Λ_0 and an interaction constant g_0. The non-interacting Green function is then given by Eq. (6.141). Evaluating the analytical expression corresponding to the Feynman graph in Fig. 7.1 we obtain the following two results for the self-energy where no approximation has been made,

$$\begin{aligned}\Sigma^{(ic)}_{\rm PT}(k_F+p,i\omega) &= \left(\frac{g_0}{4\pi v_F}\right)^2\Bigg\{\Theta(|p|<p_c)\Big[-2v_Fp+(i\omega-v_Fp)\\ &\qquad\times\ln\left(\frac{\omega^2+(v_Fp)^2}{4(v_Fp_c)^2-(i\omega-v_Fp)^2}\right)\Big]\\ &\quad+\Theta(p_c<|p|)\Big[-2s_pv_Fp_c+(i\omega-v_Fp)\\ &\qquad\times\ln\left(\frac{i\omega-v_Fp}{i\omega-v_Fp-2s_pv_Fp_c}\right)\Big]\Bigg\},\end{aligned}\tag{7.1}$$

for the model with interaction cutoff p_c and

$$\begin{aligned}\Sigma^{(bc)}_{\rm PT}(k_F+p,i\omega) &= \left(\frac{g_0}{4\pi v_F}\right)^2\Bigg\{\Theta(|v_Fp|<\Lambda_0)\\ &\quad\times\Big[-2v_Fp+(i\omega-v_Fp)\ln\left(\frac{\omega^2+(v_Fp)^2}{\omega^2+(|v_Fp|-2\Lambda_0)^2}\right)\\ &\quad+(i\omega-v_Fp+4s_p\Lambda_0)\ln\left(\frac{i\omega+v_Fp+2s_p\Lambda_0}{i\omega-v_Fp+2s_p\Lambda_0}\right)\Big]\\ &\quad+\Theta(\Lambda_0<|v_Fp|<2\Lambda_0)\Big[-4\Lambda_0+2|v_Fp|\\ &\quad+(i\omega-v_Fp+4s_p\Lambda_0)\ln\left(\frac{i\omega-v_Fp+4s_p\Lambda_0}{i\omega+v_Fp}\right)\Big]\Bigg\},\end{aligned}\tag{7.2}$$

for the model with band cutoff Λ_0. Obviously the detailed dependence on frequencies and momenta is rather different for both expressions. However, if we choose $\Lambda_0 = v_F p_c$ we get a common low-energy form for $|\omega|, |v_Fp| \ll \Lambda_0$

$$\Sigma^{(bc/ic)}_{\rm PT}(k_F+p,i\omega) \approx \pm\frac{\tilde{g}_0^2}{8}v_Fp+\frac{\tilde{g}_0^2}{16}(i\omega-v_Fp)\ln\left(\frac{\omega^2+(v_Fp)^2}{4\Lambda_0^2}\right).\tag{7.3}$$

Here we have again introduced $\tilde{g}_0 = g_0/\pi v_F$. The plus sign in front of the first term on the r.h.s. of Eq. (7.3) appears for the band cutoff and the minus sign for

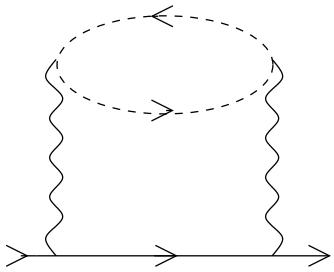

Figure 7.1: Feynman diagram determining the self-energy at second order perturbation theory. The wavy lines again correspond to the g_2-interaction.

the interaction cutoff. Note that in the band-cutoff case this is due to the expansion of the second logarithm on the r.h.s. of Eq. (7.2), the leading contribution of which is $v_F|p|/\Lambda_0$. The first term on the r.h.s. of Eq. (7.3) is responsible for a renormalization of the Fermi velocity. This confirms that different cutoff procedures lead to different renormalizations of the Fermi velocity, a result we have already stated with the aid of our RG techniques. Consequently, to obtain this no sophisticated methods like the RG are necessary. Explicitly, the renormalized values for the Fermi velocity are

$$\tilde{v}_F = \left(1 \pm \frac{\tilde{g}_0^2}{8}\right) v_F \,, \tag{7.4}$$

with the plus sign corresponding to the band cutoff. Note that $\tilde{v}_F$ depends on the cutoff *procedure* but not on the cutoff itself.

Let us now turn our attention to the spectral function obtained from Eqs. (7.1) and (7.2). For convenience we will restrict our considerations to the case of the interaction cutoff, although our RG results derived later on have to be compared to the band-cutoff expressions. The reason for our choice is that in case of an interaction cutoff we have $\tilde{v}_F < v_F$, while for the band cutoff $\tilde{v}_F > v_F$. In the first case this leads to an undamped δ-like quasi-particle peak in the spectral function located outside the support of the branch cut associated with the first logarithm in Eq. (7.1). This allows for neatly separating the features of the spectral line shape which are Fermi-liquid like from those which characterize a Luttinger liquid. In the band-cutoff case this is more difficult as we find a damped quasi-particle peak[2] with its maximum value for frequencies located inside the support of the branch cut, leading to an overlap with the plasmon background; see also Fig.

[2]Strictly speaking the peak-like feature does not correspond to a real quasi-particle in the Luttinger sense [79], since the imaginary part of the self-energy is found to be *linear* instead of quadratic in the frequency ω.

7.7 . It is important to emphasize that the physical system we describe here is of course a Luttinger liquid. The remainders of Fermi-liquid behavior we will find shortly are most likely an artifact of perturbation theory.
Let us adopt here the viewpoint of expression (7.1) being the *exact* self-energy of some *toy model* and imagine that we would like to investigate if the system is a Fermi or a non-Fermi liquid. This question is best answered by considering the retarded self-energy $\Sigma^{(ic)}_{\rm PT}(k_F+p,\omega+i0^+)$.[3] For $|p|\leq p_c$ we obtain from Eq. (7.1)

$$\begin{aligned}\mathrm{Re}\,\Sigma^{(ic)}_{\rm PT}(k_F+p,\omega+i0^+) \;&=\\ -\frac{\tilde{g}_0^2}{8}v_Fp+\;&\frac{\tilde{g}_0^2}{16}(\omega-v_Fp)\ln\left|\frac{\omega^2-(v_Fp)^2}{4(v_Fp_c)^2-(\omega-v_Fp)^2}\right|,\end{aligned}\tag{7.5}$$

and

$$\begin{aligned}\mathrm{Im}\,\Sigma^{(ic)}_{\rm PT}(k_F+p,\omega+i0^+) \;&=\\ -\pi\frac{\tilde{g}_0^2}{16}\,&|\omega-v_Fp|\,\Theta(|v_Fp|<|\omega|<2v_Fp_c+\mathrm{sgn}(\omega)v_Fp)\,,\end{aligned}\tag{7.6}$$

Note that the imaginary part arises due to the branch cut of the logarithm, located on the real ω-axis within the interval described by the argument of the Θ-function. The spectral function for the right-moving fermions is given by [84]

$$A^{(ic)}_{\rm PT}(k_F+p,\omega) \;=\; -\frac{1}{\pi}\,\mathrm{Im}\,G^{(ic)}_{\rm PT}(k_F+p,\omega+i0^+)\tag{7.7}$$

$$=\;-\frac{1}{\pi}\,\mathrm{Im}\left[\frac{1}{\omega-v_Fp-\Sigma^{(ic)}_{\rm PT}(k_F+p,\omega+i0^+)+i0^+}\right].\tag{7.8}$$

In regions where the imaginary part of $\Sigma^{(ic)}_{\rm PT}(k_F+p,\omega+i0^+)$ equals zero we have to check if the denominator on the r.h.s. has a zero or not. If this is indeed the case we get a δ-like contribution to the spectral function. In our example we find such a zero which is approximately given by

$$\omega_p=\left(1-\frac{\tilde{g}_0^2}{8}\right)v_Fp+\mathcal{O}(\tilde{g}_0^4\ln(\tilde{g}_0))\approx\tilde{v}_Fp\,,\tag{7.9}$$

which is hence located outside the branch cut of the logarithm. Consequently, the spectral function splits up in a δ-like and a continuous part, i.e.

[3] Actually, physical systems with a retarded self-energy of the form $\Sigma(\mathbf{k}_F,\omega+i0^+)\sim\omega\ln|\omega|+i\omega$ are sometimes called *marginal Fermi liquids* [95,96]. Note that this is precisely the form we get if we set $p=0$ in Eqs. (7.5) and (7.6).

$$A^{(ic)}_{\rm PT}(k_F+p,\omega) = A^{(ic)}_{\delta}(k_F+p,\omega) + A^{(ic)}_{cont}(k_F+p,\omega)\,. \tag{7.10}$$

The quasi-particle peak is explicitly given by

$$A^{(ic)}_{\delta}(k_F+p,\omega) = Z_{\rm PT}(p)\,\delta(\omega-\omega_p)\,, \tag{7.11}$$

with residue

$$\begin{aligned} Z_{\rm PT}(p) &= \left[\frac{\partial {\rm Re}\,(G^{(ic)}_{\rm PT})^{-1}(p,\omega+i0^+)}{\partial\omega}\right]^{-1}_{\omega=\omega_p} \\ &\approx \frac{1}{1-\frac{\tilde g_0^2}{16}[1+2\ln|\frac{p}{p_c}|]}\,, \end{aligned} \tag{7.12}$$

while the continuous part reads

$$\begin{aligned} &A^{(ic)}_{cont}(k_F+p,\omega) = \\ &-\frac{1}{\pi}\,\frac{{\rm Im}\,\Sigma^{(ic)}_{\rm PT}(k_F+p,\omega+i0^+)}{[\omega-v_Fp-{\rm Re}\,\Sigma^{(ic)}_{\rm PT}(k_F+p,\omega+i0^+)]^2+[{\rm Im}\,\Sigma^{(ic)}_{\rm PT}(k_F+p,\omega+i0^+)]^2}\,. \end{aligned} \tag{7.13}$$

Let us fist discuss the simple case of vanishing p. Setting $p=0$ in Eq. (7.12) we immediately get $Z_{\rm PT}(0)=0$. This result can also be obtained by the usual Fermi-liquid definition of the quasi-particle residue, which relies on an expansion of the self-energy in powers of ω *and* p, that is $Z_F = (1-\partial_{i\omega}\Sigma(k_F,i\omega))^{-1}|_{\omega=0}$. But note that this definition cannot be used unambiguously for our toy model, as the radius of convergence of an expansion in both variables around $p=\omega=0$ is zero. However, for this singular point we still get the correct result, which implies that our toy model does not describe a Fermi liquid. For the continuous part we explicitly get from Eqs. (7.5) and (7.6)

$$\begin{aligned} A^{(ic)}_{\rm PT}(k_F,\omega) &= A^{(ic)}_{cont}(k_F,\omega) \\ &= \frac{\tilde g_0^2}{16}\frac{1}{|\omega|}\,\frac{\Theta(|\omega|<2v_Fp_c)}{[1-\frac{\tilde g_0^2}{16}\ln|\frac{\omega^2}{4(v_Fp_c)^2-\omega^2}|]^2+[\pi\frac{\tilde g_0^2}{16}]^2}\,, \end{aligned} \tag{7.14}$$

In Fig. 7.2 we show the line shape of this function for $\tilde g_0 = 0.5$ and compare it to the corresponding weak-coupling result obtained by means of the bosonization approach, see Eq. (7.48). The nature of the singularity at $\omega=0$ can easily be read off Eq. (7.14) to be $A^{(ic)}_{\rm PT}(k_F,\omega)\sim 1/(|\omega|\ln^2|\omega|)$, while the asymptotically

exact bosonization result predicts a power-law singularity characterized by the anomalous dimension. At weak coupling this qualitatively different behavior is nearly invisible on a linear ω scale. This is why we have also compared the two results on a logarithmic scale in Fig. 7.3. By numerical integration it can be checked that the sum rule for the spectral function, which explicitly reads

$$\mathcal{S}(p) = \int_{-\infty}^{\infty} d\omega\, A(p,\omega) = 1\,, \tag{7.15}$$

is exactly fulfilled for our toy model. This is true not only for $p = 0$ but for all values $|p| < p_c$ as well. In this case the spectral weight is split up into a contribution $\mathcal{S}_\delta(p)$ related to the δ-like part of the spectral function (which just equals $Z_{\rm PT}(p)$) and a contribution $\mathcal{S}_{cont}(p)$ which is due to the continuous part. Both contributions add up to one as demanded by Eq. (7.15). This is shown in Fig. 7.6 for two values of the interaction strength. We see that down to values $|p/p_c| = 10^{-4}$ the δ-like part is strongly dominant. This can directly be understood from Eq. (7.12), which we may approximately be inverted for $|p/p_c| \ll 1$,

$$\left|\frac{p}{p_c}\right| \simeq \exp\Big(-\frac{1}{(\tilde{g}_0^2/8)Z_{\rm PT}}\Big)\,. \tag{7.16}$$

Note that at first sight this equation seems to be the perturbative analogue of Eq. (6.140), but its interpretation is actually quiet different. For our toy model we know from the result for spectral function, that a quasi-particle peak indeed exists, *but no such conclusion must be drawn upon Eq. (6.140) as long as* Λ *can be reduced to zero.*[4] Eq. (7.16) predicts that the momentum range for which the continuous part of the spectral function dominates is exponentially small.
Finally let us elaborate a little more on the continuous part $A^{(ic)}_{cont}$. For convenience we neglect the imaginary part in the denominator of Eq. (7.13) as it gives rise to terms of order $\tilde{g}_0^4$. This is allowed if the remaining denominator has no zero[5],

$$\begin{aligned} A^{(ic)}_{cont}(k_F+p,\omega) \;&\approx\; \frac{\tilde{g}_0^2}{16}\,|\omega - v_F p| \\ &\times \frac{\Theta(|v_F p| < |\omega| < 2v_F p_c - s_\omega v_F p)}{\Big[\omega - \tilde{v}_F p - \frac{\tilde{g}_0^2}{16}(\omega - v_F p)\ln\Big|\frac{\omega^2-(v_F p)^2}{4(v_F p_c)^2-(\omega - v_F p)^2}\Big|\Big]^2}\,. \end{aligned} \tag{7.17}$$

[4]This will become completely evident in the next section when we describe the toy model by means of our RG approach.

[5]Actually there is a second zero located at the high-energy ends of the branch-cut region, where the imaginary part has to be kept. But this is of no importance for our discussion here and we keep the simpler expression.

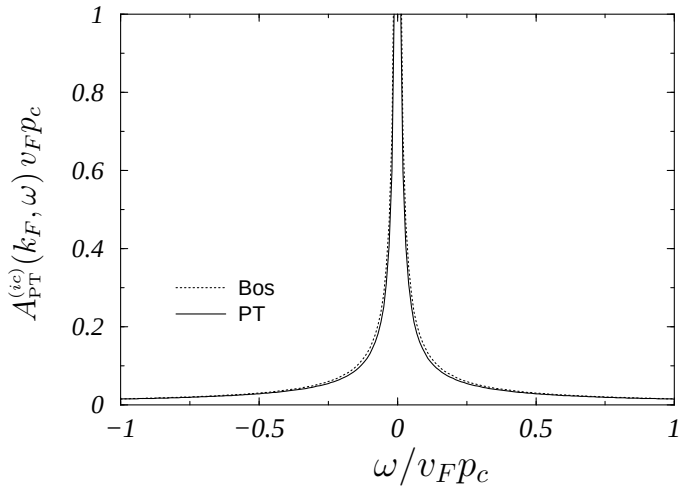

Figure 7.2: Comparison of the perturbative result for the $k = k_F$ spectral function given by Eq. (7.14) with the bosonization result in Eq. (7.48). Both expressions are singular at $\omega = 0$, but the nature of the singularity is different. At weak coupling this is almost invisible on a linear ω scale. We have chosen $\tilde{g}_0 = 0.5$.

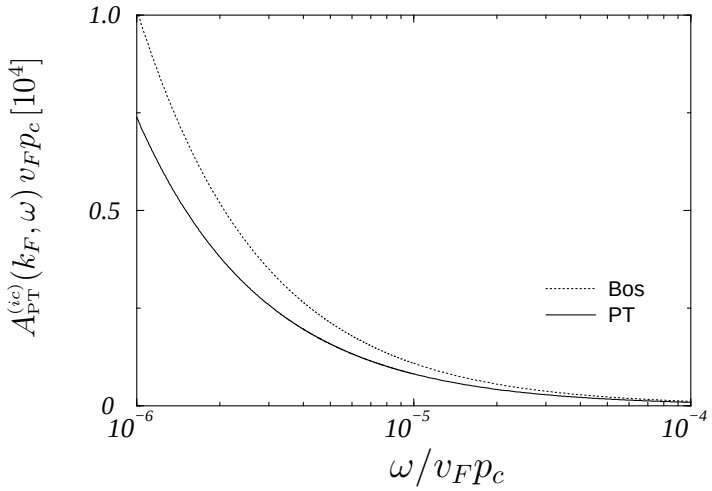

Figure 7.3: The same as above but plotted on a logarithmic ω scale. Here the differences become apparent when $\omega = 0$ is approached. Note that the y-axis is scaled by a factor of 10^4.

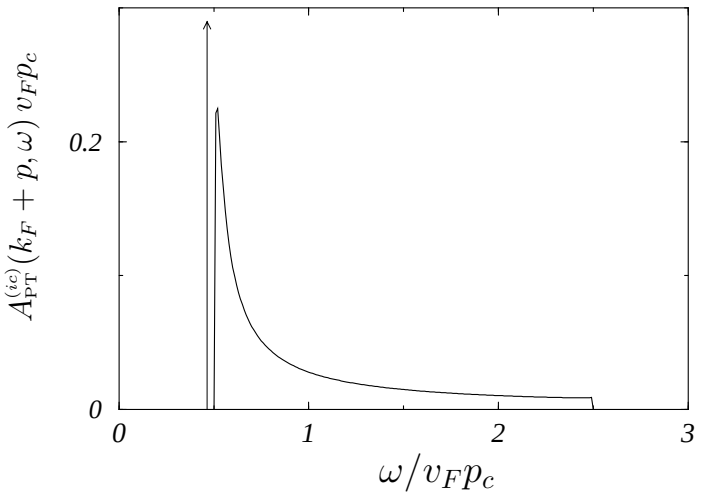

Figure 7.4: The spectral function at second order perturbation theory for $p/p_c = 0.5$ and $\tilde{g}_0 = 0.5$. We only show the relevant part for $\omega > 0$ splitting up in a δ-like contribution at $\omega \approx \tilde{v}_F p$ sketched by the arrow and a continuous background peaked out near $\omega = v_F p$.

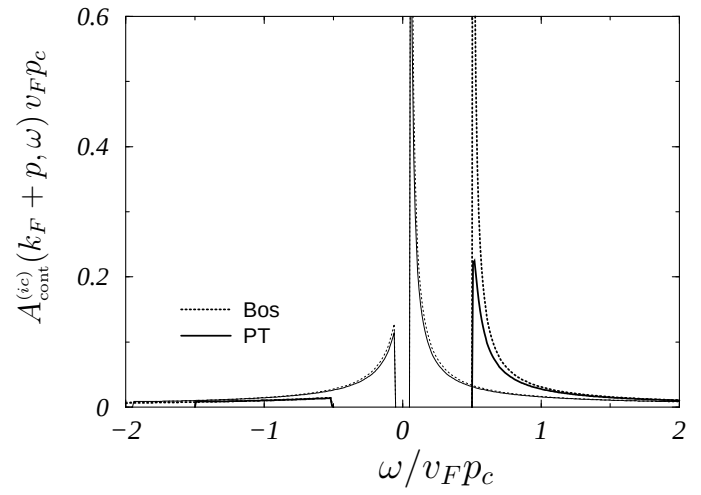

Figure 7.5: Comparison of the continuous part of the perturbative spectral function, Eq. (7.17), with the bosonization result. For convenience we have set the charge velocity $v_c = v_F\sqrt{1-\tilde{g}_0^2/4}$ equal to v_F. We show the line shapes for $p/p_c = 0.5$ (thick lines) and $p/p_c = 0.05$ (light curves) with $\tilde{g}_0 = 0.5$ in both cases. When $|p|$ decreases the continuous part of the perturbative expression approaches more and more the bosonization result.

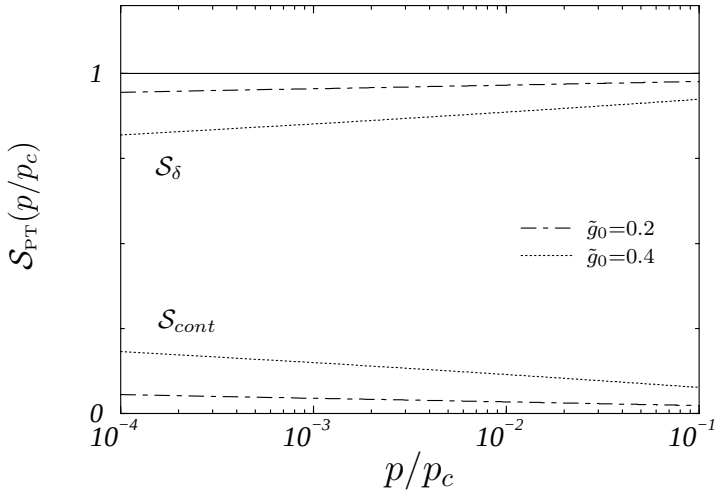

Figure 7.6: Plot of the sum rule (7.15) applied to the perturbative spectral function. The contribution of the δ-like part equals $Z_{\rm PT}(p)$ in Eq. (7.12), while the contribution of $A^{(ic)}_{cont}$ has been obtained by numerical integration. The solid line is the sum of the upper and the lower pair of curves for the two values of $\tilde{g}_0$ depicted in the legend.

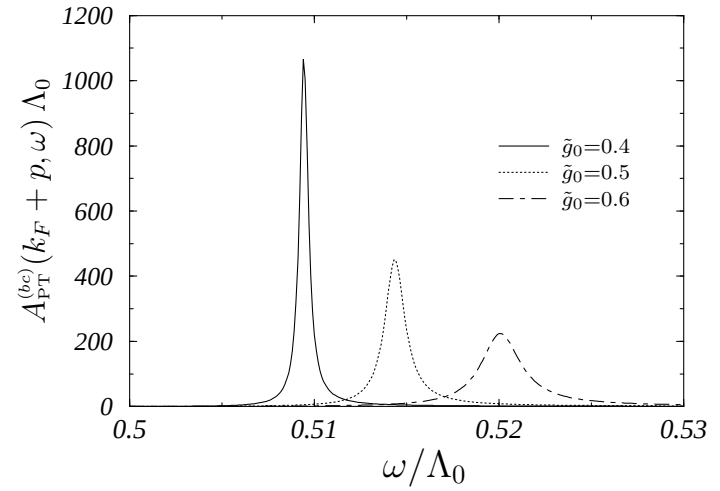

Figure 7.7: The perturbative spectral function corresponding to the analytical continuation of the self-energy given in Eq. (7.2), where a band cutoff has been used. We only show the part for $\omega > v_F p$ where we have chosen $p/p_c = 0.5$ in all three cases. The undamped quasiparticle peak of Fig. 7.4 now appears within the branch cut of the logarithm and is broadened due to the finite imaginary part of the self-energy in this region. The continuous background corresponding to plasmon excitations is completely overlapped.

In Fig. 7.4 we show a plot of this function for $\tilde{g}_0 = 0.5 = p/p_c$ and $\omega > 0$, together with the adjacent δ-peak. In Fig. 7.5 we exclusively show the continuous part of the spectral function and compare it with the bosonization result for the two values $p/p_c = 0.5$ and $p/p_c = 0.05$. We see that with decreasing momentum $A^{(ic)}_{cont}$ more and more approaches the bosonization result with best correspondence at $p = 0$. An important difference is the behavior at $\omega = v_F p$ (for a better comparison we have set the charge velocity v_c of the exact solution equal to v_F). While the exact result exhibits an algebraic singularity, the perturbative expression drops logarithmically down to zero at this point, i.e. with infinite slope, and develops its maximum value very close to the zero. This is also evident from Eq. (7.17) due to the fact that the denominator is non-zero at $\omega = v_F p$ while the numerator vanishes. By closer observation we find that the term $\tilde{v}_F p$ is responsible for this different behavior. If we just drop this term in Eq. (7.17) the expression develops a $1/(x \ln^2 x)$ singularity at $\omega = v_F p$, just like we have found for $p = 0$ at $\omega = 0$. At the same time the quasi-particle peak is removed such that the whole spectral weight will be carried by the logarithmic singularity. This is what is believed to happen in the exact solution, for which our toy model is only a first and rather crude approximation: The terms linear in p and ω are expected to be canceled at higher loop orders and the logarithmic singularity will be turned into an algebraic one. We will indeed find this scenario when we use our non-perturbative RG approach. However, it cannot be excluded, neither by our RG method nor by the bosonization approach, that this cancellation is *not* exact to all orders in the coupling $\tilde{g}_0$. *In this case the energy regime where we can expect to find the generic Luttinger-liquid behavior might be extremely small.* Finally let us sketch what happens if a band-cutoff is used. In this case we have to analytically continue the self-energy expression given by Eq. (7.2). The most important difference appears due to the different renormalization of the Fermi velocity which is now given by $\tilde{v} \approx (1 + \tilde{g}_0^2) v_F$, see Eq. (7.3). Here $\tilde{v}_F p > v_F p$ such that the denominator in Eq. (7.8) exhibits a zero where the imaginary part of $\Sigma^{(bc)}_{\mathrm{PT}}(k_F + p, \omega + i0^+)$ is non-zero. This leads to a broadening of the quasi-particle peak and a complete overlap with the plasmon background, as is shown in Fig. 7.7. Note, however, that the imaginary part of the self-energy is *linear* in ω such that we do not deal with the quasi-particle peak of a Fermi-liquid (for which the imaginary part has to be quadratic in ω), but rather with that of a marginal Fermi liquid, see the footnote above Eq. (7.5). For $p = 0$ we get of course the same picture as before with some less important differences at large ω. The process of spectral-weight transfer from the quasi-particle peak to the plasmon excitations when $p = 0$ is approached is expected to be qualitatively the same as for the interaction-cutoff.

7.2 Scenario Behind the Coupling Flow

The importance of studying the above toy model is not primarily due to its physical significance, although the most important features of the bosonization result are already visible at second-order perturbation theory. Instead it provides us with an example for which the RG flow predicts a vanishing quasi-particle residue Z_l while on the other hand the spectral function exhibits a quasi-particle peak whenever k is different from the Fermi points. This is a paradigm for a situation where the applicability of the scaling hypothesis fails. The result for the fixed-point value of Z_l cannot be extended to the vicinity of the Fermi points: It exclusively applies to the single momentum values $k = \pm k_F$.
To prove this we will first try to recover the band-cutoff result (7.2) for the perturbative self-energy by means of our RG approach. From the explanations of Sec. 6.5 and the fact that $\Sigma^{(bc)}_{\rm PT}(k_F + p, \omega)$ is not a homogeneous function in the variables p and ω we *cannot* expect to get a finite and correct result when we make use of the scaling hypothesis, see also the remarks below Eq. (5.10). Consequently, we have to scale back to the physical variables before the limit $l \to \infty$ is taken. The most convenient way to calculate the self-energy is then to use Eq. (5.13), which in one dimension reads

$$\Sigma_\Lambda(k_F + p, i\omega) = -\Lambda_0 \int_0^l dt\, e^{-t}\, \dot\Gamma^{(2)}_t\big(e^t \tfrac{v_F p}{\Lambda_0}, e^t \tfrac{i\omega}{\Lambda_0}\big)\,. \tag{7.18}$$

Note that we have replaced the upper integration boundary by l , as we are interested not only in the fixed-point result for Σ_Λ but also its flow at finite Λ. On the r.h.s. of Eq. (7.18) we have to insert our explicit two-loop result for $\dot\Gamma^{(2)}_l$ given in Eq. (6.57). The constant term $-\tilde g_l/2$ then cancels the contribution of the counter term $\Sigma(k_F, i0)$ appearing in Eq. (5.12) when the limit $l \to \infty$ is taken. However, at finite l it gives rise to a small energy shift that we shall neglect as it is of no importance for our present discussion. If we set $\tilde v_l = 1$ and distinguish again between the zero-sound and the Peierls-BCS contribution, we get after some lengthy calculations

$$\begin{aligned}
\Sigma^{(\rm ZS)}_\Lambda(k_F + p, i\omega) \;=\; & s_p\, \frac{\tilde g_0^2}{16} \Bigg\{ \Theta(\Lambda < |v_F p| < \Lambda_0) \Big[2(\Lambda - |v_F p|) \\
& + (i\omega s_p + 3|v_F p|) \ln\left(\frac{i\omega s_p + 3|v_F p|}{i\omega s_p + |v_F p| + 2\Lambda} \right) \Big] \\
& + \Theta(\Lambda_0 < |v_F p| < 2\Lambda_0 - \Lambda) \Big[2(|v_F p| + \Lambda - 2\Lambda_0) \\
& + (i\omega s_p - |v_F p| + 4\Lambda_0) \ln\left(\frac{i\omega s_p - |v_F p| + 4\Lambda_0}{i\omega s_p + |v_F p| + 2\Lambda} \right) \Big] \Bigg\}\,,
\end{aligned}$$

(7.19)

and

$$\begin{aligned}\Sigma_\Lambda^{(\mathrm{PB})}(k_F+p,i\omega) &= s_p\,\frac{\tilde{g}_0^2}{16}\Big\{\Theta(2\Lambda-\Lambda_0<|v_Fp|<\Lambda)\Big[2(|v_Fp|+\Lambda_0-2\Lambda)\\ &\quad+(i\omega s_p-|v_Fp|+4\Lambda)\ln\left(\frac{i\omega s_p-|v_Fp|+4\Lambda}{i\omega s_p+|v_Fp|+2\Lambda_0}\right)\Big]\\ &\quad+\Theta(\Lambda<|v_Fp|<\Lambda_0)\Big[2(\Lambda_0-|v_Fp|)\\ &\quad-(i\omega s_p+3|v_Fp|)\ln(i\omega s_p+3|v_Fp|)\\ &\quad+(i\omega s_p-|v_Fp|+4\Lambda_0)\ln(i\omega s_p+|v_Fp|+2\Lambda_0)\\ &\quad-2\,(i\omega s_p-|v_Fp|+2\Lambda_0+2\Lambda)\\ &\qquad\qquad\times\ln(i\omega s_p-|v_Fp|+2\Lambda_0+2\Lambda)\\ &\quad+2\,(i\omega s_p+|v_Fp|+2\Lambda)\ln(i\omega s_p+|v_Fp|+2\Lambda)\Big]\\ &\quad+\Theta(|v_Fp|<\Lambda_0-2\Lambda)\Big[2(|v_Fp|-\Lambda_0+2\Lambda)\\ &\quad+(i\omega s_p-|v_Fp|-4\Lambda)\ln\left(\frac{i\omega s_p-|v_Fp|-4\Lambda}{i\omega s_p+|v_Fp|-2\Lambda_0}\right)\Big]\Big\}.\end{aligned} \tag{7.20}$$

The first thing we can check is that in the limit $\Lambda\to 0$ the sum of $\Sigma_\Lambda^{(\mathrm{ZS})}$ and $\Sigma_\Lambda^{(\mathrm{PB})}$ *exactly* reproduces our band-cutoff result $\Sigma_{\mathrm{PT}}^{(bc)}$ given in Eq. (7.2), i.e. including the full dependence on the ultraviolet cutoff Λ_0. This is a rather technical point and we do not want to show this here explicitly. But what we have gained with the results (7.19) and (7.20) is much more: It enables us to follow the complete flow of the self-energy (and hence the flow of the spectral function as well) from $\Lambda=\Lambda_0$ to $\Lambda=0$. Before we proceed so let us see what the flow of the couplings Z_l and v_Λ defined in Eqs. (4.16) and (5.32) predict at this level. Setting $p=0$ in Eq. (7.19) we immediately find that the zero-sound channel does not contribute to the flow, just like it was the case in our non-perturbative RG calculations. The quasi-particle residue is then explicitly given by

$$\begin{aligned}Z_l &= \frac{1}{1-\partial_{i\omega}\Sigma_\Lambda^{(\mathrm{PB})}(k_F,i\omega)|_{\omega=0}}=\frac{1}{1-\frac{\tilde{g}_0^2}{8}[\ln(\frac{2\Lambda}{\Lambda_0})+1-2\frac{\Lambda}{\Lambda_0}]\,\Theta(\Lambda_0-2\Lambda)}\\ &= \frac{1}{1+\frac{\tilde{g}_0^2}{8}[\,l-\ln 2-1+2e^{-l}]\,\Theta(e^l-2)}\,,\end{aligned} \tag{7.21}$$

where for the third equality we have used $\Lambda = \Lambda_0 e^{-l}$. Note that the result in the first line very much resembles that of $Z_{\rm PT}(p)$ in Eq. (7.12), with $|v_F p|$ replaced by Λ. What we find here is that Z_l vanishes in the limit $\Lambda \to 0$. At first sight this seems to be a contradiction to what we have shown in the previous section, where this result only applied to the special case $p = 0$. For finite p we rather found a finite $Z_{\rm PT}(p)$ that even carries most of the spectral weight down to exponentially small values of p. What we see here explicitly is, that *for non-Fermi liquids the vanishing of the radius of convergence for expansions of the vertex functions in powers of frequencies and momenta has to be taken seriously.* Rigorously speaking the perturbative expression (7.21) is only valid for the single point $p = 0$, for which $Z_{\rm PT}(p)$ and Z_l both predict a vanishing quasi-particle residue. However, *the validity of the Z_l flow must not be extended to a finite region close to the Fermi points.* As we have seen in the previous section, for our toy model the region where $Z_{\rm PT}(p) \approx 0$ is exponentially small. For any measurable non-zero momentum$p$ we would find a dominating quasi-particle peak instead of exclusively plasmon excitations.

Let us elaborate a little more on our result for Z_l. Note that the last equality in Eq. (7.21) is precisely what we get if we approximate our non-perturbative RG result given in Eq. (6.115) as follows,

$$Z_l = e^{-\bar{\eta}_l\, l} \approx \frac{1}{1 + \bar{\eta}_l\, l}\,, \tag{7.22}$$

and insert the explicit expression for the scale-averaged anomalous dimension $\bar{\eta}_l$ given in Eq. (6.116) on the r.h.s. of (6.116). Furthermore for large l the perturbative result predicts

$$Z_l \simeq \frac{1}{\eta\, l} \quad \stackrel{l\to\infty}{\longrightarrow} \quad 0\,, \tag{7.23}$$

but also

$$\eta_l = -\,\frac{\partial_l Z_l}{Z_l} \simeq \frac{1}{l} \quad \stackrel{l\to\infty}{\longrightarrow} \quad 0\,. \tag{7.24}$$

The last result just reflects the fact that at perturbative level the physical spectral function does not yet have developed an anomalous dimension but only a logarithmic singularity. Nonetheless the quasi-particle residue vanishes for $p = 0$, such that also the flow of the couplings Z_l and η_l suggests the properties of a marginal Fermi liquid.

The next thing we are going to study in more detail is the renormalized Fermi velocity. We have already pointed out that the dimensionless coupling $\tilde{v}_l$ defined in Eq. (5.21) only corresponds to the renormalization factor of the Fermi velocity in case that the physical system indeed behaves like a Fermi liquid. But we have

just found out that our toy model describes a non-Fermi liquid. So how should $\tilde{v}_l$ or its analogue v_Λ defined in Eq. (5.32) be interpreted? This question is actually not so easy to answer. First of all observe that in the perturbative spectral function (7.17) two different velocities are present: The renormalized velocity $\tilde{v}_F \approx (1 - \tilde{g}_0^2/8)v_F$ and the bare Fermi velocity v_F within the argument of the logarithm. In the asymptotically exact bosonization result for spinless fermions only a single velocity is present, which turns out to be the charge velocity v_c of the plasmon excitations. At second-order PT the values of v_c and $\tilde{v}_F$ numerically coincide and one is thus tempted to interpret $\tilde{v}_F$ as the charge velocity at the perturbative level. But in the previous section we have found that it is the quasi-particle peak that appears approximately at $\omega = \tilde{v}_F p$, while the plasmon background only starts at $\omega = v_F p$. Consequently, such an interpretation is somewhat vague. Note as well that the proper definition of the charge velocity is related to the density-density correlation function, where it appears as the zero of the dielectric function, rather than to the single-particle Green function. However, it is the common belief supported by the knowledge about the exact result, that $\tilde{v}_F$ "somehow" will take the place of v_c in higher loop orders, and we will also adopt this viewpoint here.

Now, if we compare our fixed-point result $\tilde{v}$ in Eq. (6.117) with $\tilde{v}_F/v_F$ we see that the explicit values are different as well as $\tilde{v}$ is different from v_F itself. This at least has a simple reason: We have determined $\tilde{v}$ in the hydrodynamic regime, where the logarithms of Eq. (6.59) contribute to expansions in powers of the dimensionless variables q and ϵ. In contrast an expansion of the fixed-point self-energy given by Eq. (7.2) in powers of p and ω is not justified, and we hence cannot expect the results to coincide. Consequently there is no obvious physical interpretation of the parameter $\tilde{v}_l$ for non-Fermi liquids, and we should just take it as a parameter of the RG flow.

Let us determine the flow of $v_\Lambda = \tilde{v}_l v_F$ at perturbative level. First of all we need the momentum derivative of the self-energy, which explicitly yields

$$\partial_p \Sigma_\Lambda^{(\mathrm{PB})}(k_F + p, i0)\big|_{p=0} = v_F \frac{\tilde{g}_0^2}{8}\left[1 + \ln\left(\frac{2\Lambda}{\Lambda_0}\right) - 2\frac{\Lambda}{\Lambda_0}\right]\Theta(\Lambda_0 - 2\Lambda)\,, \tag{7.25}$$

diverging logarithmically when $\Lambda \to 0$. But $\partial_p \Sigma_\Lambda^{(\mathrm{PB})}(k_F + p, i0)\big|_{p=0}$ does not determine v_Λ alone. According to its definition in Eq. (5.32) we have

$$v_\Lambda = Z_l\left[v_F - \partial_p \Sigma_\Lambda^{(\mathrm{PB})}(k_F + p, i0)\big|_{p=0}\right] = v_F\,. \tag{7.26}$$

For the second equality we have inserted our PT result (7.21) for Z_l and Eq. (7.25). Both contributions cancel each other exactly, such that the whole expression remains not only finite but even constant during the whole flow. Keeping

in mind that we have identified $\tilde{v}_l = v_\Lambda/v_F$ in Eq. (5.35), this is at first sight a rather puzzling result. Note that we have found $\tilde{v} \approx 1 + \tilde{g}^2/4$ using the RG and one is tempted to believe that at two-loop order perturbation theory this result should be recovered. Instead we have found $\tilde{v}_l = 1$. The misapprehension in this reasoning is due to the fact that *both* results are non-perturbative in nature. A usual perturbative velocity renormalization cannot be defined for a non-Fermi liquid, at least not in our explicit example, as the p- and ω-derivatives of the self-energy are divergent at the fixed point. In light of this our present result $v_\Lambda = v_F$, i.e. $\tilde{v}_l = 1$, is just the lowest *non-perturbative* order in an expansion of $\tilde{v}_l$ in powers of $\tilde{g}_0$.

Having determined the coupling flow at perturbative level we shall now try to calculate the flow of the corresponding spectral function, providing us with a proper interpretation of the above results. Our main interest is the change of Z_l with the energy-scale parameter Λ, and we will thus restrict ourselves to the flow of the spectral function for $p = 0$. Eq. (7.21) predicts that down to extremely small values of Λ/Λ_0 the quasi-particle residue persists. On the other hand we have seen in the previous section that the spectral function for $p = 0$ shows no quasi-particle peak but a logarithmic singularity at $\omega = 0$, see Fig. 7.2. Intuitively the spectral function must somehow change its shape from a δ-peak at $\Lambda = \Lambda_0$ to the fixed-point structure at $\Lambda = 0$ given by Eq. (7.14). To see this we shall now analytically continue the scale-dependent self-energy. For $p = 0$ only the Peierls-BCS channel contributes, and from Eq. (7.20) we get

$$\begin{aligned} \mathrm{Re}\,\Sigma_\Lambda^{(\mathrm{PB})}(k_F, \omega + i0^+) &= \frac{\tilde{g}_0^2}{16}\,\Theta(\Lambda_0 - 2\Lambda) \\ &\times \left[(\omega + 4\Lambda)\,\ln\left|\frac{\omega + 4\Lambda}{\omega + 2\Lambda_0}\right| + (\omega - 4\Lambda)\,\ln\left|\frac{\omega - 4\Lambda}{\omega - 2\Lambda_0}\right| \right], \end{aligned} \tag{7.27}$$

as well as

$$\begin{aligned} \mathrm{Im}\,\Sigma_\Lambda^{(\mathrm{PB})}(k_F, \omega + i0^+) &= -\pi\frac{\tilde{g}_0^2}{16}\,\Theta(\Lambda_0 - 2\Lambda)\,\Theta(4\Lambda < |\omega| < 2\Lambda_0) \\ &\times (|\omega| - 4\Lambda)\,. \end{aligned} \tag{7.28}$$

The spectral function can easily be derived from this expression using Eq. (7.8). First of all note that the retarded self-energy is only non-zero for $\Lambda < \Lambda_0/2$. Consequently, the spectral function for $\Lambda > \Lambda_0/2$ is just a δ-peak at $\omega = 0$ with spectral weight $Z_l = 1$. But also for $\Lambda < \Lambda_0/2$ this δ-peak persists, which is seen from the fact that the imaginary part of $\Sigma_\Lambda^{(\mathrm{PB})}$ is non-zero only for $|\omega| > 4\Lambda$,

together with the fact that for all values of Λ we have $\mathrm{Re}\,\Sigma_\Lambda^{(\mathrm{PB})}(k_F, i0^+) = 0$. Consequently we get

$$A_\Lambda^{(\mathrm{PT})}(k_F,\omega) = A_{\Lambda,\delta}^{(\mathrm{PT})}(k_F,\omega) + A_{\Lambda,cont}^{(\mathrm{PT})}(k_F,\omega)\,, \tag{7.29}$$

with

$$\boxed{A_{\Lambda,\delta}^{(\mathrm{PT})}(k_F,\omega) = Z_l\,\delta(\omega)\,,} \tag{7.30}$$

where Z_l is given by Eq. (7.21) and

$$\boxed{\begin{aligned} A_{\Lambda,cont}^{(\mathrm{PT})}(k_F,\omega) &= \frac{\tilde{g}_0^2}{16}\,\Theta(\Lambda_0 - 2\Lambda) \\ &\times \frac{\Theta(4\Lambda < |\omega| < 2\Lambda_0)\,(|\omega| - 4\Lambda)}{\left[\omega - \frac{\tilde{g}_0^2}{16}\sum\limits_{\alpha=\pm1}\left((\omega+\alpha 4\Lambda)\ln\left|\frac{\omega+\alpha 4\Lambda}{\omega+\alpha 2\Lambda_0}\right|\right)\right]^2 + \left[\pi\frac{\tilde{g}_0^2}{16}(|\omega|-4\Lambda)\right]^2}\,. \end{aligned}} \tag{7.31}$$

First note that in the limit $\Lambda \to 0$ the PT result given by Eq. (7.14) is recovered[6], in particular the δ-peak vanishes due to the fact that $\lim_{\Lambda\to 0} Z_l = 0$. A graphical representation of Eq. (7.29) is given in Fig. 7.8 for $\tilde{g}_0 = 0.5$ and in Fig. 7.9 for $\tilde{g}_0 = 0.25$. In both figures $A_{\Lambda,cont}^{(\mathrm{PT})}(k_F,\omega)$ has been plotted for values $\Lambda/\Lambda_0 = 2^{-n}$ with $n = 2,3,4,5,6$. The line shapes are compared with the PT result in Eq. (7.14) ($\Leftrightarrow n = \infty$), where we have set $\Lambda_0 = v_F p_c$. For $\Lambda > \Lambda_0/2$ the continuous part of the spectral function equals zero, such that $A_\Lambda^{(\mathrm{PT})}(k_F,\omega) = \delta(\omega)$ with quasi-particle residue $Z_l = 1$. When $\Lambda < \Lambda_0/2$ the continuous part $A_{\Lambda,cont}^{(\mathrm{PT})}(k_F,\omega)$ grows with decreasing scale ratio Λ/Λ_0 until the PT result with a logarithmic singularity at $\omega = 0$ is reached at $\Lambda/\Lambda_0 = 0$. At the same time Z_l reduces to zero. One might now wonder if the sum rule defined in Eq. (7.15) is conserved as a function of scale? Indeed, if we generally define

$$\mathcal{S}_\Lambda(k_F) = \int_{-\infty}^{\infty} d\omega\, A_\Lambda(k_F,\omega) = \mathcal{S}_{\Lambda,\delta}(k_F) + \mathcal{S}_{\Lambda,cont}(k_F)\,, \tag{7.32}$$

then, according to Eq. (7.29), $\mathcal{S}_{\Lambda,\delta}^{(\mathrm{PT})}(k_F) = Z_l$ is the spectral weight of the quasi-

[6]Eq. (7.14) has been derived for an interaction cutoff, while here we have used a band cutoff. However, for $p = 0$ our two results for the self-energy in Eqs. (7.1) and (7.2) coincide if we identify $\Lambda_0 = v_F p_c$.

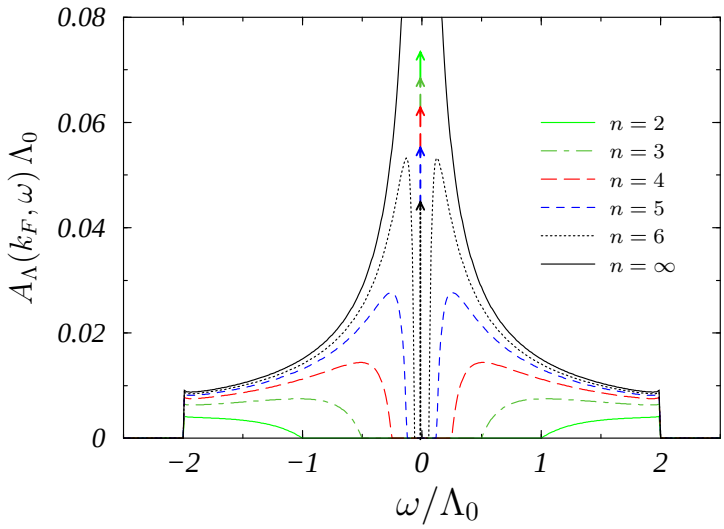

Figure 7.8: Flow of the spectral function determined by Eq. (7.29) for $\tilde{g}_0 = 0.5$ and $\Lambda/\Lambda_0 = 2^{-n}$. The various curves correspond to the values of n depicted in the legend. The straight arrows at $\omega = 0$ represent the δ-contributions, with a quasi-particle weight changing with Λ, which is symbolized by the length of the arrows. For $n \leq 1$ the continuous part of $A_\Lambda(k_F,\omega)$ vanishes and only the δ-peak remains.

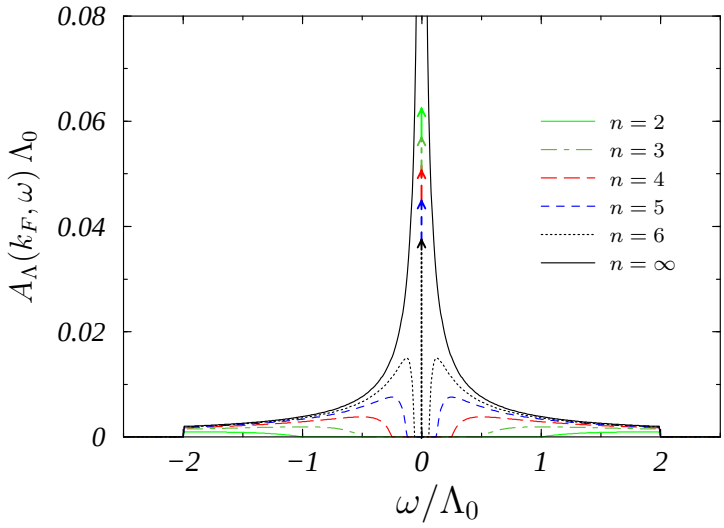

Figure 7.9: The same as in Fig. 7.8 but with $\tilde{g}_0 = 0.25$.

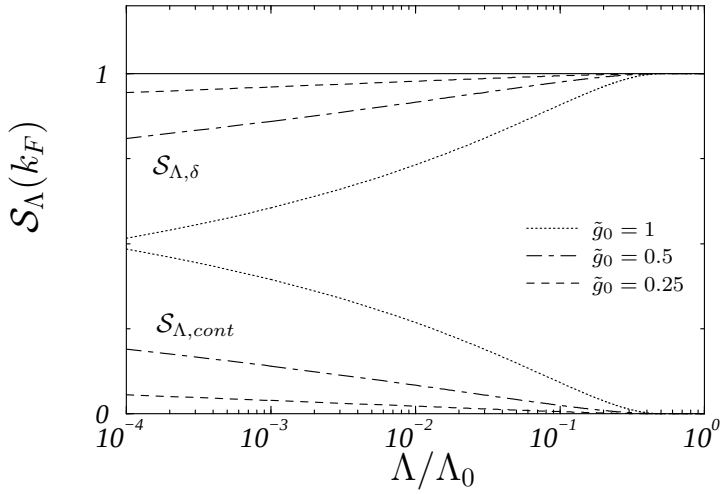

Figure 7.10: The sum rule of the scale-dependent spectral function given in Eq. (7.29) as a function of scale. Like in Fig. 7.6 the lower curves correspond to the contribution of $A_{\Lambda,cont}(k_F,\omega)$ while the upper ones belong to $A_{\Lambda,\delta}(k_F,\omega)$. Each pair corresponding to the same value of $\tilde{g}_0$ adds up to one, which is shown by the solid line.

particle peak at $\omega = 0$ and $\mathcal{S}^{(\mathrm{PT})}_{\Lambda,cont}(k_F)$ denotes the contribution of the continuous part. We find that both contributions add up to one independently of the scale. Analogous to our calculations of the spectral-weight distribution in the previous section this result is numerically exact, which is shown in Fig. 7.10 . Consequently, *our RG transformation conserves the sum rule for the spectral function as a function of scale*, which is indeed a remarkable property.
Furthermore it is now evident how the flow of the quasi-particle residue determined Eq. (7.21) has to be interpreted properly: As long as there is no physical low-energy cutoff like, e.g. , a transverse hopping parameter that effectively replaces Λ at a certain scale, the spectral function for $p = 0$ will assume the Luttinger-liquid form, which at perturbative level is given by Eq. (7.14) . The quasi-particle peak which appears for finite Λ at $\omega = 0$ is then unphysical and vanishes when Λ is reduced to zero. However, the vanishing of Z_l does not exclude the possibility of a finite quasi-particle peak for $p \neq 0$, as we have emphasized below Eq. (7.21). Now imagine that a low-energy scale indeed exists, say a transverse hopping amplitude $\tau_\perp$ to neighboring chains. Then we expect Fig. 7.8 to give the qualitatively correct picture of the spectral function for $p = 0$ if we effectively replace Λ/Λ_0 with $\tau_\perp/\Lambda_0 \equiv \tau_\perp//v_F p_c$ for $\Lambda \leq \tau_\perp$. In this case the quasi-particle peak will persist, as a further reduction of Λ cannot remove it anymore. Depending on the actual value of the ratio $\tau_\perp/v_F p_c$ the physical system will

then behave more or less Fermi-liquid like. We will recover this scenario in our non-perturbative approach to the spectral function in Sec. 7.5 , where we discuss this point in more detail.
Here, these rather far reaching conclusions rely on insights gained by studying our toy model, the importance of which is due to its exact solubility by means of our RG method. Note that we do not claim that the quasi-particle peak we have found in the PT result for the spectral function at $p \neq 0$ will also be present in the exact solution of the g_2-model. *What we have shown here is that RG results predicting a vanishing Z_l exclusively describe a feature of the spectral function at $k = \pm k_F$.*

7.3 Bosonization and Cutoff Dependence

In the previous sections we have repeatedly studied the influence of different cutoff procedures within our RG formalism, and we have seen that important quantities like the renormalized Fermi velocity are changed in the next-to-leading orders. As we have seen in the previous section for a non-Fermi liquid typical Fermi-liquid features like a quasi-particle peak may coexist with non-Fermi liquid properties even in the infrared limit. Furthermore we have speculated that provided that the cancellation between the bare inverse propagator $i\omega - v_F p$ and parts of the exact self-energy Σ in the defining equation for the spectral function (7.8) is not exact to all orders in the coupling $\tilde{g}_0$, this could lead to a scenario similar to that obtained at second-order PT. This would of course drastically reduce the range of validity of the generic TLM result for the spectral function derived by Meden and Schönhammer in Ref. [93] ; it was indeed Meden himself who later on questioned the universality of his earlier result [82].
In this section we do not want to address this difficult question in its full complexity. Instead, we shall point out the most problematic assumptions on which the derivation of the generic Luttinger-liquid result is based. For definiteness we will adopt the notations used in Ref. [82].[7] The interacting Green function in real-time and real-space as obtained within the bosonization approach can be written as follows,

$$G_+^<(x,t) = [G_+^<]_0(x,t)\, e^{F(x,t)}\,, \tag{7.33}$$

where the non-interacting Green function is given by

[7] In particular the relative momentum will in this section be defined by the usual bosonization convention, i.e. $p = k - \alpha k_F$. The two-point function then depends on the branch index α , such that the Green function $G_+^<(x,t)$ refers to the right Fermi point.

$$[G_+^<]_0(x,t) = -\frac{1}{2\pi}\,\frac{e^{ixk_F}}{x - v_F t - i0^+}\,. \tag{7.34}$$

Here the index $<$ referes to the time ordering of the real-time Greenfunction [84]. The Debye-Waller factor for spinless fermions is determined by the equation

$$\begin{aligned} F(x,t) \;&=\; \int_0^\infty \frac{dp}{p}\Big\{\, e^{-ip(x-v_c(p)t)} - e^{-ip(x-v_F t)} \\ &\qquad + \eta(p)\,\big[cos(px)\, e^{iv_c(p)pt} - 1\,\big]\Big\}\,, \end{aligned} \tag{7.35}$$

where the charge velocity $v_c(p)$ for the spinless g_2-model is given by $v_c(p) = v_F\sqrt{1-\tilde{g}_0^2(p)/4} \approx v_F(1-\tilde{g}_0^2(p)/8)$ and the anomalous dimension at weak coupling reads $\eta(p) \approx \tilde{g}_0^2(p)/8$. Again, $\tilde{g}_0(p)$ is the dimensionless Landau parameter defined by $\tilde{g}_0(p) = g_0(p)/\pi v_F$, where the g_2 scattering amplitude $g_0(p)$ is assumed to have a so far unspecified momentum dependence characterized by some effective low-momentum cutoff p_c. Unfortunately there is only a single case for which the integrations in Eq. (7.35) can be performed *exactly*. This is for a constant Landau parameter $g_0(p) = g_0$. However, for the derivation of the spectral function the use of constant Landau parameters is illdefined, as a finite interaction cutoff is needed to obtain a finite result. We will see this shortly. For all other forms of the function $g_0(p)$ only an approximate expression for the Debye-Waller factor can be given, which is obtained by a regularization procedure where $\tilde{g}_0(p)$ in Eq. (7.35) is effectively replaced by $\tilde{g}_0(0) \equiv \tilde{g}_0$. The whole integrand is then multiplied by a factor e^{-p/p_c} to mimic the effect of the finite interaction range. This procedure is justified as follows: As we are interested in the low-energy properties of the spectral function, it will mainly be the values of $G_+^<(x,t)$ for large x and t that contribute to the Fourier transform in momentum and frequency space, where the spectral function is defined. But for large x and t the integrand in Eq. (7.35) is highly oscillatory due to the exponentials, unless p is small. Thus the value of the integral will be dominated by small values of p and the regularization should qualitatively be correct. This intuitive picture is believed to be asymptotically exact. However, it would be interesting to quantify how small p and ω in the spectral function must actually be for the asymptotic result to represent the correct physics. To the best of our knowledge this is still an open question.

As mentioned above, Meden [82] has shown by means of an asymptotic expansion of the Debye-Waller factor that the anomalous dimension picks up non-universal features related to the explicit form of the function $g_0(p)$, in particular due to its smoothness at $p = 0$. He argued that it is not even clear that the spectral function will always show the algebraic singularities calculated in his earlier publication. Only for a box potential, i.e. $g_0(p) = g_0\,\Theta(p_c - |p|)$, he claims his former result

to apply without corrections. We will show here that even this limited statement is questionable.
Introducing the dimensionless variables $\bar{x} = xp_c$ and $\bar{t} = v_F p_c t$ and using a box potential for the Landau parameters, Eq. (7.35) turns into

$$\begin{aligned}\tilde{F}(\bar{x},\bar{t}) &= \int_0^1 \frac{dp}{p}\Big\{ e^{-ip(\bar{x}-\bar{v}_c\bar{t})} - e^{-ip(\bar{x}-\bar{t})} \\ &\qquad + \eta\left[cos(p\bar{x})\, e^{i\bar{v}_c\bar{p}t} - 1\right]\Big\}, \end{aligned} \tag{7.36}$$

where $\bar{v}_c = v_c(0)/v_F \approx 1 - \tilde{g}_0^2/8$ and $\eta = \tilde{g}_0^2/8$. Eq. (7.36) may be expressed in terms of the Exponential Integral $E_1(z) = \int_z^\infty dt\, e^{-t}/t$ [91],[8]

$$\begin{aligned}\tilde{F}(\bar{x},\bar{t}) &= C + \ln(i((\bar{x}-\bar{t})) + E_1(i(\bar{x}-\bar{t})) \\ &- \left[C + \ln(i(\bar{x}-\bar{v}_c\bar{t})) + E_1(i(\bar{x}-\bar{v}_c\bar{t}))\right] \\ &- \frac{\eta}{2}\left[C + \ln(i(\bar{x}+\bar{v}_c\bar{t})) + E_1(i(\bar{x}+\bar{v}_c\bar{t}))\right. \\ &+ \left. C + \ln(-i((\bar{x}-\bar{v}_c\bar{t})) + E_1(-i(\bar{x}-\bar{v}_c\bar{t}))\right], \end{aligned} \tag{7.37}$$

where $C \approx 0.577$ is the Euler constant. To obtain the widely accepted asymptotic result for $\tilde{F}$ when $|\bar{x}|, |\bar{t}| \to \infty$, the following property of the Exponential Integral is used,

$$\lim_{|y|\to\infty} E_1(iy) = 0\,. \tag{7.38}$$

If we naively apply this property to all terms containing E_1 in Eq. (7.37) in the limit $|\bar{x}|, |\bar{t}| \to \infty$, we obtain the following asymptotic expression for the Debye-Waller factor,

$$\tilde{F}(\bar{x},\bar{t}) \simeq -\frac{\eta}{2}\,\ln|\bar{x}^2 - (\bar{v}_c\bar{t})^2| + \ln\left|\frac{\bar{x}-\bar{t}}{\bar{x}-\bar{v}_c\bar{t}}\right|. \tag{7.39}$$

The factor $e^{\tilde{F}(\bar{x},\bar{t})}$ in Eq. (7.33) then leads to the well-known algebraic decay of the Green function $G_+^<(x,t)$ for large values of x and t,

$$G_+^<(sx,st) \simeq s^{-1-\eta} G_+^<(x,t)\,, \tag{7.40}$$

for some positive real number s. This result suggests that $G_+^<(x,t)$ asymptotically represents a homogeneous function of degree $-1-\eta$ independently of the direction

[8] For complex numbers z the path of integration must be chosen such that it does not cross the branch cut extending over the whole negative real axis.

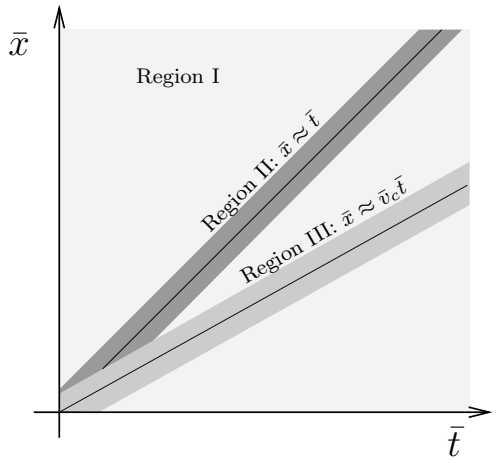

Figure 7.11: Schematical representation of the regions in the $(\bar{t}, \bar{x})$ plane for $\bar{t}, \bar{x} > 0$ where the Green function $G_+^<$ defined in Eq. (7.33) shows different algebraic decay. For detailed explanations see the text.

in the $(\bar{t}, \bar{x})$ plane. However, the problem with this procedure is that even if $|\bar{x}|$ and $|\bar{t}\,|$ are both large, the relevant combinations $|\bar{x} \pm \bar{t}\,|$ and $|\bar{x} \pm \bar{v}_c \bar{t}\,|$ in Eq. (7.37) may remain small. The crucial observation in this context is that the function E_1 has the following series expansion [91],

$$C + \ln z + E_1(z) = \sum_{n=1}^{\infty} (-1)^n \, \frac{z^n}{n \, n!} \,. \tag{7.41}$$

It is then easy to see that there are regions in the $(\bar{t}, \bar{x})$ plane where the approximation (7.39) fails. This is shown in Fig. 7.11 where the situation is sketched for $\bar{x}, \bar{t} > 0$. In region II we have $\bar{x} \approx \bar{t}$ such that Eq. (7.41) must be applied to all terms involving the combination $\bar{x} - \bar{t}$. Equivalently in region III $\bar{x} \approx \bar{v}_c \bar{t}$ such that Eq. (7.41) must be applied to all terms involving the combination $\bar{x} - \bar{v}_c \bar{t}$, and so on. While in region I the approximation given by Eq. (7.39) will be correct in the asymptotic limit $|\bar{x}|, |\bar{t}| \to \infty$, in region II we should rather use the series expansion (7.41) in the first line of Eq. (7.37). The logarithms of the second, third and the fourth line will then dominate for large $\bar{x}$ and $\bar{t}$, such that in this region we get

$$\tilde{F}(\bar{x}, \bar{t}\,) \simeq - \ln |\bar{x} - \bar{v}_c \bar{t}\,| - \frac{\eta}{2} \ln |\bar{x}^2 - (\bar{v}_c \bar{t})^2\,| \,, \qquad \text{Region II} \,. \tag{7.42}$$

Here the algebraic decay is characterized by

$$G_+^<(sx, st) \simeq s^{-2-\eta} G_+^<(x, t) \,, \tag{7.43}$$

which is one power stronger than the generic behavior given by Eq. (7.40). On the other hand in region III we get,

$$\tilde{F}(\bar{x},\bar{t}\,) \simeq \ln|\bar{x}-\bar{t}\,| - \frac{\eta}{2}\,\ln|\bar{x}+\bar{v}_c\bar{t}\,|\,, \qquad \text{Region III}\,, \tag{7.44}$$

leading to

$$G_+^<(sx,st) \simeq s^{-\eta/2} G_+^<(x,t)\,, \tag{7.45}$$

which now decays more than one power weaker than in Eq. (7.40). Finally, in the region where $|\bar{x}+\bar{v}_c\bar{t}\,|$ is small but $|\bar{x}|$ and $|\bar{t}\,|$ are large we get

$$\tilde{F}(\bar{x},\bar{t}\,) \simeq \ln\left|\frac{\bar{x}-\bar{t}}{\bar{x}-\bar{v}_c\bar{t}}\right| - \frac{\eta}{2}\,\ln|x-\bar{v}_c\bar{t}\,|\,, \tag{7.46}$$

and

$$G_+^<(sx,st) \simeq s^{-1-\eta/2} G_+^<(x,t)\,. \tag{7.47}$$

What we see here is that the algebraic decay of the function $G_+^<$ strongly depends on the direction in the $(\bar{t},\bar{x})$ plane. One might now argue that the region where the asymptotic result given by Eq. (7.39) is correct is much larger than the small regions indicated in Fig. 7.11 where it does not apply, such that the influence of the above consideration might be negligible. However, by using the methods described in Ref. [93] for the calculation of the spectral function it becomes evident that it is precisely these small regions that dominate the Fourier transform to the frequency and momentum variables. We do not want to follow this track further, as an analytic expression for the spectral function using the above results seems rather hard to obtain. All we want to stress here is that the so-called asymptotically exact result for the TLM spectral function is at least questionable. It is obtained from Eqs. (7.33) and (7.39) and reads

$$\begin{aligned} A_{\mathrm{TL},+}(p,\omega) &= \frac{\eta}{2}\,(v_c\,p_c)^{-\eta}\,\Theta(|\omega|-|v_cp|) \\ &\quad \times |\omega - v_cp|^{\eta/2-1}|\omega+v_cp|^{\eta/2}\,, \end{aligned} \tag{7.48}$$

at weak coupling. Especially the detailed nature of the algebraic singularities is to our opinion not necessarily correct. Note also that Eq. (7.48) solely depends on the charge velocity v_c while $G_+^<(x,t)$ depends on the bare Fermi velocity v_F as well. Only if we use Eq. (7.39) for all directions in the $(\bar{t},\bar{x})$ plane, the contribution of the Green function $[G_+^<]_0(x,t)$ in the prefactor is asymptotically canceled and the dependence on v_F drops out of the explicit result for $A_{\mathrm{TL},+}$. As we have seen by studying our toy model the presence of a second velocity can lead to

additional features in the line shape of the spectral function, like for instance a δ-peak. This is also known from the model including the spin degree of freedom, where the spin-wave excitations propagate with a velocity different from the plasmon modes (spin-charge separation). Here two algebraic non-analyticities exist, each being directly related to one of the two velocities [93].

Finally let us turn our attention to the question of cutoff dependence of the bosonization results. Note that the spectral function given by Eq. (7.48) is proportional to the inverse momentum cutoff p_c. This means that the overall prefactor of the interacting spectral function depends crucially on *non-universal* features of the model. In particular we cannot send p_c to infinity, i.e. use an infinite-range interaction in momentum space, as it would lead to a vanishing spectral function. In the next section we will find an asymptotic low-energy expression for the spectral function by means of our RG approach, which is essentially equivalent to Eq. (7.48) but with the prefactor $(v_c p_c)^{-\eta}$ replaced by $(\Lambda_0)^{-\eta}$. This again underlines the dual role of the band-width cutoff Λ_0, which also simulates the interaction range if constant Landau parameters are used. It would however be desirable to find an explicit result for the spectral function where p_c or Λ_0 are replaced by more physical quantities. We can indeed give such an example if we combine results obtained in Refs. [97] and [98], where we studied the influence of a non-linear energy dispersion on the spectral function of the TLM and assumed equal g_2 and g_4 scattering amplitudes. In Ref. [98] we showed that the dynamic structure factor of the model splits up in a δ-like part related to the excitation energies of the plasmon modes and a continuous part centered around the energy $v_F p$. The f-sum rule for the dynamic structure factor of the model was shown to be fulfilled exactly with the spectral weight switching from the continuous part at large momentum to the δ-like part when p approaches zero. Here p denotes the transfered momentum of a scattering process. Via the threshold where both contributions to the f-sum rule coincide we defined an additional momentum cutoff besides p_c, which is explicitly given by

$$p_m = \frac{m g_0}{\pi}\,, \tag{7.49}$$

where m is the bare mass of the spinless fermions and g_0 is the common scattering amplitude of g_2-and g_4-processes at zero momentum. The model with linear energy dispersion corresponds to the limit $m \to \infty$ (see for instance Eq. (4.3)) where this cutoff is absent. In Ref. [97] we considered the case $p_c < p_m$ and neglected the contribution of the continuous part of the dynamic structure factor. The result for the spectral function is then given by Eq. (7.48), but with an anomalous dimension that explicitly depends on the curvature of the energy dispersion which is closely related to the bare mass m. There is another interesting

regime which can be treated analytically by precisely the same methods that led to the result in Ref. [97]. This is the case when $p_m < p_c$, but with p_m still being of the same order of magnitude as p_c. The continuous part of the dynamic structure factor will then be negligible like before and the whole calculation remains the same with p_c simply replaced by p_m. At weak coupling the explicit result for the spectral function then reads,

$$\boxed{\begin{aligned} A_{\mathrm{curv},+}(p,\omega) \approx \tfrac{\eta}{2}\left(\tfrac{\pi}{m\, v_F g_0}\right)^{\eta} \Theta(|\omega| - |v_c p|) \\ |\omega - v_c p|^{\eta/2-1} |\omega + v_c p|^{\eta/2}\,, \end{aligned}} \tag{7.50}$$

where we have neglected the curvature corrections to the anomalous dimension as they give rise to terms of order $\sim g_0^4$, see Ref. [97]. Of course, just like p_c the cutoff p_m is introduced here as an effective hard-core momentum cutoff that sharply separates the δ-like part of the dynamic structure factor from the continuous part. However, Eq. (7.50) explicitly shows that the prefactor of the spectral function is essentially determined by *irrelevant* couplings in the RG sense, which in our example is just the fermionic bare mass m.

7.4 Non-Perturbative Scaling Function

In Sec. 7.2 we have shown that the complete flow of the perturbative spectral function can exactly be described by means of our RG approach, in a way that even the sum rule is fulfilled independently of the scale. Encouraged by this rather promising result one might wonder if it is possible to derive a non-perturbative expression for the self-energy, resumming infinite orders of the coupling $\tilde{g}_l$. We will now present such a procedure making use of the scaling hypothesis as described below Eq. (5.10). We have suggested that results obtained in this way will represent some generic low-energy form of the spectral function, comparable to the situation we have found for the susceptibility $\tilde{\Pi}_l$ in Sec. 6.5. However, keeping in mind the discussion of the previous sections, it may well be that the validity of our result might be restricted to extremely small values of the relative momentum p and the frequency ω. Using the methods presented in this section no information about this range of validity can be gained.

To obtain a non-perturbative expression for the spectral function in a first step we shall calculate the fixed-point scaling function $\tilde{\Gamma}^{(2)}_{\infty}(q, i\epsilon)$. In Sec. 5.4 we have emphazised that for this purpose we need the *subtracted* version of the integral representation Eq. (4.57) for $n = 1$, which reads

$$\tilde{\Gamma}_l^{(2,sub)}(q,i\epsilon) = \int_0^l dt\, e^{(1-\bar{\eta}_l(t))\,t}\, \dot{\Gamma}_{l-t}^{(2,sub)}(e^{-t}\,q, e^{-t}\,\epsilon)\,. \tag{7.51}$$

The functions $\tilde{\Gamma}_l^{(2,sub)}$ and $\dot{\Gamma}_l^{(2,sub)}$ are defined by Eqs. (5.39) and (5.43). Eq. (7.51) can be derived from Eq. (4.57) by changing the integration variable according to $t \to l - t$ and by using the fact that $\dot{\Gamma}_{l=0}^{(2,sub)} = 0$. We have introduced here a scale averaged anomalous dimension slightly different from our previous definition in Eq. (4.48),

$$\bar{\eta}_l(t) = \frac{1}{t}\int_0^t d\tau\, \eta_{l-\tau}\,. \tag{7.52}$$

Setting $\bar{\eta}_l(t) = 0$ and inserting the subtracted versions of our two-loop results for the function $\dot{\Gamma}_l^{(2)}$ given by Eqs. (6.58) and (6.59) on the r.h.s. of Eq. (7.51), we simply get back to the perturbative self-energy derived in Sec. 7.2. Yet, if we proceed in the same way but keep $\bar{\eta}_l(t)$ finite this will provide us with an expression for the two-point scaling function that re-sums infinite orders of the coupling $\tilde{g}_l$ and is hence non-perturbative in nature. The calculation will be considerably simplified if we make use of the scaling hypothesis, i.e. if we approximate

$$\tilde{\Gamma}_l^{(2,sub)}(q,i\epsilon) \approx \tilde{\Gamma}_\infty^{(2,sub)}(q,i\epsilon)\,, \qquad \text{for} \quad 1 \ll |q|, |\epsilon| \ll e^l\,. \tag{7.53}$$

Note however that the limit $l \to \infty$ cannot be performed trivially in Eq. (7.51) since both the upper integration boundary and the integral kernel depend on l. We will follow here the same approximation strategy we used for the derivation of the susceptibilities and neglect the non-local dependence of $\tilde{\Gamma}_l^{(2)}$ on the logarithmic scale factor l. To be concrete, we rewrite Eq. (7.51) for $l = \infty$ and obtain

$$\begin{aligned}\tilde{\Gamma}_\infty^{(2,sub)}(q,i\epsilon) &\approx \int_0^\infty dt\, e^{(1-\eta)t}\, \dot{\Gamma}_\infty^{(2,sub)}(e^{-t}q, e^{-t}\epsilon) \\ &= \int_0^1 d\lambda\, \lambda^{\eta-2}\, \dot{\Gamma}_\infty^{(2,sub)}(\lambda q, \lambda\epsilon)\,. \end{aligned} \tag{7.54}$$

We have used that $\bar{\eta}_\infty(t) = \eta$ according to Eq. (7.52), with η being the fixed-point value of the anomalous dimension. For the function $\dot{\Gamma}_\infty^{(2,sub)}$ we insert the subtracted versions of the zero-sound and the Peierls-BCS contribution of the function $\dot{\Gamma}_l^{(2)}$ determined by Eqs. (6.58) and (6.59), which for $l = \infty$ add up to

$$\dot{\Gamma}_\infty^{(2,sub)}(q,i\epsilon) = \eta s_q\,\Theta(1<|q|) + \eta s_q \Big\{ 2\Theta(1<|q|)\,\ln(\tilde{v}(2+|q|) + i\epsilon s_q)$$

$$+\,\Theta(|q|<1)\,\ln(\tilde{v}(4-|q|)+i\epsilon s_q)-2\ln(\tilde{v}(4+|q|)-i\epsilon s_q)$$
$$-\,\Theta(1<|q|)\,\frac{3\tilde{v}|q|+i\epsilon s_q}{\tilde{v}(2+|q|)+i\epsilon s_q}-(i\epsilon s_q-\tilde{v}|q|)\Big\}\,. \qquad (7.55)$$

Several remarks about this equation are in order. First of all, it is important to notice that in contrast to the hydrodynamic regime, in the scaling regime the zero-sound channel contributes to the self-energy. Furthermore, on the r.h.s. of Eq. (7.55) the fixed-point value $\tilde{v}$ of the velocity renormalization factor $\tilde{v}_l$ appears, which we had kept self-consistently in our calculation of $\dot{\Gamma}_l^{(2)}$. But we should not identify $\tilde{v}$ with the fixed-point value given by Eq. (6.117) as it has been calculated in the hydrodynamic regime, while now we are interested in the properties of the scaling function in the scaling regime. On the other hand, we have seen in Sec. 7.1 that our RG approach reproduces the correct velocity renormalization predicted by simple perturbation theory. For a better comparison with the bosonization result we will thus set $\tilde{v}=1-\tilde{g}_0^2/8=1-\eta$, which corresponds to the velocity renormalization obtained at the perturbative level in the model with an *interaction* cutoff. If we proceed so we should weed out all terms in Eq. (7.55) that lead to a velocity renormalization at the perturbative level. This is found to be the term $\eta s_q\,\Theta(1<|q|)$ on the r.h.s. of the equation which we shall neglect in our subsequent calculations.

Before we proceed, it should be checked if the application of the scaling hypothesis is indeed justified. – This is not obvious at all, since at the perturbative level we have seen that the fixed-point expression is not a homogeneous function and we had to use other methods. Furthermore, if we replace q and ϵ by sq and $s\epsilon$ in Eq. (7.54), with s being a positive scale factor, and change the integration variable on the r.h.s. according to $\lambda\to s\lambda$ we see that the homogeneity is spoiled by the upper integration boundary. On the other hand the bosonization result for the spectral function, Eq. (7.48), is manifestly a homogeneous function in the variables p and ω. The crucial outcome is that not $\tilde{\Gamma}_\infty^{(2,sub)}(q,i\epsilon)$ itself but $\tilde{r}_\infty(q,i\epsilon)=i\epsilon-\tilde{v}q+\tilde{\mu}+\tilde{\Gamma}_\infty^{(2,sub)}(q,i\epsilon)$ will be homogeneous in the scaling regime, with the correct scaling behavior ensuring a finite result for the physical spectral function.

Now, if we insert Eq. (7.55) on the r.h.s. of Eq. (7.54) the following expression for the two-point scaling function *in the scaling regime* can be found,

$$\tilde{\Gamma}_\infty^{(2,sub)}(q,i\epsilon)\;\simeq\;\frac{i\epsilon-\tilde{v}q}{2}\Big\{-2+F_\eta\Big(-\frac{i\epsilon s_q+\tilde{v}|q|}{2\tilde{v}}\Big)+F_\eta\Big(\frac{i\epsilon s_q-\tilde{v}|q|}{4\tilde{v}}\Big)$$
$$+|q|^{-\eta}\Big[F_\eta\Big(-\frac{i\epsilon s_q-\tilde{v}|q|}{4\tilde{v}|q|}\Big)-F_\eta\Big(-\frac{i\epsilon s_q+\tilde{v}|q|}{2\tilde{v}|q|}\Big)\Big]\Big\}\,, \qquad (7.56)$$

where we have defined

$$F_\eta(z) = \eta \int_0^1 d\lambda \, \frac{\lambda^{\eta-1}}{1-\lambda z} \approx {}_2F_1(1,\eta;1+\eta;z)\,. \tag{7.57}$$

Here, ${}_2F_1(a,b;c;z)$ is the Gauss hyper-geometric function [91]. In deriving Eq. (7.56) we have neglected terms vanishing in the scaling regime $|q|, |\epsilon| \gg 1$ and we have only retained the leading orders in η in the prefactors. Note that the first term on the r.h.s. of Eq. (7.56) is of order unity in the prefactor while the terms involving the function $F_\eta(z)$ are proportional to η. The rescaled inverse propagator $\tilde{r}_\infty$ in the scaling regime then reads,

$$\begin{aligned}
\tilde{r}_\infty(q,i\epsilon) &\simeq i\epsilon - \tilde{v}q + \tilde{\Gamma}_\infty^{(2,sub)}(q,i\epsilon) \\
&= \frac{i\epsilon - \tilde{v}q}{2}\left\{ F_\eta\Big(-\frac{i\epsilon s_q + \tilde{v}|q|}{2\tilde{v}}\Big) + F_\eta\Big(\frac{i\epsilon s_q - \tilde{v}|q|}{4\tilde{v}}\Big)\right. \\
&\left. +|q|^{-\eta}\Big[F_\eta\Big(-\frac{i\epsilon s_q - \tilde{v}|q|}{4\tilde{v}|q|}\Big) - F_\eta\Big(-\frac{i\epsilon s_q + \tilde{v}|q|}{2\tilde{v}|q|}\Big)\Big]\right\}.
\end{aligned} \tag{7.58}$$

Note that the inverse propagator $i\epsilon - \tilde{v}q$ in the first equality has been canceled by a corresponding contribution of $\tilde{\Gamma}_\infty^{(2,sub)}(q,i\epsilon)$. For later convenience we have kept the hypergeometric functions $F_\eta(z)$ irrespective of the explicit value of the argument z. However, for $z = -(i\epsilon s_q + \tilde{v}|q|)/2\tilde{v}$ and $z = (i\epsilon s_q - \tilde{v}|q|)/4\tilde{v}$ we should better use the transformation formula [91],

$$F_\eta(z) = \frac{\eta\pi}{\sin(\eta\pi)}\,(-z)^{-\eta} + \frac{\eta}{1-\eta}\,z^{-1}\,F_{1-\eta}(-z^{-1})\,, \tag{7.59}$$

valid for $|\arg(-z)| < \pi$, so that for large $|z|$ (scaling regime) we approximately have $F_\eta(z) \sim (-z)^{-\eta}$ to leading order in the prefactor. Note however, that for instance for $z = -(i\epsilon s_q + \tilde{v}|q|)/2\tilde{v}|q|$ the transformation (7.59) does not lead to a simplification, since $|z|$ remains of the order of unity even in the scaling regime and the hypergeometric function has to be kept. From Eq. (7.58) it is then easy to show that

$$\tilde{r}_\infty(sq, s\,i\epsilon) = s^{1-\eta}\,\tilde{r}_\infty(q,i\epsilon) \qquad \text{for} \quad |q|, |\epsilon| \gg 1\,, \tag{7.60}$$

i.e. $\tilde{r}_\infty(q,i\epsilon)$ is indeed a homogeneous function of degree $1-\eta$ in the scaling regime. This a posteriori confirms the applicability of the scaling hypothesis, and according to Eq. (5.11) the physical Green function G at the fixed point may now be written as

$$G(\alpha(k_F+p), i\omega) \approx \frac{(\Lambda_0)^{-\eta}}{\tilde{r}_\infty(p,i\omega)} \equiv (\Lambda_0)^{-\eta}\,\tilde{G}_\infty(p,i\omega)\,, \tag{7.61}$$

which makes explicit use of the property (7.60). The function $\tilde{G}_\infty$ is hence indeed a scaling function in the sense of Sec. 5.1.[9]
Let us now deduce the spectral function from Eq. (7.56) . To this end we need the analytic continuation of $\tilde{\Gamma}^{(2,sub)}_\infty(q, i\epsilon)$ to the real frequency axis, i.e. the retarded two-point vertex $\tilde{\Gamma}^{(2,sub)}_\infty(q, \epsilon + i0^+)$. This can be achieved by using the integral representation of the hypergeometric function F_η given in Eq. (7.57). For the real part the analytic continuation is a rather involved and technical matter which we postpone to appendix C . There we show in detail that to leading order in the prefactors and in the scaling regime the imaginary and the real part of the retarded two-point vertex are given by

$$\begin{aligned}
\mathrm{Im}\,\tilde{\Gamma}^{(2,sub)}_\infty(q, \epsilon + i0^+) &= 2\pi\eta \Bigg\{ \Theta(\epsilon s_q < -3\tilde{v}|q|) \left|\frac{\epsilon - \tilde{v}q}{4\tilde{v}}\right|^{1-\eta} \\
&\quad + \Theta(-3\tilde{v}|q| < \epsilon s_q < -\tilde{v}|q|) \left|\frac{\epsilon - \tilde{v}q}{4\tilde{v}}\right| \left|\frac{\epsilon + \tilde{v}q}{2\tilde{v}}\right|^{-\eta} \\
&\quad + \Theta(\tilde{v}|q| < \epsilon s_q) \left|\frac{\epsilon - \tilde{v}q}{4\tilde{v}}\right|^{1-\eta} \Bigg\}, \qquad (7.62)
\end{aligned}$$

and

$$\begin{aligned}
\mathrm{Re}\,\tilde{\Gamma}^{(2,sub)}_\infty(q, \epsilon + i0^+) &= -(\epsilon - \tilde{v}q) \\
&\quad + \Theta(\epsilon s_q < -3\tilde{v}|q|)\,(\epsilon - \tilde{v}q) \left|\frac{\epsilon - \tilde{v}q}{4\tilde{v}}\right|^{-\eta} \\
&\quad + \Theta(-3\tilde{v}|q| < \epsilon s_q)\,(\epsilon - \tilde{v}q)\,\frac{1}{2} \left[\left|\frac{\epsilon - \tilde{v}q}{4\tilde{v}}\right|^{-\eta} + \left|\frac{\epsilon + \tilde{v}q}{2\tilde{v}}\right|^{-\eta}\right]. \qquad (7.63)
\end{aligned}$$

In analogy with Eq. (7.13) the dimensionless spectral function in the scaling regime will then be given by

$$\tilde{A}_\infty(q, \epsilon) = -\frac{1}{\pi}\,\mathrm{Im}\left[\frac{1}{\epsilon - \tilde{v}q + \tilde{\Gamma}^{(2,sub)}_\infty(q, \epsilon + i0^+) + i0^+}\right]. \qquad (7.64)$$

First of all we have to check if in the interval $-\tilde{v}q < \epsilon < \tilde{v}q$, where the imaginary part of $\tilde{\Gamma}^{(2,sub)}_\infty$ vanishes, the function $\mathrm{Re}\,\tilde{r}_\infty(q, \epsilon + i0^+)$ is non-zero, as otherwise we

[9] Strictly speaking what we have called the two-point scaling function, i.e. $\tilde{\Gamma}^{(2)}_l$, does not have the property of a scaling function at the fixed point. We used this nomenclature in Chap. I since $\tilde{\Gamma}^{(2)}_l$ is closely related to the real scaling function $\tilde{G}_\infty$ and to distinguish it from the physical two-point vertex $\Gamma^{(2)}_\Lambda$.

would again find a δ-like contribution to the spectral function. Using Eq. (7.63) it is easy to show that for $\epsilon s_q < \tilde{v}|q|$ we have $\mathrm{Re}\,\tilde{r}_\infty(q, \epsilon + i0^+) < 0$ for $q > 0$ and $\mathrm{Re}\,\tilde{r}_\infty(q, \epsilon + i0^+) > 0$ for $q < 0$, such that the quasi-particle peak we found in the perturbative spectral function is absent in our non-perturbative result (see also Fig. 7.12). It should however be mentioned that we have eliminated this feature of the perturbative expression by hand, a point we will discuss after having stated the explicit result for the spectral function. Due to the fact that no δ-like contribution exists the function $\tilde{A}_\infty$ can be approximated by

$$\tilde{A}_\infty(q,\epsilon) \approx \frac{1}{\pi} \frac{\mathrm{Im}\,\tilde{\Gamma}_\infty^{(2,sub)}(q, \epsilon + i0^+)}{\left[\epsilon - \tilde{v}q + \mathrm{Re}\,\tilde{\Gamma}_\infty^{(2,sub)}(q, \epsilon + i0^+)\right]^2} = \frac{1}{\pi} \frac{\mathrm{Im}\,\tilde{r}_\infty(q, \epsilon + i0^+)}{[\mathrm{Re}\,\tilde{r}_\infty(q, \epsilon + i0^+)]^2}\,, \tag{7.65}$$

where in the denominators we have neglected the contribution of $\mathrm{Im}\,\tilde{\Gamma}_\infty^{(2,sub)}$. This is justified by observing that the imaginary part of $\tilde{\Gamma}_\infty^{(2,sub)}$ is proportional to η while the prefactor of the real part is of the order of unity.
Let us first consider the special case $q = 0$, which in principle needs a separate treatment, since in deriving Eq. (7.56) we made explicit use of the scaling limit where $|q| \gg 1$. The result of a separate calculation is however the same as obtained by simply setting $q = 0$ in Eqs. (7.62) and (7.63). Since in the next section we will study this special case in detail, let us just state the result here. We obtain

$$\boxed{\tilde{A}_\infty(0,\epsilon) \simeq \frac{\eta}{2}\,|\epsilon|^{\eta-1}\,,} \tag{7.66}$$

leading to the physical spectral function

$$A(\alpha k_F, \omega) \approx Z_l\,\Lambda^{-1}\,\tilde{A}_\infty(0, \omega/\Lambda) = \Lambda_0^{-\eta}\,\frac{\eta}{2}\,|\omega|^{\eta-1}\,, \tag{7.67}$$

with $\alpha = \pm 1$ labeling the two Fermi points $k = \pm k_F$. This is precisely the weak-coupling result obtained by the bosonization method if we identify $\Lambda_0 = v_c\,p_c$, see Eq. (7.48) for $p = 0$. For $q \neq 0$ our result will be more complicated and we first notice that the bare inverse propagator given by Eq. (7.58) may be written in the dynamic scaling form [81] as follows,

$$\tilde{r}_\infty(q, \epsilon + i0^+) = |q|^{\eta-1}\,\tilde{f}_\infty^{\pm}(\epsilon/\tilde{v}q)\,, \tag{7.68}$$

with

$$\mathrm{Im}\tilde{f}_\infty^{\pm}(x) \;=\; 2\pi\eta \left\{ \Theta(x < -3) \left|\frac{x-1}{4}\right|^{1-\eta}\right.$$

$$+\,\Theta(-3<x<-1)\,\left|\frac{x-1}{4}\right|\,\left|\frac{x+1}{2}\right|^{-\eta}$$
$$+\,\Theta(1<x)\,\left|\frac{x-1}{4}\right|^{1-\eta}\,\Bigg\}\,, \tag{7.69}$$

and

$$\begin{aligned}\mathrm{Re}\tilde{f}^{\pm}_{\infty}(x) &= \pm\,(x-1)\,\Bigg\{\,\Theta(x<-3)\,\left|\frac{x-1}{4}\right|^{-\eta}\\ &\quad+\,\Theta(-3<x)\,\frac{1}{2}\left[\,\left|\frac{x-1}{4}\right|^{-\eta}+\left|\frac{x+1}{2}\right|^{-\eta}\,\right]\Bigg\}\,.\end{aligned} \tag{7.70}$$

Here, the functions $\tilde{f}^{+}_{\infty}(x)$ and $\tilde{f}^{-}_{\infty}(x)$ refer to $q>0$ and $q<0$ respectively, and a graph of $\tilde{f}^{+}_{\infty}(\epsilon/\tilde{v}q)$ is shown in Fig. 7.12 for $\eta=0.2$. Note that at $x=-1$ both the real and the imaginary part of $\tilde{f}^{\pm}_{\infty}(x)$ diverge like $\sim|x+1|^{-\eta}$, such that $\tilde{A}_{\infty}$ in Eq. (7.65) vanishes like $\sim|x+1|^{\eta}$ at this point. On the other hand, at $x=1$ both contributions vanish like $\sim|x-1|^{1-\eta}$, leading to an algebraic singularity of degree $\eta-1$. For $q\neq 0$ we get

$$\boxed{\tilde{A}_{\infty}(q,\epsilon)\simeq|q|^{\eta-1}\,\tilde{h}_{\infty}(\epsilon/\tilde{v}q)\,,} \tag{7.71}$$

with the scaling function $\tilde{h}_{\infty}$ given by

$$\tilde{h}_{\infty}(x)=\frac{\eta}{2}\,|x-1|^{\eta-1}\,\begin{cases}1 & \text{for}\quad x<-3\\ 4\left[\,\left|2\frac{x+1}{x-1}\right|^{\eta/2}+\left|\frac{1}{2}\frac{x-1}{x+1}\right|^{\eta/2}\,\right]^{-2} & \text{for}\,-3<x<-1\\ 0 & \text{for}\,-1<x<1\\ 4\left[1+\left|\frac{x-1}{x+1}\right|^{\eta}\,\right]^{-2} & \text{for}\quad 1<x\end{cases}\,. \tag{7.72}$$

In Fig. 7.13 we compare the graph of $\tilde{h}_{\infty}$ with the corresponding scaling function obtained from the bosonization result in Eq. (7.48). For $\eta=0.2$ the two graphs coincide very well on a linear ω-scale, although the nature of the algebraic singularity at $\omega=v_c p$ is slightly different for $p\neq 0$. To amplify the differences we have plotted the same functions on a logarithmic scale in the vicinity of $\omega=v_c p$ in Fig. 7.14. Here, we also display the result obtained from second-order perturbation theory, Eq. (7.17), which shows a qualitatively different behavior.

Analytically it is easy to check that $\tilde{h}_{\infty}(x)$ is continuous and differentiable at $x=-3$, such that $\tilde{h}_{\infty}(\epsilon/\tilde{v}q)$ is a smooth function in the interval $-\infty<\epsilon/\tilde{v}q<-3$

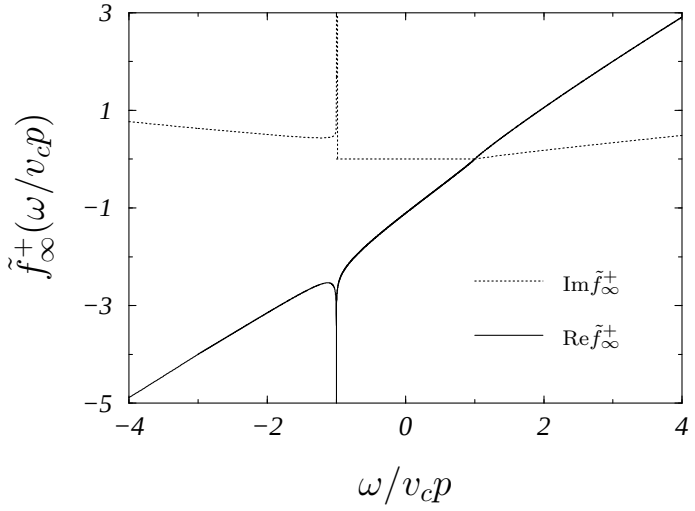

Figure 7.12: Graph of the function $\tilde{f}^+_\infty(\omega/v_cp)$ defined by Eq. (7.70) for $\eta = 0.2$. Note that the real part of $\tilde{f}^+_\infty$ is strictly negative in the interval $-1 < \omega/v_cp < 1$ where the imaginary part vanishes.

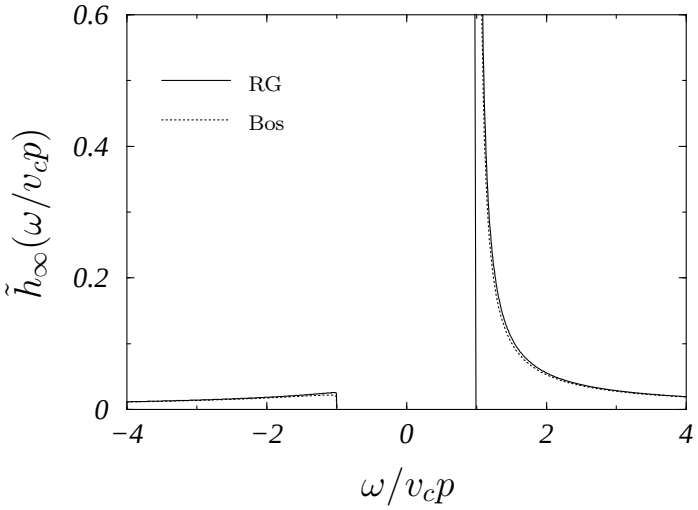

Figure 7.13: Graph of the functions $\tilde{h}_\infty(\omega/v_cp)$ defined by Eq. (7.72) and $\tilde{h}_{\mathrm{TL}}(\omega/v_cp) = A_{\mathrm{TL}}(k_F + p, \omega)(v_cp_c)|v_cp|^{1-\eta}$ for $\eta = 0.2$. Even for this value of the anomalous dimension, which is out of range of a weak-coupling expansion in $\tilde{g}_0$, the differences of the bosonization and the RG result are nearly invisible on a linear scale in ω/v_cp.

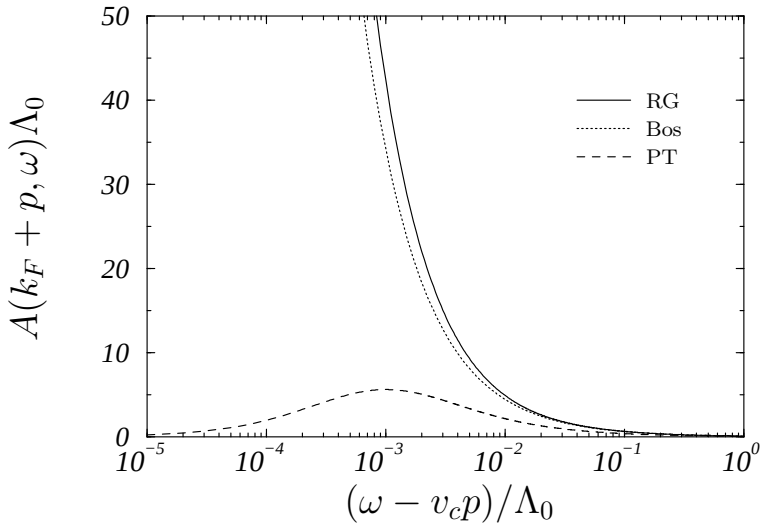

Figure 7.14: Graph of the spectral function near $\omega = v_c p$ for $p/p_c = 0.01$ and $\eta = 0.2$ on a logarithmic ω-scale. We compare the results obtain from second-order perturbation theory (PT), bosonization (Bos) and from our RG approach (RG) . For a better comparison we have set the bare Fermi velocity v_F present in the continuous part of the perturbative result (7.17) equal to the charge velocity v_c . We have identified $\Lambda_0 = v_c p_c$.

as well as for $1 < \epsilon/\tilde{v}q$. For a better comparison with the bosonization result let us transform back to the physical variables p and ω . To this end notice that $\tilde{A}_\infty$ satisfies a simple scaling law,

$$\tilde{A}_\infty(sq, s\epsilon) = s^{\eta-1}\,\tilde{A}_\infty(q,\epsilon)\,. \tag{7.73}$$

Using equation (4.29) the relation between the physical spectral function $A(\alpha(k_F+p),\omega)$ and the scaling function $\tilde{A}_\infty(q,\epsilon)$ is then given by

$$\begin{aligned} A(\alpha(k_F+p),\omega) &\approx \Lambda^{-1} Z_l\,\tilde{A}_\infty\big(\tfrac{v_F p}{\Lambda}, \tfrac{\omega}{\Lambda}\big) \\ &\approx \tau\Big(\frac{\xi_0}{\xi}\Big)^{\eta}\,\tilde{A}_\infty(p\xi,\omega\tau) = \tau_0^{\eta}\tilde{A}_\infty(v_F p,\omega)\,. \end{aligned} \tag{7.74}$$

The first line represents nothing but the scaling hypothesis for the analytically continued Green function in the form stated in Eq. (5.10), and the second approximate relation uses the definitions of the length and time-scales introduced in Eq. (5.1). We have used the fact that for large values of l we may write $Z_l = e^{-\bar{\eta}_l l} \approx e^{-\eta l} = (\xi_0/\xi)^{\eta}$. From this equation the formal analogy of the function $\tilde{A}_\infty$ with the scaling functions introduced in the theory of dynamical critical

phenomena becomes completely evident.
Let us now compare the analytic properties of the bosonization and the RG results which are, in contrast to the $p = 0$ case, slightly different. In Fig. 7.13 the line shapes of the scaling functions $\tilde{h}_\infty(\epsilon/\tilde{v}q) = \tilde{h}_\infty(\omega/v_c p)$ given by Eq. (7.72) and $\tilde{h}_{\rm TL}(\omega/v_c p) = A_{\rm TL}(k_F + p, \omega)/|v_c p|^{\eta-1}$, following from Eq. (7.48), are shown for $\eta = 0.2$.[10] Although the two plots coincide very well at first sight, by closer observation we see that the analytical properties at $\omega = \pm v_c p$ are different. In particular, for $\omega \to v_c p + 0^+$ the bosonization result predicts

$$A_{\rm TL}(k_F + p, \omega) \sim \Lambda_0^{-\eta} \frac{\eta}{2} |2v_c p|^{\eta/2} |\omega - v_c p|^{\eta/2-1} , \tag{7.75}$$

while our RG result yields

$$A(k_F + p, \omega) \sim \Lambda_0^{-\eta}\, 2\eta |\omega - v_c p|^{\eta-1} , \tag{7.76}$$

which diverges with a different exponent. Similarly, for $\omega \to -v_c p - 0^+$ we get

$$A_{\rm TL}(k_F + p, \omega) \sim \Lambda_0^{-\eta} \frac{\eta}{2} |2v_c p|^{\eta/2-1} |\omega + v_c p|^{\eta/2} , \tag{7.77}$$

while Eq. (7.72) predicts

$$A(k_F + p, \omega) \sim \Lambda_0^{-\eta}\, 2\eta |2v_c p|^{-1} |\omega + v_c p|^{\eta} , \tag{7.78}$$

which drops down to zero with a different exponent than the bosonization result. Note however that the overall scaling law (7.73) applies to both results.
What are the reason for this different behavior and which expression is the correct one? In the previous section we have shown in some detail that the widely accepted asymptotic low-energy result for the spectral function with a hard-core potential energy, obtained by means of the bosonization technique, is at least questionable. It is however fair to mention that problems similar to those presented in Sec. 7.3 also appear in the RG approach. Note for instance that the result (7.71) has been derived in the scaling limit and relies not only on the fact that both $|q|$ and $|\epsilon|$ are large compared with unity, but the combinations $|i\epsilon \pm \tilde{v}q|$ entering the explicit expression for $\tilde{r}_\infty(q, i\epsilon)$ in Eq. (7.58) have to be large as well. For the imaginary frequency representation this poses no problem, but after analytic continuation the condition reads $|\epsilon \pm \tilde{v}q| \gg 1$, which may well be violated even if $|q|$ and $|\epsilon|$ both are large. If we now draw a picture in the (q, ϵ) plane the situation is very similar to the picture sketched in Fig. 7.11. However, in contrast to the discussion of the Debye-Waller factor here we are already in Fourier space

[10] We have chosen $\eta = 0.2$ to make the differences visible, although this value for the anomalous dimension corresponds to $\tilde{g} \approx 1.3$, being out of range of a weak-coupling expansion. For $\tilde{g} = 0.3$ we obtain $\eta \approx 0.01$ in which case the two plots are indistinguishable.

where the spectral function is defined, and the subtleties related to the scaling limit can be discussed in a controlled manner. In deriving our result for $\tilde{A}_\infty$ we indeed have assumed that $|\epsilon \pm \tilde{v}q| \gg 1$, as well as $|q| \gg 1$ and $|\epsilon| \gg 1$ separately. Whether the condition $|\epsilon \pm \tilde{v}q| \gg 1$ will be satisfied or not depends crucially on the fact if the infrared cutoff Λ can be reduced to zero. More precisely, if a finite low-energy cutoff $\Lambda_\star$ like a finite transverse-hopping amplitude exists that effectively replaces Λ for $\Lambda < \Lambda_\star$, we get

$$|\epsilon \pm \tilde{v}q| \approx \left| \frac{\omega - v_c p}{\Lambda_\star} \right| . \tag{7.79}$$

In this case $|\epsilon \pm \tilde{v}q|$ may remain small even for small $\Lambda_\star$ if only ω is close enough to $v_c p$. However, $\Lambda_\star \to 0$ implies $|\epsilon \pm \tilde{v}q| \to \infty$ unless precisely $\omega = v_c p$, such that our result for the spectral function is expected to be correct. It hence describes the physical system at the quantum critical point where the correlation length $\xi = v_F/\Lambda$ diverges.

Keeping in mind that in practice the TLM only describes a one-dimensional conductor above some finite energy scale $\Lambda_\star$ below which a crossover to higher dimensionality or a superconducting state sets in, it is instructive to elaborate a little more on the case of a small but finite $\Lambda_\star$. To elucidate the nature of the singularity of the spectral function at $\omega \approx v_c p$ a different limiting procedure is then relevant. This is given by first taking the limit $|\epsilon - \tilde{v}q| \to 0$ followed by $|\epsilon|, |q| \gg 1$. In appendix C we show that the real part of $\tilde{r}_\infty(q, \epsilon + i0^+)$ is in this limit to leading order given by

$$\mathrm{Re}\, \tilde{r}_\infty(q, \epsilon + i0^+) \approx \frac{1}{2} (\epsilon - \tilde{v}) , \tag{7.80}$$

while the imaginary part vanishes. According to Eq. (7.64) the dimensionless scaling function is then given by

$$\tilde{A}_\infty(q, \epsilon) = 2\, \delta(\epsilon - \tilde{v}q + \tilde{\mu}) , \tag{7.81}$$

leading to the physical spectral function

$$A(k_F + p, \omega) = Z_{l_\star} \delta(\omega - v_c p) . \tag{7.82}$$

Here the quasi-particle residue is determined by $Z_{l_\star} = 2(\Lambda_\star/\Lambda_0)^\eta$. The predicted line-shape for the spectral function shows a typical Fermi-liquid feature and is thus qualitatively different if a finite low-energy cutoff is present. However, we should not trust Eq. (7.82) too far. In particular the factor of two present in the result for the quasi-particle residue $Z_{l_\star}$ is not reliable. The reason for this is that we used Eq. (7.58) for the derivation of the above result, which in turn has been derived by using the scaling hypothesis, which is not necessarily applicable

when Λ cannot be reduced to zero. Nonetheless, Eq. (7.82) should at least be qualitatively correct. In the next section, when we calculate the complete flow of the spectral function for $p = 0$, we will recover the result (7.82) but with $Z_{l_\star} \approx (\Lambda_\star/\Lambda_0)^\eta$. A further discussion of this result will hence be postponed to this section.

Finally let us address the question if a quasi-particle peak exists in the spectral function when the infrared cutoff Λ *can* be reduced to zero, i.e. when $\Lambda_\star = 0$. In Sec. 7.1 we have seen that in the perturbative spectral function such a peak is present for $p \neq 0$. If we keep the considerations of Sec. 7.3 in mind, in our opinion it remains an open question if Eq. (7.48) correctly describes the low-energy excitation spectrum of the TLM for all momenta k. The problem with the bosonization approach is that even if we knew a reliable approximation for the Green function in real-time and real-space representation, the double Fourier transform to the momentum and frequency variables would still be a very hard calculational task. On the other hand our RG formalism directly works in Fourier space, such that at least this problem does not occur. Here we are able to calculate an explicit expression for the self-energy. From the definition (7.65) of the spectral function it is then clear that the analytic properties of $\tilde{A}_\infty$ at $\epsilon = \tilde{v}q$ depend crucially on the fact if the bare inverse propagator $\epsilon - \tilde{v}q$ is canceled *exactly* by a corresponding contribution of the self-energy or not. By the approximation scheme we presented in this section this was indeed the case, leading to the famous algebraic singularity of the spectral function at $\omega = v_c p$. However, in deriving our result we eliminated the terms leading to a renormalization of the Fermi velocity at perturbative level by hand. If we keep these terms they give rise to contributions to $\tilde{r}_\infty(q, \epsilon + i0^+)$ in the subleading η-order in the prefactors, which indeed qualitatively change the line-shape of the spectral function in Fig. 7.13. The quasi-particle peak present at second-order PT then reappears and the continuous part of the spectral function related to the plasmon excitations drops down to zero with an algebraic power law at $\omega = v_F p$.[11] The shape of the spectral function is then very similar to that of second-order perturbation theory given in Fig. 7.4. However, the next-to-leading orders in the prefactors of $\mathrm{Re}\,\tilde{r}_\infty(q, \epsilon + i0^+)$ cannot be trusted in our non-perturbative approach to the spectral function for the following reason: On the r.h.s. of Eq. (7.54) we have inserted all two-loop contributions to $\dot{\Gamma}_\infty^{(2,sub)}$, i.e. all terms of order $\sim \tilde{g}^2 \sim \eta$. Due to the λ-integration in Eq. (7.54) the real part of $\tilde{r}_\infty$ picks up a prefactor $\sim 1/\eta$, such that the leading contributions are of the order of unity in the prefactor. This is a strongly non-perturbative effect that "shifts" the η-orders in the prefactor of the real part of the retarded self-energy, while no such shift appears for the imaginary part, see

[11] If we keep the term responsible for the velocity renormalization in the *hydrodynamic* regime we should also use v_F instead of v_c for consistency reasons.

Eqs. (7.62) and (7.63) . The imaginary part hence remains proportional to η . For the same reason we expect that the leading contributions to the real part which are due to contributions of $\dot{\Gamma}_{\infty}^{(2,sub)}$ proportional to $\tilde{g}^4 \sim \eta^2$ will be of order $\sim \eta$ in the prefactor as well. Consequently, if we would like to clarify if the quasi-particle peak persists, we would at least have to retain all contributions to $\dot{\Gamma}_{\infty}^{(2,sub)}$ up to order $\sim \tilde{g}^4$, implying the inclusion of all four-loop Feynman diagrams. This of course seems to be a rather formidable task.
In summary, it remains an open question if the quasi-particle peak in the spectral function for $p \neq 0$ is an artifact of perturbation theory and if it is removed in the exact solution. If we follow the general belief that it *is* removed we still have to explain the discrepancy in the nature of the algebraic singularities at $\omega = \pm v_c p$ following from the RG and the bosonization result. Here, we have to be modest as well, although we have doubted the correctness of the bosonization result in Sec. 7.3. On the other hand, it is also clear that our RG result only resums a subclass of Feynman diagrams, and the missing factor one half in the algebraic exponents might well be related to this fact. However, at least for $p = 0$ both methods predict the same line-shape at weak-coupling, including the non-universal prefactor of the spectral function.

7.5 Flow of the Spectral Function at Fermi Momentum

In the previous section we have calculated a good approximation to the spectral function of the g_2-TLM making explicit use of the scaling hypothesis. In Sec. 5.1 we claimed that results obtained in this way represent a generic low-energy form, valid only in the the asymptotic regime $p, \omega \to 0$ and representative of a larger class of Hamiltonians (universality). In Sec. 6.5 we gave a first and simple example for these assertions by considering the susceptibility $\tilde{\Pi}_l(q, i\epsilon)$, which turned out to be a homogeneous function at the fixed point. We will now give a second and more important example considering the non-perturbative spectral function at Fermi momentum, the complete flow of which we shall calculate in this section. The procedure is very much the same as the one that led us to the flow of the perturbative spectral function for $p = 0$, only that now we keep the anomalous dimension in the exponential of Eq. (5.13) finite. In analogy with Eq. (7.18) we start with

$$\Sigma_\Lambda(\pm k_F, i\omega) = -\,\Lambda_0 \int_0^l dt\, e^{(\bar{\eta}_t - 1)t}\, \dot{\Gamma}_t^{(2)}\big(0, e^t \tfrac{i\omega}{\Lambda_0}\big)\,, \tag{7.83}$$

where again we will neglect the momentum- and frequency-independent part of the self-energy, which gives rise to a small energy shift that vanishes in the limit $\Lambda \to 0$. Like before we neglect non-localities in the dependence of $\tilde{g}_t$ and $\tilde{v}_t$ on t and replace the couplings by their fixed-point values $\tilde{g}$ and $\tilde{v} = v_c/v_F$, respectively. In case of the scale-averaged anomalous dimension we have to be more careful, since here an explicit t-dependence is present, see Eq. (6.116). However, in favor of an analytical treatment we simply approximate

$$\bar{\eta}_l \approx \Theta(e^l - 2)\, \eta\, (1 - \ln 2/l)\,, \tag{7.84}$$

with $\eta = \bar{\eta}_\infty = \tilde{g}^2/8$. We have kept the term $\ln 2/l$ for $\bar{\eta}_l$ to be continuous at $l = \ln 2$. However, it turns out that this term just leads to an overall prefactor $2^{-\eta}$ of the self-energy, which we will subsequently set equal to one again, as generally we shall only keep the leading orders in η in the prefactors. We will discuss the consequences of the approximation (7.84) at the end of this section. In fact it turns out that even the Θ-function in Eq. (7.84) can be dropped, since the flow of $\dot{\Gamma}^{(2)}_l\big(0, e^l \frac{i\omega}{\Lambda_0}\big)$ only starts at $e^l = 2$ anyway. Changing the integration variable according to $\lambda = e^l$, Eq. (7.83) then turns into

$$\Sigma_\Lambda(k_F, i\omega) = -\,\Lambda_0 \int_1^{e^l} d\lambda\, \lambda^{\eta-2}\, \dot{\Gamma}^{(2)}_{\ln\lambda}\big(0, \lambda \tfrac{i\omega}{\Lambda_0}\big)\,, \tag{7.85}$$

where here and subsequently we only refer to the right Fermi point $+k_F$. From Eqs. (6.58) and (6.59) we obtain

$$\begin{aligned} \dot{\Gamma}^{(2)}_{\ln\lambda}\big(0, \lambda \tfrac{i\omega}{\Lambda_0}\big) &= \dot{\Gamma}^{(2,\mathrm{PB})}_{\ln\lambda}\big(0, \lambda \tfrac{i\omega}{\Lambda_0}\big) \\ &= 2\eta\, \Theta(\lambda - 2) \left[\ln\left(\frac{4\tilde{v}\Lambda_0 + \lambda i\omega}{4\tilde{v}\Lambda_0 - \lambda i\omega}\right) + \ln\left(\frac{2\tilde{v}\Lambda_0 - i\omega}{2\tilde{v}\Lambda_0 + i\omega}\right) \right]. \end{aligned} \tag{7.86}$$

Inserting this result in Eq. (7.85) the λ-integrations can be performed and we get to leading order in the prefactors

$$\begin{aligned} \Sigma_\Lambda(k_F, i\omega) &= -2\eta\, \Lambda_0\, \Theta(\Lambda_0 - 2\Lambda) \\ &\quad \times \Bigg\{ 2^{\eta-1} \left[F_{1-\eta}\Big(-\frac{2\tilde{v}\Lambda_0}{i\omega}\Big) - F_{1-\eta}\Big(\frac{2\tilde{v}\Lambda_0}{i\omega}\Big) \right] \\ &\quad - \Big(\frac{\Lambda}{\Lambda_0}\Big)^{1-\eta} \left[F_{1-\eta}\Big(-\frac{4\tilde{v}\Lambda}{i\omega}\Big) - F_{1-\eta}\Big(\frac{4\tilde{v}\Lambda}{i\omega}\Big) \right] \\ &\quad + \Big(\frac{\Lambda}{\Lambda_0}\Big)^{1-\eta} \ln\left(\frac{(2\tilde{v}\Lambda_0 + i\omega)(4\tilde{v}\Lambda - i\omega)}{(2\tilde{v}\Lambda_0 - i\omega)(4\tilde{v}\Lambda + i\omega)}\right) \Bigg\}, \end{aligned} \tag{7.87}$$

This expression displays a rather complex behavior and cannot easily be simplified if we are interested in the complete flow of the spectral function. Note however that Eq. (7.87) explicitly satisfies $\Sigma_\Lambda(k_F, -i\omega) = -\Sigma_\Lambda(k_F, i\omega)$ and thus conserves the particle-hole symmetry at all scales Λ. Like for our perturbative result determined by Eqs. (7.27) and (7.28) the flow only sets in at $\Lambda = \Lambda_0/2$ and is easily shown to be continuous at this scale, i.e.

$$\Sigma_{\Lambda_0/2-0^+}(k_F, i\omega) = 0\,. \tag{7.88}$$

Before we turn our attention to the change of Σ_Λ with the scale Λ, let us derive the fixed-point expression following from Eq. (7.87). Performing the limit $\Lambda \to 0$ and using the analogy of the transformation formula (7.59) for the hypergeometric function $F_{1-\eta}(z)$, we find

$$\boxed{\begin{aligned}\Sigma(k_F, i\omega) \;=\; \Lambda_0 \Big[\Big(-\frac{i\omega}{2\tilde{v}\Lambda_0}\Big)^{1-\eta} - \Big(\frac{i\omega}{2\tilde{v}\Lambda_0}\Big)^{1-\eta} \\ + \tilde{F}_\eta\Big(\frac{i\omega}{2\tilde{v}\Lambda_0}\Big) - \tilde{F}_\eta\Big(-\frac{i\omega}{2\tilde{v}\Lambda_0}\Big)\Big]\,.\end{aligned}} \tag{7.89}$$

Here we have defined $\tilde{F}_\eta(z) = z\, F_\eta(z)$. For $|z| \ll 1$ the hypergeometric functions can be expanded in a power series, which to leading order yields $\tilde{F}_\eta(z) - \tilde{F}_\eta(-z) = 2z + \mathcal{O}(z^2)$. The interacting Green function $G(k_F, i\omega) = [i\omega - \Sigma(k_F, i\omega)]^{-1}$ in imaginary frequency representation is then easily be obtained from Eq. (5.12),

$$\boxed{G(k_F, i\omega) \approx \Lambda_0^{-\eta}\Big[\Big(\frac{i\omega}{2}\Big)^{1-\eta} - \Big(-\frac{i\omega}{2}\Big)^{1-\eta}\Big]^{-1}\,.} \tag{7.90}$$

However, for the derivation of the spectral function let us rather start from Eq. (7.89), since we are also interested in non-universal features of the spectral function, in particular in the behavior for large ω. The analytic continuation of Eq. (7.89) can be obtained with the aid of Eq. (C.11) together with the observation that $(x \pm i0^+)^{1-\eta} = e^{(1-\eta)\ln(x\pm i0^+)} \approx |x|^{1-\eta}[\mathrm{sgn}(x) \pm \Theta(-x)\, i\eta\pi]$. It is then not difficult to see that

$$\mathrm{Im}\,\Sigma(k_F, \omega + i0^+) = -\,\pi\,\frac{\eta}{2}\,\Big|\frac{\omega}{\Lambda_0}\Big|^{1-\eta}\,\Theta(|\omega| < 2\Lambda_0)\,, \tag{7.91}$$

and

$$\mathrm{Re}\,\Sigma(k_F, \omega + i0^+) \;=\; \mathrm{sgn}(\omega)\,\Lambda_0\,\Theta(|\omega| < 2\Lambda_0)$$

$$\times \Big[\Big|\frac{\omega}{\Lambda_0}\Big|^{1-\eta} + \tilde{F}_\eta\Big(\Big|\frac{\omega}{2\Lambda_0}\Big|\Big) - \tilde{F}_\eta\Big(-\Big|\frac{\omega}{2\Lambda_0}\Big|\Big)\Big]\,, \tag{7.92}$$

where for the real part we have only retained the contributions within the interval $-2\Lambda_0 < \omega < 2\Lambda_0$, which equals to the support of the spectral function. In addition we have set $\tilde{v} = 1$ as keeping $\tilde{v}$ gives rise to higher η-orders in the prefactors. It would now be desirable to simplify the contribution of the hypergeometric functions $\tilde{F}_\eta$ in the expression for the real part. Below Eq. (7.89) we have already seen that for small values of the argument the leading contribution is linear. However, at $\omega = \pm 2\Lambda_0$ the first hypergeometric function on the r.h.s. of Eq. (7.92) diverges logarithmically, such that a linear approximation fails at first sight. On the other hand, *for the spectral function* this divergence simply leads to a steep and continuous decrease to zero at these points, which represent the high-energy ends of its support. Comparing the graphs for the spectral functions obtained from the linear approximation of the hypergeometric contributions with the one given by the full expression, one indeed finds that up to a high degree on accuracy the linear approximation simulates the correct behavior even for values of ω close to the edges of the support. The approximation

$$\tilde{F}_\eta\Big(\Big|\frac{\omega}{2\Lambda_0}\Big|\Big) - \tilde{F}_\eta\Big(-\Big|\frac{\omega}{2\Lambda_0}\Big|\Big) \approx \Big|\frac{\omega}{\Lambda_0}\Big|\,, \tag{7.93}$$

may hence safely be extended to the whole support of the spectral function. In this approximation we finally obtain

$$\boxed{A(k_F,\omega) = \Lambda_0^{-\eta}\,\frac{\eta}{2}\,|\omega|^{\eta-1}\,\Theta(|\omega| < 2\Lambda_0)\,.} \tag{7.94}$$

Obviously, for $|\omega| < 2\Lambda_0$ this result just equals to the expression obtained by means of the scaling hypothesis in Eq. (7.67). At larger frequencies the step function has however an important effect: it leads to a finite result for the sum rule (7.15), while the expression given by Eq. (7.67) falls off like $\sim |\omega|^{\eta-1}$ for large frequencies and is hence not integrable over the whole frequency axis. From Eq. (7.94) we get

$$\int_{-\infty}^{\infty} d\omega\, A(k_F,\omega) = 2^\eta = 1 + \eta \ln 2 + \mathcal{O}(\eta^2) \approx 1\,. \tag{7.95}$$

Keeping in mind that we have consistently neglected subleading orders in η in the prefactors, it is even justified to say that within our approximation scheme the sum rule is satisfied exactly.

We hence have found again that vertices calculated by the methods presented in this section contain more information than those obtained by means of the scaling hypothesis, which can be viewed as a low-energy version of Eq. (7.94).

Let us now turn our attention to the flow of the spectral function. For this purpose we need to analytically continue Eq. (7.87) , which is possible using the same methods as presented in appendix C. Again we keep only the leading orders in the prefactors and obtain for the imaginary part of the self-energy,

$$\begin{aligned}\operatorname{Im}\Sigma_\Lambda(k_F,\omega+i0^+) &= -\pi\,\frac{\eta}{2}\,\Lambda_0\,\Theta(\Lambda_0-2\Lambda)\\ &\quad\times\Theta(4\Lambda<|\omega|<2\Lambda_0)\,\Big[\,\Big|\frac{\omega}{\Lambda_0}\Big|^{1-\eta}-\Big|\frac{4\Lambda}{\Lambda_0}\Big|^{1-\eta}\Big]\,. \end{aligned}\tag{7.96}$$

The second Θ-function is related to the branch cuts of the hypergeometric functions and the logarithm in Eq. (7.87). In the interval $|\omega|<4\Lambda$ where the imaginary part vanishes, we will find a zero of the real part at $\omega=0$, leading to a δ-like contribution to the spectral function. This is very similar to the calculations in the context of our perturbative result in Sec. 7.2 , and we will be rather brief here. For the real part we get

$$\begin{aligned}\operatorname{Re}\Sigma_\Lambda(k_F,\omega+i0^+) &= -2\operatorname{sgn}(\omega)\,\Lambda_0\,\Theta(\Lambda_0-2\Lambda)\\ &\times\Big\{\,\eta\,\big(\tfrac{\Lambda}{\Lambda_0}\big)^{1-\eta}\ln\Big|\frac{(|\omega|+2\Lambda_0)(|\omega|-4\Lambda)}{(|\omega|-2\Lambda_0)(|\omega|+4\Lambda)}\Big|\\ &\quad+\Theta(|\omega|<4\Lambda)\Big\{\,\big(\tfrac{\Lambda}{\Lambda_0}\big)^{1-\eta}\Big[\tilde F_\eta\Big(\Big|\frac{\omega}{4\Lambda}\Big|\Big)-\tilde F_\eta\Big(-\Big|\frac{\omega}{4\Lambda}\Big|\Big)\Big]\\ &\qquad\qquad-2^{\eta-1}\Big[\tilde F_\eta\Big(\Big|\frac{\omega}{2\Lambda_0}\Big|\Big)-\tilde F_\eta\Big(-\Big|\frac{\omega}{2\Lambda_0}\Big|\Big)\Big]\Big\}\\ &\quad+\Theta(4\Lambda<|\omega|<2\Lambda_0)\Big\{\,2\,\Big|\frac{\omega}{4\Lambda_0}\Big|^{1-\eta}\\ &\qquad\qquad+\eta\,\big(\tfrac{\Lambda}{\Lambda_0}\big)^{1-\eta}\Big[\,F_{1-\eta}\Big(\Big|\frac{4\Lambda}{\omega}\Big|\Big)-F_{1-\eta}\Big(-\Big|\frac{4\Lambda}{\omega}\Big|\Big)\Big]\\ &\qquad\qquad-2^{\eta-1}\Big[\tilde F_\eta\Big(\Big|\frac{\omega}{2\Lambda_0}\Big|\Big)-\tilde F_\eta\Big(-\Big|\frac{\omega}{2\Lambda_0}\Big|\Big)\Big]\Big\}\\ &\quad+\Theta(2\Lambda_0<|\omega|)\Big\{\,\eta\,\Big[\,\big(\tfrac{\Lambda}{\Lambda_0}\big)^{1-\eta}F_{1-\eta}\Big(\Big|\frac{4\Lambda}{\omega}\Big|\Big)-2^{\eta-1}F_{1-\eta}\Big(\Big|\frac{2\Lambda_0}{\omega}\Big|\Big)\Big]\\ &\qquad\qquad+2^{\eta-1}\Big[\tilde F_\eta\Big(-\Big|\frac{\omega}{2\Lambda_0}\Big|\Big)-\tilde F_\eta\Big(-\Big|\frac{\omega}{4\Lambda}\Big|\Big)\Big]\Big\}\Big\}\,. \end{aligned}\tag{7.97}$$

The analytic structure of this equation is rather rich and shown in Fig. 7.15 for $\Lambda=\Lambda_0/8$ and in Fig. 7.16 for $\Lambda=\Lambda_0/16$ together with the imaginary part. It is important to recognize that for the properties of the spectral function it is important to search for zeros of $\operatorname{Re}\Sigma_\Lambda(k_F,\omega+i0^+)$ in the intervals where the imaginary part vanishes. This is the case in the regions $|\omega|<4\Lambda$ and $2\Lambda_0<|\omega|$, and it can be shown from Eq. (7.97) that the only zero in these intervals is located

at $\omega = 0$. Like for the fixed-point result for the real part of Σ_Λ in Eq. (7.92) we would like to simplify Eq. (7.97), here in the interval $4\Lambda < |\omega| < 2$ where the continuous part of the spectral function is non-zero, and we meet again the same problems. Note that the subleading terms proportional to η and the other hypergeometric functions lead to logarithmic divergencies at the borders of the support. A neglect or an expansion in powers of $|\omega/2\Lambda_0|$ is hence not justified within the whole interval. Nonetheless, the main effect of these divergences is the vanishing spectral function at these points, and here this may safely be neglected (just like is was the case for the fixed-point expression). Hence in the interval $4\Lambda < |\omega| < 2$ Eq. (7.97) can be approximated by

$$\mathrm{Re}\,\Sigma_\Lambda(k_F, \omega + i0^+) \approx \mathrm{sgn}(\omega)\,\Lambda_0\,\Theta(\Lambda_0 - 2\Lambda)\Big[\,\Big|\frac{\omega}{\Lambda_0}\Big| - \Big|\frac{\omega}{\Lambda_0}\Big|^{1-\eta}\,\Big]\,. \tag{7.98}$$

For the spectral function we finally obtain

$$A_\Lambda(k_F, \omega) = A_{\Lambda,\delta}(k_F, \omega) + A_{\Lambda,cont}(k_F, \omega)\,, \tag{7.99}$$

with

$$\boxed{A_{\Lambda,\delta}(k_F, \omega) \approx \Big[\,\Theta(2\Lambda - \Lambda_0) + \Theta(\Lambda_0 - 2\Lambda)\,\Big(\frac{2\Lambda}{\Lambda_0}\Big)^\eta\,\Big]\,\delta(\omega)\,,} \tag{7.100}$$

where we have inserted the explicit expression for the quasi-particle residue which can be obtained from Eq. (7.97) using the fact that $\frac{d}{dz}F_\eta(z) = \frac{\eta}{1+\eta}\,{}_2F_1(2, 1+\eta; 2+\eta; z)$ [91],

$$\begin{aligned} Z_l &= \frac{1}{1 + \partial_\omega \mathrm{Re}\,\Sigma_\Lambda(k_F, \omega + i0^+)|_{\omega=0}} \\ &= \Theta(2\Lambda - \Lambda_0) + \Theta(\Lambda_0 - 2\Lambda)\,\Big[\Big(\frac{2\Lambda}{\Lambda_0}\Big)^\eta + \mathcal{O}\Big(\eta\Big(\frac{\Lambda}{\Lambda_0}\Big)^\eta\Big)\,\Big]\,. \end{aligned} \tag{7.101}$$

For the continuous part we get from Eqs. (7.96) and (7.98)

$$\boxed{\begin{aligned} A_{\Lambda,cont}(k_F, \omega) &= \Lambda_0^{-\eta}\,\frac{\eta}{2}\,\Theta(\Lambda_0 - 2\Lambda) \\ &\quad \times \Theta(4\Lambda < |\omega| < 2\Lambda_0)\,\Big[\,|\omega|^{\eta-1} - (4\Lambda)^{\eta-1}\Big|\frac{\omega}{4\Lambda}\Big|^{2(\eta-1)}\,\Big]\,. \end{aligned}} \tag{7.102}$$

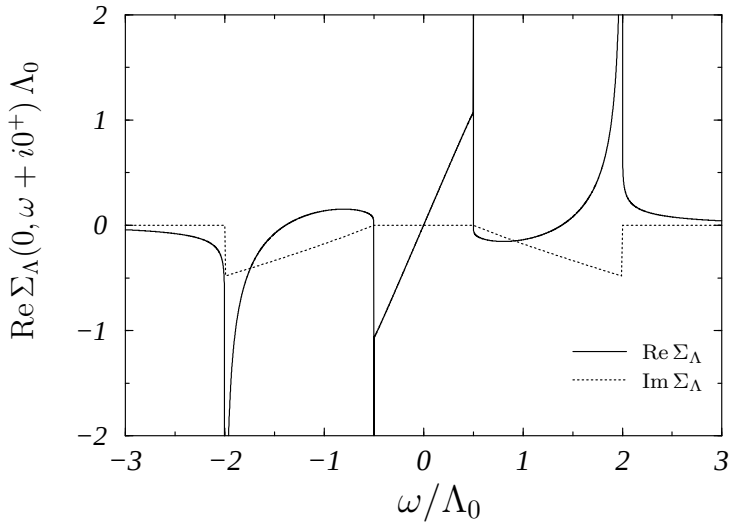

Figure 7.15: Real and imaginary part of the retarded self-energy at scale $\Lambda/\Lambda_0 = 1/8$ as determined by Eqs. (7.96) and (7.97). We have chosen $\eta = 0.2$. The support of both functions is split into the three regions $|\omega/\Lambda_0| < 0.5$, $0.5 < |\omega/\Lambda_0| < 2$ and $2 < |\omega/\Lambda_0|$. In the first interval the real part is approximately linear in ω and approaches a finite limit when $|\omega/\Lambda_0| \to 0.5 - 0^+$. On the other hand, for $|\omega/\Lambda_0| \to 0.5 + 0^+$ we get a logarithmic divergence. The real part exhibits five zeros, but only the zero at $\omega = 0$ is located in a region where the imaginary part vanishes.

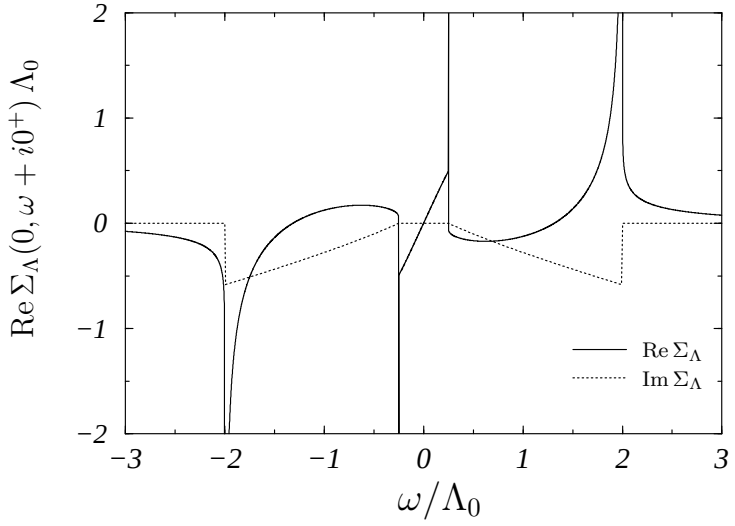

Figure 7.16: The same as in Fig. 7.15 but with $\Lambda/\Lambda_0 = 1/16$. The three disjoint intervals are now given by $|\omega/\Lambda_0| < 0.25$, $0.25 < |\omega/\Lambda_0| < 2$ and $2 < |\omega/\Lambda_0|$.

First of all it is easy to check that in the limit $\Lambda \to 0$ the fixed-point result given by Eq. (7.99) is recovered. Analogous to the picture we got for the perturbative spectral function this is due to the fact that the quasi-particle residue (7.101) vanishes in this limit, and the continuous part (7.102) approaches the fixed-point expression. In Fig. 7.17 we compare $A_\Lambda(k_F, \omega)$ for $\tilde{g}_0 = 0.5$, which corresponds to $\eta \approx 0.03$, with the perturbative spectral function (7.29). We have chosen $\Lambda/\Lambda_0 = 2^{-n}$ for the three values $n = 3, 4, 5$. The qualitative picture is very similar to the one predicted by perturbation theory: With decreasing ratio Λ/Λ_0 the continuous part of the spectral function increases until it approaches the fixed-point result, which now displays the well-known algebraic singularity of the TLM instead of a logarithmic singularity at $\omega = 0$. The most important difference is contained in the sum rule for the spectral weight, given by Eq. (7.32). Of course we cannot expect it to be satisfied exactly anymore. But at least to leading order in η it should hold independently of the scale. This can be checked analytically from Eq. (7.99) with the explicit expressions for $A_{\Lambda,\delta}(k_F, \omega)$ and $A_{\Lambda,cont}(k_F, \omega)$. Performing the integration in Eq. (7.32) yields

$$\mathcal{S}_{\Lambda,\delta}(k_F) = \Theta(2\Lambda - \Lambda_0) + \Theta(\Lambda_0 - 2\Lambda) \left(\frac{2\Lambda}{\Lambda_0}\right)^\eta + \mathcal{O}\Big(\eta\Big(\frac{\Lambda}{\Lambda_0}\Big)^\eta\Big)\,, \tag{7.103}$$

and

$$\mathcal{S}_{\Lambda,cont}(k_F) = \Theta(\Lambda_0 - 2\Lambda) \left[1 - \left(\frac{2\Lambda}{\Lambda_0}\right)^\eta\right] + \mathcal{O}\Big(\eta, \eta\Big(\frac{\Lambda}{\Lambda_0}\Big)^\eta\Big)\,, \tag{7.104}$$

thus

$$\boxed{\mathcal{S}_\Lambda(k_F) = 1 + \mathcal{O}\big(\eta, \eta\big(\tfrac{\Lambda}{\Lambda_0}\big)^\eta\big)\,.} \tag{7.105}$$

Hence we recover the picture already found at perturbative level: With decreasing scale the spectral weight is transfered from the quasi-particle peak at $\omega = 0$ to the continuous background that becomes more and more coherent, in a way that the sum of both contributions adds up to one. At the fixed point the complete weight is carried by the continuous part and the δ-like contribution vanishes.
It is important to recognize that this result is not only of academic interest. We have already argued in the context of our perturbative result in Sec. 7.2 that the presence or absence of a finite low-energy cutoff $\Lambda_\star$ will finally decide if the physical system behaves like a Fermi or a non-Fermi liquid. Let us make this point completely clear. Note that Luttinger's definition of the Landau Fermi liquid [75] relies crucially on the analytic properties of the self-energy. As we have

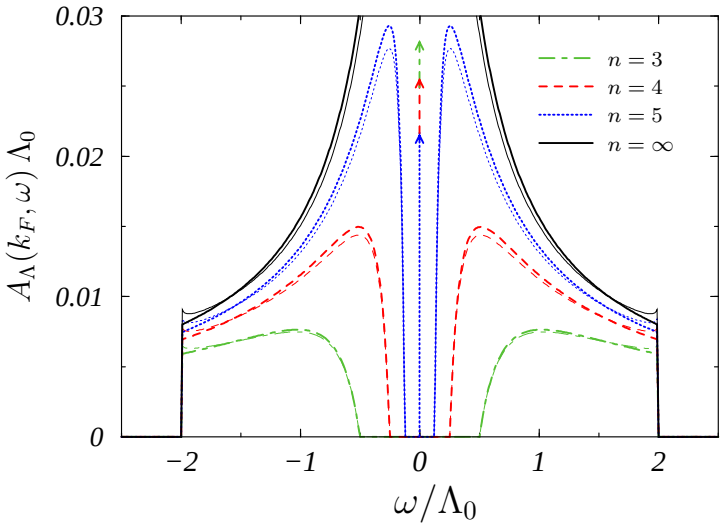

Figure 7.17: Comparison of $A_\Lambda(k_F,\omega)$ (bold lines) with the perturbative spectral function $A_\Lambda^{(\mathrm{PT})}(k_F,\omega)$ (thin lines) as predicted by Eqs. (7.29) and (7.99), respectively. We have plotted graphs for scale ratios $\Lambda/\Lambda_0 = 2^{-n}$, with the values for n depicted in the legend. For all graphs $\eta = 0.03125$, which corresponds to $\tilde{g}_0 = 0.5$.

emphasized in Sec. 5.2, the self-energy of a Fermi liquid is assumed to be an analytic function in both the momentum and the frequency variables p and ω at $\omega = p = 0$, with a finite radius of convergence. At *high* energies non-analyticities related to branch cuts of the retarded self-energy may appear as well, which physically are due to dissipation in the system. The radius of convergence (ROC) of a Taylor expansion in powers of p and ω is then determined by the branch point closest to the origin. Note, however, that this description treats ω and p on an equal footing, as we simultaneously expand in both variables. If on the other hand we proceed slightly differently, it is possible to understand Fermi- and non-Fermi liquid behavior on a more common ground.

Let us consider the analytic continuation of the self-energy to the complex-frequency plane, i.e. $\Sigma(k_F+p,z)$, where z denotes an arbitrary complex number.[12] In Fig. 7.18 we have sketched a situation where two branch cuts are located on the real-frequency axis, where the retarded self-energy is defined. We have seen in the previous sections that the spectral function is determined by the analytic continuation of $\Sigma(k_F+p,z)$ from the imaginary z-axis to the real z-axis, formally obtained by $z \to \omega + i0^+$. In the regions of the branch cut the retarded self-energy

[12] In dimensions $D > 1$ $\Sigma(k_F+p,z)$ has to be replaced by $\Sigma(\mathbf{n}(k_F+p),z)$, using the decomposition of $\mathbf{k}$ given in Eq. (4.5).

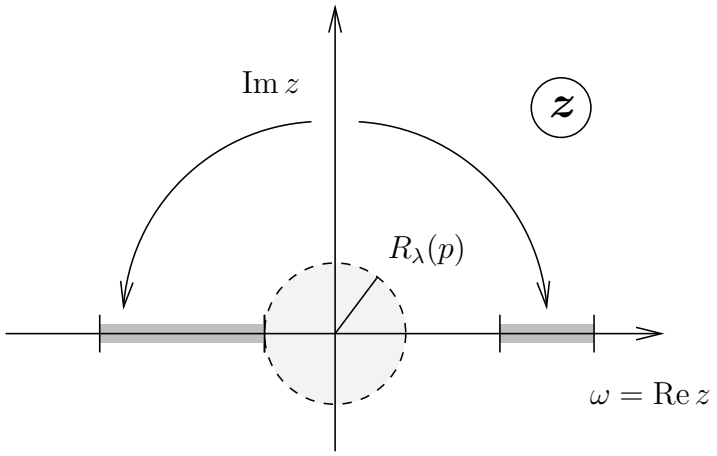

Figure 7.18: Schematical representation of the complex z-plane, where the analytically continued self-energy $\Sigma(k_F + p, z)$ is defined. The gray-shaded regions on the real z-axis represent branch cuts due to non-analytic parts of $\Sigma(k_F + p, z)$. The gray-shaded circle symbolizes the circle of convergence for an expansion of $\Sigma(k_F + p, z)$ in powers of z, with the ROC given by $R_\lambda(p)$. Finally the arrows are symbolic for the process of analytic continuation from the imaginary z-axis to the real z-axis according to $z \to \omega + i0^+$.

assumes a finite imaginary part, leading to the continuous excitation spectrum of the spectral function. On the other hand the branch cut closest to the origin at $z = 0$ determines the ROC of an expansion of $\Sigma(k_F + p, z)$ in powers of z, which in Fig. 7.18 we have denoted by $R_\lambda(p)$. The crucial point is that the ROC will in general depend on the momentum p as well as on other physical parameters, which we express by a so far unspecified λ-dependence. It is important to emphasize that we do not claim that the imaginary part of the retarded self-energy vanishes within the circle of convergence, only it is not related to a branch cut in this region. We get back to Luttinger's definition of a Fermi liquid if $R_\lambda(p)$ itself is an analytic function of p at $p = 0$ *and* provided that $R_\lambda(0) > 0$. The ROC of an expansion in *both* variables will then essentially be determined by the magnitude of $R_\lambda(0)$. Now, the paradigm of a non-Fermi liquid is the one-dimensional electron gas. Within the TLM description in the spinless case the spectral function has the line-shape shown in Fig. 7.13. Keeping in mind that here the spectral function is only non-zero in the branch-cut region of the self-energy, it is easy to see that in this case $R_\lambda(p) = |v_c p|$. Note that this can also be seen from our RG result for the imaginary part of the retarded self-energy, Eq. (7.62). Hence we have $R_\lambda(0) = 0$, extending the branch cut down to zero frequency. According to this a physical system will behave like a Fermi liquid, provided the self-energy $\Sigma(\mathbf{n}(k_F + p), z)$ satisfies the following three conditions

$$\textbf{\textit{i)}} \qquad R_\lambda(p) \quad \text{is analytic at } p = 0\,, \tag{7.106}$$

$$\textbf{\textit{ii)}} \qquad R_\lambda(0) > 0\,, \tag{7.107}$$

$$\textbf{\textit{iii)}} \qquad \mathrm{Im}\,\Sigma(k_F + p, \omega + i0^+) \sim \omega^2\,, \quad \text{for} \quad |\omega| < R_\lambda(0)\,. \tag{7.108}$$

The last condition refers to the decay rate of the quasi-particle, which due to this condition will be asymptotically free in the limit $\omega \to 0$. The advantage of this rather formal definition of a Fermi liquid is that it allows for a qualitative understanding of the crossover from Fermi-liquid to non-Fermi-liquid behavior. Note that for $p \neq 0$ nothing a priori forbids the real part of the self-energy to vanish in the region $|\omega| < R_\lambda(p)$. If a zero is found, the spectral function will indeed exhibit a δ-like contribution, just like it was the case within our toy model in Sec. 7.1.

So far we did not speak about the λ-dependence of $R_\lambda(p)$. For definiteness let us consider a quasi-one-dimensional system, with a transverse-hopping amplitude $\tau_\perp$ to neighboring chains and first identify $\lambda = \tau_\perp$. In RG language $\tau_\perp$ is a relevant parameter, since an arbitrarily small $\tau_\perp$ destroys the Luttinger liquid state, see e.g. Ref. [16]. Consequently and according to the above definition, we would express this fact by $R_{\tau_\perp}(0) > 0$ for $\tau_\perp > 0$ together with $R_{\tau_\perp=0}(0) = 0$, since for $\tau_\perp = 0$ we simply get back to the Luttinger-liquid behavior of a single chain. The limit $\tau_\perp \to 0$ can now qualitatively be understood by the RG flow of the $p = 0$ spectral function given in Fig. 7.17. Let us first consider the RG flow of the single chain with $\tau_\perp = 0$. In this case we may identify λ with the infrared cutoff Λ, and from Eq. (7.102) it is easy to see that $R_\Lambda(0) = 4\Lambda$. Of course, for finite Λ this is different from zero, but the physical system is only described by the limit $\Lambda \to 0$, when all degrees of freedom are integrated out. Consequently, in the physically relevant limit $R_{\Lambda=0}(0) = 0$ and the system is correctly found to be a non-Fermi liquid. Now imagine we were able to calculate to flow of the $p = 0$ spectral function with a finite and small $\tau_\perp$. What kind of scenario would we expect? In this case we should interpret λ as a composite label, i.e. $\lambda = (\Lambda, \tau_\perp)$, with $\tau_\perp = \tau_\perp(\Lambda)$ depending itself on the flow parameter. At finite Λ we expect again $R_{(\Lambda,\tau_\perp)}(0) > 0$, but this condition should now even be satisfied in the limit $\Lambda \to 0$, i.e.

$$\lim_{\Lambda\to 0} R_{(\Lambda,\tau_\perp)}(0) = R_{(0,\tau_\perp^\star)}(0) > 0\,, \tag{7.109}$$

provided that $\lim_{\Lambda\to 0} \tau_\perp(\Lambda) \equiv \tau_\perp^\star > 0$. The system hence remains Fermi-liquid like. A qualitatively correct picture of the RG flow of the spectral function should then be given by Fig. 7.17 if we stop the flow at the low-energy scale $\Lambda_\star = \tau_\perp^\star$. If we naively use our result (7.99) the fixed-point spectral function for quasi-one-dimensional systems in the vicinity of $\omega = 0$ will be of the form

$$\boxed{A_{\tau_\perp^\star}(k_F,\omega) \sim (\tau_\perp^\star)^\eta\, \delta(\omega)\,,} \tag{7.110}$$

hence

$$Z_{l_\star} \sim (\tau_\perp^\star)^\eta\,. \tag{7.111}$$

Note that this is precisely the result predicted for coupled chains in Ref. [16] and the references therein. Here we have even more information, since we also know a qualitative picture of the continuous part and the smooth crossover when the limit $\tau_\perp^\star \to 0$ is taken. Depending on the actual value of $\tau_\perp^\star$ there will be more or less important remainders of Luttinger-liquid behavior. In particular we have $R_{(0,\tau_\perp^\star)}(0) = 4\tau_\perp^\star$, such that for small $\tau_\perp^\star$ the support of the plasmon part can be very close to zero frequencies. The spectral weight of the plasmon background is then simply given by $1 - Z_{l_\star}$.

Keeping this and the fact in mind that real physical systems are always quasi-one-dimensional, it is questionable if the generic Luttinger-liquid scaling behavior is indeed measurable provided the above result is qualitatively correct. In Fig. 7.19 we compare the decay of the quasi-particle residue as a function of the ratio $\tau_\perp^\star/v_F p_c$ obtained from perturbation theory in Eq. (7.21) and the non-perturbative RG results (6.115) and (7.84). We show the decay for the two values $\eta = 0.03125$ which corresponds to $\tilde{g}_0 = 0.5$ and for $\eta = 0.2$. At weak coupling the three curves remain close together and predict a quasi-particle residue of the order of one down to very small scales. At strong coupling ($\eta = 0.2$) the results obtained by perturbation theory and the RG significantly differ for $\tau_\perp^\star/v_F p_c < 10^{-2}$, and the latter predicts a faster decay. However, in both cases $\tau_\perp^\star/v_F p_c$ has to be very small for the spectral weight of the δ-function to be negligible, which is due to the power-law behavior in Eq. (7.111), see also Fig. 6.10. If the above picture for the spectral function of a quasi-one-dimensional system is qualitatively correct, we cannot expect the spectral function to assume the scaling form given in Eq. (7.67) unless $\tau_\perp^\star$ is extremely small.

Note, however, that only recently D. Orgad et al. [17] made the attempt to calculate the spectral function of the TLM at finite temperatures in favor of a better comparison with experiments. In deriving their results the authors used a scaling form for the spectral function of the model including the spin degree of freedom, and at least for the most important features they found qualitative agreement with experiments. On the other hand, following a suggestion of D. Zanchi [58], who identifies the scale Λ with an effective temperature T_{eff}, we would obtain a crossover scenario for the $k = k_F$ spectral function as a function of T_{eff} which is qualitatively similar to that for a non-zero $\tau_\perp$. Here we would obtain a quasi-particle residue $Z_{l_\star} \sim (T_{\text{eff}})^\eta$, such that the generic scaling behavior

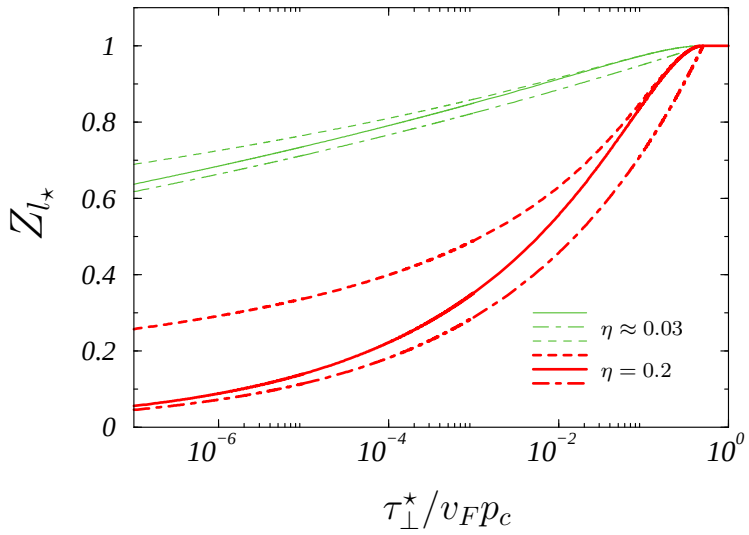

Figure 7.19: The quasi-particle residue as a function of the hopping parameter $\tau_\perp^\star$. We compare the results obtained by perturbation theory in Eq. (7.21) (dashed lines) with those following from our non-perturbative RG approaches where $Z_{l_\star} = e^{-\bar{\eta}_{l_\star} l_\star}$. We have set $l_\star = -\ln(\tau_\perp^\star / v_F p_c)$. For the non-perturbative expressions we distinguish the two cases with the scale-averaged anomalous dimension $\bar{\eta}_{l_\star}$ given by Eq. (6.116) (solid lines) and by the approximate expression (7.84) (dot-dashed lines).

of the TLM could only be expected very close to the quantum critical point at $T_{\text{eff}} = 0$. Although this interpretation of Λ has qualitatively been confirmed in the context of the two-dimensional Hubbard model by Honerkamp and Salmhofer [73,74], who introduced a new RG formalism that explicitly uses the temperature itself as the flow parameter of the RG, it is to our opinion questionable if such an interpretation is generally correct. At least applied to the one-dimensional electron gas the above crossover scenario as a function of T_{eff} would contradict the assumptions in Ref. [17]. Since the results of this paper have repeatedly been compared to experiments [24, 30] with a rather promising agreement, we believe that this statement reaches too far and cannot replace a true finite-temperature calculation.

Chapter 8

Effects of Non-Linear Energy Dispersion

In this chapter we are going to study the effects of the quadratic term of the expansion of the energy dispersion (4.7) within the spinless g_2-model. As we have emphasized in the introduction our RG approach principally opens up the possibility to take the flow of irrelevant couplings systematically into account. We will show that the fixed-point values of the couplings $\tilde{v}_l$ and $\tilde{g}_l$ depend on the initial curvature of the energy dispersion, which is represented by an irrelevant coupling. In case of $\tilde{g}_l$ this is already evident at one-loop level, leading in turn to a renormalization of the anomalous dimension beyond the leading order. The corrections compared to our former results obtained for a strictly linear dispersion are small, but they further reduce the universality of the Luttinger-liquid fixed-point manifold.

8.1 The Spectral Function at Perturbative Level

In this section we will derive some results within second-order perturbation theory as a guide line for the subsequent non-perturbative approach. We have seen in Sec. 7.1 that the perturbative spectral function for a strictly linear energy dispersion exhibits the most important features of the exact result, at least at the Fermi momentum k_F. The breakdown of Fermi-liquid theory manifests itself already at this level in a logarithmic singularity instead of a δ-like excitation at $\omega = 0$. The main effect of the non-perturbative approach was to turn this logarithmic singularity into an algebraic one. Furthermore we have shown in Sec. 7.2 that the RG flow of the couplings related to the two-point vertex exclusively describe its properties at $k = k_F$. This is why we restrict ourselves to this special

momentum value in the present section.
Already in Haldanes seminal work [10] the influence of the non-linear term in the expansion of the energy dispersion (4.7) around $k = k_F$ has been discussed in the framework of the bosonization technique. His treatment relied on an expansion of the bare propagators in powers of the inverse electron mass, such that the leading order was given by the model with a strictly linear dispersion. Haldane showed the mass corrections to be responsible of turning a system of free bosons of the linear theory into a system of weakly interacting bosons, thus constituting the concept of a Luttinger *liquid*. The low-energy physics was shown to be correctly described by the TLM, at least as long as the mass term is not too large. Furthermore Haldane speculated that the value of the renormalized interaction coupling will be affected by curvature, but he did not show explicit results. The interest in studying this field in one-dimensional systems has subsequently decreased, most likely due to the fact that results are rather hard to obtain. In Refs. [97] and [98] we already made the attempt to calculate the single particle Green function of the TLM for a non-linear energy dispersion within the bosonization approach. Most reliably we found a finite renormalization of the anomalous dimension in subleading orders of a weak coupling expansion. The detailed structure of the spectral function has also been calculated and was found to exhibit a second algebraic singularity besides the one known from the linear theory. However, we were not able to exclude that this feature will be suppressed by higher-order contributions of our approximation scheme.

Let us now turn our attention to second-order perturbation theory. What can we expect from a calculation using $\xi(p) = v_F p + p^2/2m$ as the bare excitation energy, compared to our former result obtained by using $\xi(p) = v_F p$? Intuitively it seems clear that the low-energy properties of the spectral function should be the same as before when $p \to 0$. Nonetheless it is obvious as well that the momentum integrations within the analytical expression corresponding to the Feynman diagram shown in Fig. 7.1 will range over a finite interval. If for simplicity we use again the interaction cutoff p_c of a box potential, this range will be given by $2p_c$. Compared to the linear model the momentum integrations will then differ by a contribution which is proportional to the area of the dark-gray shaded region in Fig. 1.1, such that even at $k = k_F$, i.e. at $p = 0$, the non-linear term $p^2/2m$ will affect the line-shape of the spectral function. The most evident difference is the absence of the perfect particle-hole symmetry present in the linear model. In terms of the fermionic excitation energy $\xi(p)$ this symmetry is reflected by the property $|\xi(-p)| = |\xi(p)|$ at non-interacting level. While for $\xi(p) = v_F p$ this condition is satisfied, for $\xi(p) = v_F p + p^2/2m$ we rather have $|\xi(-p)| \leq |\xi(p)|$ for small p. Hence a particle with momentum $k = k_F + |p|$ carries more kinetic energy than the corresponding hole with $k = k_F - |p|$, the difference being equal

to p^2/m. In the spectral function the particle-hole symmetry is reflected by the property $A(k_F + p, \omega) = A(k_F - p, -\omega)$. For the special case $p = 0$ this implies that $A(k_F, \omega)$ is mirror symmetric with respect to the ordinate, see e.g. Fig. 7.2. We will see shortly that for non-linear dispersion this symmetry will only by given in the limit $\omega \to 0$.
Let us now evaluate the Feynman diagram of Fig. 7.1, this time using

$$G_0(k_F + p, i\omega) = \frac{1}{i\omega - v_F p - p^2/2m} \tag{8.1}$$

as bare propagator. For convenience we will still use the classification of the spinless Fermions in right- and left-movers, although this construction is not strictly necessary anymore, at least not for the one-dimensional electron gas. This is due to the fact that the two Fermi points where the excitation energy vanishes could as well be included in the formalism by allowing p to range over all momenta. The Fermi point $k = +k_F$ would then correspond to $p = 0$, while $k = -k_F$ would be given by $p = -2k_F$. However, for a better comparison with our former results obtained within the linear model we will keep the construction making use of two different types of fermions. Furthermore we will again work with a single g_2-coupling constant within the region of width $2\Lambda_0 \equiv 2v_F p_c$ around $k = \pm k_F$. To avoid double counting of momenta we have to make sure that p_c does not exceed the Fermi vector k_F. Introducing the dimensionless parameter

$$\lambda = \frac{p_c}{2k_F} \equiv \frac{\Lambda_0}{4E_F}\,, \tag{8.2}$$

this condition will be satisfied when

$$\lambda \leq \frac{1}{2}\,. \tag{8.3}$$

Note that the second equality in Eq. (8.2) only holds for the one-dimensional electron gas, where $k_F = mv_F$. It is important to notice that the condition (8.3) also implies that we cannot send Λ_0 to infinity anymore. This is best appreciated by considering Fig. 1.1: For $\lambda > 1/2$ the gray-shaded stripes overlap near $k = 0$ and the momenta in this region would be counted twice within k-integrations.
Note also that the limit of linear energy dispersion is formally obtained by sending $1/m \to 0$ while keeping the density, i.e. k_F, fixed. On the other hand, for the one-dimensional electron gas we have $k_F = mv_F$, which allows us to write

$$\xi(p) = v_F p\Big(1 + \lambda\,\frac{p}{p_c}\Big) \equiv v_F p\Big(1 + \lambda\,\frac{v_F p}{\Lambda_0}\Big)\,. \tag{8.4}$$

Formulated in this way we of course have to keep the fermion mass finite, as otherwise we would send k_F to infinity. The linear theory is then recovered by

the limit $\lambda \to 0$, expressing the fact that the quadratic term $p^2/2m$ becomes negligible when the ratio p_c/k_F tends to zero: The gray-shaded stripes in Fig. 1.1 become smaller and smaller, such that the linear approximation finally becomes exact. However, apart from these subtleties related to the limit of linear energy dispersion, sending $\lambda \to 0$ yields the same result as the limit $1/m \to 0$, since the Fermi vector k_F does not appear explicitly within the calculations.[1]
Similar to the linear case the only momentum- and frequency-dependent Feynman diagram that contributes in the spinless g_2-model at second order perturbation theory is the one shown in Fig. 7.1. However, the corresponding analytical expression cannot be stated in terms of elementary functions anymore. Using for simplicity the box potential $g_0(p) = g_0\,\Theta(p_c - |p|)$ we obtain for $k = k_F$

$$\begin{aligned}\bar{\Sigma}^{(ic)}_{\rm PT}(k_F, i\omega) &= \Sigma^{(ic)}_{\rm PT}(k_F, i\omega) - \Sigma^{(ic)}_{\rm PT}(k_F, i0) \\ &= -v_F p_c \frac{\tilde{g}_0^2}{8\lambda} \int_0^1 \frac{dx}{x} \left[\ln \left(\frac{x^2 - \left(\lambda x^2 - \frac{i\omega}{2v_F p_c}\right)^2}{x^2 - \left(\frac{i\omega}{2v_F p_c}\right)^2} \right) - \ln(1 - \lambda^2 x^2) \right], \quad (8.5)\end{aligned}$$

with $\tilde{g}_0 = g_0/\pi v_F$. The second logarithm on the r.h.s. is due to the counter term $\Sigma(k_F, i0)$ of the self-energy and insures that $\bar{\Sigma}^{(ic)}_{\rm PT}(k_F, i0) = 0$. The remaining integration cannot be performed exactly, but it is not difficult to see that in the limit $\lambda \to 0$ we precisely recover the linear result (7.1) for $p = 0$. To obtain the spectral function we again have to analytically continue Eq. (8.5) according to $i\omega \to \omega + i0^+$. The imaginary part of the retarded self-energy will then occur due to the branch cut of the first logarithm in Eq. (8.5), and in this case the integration can be performed after the analytic continuation. For the real part however we have to resort to numerics. Proceeding in this way yields

$$\begin{aligned}\mathrm{Im}\,\bar{\Sigma}^{(ic)}_{\rm PT}(k_F, \omega + i0^+) &= \pi\, v_F p_c \frac{\tilde{g}_0^2}{8\lambda} \\ &\times \Bigg\{ \left[\Theta(-2v_F p_c < \omega < 0)) - \Theta(0 < \omega < 2v_F p_c(1-\lambda)) \right] \\ &\qquad \times \ln \left| \frac{v_F p_c}{\lambda\,\omega} \left[1 - \sqrt{1 - 2\lambda \tfrac{\omega}{v_F p_c}} \right] \right| \\ &+ \Theta(-2v_F p_c(1+\lambda) < \omega < -2v_F p_c)\, \ln \left| \frac{1}{2\lambda} \left[1 + \sqrt{1 - 2\lambda \left| \tfrac{\omega}{v_F p_c} \right|} \right] \right| \\ &+ \Theta(2v_F p_c(1-\lambda) < \omega < 2v_F p_c)\, \ln \left| \frac{\omega}{2v_F p_c} \right| \Bigg\}, \quad (8.6)\end{aligned}$$

[1] Later on we shall use k_F as a shorthand notation for mv_F which is justified in case of the one-dimensional electron gas. When the limit $1/m \to 0$ is taken this implies $k_F \to \infty$ but has of course nothing to do with a diverging density.

and

$$\begin{aligned}\mathrm{Re}\,\Sigma^{(ic)}_{\mathrm{PT}}(k_F,i\omega) \;&=\\ &-v_F p_c\,\frac{\tilde{g}_0^2}{8\lambda}\int_0^1\frac{dx}{x}\left[\ln\left|\frac{x^2-\left(\lambda x^2-\frac{\omega}{2v_Fp_c}\right)^2}{\left[x^2-\left(\frac{\omega}{2v_Fp_c}\right)^2\right]\left[1-\lambda^2x^2\right]}\right|\right].\end{aligned}\tag{8.7}$$

Using the fact that

$$\begin{aligned}\ln\left|\frac{v_Fp_c}{\lambda\,\omega}\left[1-\sqrt{1-2\lambda\tfrac{\omega}{v_Fp_c}}\right]\right| \;&=\; \ln\left|\frac{v_Fp_c}{\lambda\,\omega}\left[\frac{\lambda\,\omega}{v_Fp_c}+\frac{\lambda^2}{2}\left(\frac{\omega}{v_Fp_c}\right)^2+\mathcal{O}(\lambda^3)\right]\right|\\ &=\; \frac{\lambda}{2}\,\frac{\omega}{v_Fp_c}+\mathcal{O}(\lambda^2)\,,\end{aligned}\tag{8.8}$$

it is easy to see that

$$\lim_{\lambda\to0}\mathrm{Im}\,\Sigma^{(ic)}_{\mathrm{PT}}(k_F,\omega+i0^+)=-\,\pi\,\frac{\tilde{g}_0^2}{16}\,|\omega|\,\Theta(|\omega|<2v_cp_c)\,.\tag{8.9}$$

Comparing with Eq. (7.6) for $p=0$ we see that the limit of linear energy dispersion is correctly recovered from Eq. (8.6). In the same way this can be shown for the real part. In Figs. 8.1 and 8.2 we show the graphs of the imaginary and the real part of $\Sigma^{(ic)}_{\mathrm{PT}}(k_F,\omega+i0^+)$ for several values of λ as predicted by Eqs. (8.6) and (8.7), and compare it with the linear results obtained from Eqs. (7.5) and (7.6). In all plots we have chosen $\tilde{g}_0^2/8=0.1$ which is in principle out of range of a perturbative expansion in $\tilde{g}_0$. Note however that this quantity only appears as an overall prefactor in the equations under consideration, such that results for smaller values are simply obtained by an appropriate scaling of the ordinate; the structure of the curves remains unchanged. The line-shapes for the real part have been obtained by means of numerical integration. For both functions it can be seen in the figures that the curves approach the one for linear dispersion when λ decreases. The particle-hole symmetry, which for the linear result is reflected by the properties $\mathrm{Im}\,\Sigma^{(ic)}_{\mathrm{PT}}(k_F,-\omega+i0^+)=\mathrm{Im}\,\Sigma^{(ic)}_{\mathrm{PT}}(k_F,\omega+i0^+)$ and $\mathrm{Re}\,\Sigma^{(ic)}_{\mathrm{PT}}(k_F,-\omega+i0^+)=-\mathrm{Re}\,\Sigma^{(ic)}_{\mathrm{PT}}(k_F,\omega+i0^+)$ is obviously broken for finite curvature. However, in the vicinity of $\omega=0$ the above symmetries are reestablished. Of course, the most interesting result is the spectral function itself, which can numerically be obtained form Eqs. (8.6), (8.7) and (7.13). The line-shape is shown in Fig. 8.3, again in comparison with the linear result. As one would expect the most important differences occur for $\lambda=0.5$, which represents the maximum value we are allowed to choose, see Eq. (8.3) and the discussion above. We have so far not been able to obtain a reliable result for the spectral weight

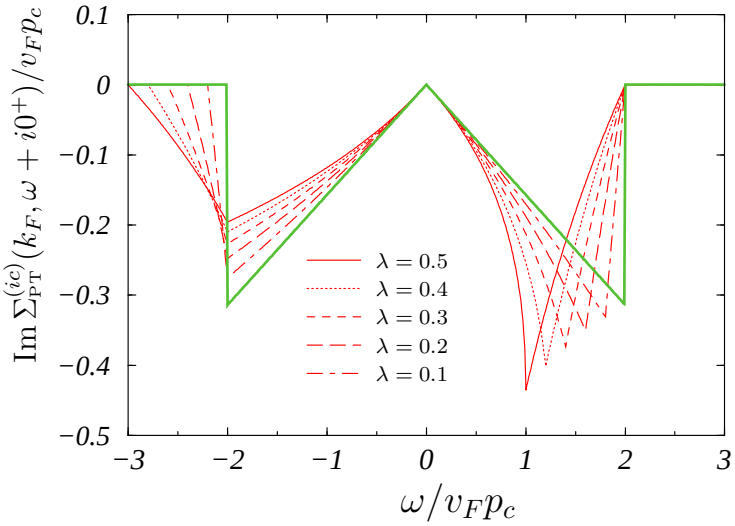

Figure 8.1: The imaginary part of the retarded self-energy at second-order perturbation theory as obtained from Eq. (8.6) for several values of $\lambda = p_c/2k_F$ (light curves). The thick solid line represents the corresponding result for linear energy dispersion. All curves are plotted for $\tilde{g}_0^2/8 = 0.1$.

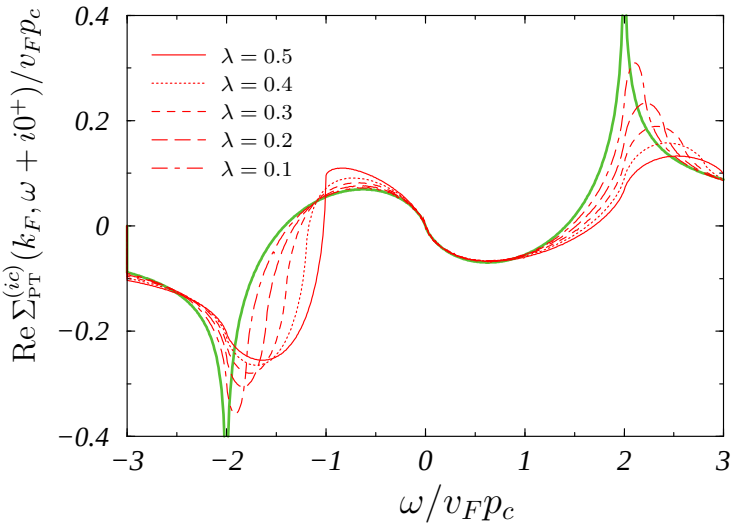

Figure 8.2: The corresponding plots of the real part of the retarded self-energy, obtained by numerical integration of Eq. (8.7). Again the thick solid curve represents the result for linear dispersion as given by Eq. (7.5). All curves are plotted for $\tilde{g}_0^2/8 = 0.1$.

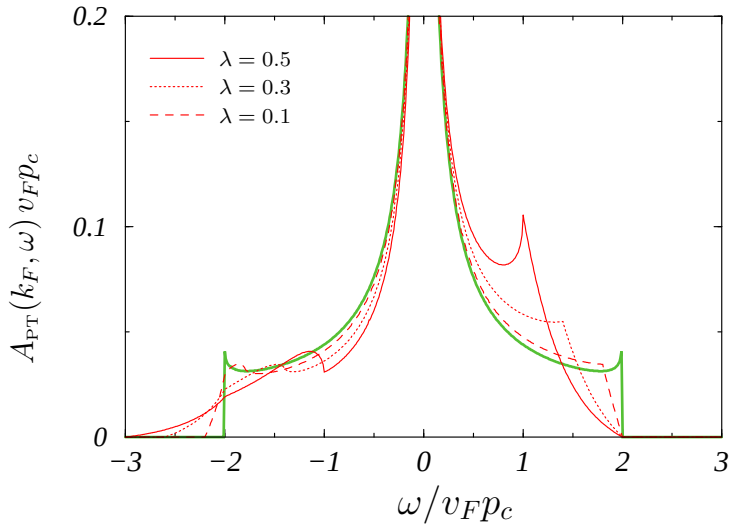

Figure 8.3: The spectral function at perturbative level obtained from Eqs. (8.6), (8.7) and (7.13). The thick solid line corresponds to the result for linear energy dispersion. We have chosen $\tilde{g}_0^2/8 = 0.1$ for all curves.

distribution in the two half-planes $\omega < 0$ and $\omega > 0$, as here a two-dimensional numerical integration is needed, with a rather singular integrand. However, at least if we restrict ourselves to the regions $-v_F p_c < \omega < 0$ and $0 < \omega < v_F p_c$ one can see from Fig. 8.3 that there is an enhancement of spectral weight for positive frequencies, while for negative frequencies the spectral weight is slightly suppressed compared to the symmetric linear case. For $\lambda = 0.5$ the enhancement in the positive-frequency region can be estimated to be of the order of two or three per cent.

This estimate relies on the assumption that the spectral function with finite curvature approaches the curve for linear dispersion when $\omega \to 0$, i.e. that the nature of the singularity at $\omega = 0$ is the same in both cases. Indeed, this can be shown analytically from Eqs. (8.6) and (8.7). For the imaginary part the limit $\omega \to 0$ is easily seen to yield the same result as the limit $\lambda \to 0$, since in the relevant ω-region both quantities exclusively appear in the combination $\lambda\,\omega$. According to Eq. (8.9) we thus have

$$\mathrm{Im}\,\Sigma^{(ic)}_{\rm PT}(k_F,\omega+i0^+) \sim -\,\pi\,\frac{\tilde{g}_0^2}{16}\,|\omega|\,, \qquad \text{for} \quad \omega \to 0\,. \tag{8.10}$$

For the real part the asymptotic behavior is less obvious, since the r.h.s. of Eq. (8.7) does not solely depend on the combination $\lambda\,\omega$ but also on λ and ω separately. However, for small ω the integrand can be approximated by

$$\frac{1}{x}\,\ln\left|\frac{x^2-\left(\lambda x^2-\frac{\omega}{2v_Fp_c}\right)^2}{\left[x^2-\left(\frac{\omega}{2v_Fp_c}\right)^2\right]\left[1-\lambda^2x^2\right]}\right|\Bigg] \approx -\,\frac{2\lambda x\frac{\omega}{2v_Fp_c}}{\left[x^2-\left(\frac{\omega}{2v_Fp_c}\right)^2\right]\left[1-\lambda^2x^2\right]}\,. \tag{8.11}$$

Setting $\omega = 0$ in the denominator the integral in Eq. (8.7) can be seen to diverge logarithmically. More precisely, if we insert Eq. (8.11) on the r.h.s. of Eq. (8.7) and perform the x-integration, it is easy to see that to leading order in ω we get

$$\mathrm{Re}\,\Sigma^{(ic)}_{\mathrm{PT}}(k_F,\omega+i0^+) \sim \frac{\tilde{g}_0^2}{8}\,\omega\ln|\omega|\,, \tag{8.12}$$

with the prefactor being independent of λ. The nature of the singularity of the spectral function can then be read off from Eq. (7.13) to be

$$A^{(ic)}_{\mathrm{PT}}(k_F,\omega) \sim \frac{4}{\tilde{g}_0^2}\,\frac{1}{|\omega|\ln^2|\omega|}\,, \tag{8.13}$$

which is precisely the analytic behavior of the linear result, see Eq. (7.14) and the discussion below.

In summary we have found that within second-order PT the $k = k_F$ spectral function for non-linear energy dispersion displays some small non-universal features at frequencies comparable to $\sim v_Fp_c$. These features reflect the absence of particle-hole symmetry, which is only recovered asymptotically for $\omega \to 0$. Similar to the case of linear energy dispersion the spectral function exhibits a $1/|\omega|\ln^2|\omega|$-singularity at $\omega = 0$, indicating the breakdown of Landau Fermi liquid theory.

Keeping this picture in mind, what can we expect to find for the flow of the couplings within a non-perturbative RG approach? If nothing drastical happens due to the resummation of infinite orders of the coupling $\tilde{g}_0$, we expect as the most important result that the quasi-particle residue Z_l will still flow to zero at the fixed point, just like it was the case for linear dispersion. The anomalous dimension η_l itself is expected to remain unchanged at least to leading order in $\tilde{g}_0$. This is suggested by the fact that in the asymptotic limit $\omega \to 0$ (which has been emphasized to be the relevant limit corresponding the fixed-point values of the couplings) the prefactors of the imaginary and the real part of $\Sigma^{(ic)}_{\mathrm{PT}}(k_F,\omega+i0^+)$ are independent of λ.[2] Hence, from the results obtained within second-order per-

[2]Note that according to Eq. (7.98) we have $\mathrm{Re}\,\Sigma(k_F,\omega+i0^+) = \omega\,(1-|\omega/\Lambda_0|^{-\eta}) = \eta\,\omega\ln|\omega/\Lambda_0| + \mathcal{O}(\eta^2)$. Hence the anomalous dimension $\eta \approx \tilde{g}_0^2/8$ appears at perturbative level as the prefactor of the real part of the retarded self-energy. Since this prefactor is unaffected by curvature in the limit $\omega \to 0$ it is natural to assume that to leading order in $\tilde{g}_0$ the anomalous dimension will also be left unchanged.

turbation theory we do not expect the Luttinger-liquid physics to be qualitatively changed when the non-linearity of the energy dispersion is taken into account. However, it is still instructive to see if the fixed-point values of the couplings η_l, $\tilde{g}_l$ and $\tilde{v}_l$ will depend on the initial curvature, and how large in magnitude an eventual renormalization can be.

In the subsequent sections we shall describe how the flow of irrelevant couplings can systematically be taken into account within our RG formalism. As this task is not straightforward it is important to compare intermediate results with the predictions of perturbation theory whenever possible. To this end we shall now state the perturbative results for the susceptibilities defined in Sec. 6.5, using Eq. (8.1) as non-interacting Green function. It is then important to notice that the Peierls and the BCS channels, which for linear dispersion yield the same response, split up into two different contributions when a non-linear dispersion is used. This is again due to lack of particle-hole symmetry. While the zero sound contribution $\Pi_{\rm PT}$ is still determined by Eq. (6.142) together with Eq. (8.1), for the Peierls and the BCS contribution we define in analogy with Eqs. (6.32) and (6.33),

$$\chi_{\rm PT}(p,i\omega) = \int_{-\infty}^{\infty}\frac{dp'}{2\pi}\int_{-\infty}^{\infty}\frac{d\omega'}{2\pi}G_0(-p',i\omega')\,G_0(p'+p,i\omega'+i\omega)\,, \tag{8.14}$$

and

$$\chi'_{\rm PT}(p,i\omega) = -\int_{-\infty}^{\infty}\frac{dp'}{2\pi}\int_{-\infty}^{\infty}\frac{d\omega'}{2\pi}G_0(p',-i\omega')\,G_0(p'+p,i\omega'+i\omega)\,. \tag{8.15}$$

Performing the integrations we obtain

$$\Pi_{\rm PT}(p,i\omega) = \frac{m}{2\pi p}\,\ln\left(\frac{i\omega+\xi(-p)}{i\omega-\xi(p)}\right), \tag{8.16}$$

for the zero sound contribution,

$$\chi_{\rm PT}(p,i\omega) = \frac{1}{4\pi v_F\big(1+\frac{p}{2k_F}\big)}\,\ln\left[\frac{\omega^2+\xi^2(p)}{\omega^2+\big(1+\frac{p}{2k_F}\big)^2\big(2\Lambda_0-|v_Fp|\big)^2}\right], \tag{8.17}$$

for the Peierls contribution and

$$\chi'_{\rm PT}(p,i\omega) \;=\; \frac{1}{4\pi v_F\sqrt{1+\frac{1}{v_Fk_F}\big(i\omega-\frac{p^2}{4m}\big)}}$$

$$\times \sum_{\alpha=\pm} \alpha \ln \left[\frac{\left(1-\alpha\sqrt{1+\frac{1}{v_F k_F}\left(i\omega-\frac{p^2}{4m}\right)}\right)^2 - \left(\frac{p}{2k_F}\right)^2}{\left(1-\alpha\sqrt{1+\frac{1}{v_F k_F}\left(i\omega-\frac{p^2}{4m}\right)}\right)^2 - \left(\frac{2\Lambda_0-|v_F p|}{2v_F k_F}\right)^2} \right] , \qquad (8.18)$$

for the BCS contribution. In all three cases we have for simplicity assumed $|v_F p| \leq \Lambda_0$. Here k_F has to be understood as short-hand for $m v_F$. Although the expressions for $\chi_{\rm PT}$ and $\chi'_{\rm PT}$ look quiet different it is not difficult to show that they reduce to the linear result given in Eq. (6.143) both in the limits $1/m \to 0$ and $\omega, p \to 0$. Similarly, $\Pi_{\rm PT}$ reduces to its linear equivalent given in Eq. (6.142) in these limits.

8.2 Irrelevant Couplings at the Fixed Point

Before we shall turn our attention to the calculation of the RG flow equations for the spinless g_2-model with non-linear energy dispersion, it is worth to discuss the destination of irrelevant couplings at the fixed-point on more general grounds in order to develop an appropriate and consistent approximation strategy. In the non-interacting case irrelevant couplings appear naturally due to an expansion of the bare energy dispersion around the true, i.e. the interacting FS. The irrelevant coupling with canonical scaling dimension $d_s = -1$ is then associated with the curvature of the energy dispersion and has already been introduced in Eq. (4.11) in its dimensionless form. In one spatial dimension we have $v_\parallel^{\mathbf{n}} = v_F$, such that

$$c_l = c_0 e^{-l} , \qquad \text{with} \qquad c_0 = \frac{\Lambda_0}{2 v_F k_F} = \lambda , \qquad (8.19)$$

is independent of the direction $\mathbf{n}$, i.e. it does not depend on the Fermi point $\pm k_F$ under consideration.

In contrast to marginal couplings irrelevant ones pick up a dependence on the flow parameter l already at non-interacting level. The simplest way to incorporate the effect of c_l on the flow of, e.g. , $\tilde{g}_l$ is a *non*-self-consistent one- or two-loop calculation. In this case we would proceed as follows. To determine the flow of $\tilde{g}_l$ at one-loop level we had to resolve the equation

$$\partial_l \tilde{g}_l = B_l , \qquad (8.20)$$

with B_l determined by Eqs. (6.29) and (6.30). The bare propagators $\tilde{G}^0_l$ and $\dot{G}^0_l$ in Eq. (6.30) would then be given by

$$\tilde{G}^0_l(Q) = \frac{\Theta(1<|q|<e^l)}{i\epsilon - \xi_l(q)} , \qquad \text{and} \qquad \dot{G}^0_l(Q) = \frac{\delta(|q|-1)}{i\epsilon - \xi_l(q)} , \qquad (8.21)$$

with

$$\xi_l(q) \approx q - c_l q^2 \,. \tag{8.22}$$

Note that we have retained the linear dispersion in the argument of the Θ- and the δ-function in Eq. (8.21) . This greatly simplifies the calculations and should not qualitatively affect the result:[3] Obviously, in this approximation we have $c_l \to 0$ for $l \to \infty$ in the propagators (8.21), and one is tempted to say that the fixed-point value of $\tilde{g}_l$ must remain unchanged. The misapprehension in this reasoning is that the processes of solving the flow-equation Eq. (8.20) and taking the limit $l \to \infty$ do not necessarily commute. To see this clearly let us anticipate the one-loop result, which we will find to be of the form

$$\partial_l \tilde{g}_l \sim c_l^2 \, \tilde{g}_l^2 \,, \tag{8.23}$$

to leading order in $c_l \ll 1$. Asymptotically, i.e. for $l \gg 1$ we hence recover the linear flow equation $\partial_l \tilde{g}_l \sim 0$, implying that $\tilde{g}_l$ does not flow at all. This procedure corresponds to first taking the limit $l \to \infty$ and solving the flow equation afterwards. But it is easy to see that this practice must fail here, since c_l depends *explicitly* on l . Integrating Eq. (8.23) first the result for $\tilde{g}_l$ will depend non-locally on the coupling c_l , and this non-local dependence does *not* just lead to higher orders in the coupling $\tilde{g}_l$, which could be neglected within a one-loop approximation. Note that in case of marginal couplings this was our general approximation strategy in Chap. 6 . Here, $c_l = c_0 e^{-l}$ exhibits an explicit l-dependence which cannot be neglected. This is easily seen by integrating Eq. (8.23), which yields

$$\tilde{g}_l \sim \tilde{g}_0 + \tilde{g}_0^2 \frac{c_0^2}{2}(1 - e^{-2l}) + \mathcal{O}(\tilde{g}_0^3) \,. \tag{8.24}$$

Taking the limit $l \to \infty$ only now shows that the fixed-point result indeed depends on the initial curvature.

This immediately raises the question whether irrelevant couplings can also qualitatively change the physical nature of the fixed point, apart from the fixed-point values themselves. The classification as *irrelevant* in the RG sense somehow takes it for granted that this will not happen. On the other hand on physical grounds it is clear that for instance the range of the interaction in momentum space has important consequences on the physics of an interacting many-body system, although this feature is exclusively incorporated by irrelevant couplings. The crucial observation is that the fixed-point value of an irrelevant coupling may

[3] Of course the RG *fixed-point* results should not depend on the detailed way *how* we integrate out degrees of freedom, but only on the fact that all of them are finally integrated out when the fixed point is reached. On the other hand the details of the flow *towards* the fixed point will depend on the particular choice of the function Ω_K introduced in Eq. (3.4).

well (and will in general) be different from zero. Consequently, if we take the flow of irrelevant couplings *self-consistently* into account, it can happen that the flow of the other marginal or relevant couplings is deviated to new fixed points. At least there are no principle reasons excluding such a scenario.
To see this more clearly let us consider the typical structure of the flow equation of an arbitrary irrelevant coupling $\tilde{x}_l$ with scaling dimension $d \lesssim -1$, which is of the form

$$\partial_l \tilde{x}_l = -d\,\tilde{x}_l + I_l(\tilde{x}_l, \tilde{y}_l)\,. \tag{8.25}$$

Here I_l plays the role of the inhomogeneity resulting from integrating out degrees of freedom and depends on the vertex under consideration. It may explicitly depend on l, on $\tilde{x}_l$ itself and on other relevant, marginal or irrelevant couplings, which we have symbolically incorporated by the dependence on $\tilde{y}_l$. For the present discussion we assume d to be a positive real number and neglect its dependence on the flow parameter l. If we start the flow at $l = 0$ Eq. (8.25) can be transformed into

$$\tilde{x}_l = \Big(\tilde{x}_0 + \int_0^l dt\, e^{dt}\, I_t(\tilde{x}_t, \tilde{y}_t)\Big)\, e^{-dl}\,. \tag{8.26}$$

Obviously, the integration can in general not be performed exactly. However, to get a glance of the solution let us assume that $\tilde{y}_l$ solely represents marginal couplings and that $\tilde{x}_l$ remains small during the whole flow. It is then reasonable to expand $I_t(\tilde{x}_t, \tilde{y}_t)$ in powers of $\tilde{x}_l$ and to neglect non-localities in the dependence on the integration variable t. We may hence to leading order replace $I_t(\tilde{x}_t, \tilde{y}_t)$ with $I_0(0, \tilde{y}_0)$ on the r.h.s. of Eq. (8.26), which leads to

$$\tilde{x}_l \approx \frac{1}{d}\, I_0(0, \tilde{y}_0) + \big[\tilde{x}_0 - \frac{1}{d}\, I_0(0, \tilde{y}_0)\,\big]\, e^{-dl}\,. \tag{8.27}$$

If nothing drastical happens due to the above approximation, the fixed-point value of $\tilde{x}_l$ will be of the form

$$\tilde{x} \approx \frac{1}{d}\, I_0(0, \tilde{y}_0)\,. \tag{8.28}$$

Now, within our weak-coupling expansion the inhomogeneity will typically be proportional to a power of $\tilde{g}_0$ (depending on the vertex to which the coupling $\tilde{x}_l$ is related), but it will in general be different from zero. This will even be the case if we start at $\tilde{x}_0 = 0$, i.e. if this coupling is not present in the initial action.
To give an explicit example for such a scenario consider Eqs. (6.52) and (6.53) for $Q' = (\bar{\alpha}, q, i\epsilon)$. We define an irrelevant coupling of canonical scaling dimension $d_s = -2$ by

$$\tilde{x}_l = \partial^2_{i\epsilon} \tilde{\Gamma}^{(4)}_l(Q, Q'; Q', Q)\big|_{q=\epsilon=0}\,. \tag{8.29}$$

According to Eqs. (6.51), (6.52) and (6.53) the flow of this coupling is given by

$$\tilde{x}_l = \tilde{g}_l^2 \, \partial_{i\epsilon}^2 \, \tilde{\chi}_l(0, 2i\epsilon)\big|_{\epsilon=0} = \frac{\tilde{g}_l^2}{2\tilde{v}_l^3} \, (1 - e^{-2l}) \,, \tag{8.30}$$

with fixed-point value

$$\tilde{x} = \frac{\tilde{g}^2}{2\tilde{v}^3} \,. \tag{8.31}$$

This confirms the above general picture: Although the initial value $\tilde{x}_0$ equals to zero the fixed-point value does not. The situation is even more intriguing: Let us define a second irrelevant coupling by

$$\tilde{x}_l' = \partial_{i\epsilon}^4 \, \tilde{\Gamma}_l^{(4)}(Q, Q'; Q', Q)\big|_{q=\epsilon=0} \,, \tag{8.32}$$

with scaling dimension $d_s = -4$. Here we find

$$\tilde{x}_l' = -3 \, \frac{\tilde{g}_l^2}{\tilde{v}_l^5} \, (1 - e^{-4l}) \,, \tag{8.33}$$

with initial value $\tilde{x}_0' = 0$ and fixed-point value

$$\tilde{x}' = -3 \, \frac{\tilde{g}^2}{\tilde{v}^5} \,. \tag{8.34}$$

Keeping in mind that according to Eq. (6.117) $\tilde{v} \approx 1 + \tilde{g}_0^2/4$ we see that $|\tilde{x}'| \approx 6 \, |\tilde{x}|$, although $\tilde{x}_l'$ is stronger irrelevant than $\tilde{x}_l$. The main effect of this stronger irrelevance is even that $\tilde{x}_l'$ approaches its larger fixed-point value much faster than $\tilde{x}_l$. This explicitly shows that Eq. (8.28) must be interpreted with care, since the factor $1/d$ in front of $I_0(0, \tilde{y}_0)$ seems to imply that with increasing irrelevance d the fixed-point value decreases.

It is then important to keep in mind that each coupling is related to a corresponding power of q and/or ϵ, resulting from the Taylor expansion of the dimensionless vertex under consideration. The higher the irrelevance of a certain coupling the larger will be the power and the smaller will be the contribution of this term in the vicinity of $q = \epsilon = 0$. Consequently, the most promising approach to a self-consistent calculation taking irrelevant couplings into account will be to keep all terms involving the same power in q and ϵ, i.e. all terms with the same canonical scaling dimension.

Applied to the two-point vertex this would imply that besides c_l we also had to keep the couplings $a_l = \partial_{i\epsilon}^2 \tilde{r}_l(Q)|_{Q=0} = \partial_{i\epsilon}^2 \tilde{\Gamma}_l^{(2)}(Q)|_{Q=0}$ and $b_l = \partial_{i\epsilon} \partial_q \tilde{r}_l(Q)|_{Q=0} = \partial_{i\epsilon} \partial_q \tilde{\Gamma}_l^{(2)}(Q)|_{Q=0}$, both with the same canonical scaling dimension $d_s = -1$ as c_l. However, a calculation keeping track of a_l, b_l and c_l in addition to the marginal couplings $\tilde{g}_l$ and $\tilde{v}_l$ is very hard to perform. We will thus proceed differently by

simply keeping c_l in a self-consistent manner. The justification of this procedure relies on the fact that only c_l has a non-zero initial value while on the other hand $a_0 = b_0 = 0$. Of course, according to the above discussion this does not exclude the possibility of non-zero fixed-point values for a_l and b_l. On the other hand, provided that the self-consistency indeed accounts for a *qualitative* change of the flow in coupling space with new fixed-points, this will happen due to conditions imposed on the initial values of the involved couplings. In particular the generic Luttinger-liquid behavior should be recovered in a parameter regime including $c_0 = 0$, as this initial value corresponds to the model with linear energy dispersion. Since the couplings a_l and b_l are simply not present in the initial action their initial values are fixed, such that only the variation of c_0 can in principle be responsible for a qualitative change of the coupling flow. For this reason we believe that the possibility of new fixed points should already be reflected in an approach that keeps track of c_l self-consistently, but that neglects a_l and b_l in a first approximation. Of course, *if* a new fixed-point is found or a runaway flow indicates an instability, the calculation should be repeated including a_l and b_l.
Finally, in a non-self-consistent approach all propagators $\tilde{r}_l(q, i\epsilon)$ will be replaced by bare propagators $\tilde{r}_l^0(q, i\epsilon) = i\epsilon - \xi_l(q)$ such that the only irrelevant coupling with scaling dimension $d_s = -1$ is given by c_l. As the fixed-point value of $c_l = c_0 e^{-l}$ is simply given by $c_\infty = 0$ we cannot expect to find new fixed-points in this case, since the latter are determined by the asymptotics of the flow equations for $l \to \infty$. Nonetheless it is then still instructive to see if and how strong the fixed-point values of the relevant and marginal couplings depend on the initial value c_0. At least for this limited task the subsequent calculations are reliable.

8.3 Self-Consistent One-Loop Flow

Conceptually the procedure of deriving the flow equations for the model with non-linear energy dispersion is almost identical to the methods presented in Chap. 6. Only one subtlety concerning the handling of irrelevant couplings still has to be explained, which will be done further below. The rest of the calculations is a rather technical and often tedious matter which we shall no longer present in all details; instead we will mostly be concerned with the results.
First let us outline the starting point of our calculations, beginning with the bare inverse propagator, which now reads

$$\tilde{r}_l(q, i\epsilon) = Z_l[i\epsilon - \xi_l(q)] + \tilde{\Gamma}_l^{(2)}(q, i\epsilon)\,, \tag{8.35}$$

with $\xi_l(q)$ given by Eq. (8.22) and initial condition $\tilde{r}_{l=0}(q, i\epsilon) = i\epsilon - q - c_0 q^2$. Expanding the dimensionless two-point vertex $\tilde{\Gamma}_l^{(2)}$ in powers of q and ϵ we obtain

$$\tilde{r}_l(q, i\epsilon) = i\epsilon - \tilde{\xi}_l(q) + \tilde{\mu}_l + \mathcal{O}(q\epsilon, \epsilon^2, q^3)\,, \tag{8.36}$$

with the definition

$$\tilde{\xi}_l(q) = \tilde{v}_l q + \tilde{c}_l q^2\,. \tag{8.37}$$

Although the couplings Z_l, $\tilde{v}_l$, $\tilde{\mu}_l$ and $\tilde{g}_l$ are defined in the same way as before, let us for convenience display the definitions of all involved couplings together. These are

$$\begin{aligned}
\tilde{\mu}_l &= \tilde{\Gamma}_l^{(2)}(0, i0)\,, && (8.38)\\
Z_l &= 1 + \partial_{i\epsilon}\tilde{\Gamma}_l^{(2)}(Q)|_{Q=0}\,, && (8.39)\\
\tilde{v}_l &= Z_l - \partial_q\tilde{\Gamma}_l^{(2)}(Q)|_{Q=0}\,, && (8.40)\\
\tilde{g}_l &= A_{\alpha_1'\alpha_2';\,\alpha_2\alpha_1}\,\tilde{\Gamma}_l^{(4)}(\alpha_1', 0, \alpha_2', 0; \alpha_2, 0, \alpha_1, 0)\,, && (8.41)\\
\tilde{c}_l &= Z_l\, c_l - \partial_q^2\tilde{\Gamma}_l^{(2)}(Q)|_{Q=0}\,, && (8.42)
\end{aligned}$$

and

$$\eta_l = \partial_{i\epsilon}\dot{\Gamma}_l^{(2)}(Q)|_{Q=0}\,. \tag{8.43}$$

The corresponding flow equations are

$$\begin{aligned}
\partial_l\tilde{\mu}_l &= (1-\eta_l)\tilde{\mu}_l + \dot{\Gamma}_l^{(2)}(0, i0)\,, && (8.44)\\
\partial_l Z_l &= -\eta_l\, Z_l\,, && (8.45)\\
\partial_l\tilde{v}_l &= -\eta_l\tilde{v}_l - \partial_q\dot{\Gamma}_l^{(2)}(Q)|_{Q=0}\,, && (8.46)\\
\partial_l\tilde{g}_l &= -2\eta_l\tilde{g}_l + B_l\,, && (8.47)\\
\partial_l\tilde{c}_l &= -(1+\eta_l)\tilde{c}_l - \partial_q^2\dot{\Gamma}_l^{(2)}(Q)|_{Q=0}\,, && (8.48)
\end{aligned}$$

with

$$B_l = \dot{\Gamma}_l^{(4)}(\alpha, 0, \bar{\alpha}, 0; \bar{\alpha}, 0, \alpha, 0)\,. \tag{8.49}$$

Again we should start by considering the flow of the relevant coupling $\tilde{\mu}_l$. Similarly to the case of linear energy dispersion, see Eq. (6.22), we now obtain

$$\partial_l\tilde{\mu}_l = \tilde{\mu}_l - \frac{\tilde{g}_l}{2}\left[\Theta(\tilde{\mu}_l + \tilde{v}_l - \tilde{c}_l) + \Theta(\tilde{\mu}_l - \tilde{v}_l - \tilde{c}_l)\right] + \mathcal{O}(\tilde{g}_l^2)\,. \tag{8.50}$$

Keeping in mind that $\tilde{v}_0 = 1$ and $\tilde{c}_0 = c_0 = \lambda \leq 1/2$ we recover the same fixed line as for the linear model, provided that $\tilde{v}_l - \tilde{c}_l$ remains of the order of unity and $\tilde{g}_l$

does not flow to strong coupling. In fact, the whole subsequent calculation rests on the assumption that $\tilde{v}_l > \tilde{c}_l$ during the entire flow of the couplings. In case that this situation changes at a certain finite scale $l_\star$ this would be visible in our solution, since our formalism provides us with information about the magnitude of the couplings at each scale value l. Note that even if both Θ-functions on the r.h.s. of Eq. (8.50) equal to one above a certain scale, for instance due to the fact that $\tilde{v}_l, \tilde{c}_l \to 0$ for large l, we had to fine-tune the initial condition for $\tilde{\mu}_l$ such that $\tilde{\mu}_l = \tilde{g}_l$ at and above this scale to avoid a runaway flow. The new fixed point of $\tilde{\mu}_l$ would now equal to $\tilde{g}$ rather than $\tilde{g}/2$. As long as $\tilde{g}_l$ does not flow to strong coupling this would not affect the flow of the other couplings within a self-consistent weak-coupling expansion, since keeping $\tilde{\mu}_l$ within the inverse propagator $\tilde{r}_l(q, i\epsilon)$ would simply give rise to higher orders in the coupling $\tilde{g}_l$.
Provided that $\tilde{v}_l - \tilde{c}_l$ remains of the order of unity we recover the result for linear energy dispersion to leading order in $\tilde{g}_l$, i.e.

$$\boxed{\partial_l \tilde{\mu}_l = \tilde{\mu}_l - \frac{\tilde{g}_l}{2}\,.} \tag{8.51}$$

For the couplings Z_l, $\tilde{v}_l$ and $\tilde{c}_l$ the one-loop flow can easily be read off Eqs. (8.45), (8.44) and (8.48) to be determined by

$$\boxed{\begin{aligned} \partial_l Z_l &= 0\,, \\ \partial_l \tilde{v}_l &= 0\,, \\ \partial_l \tilde{c}_l &= -\tilde{c}_l\,. \end{aligned}} \tag{8.52}$$

Like before the couplings Z_l and $\tilde{v}_l$ do not flow at all at this level, while the flow of $\tilde{c}_l$ simply integrates to

$$\tilde{c}_l = \tilde{c}_0 e^{-l} = c_l\,. \tag{8.53}$$

Hence the coupling related to the curvature of the energy dispersion remains unrenormalized at one-loop order and decays exponentially fast to zero.
The only case where some more work is to do is the coupling $\tilde{g}_l$, the flow of which at one-loop level is determined by

$$\partial_l \tilde{g}_l = B_l\,, \tag{8.54}$$

with B_l given by Eq. (6.40). We have already emphasized that for finite curvature the Peierls and the BCS channel yield different contributions to the flow of $\tilde{g}_l$. In terms of the auxiliary functions $\dot{\Pi}_l$, $\dot{\chi}_l$ and $\dot{\chi}'_l$ defined in Eqs. (6.31), (6.32) and (6.33) this means that $\dot{\chi}_l(q, i\epsilon) \neq \dot{\chi}'_l(q, i\epsilon)$. As an immediate consequence

we see from Eq. (6.40) that unlike in the model with linear dispersion here $\tilde{g}_l$ will already undergo a flow at one-loop order. Approximating the zeroth-order Green functions $\tilde{G}^0_l$ and $\dot{G}^0_l$ by the expressions given in Eq. (8.21) we obtain

$$\dot{\Pi}_l(q, i\epsilon) = \Theta(2 < |q| < e^l + 1)\, \frac{s_q(i\epsilon - \tilde{v}_l q)}{(i\epsilon - \tilde{v}_l q)^2 - (\tilde{c}_l q)^2 (|q| - 2)^2}\,, \tag{8.55}$$

$$\dot{\chi}_l(q, i\epsilon) = -\,\Theta(|q| < e^l - 1)\, \frac{(\tilde{v}_l + \tilde{c}_l q)(|q| + 2)}{\epsilon^2 + (\tilde{v}_l + \tilde{c}_l q)^2 (|q| + 2)^2}\,, \tag{8.56}$$

and

$$\dot{\chi}'_l(q, i\epsilon) = \frac{\Theta(|q| < e^l - 1)\, \tilde{v}_l (|q| + 2)}{[i\epsilon - \tilde{c}_l (q^2 + 2|q| + 2)]^2 - \tilde{v}_l^2 (|q| + 2)^2}\,. \tag{8.57}$$

It is not difficult to see that $\dot{\chi}_l$ and $\dot{\chi}'_l$ both reduce to their analogues for linear dispersion in Eq. (6.38) when $\tilde{c}_l \to 0$. The same can easily be seen for $\dot{\Pi}_l$. For the one-loop flow of $\tilde{g}_l$ we get from Eqs. (8.54), (8.56) and (8.57)

$$\boxed{\partial_l \tilde{g}_l = -\,\Theta(e^l - 2)\, \frac{\tilde{g}_l^2}{2\tilde{v}_l}\, \frac{\tilde{c}_l^2}{\tilde{v}_l^2 - \tilde{c}_l^2}\,.} \tag{8.58}$$

Before we discuss possible non-trivial implications of this equation at higher-loop orders let us first integrate Eq. (8.58) at one-loop level. According to Eq. (8.53) we can simply insert $\tilde{c}_l = c_0 e^{-l} = \lambda e^{-l}$ on the r.h.s. of Eq. (8.58), leading to

$$\tilde{g}_l = \frac{\tilde{g}_0}{1 + \frac{\tilde{g}_0}{4}\Theta(e^l - 2) \ln\left(\frac{1 - \lambda^2 e^{-2l}}{1 - \lambda^2/4}\right)}, \tag{8.59}$$

$$= \tilde{g}_0 - \lambda^2\, \frac{\tilde{g}_0^2}{16}\, \Theta(e^l - 2)\,(1 - 4e^{-2l}) + \mathcal{O}(\lambda^4, \tilde{g}_0^3)\,. \tag{8.60}$$

The fixed-point value of $\tilde{g}_l$ at this level is hence given by

$$\boxed{\begin{aligned} \tilde{g} &\approx \tilde{g}_0 - \frac{\tilde{g}_0^2}{16}\, \lambda^2 \\ &\equiv \tilde{g}_0 - \frac{\tilde{g}_0^2}{64} \left(\frac{p_c}{m v_F}\right)^2. \end{aligned}} \tag{8.61}$$

In the second line we have inserted the expression (8.19) for λ and identified $\Lambda_0 = v_F p_c$. Note also that due to the condition $\lambda \leq 1/2$, see Eq. (8.3) and

the discussion below, the logarithm in the first line of Eq. (8.59) is indeed small compared to unity. The dependence of the fixed-point value $\tilde{g}$ on the initial curvature of the energy dispersion in the next-to-leading order is thus evident already at one-loop level. The correction is found to be small and governed by the dimensionless parameter $p_c/mv_F \equiv p_c/k_F$. It is important to notice that the dependence of the fixed-point value on the momentum cutoff p_c should not be misinterpreted as "unphysical". As we have already emphasized p_c should rather be viewed as a representative of other irrelevant couplings determining the momentum dependence of the initial Landau parameters. Therefore Eq. (8.61) suggests that the next-to-leading order of the fixed-point value $\tilde{g}$ is strongly non-universal and so will be the next-to-leading orders of the fixed-point result for the anomalous dimension. We hence qualitatively confirm the results obtained by Meden in Ref. [82] concerning the universality of the Luttinger-liquid parameters. Finally, does Eq. (8.58) open up the possibility of new fixed points at higher loop orders? When a fixed point is approached the derivative of the involved couplings with respect to the flow parameter l must tend to zero. Setting $\partial_l \tilde{g}_l = 0$ on the l.h.s. of Eq. (8.58) we see that at one-loop level the resulting equation can be satisfied for arbitrary fixed-point values $\tilde{g}$ since $\tilde{c} \equiv \tilde{c}_\infty = 0$. This situation might change at higher loop orders as here the possibility of a non-zero fixed-point value $\tilde{c}$ occurs. For $\tilde{c} \neq 0$ Eq. (8.58) implies that $\tilde{g}_l$ must flow to zero at the fixed point. However, in this case we principally have to include the two-loop contribution to the flow of $\tilde{g}_l$ as well.

8.4 Susceptibilities at the Fixed Point

Let us now turn our attention to the susceptibilities, essentially obtained as l-integrated versions of the auxiliary functions $\dot{\Pi}_l$, $\dot{\chi}_l$ and $\dot{\chi}'_l$. We still have to clarify how the non-local dependence of the coupling $\tilde{c}_l$ on the flow parameter l can be handled in a consistent manner. For the marginal couplings $\tilde{v}_l$ and $\tilde{g}_l$ we have seen that non-localities lead to higher orders in the coupling $\tilde{g}_l$, which can be neglected within a weak-coupling expansion. In contrast $\tilde{c}_l$ exhibits an explicit l-dependence which must not be neglected. In a non-self-consistent calculation $\tilde{c}_l$ has to be replaced with $c_l = \lambda e^{-l}$, such that the l-dependence is simply given by the factor e^{-l}. For a self-consistent treatment it is then obvious to try the Ansatz

$$\tilde{c}_l = \bar{c}_l e^{-l}. \tag{8.62}$$

The flow equation for $\bar{c}_l$ is then easily obtained from the flow equation (8.48) for $\tilde{c}_l$,

$$\partial_l \bar{c}_l = -\eta_l \bar{c}_l + e^l \, \partial_q^2 \dot{\Gamma}_l^{(2)}(Q)|_{Q=0} \,. \tag{8.63}$$

Consequently, the coupling $\bar{c}_l$ is marginal in the RG sense. Now, imagine that the original coupling $\tilde{c}_l$ occurs within an integral kernel in the form $\tilde{c}_{l-t}$, where t is the integration variable. According to the above definition we have $\tilde{c}_{l-t} = e^{t-l}\bar{c}_{l-t}$. Since $\bar{c}_l$ is marginal its non-local dependence on t can be neglected for the same reasons that hold for $\tilde{v}_l$ and $\tilde{g}_l$. This means that we may approximate $\tilde{c}_{l-t} \approx e^{t-l}\bar{c}_l = e^t \tilde{c}_l$. Proceeding in this way the following expressions for the dimensionless susceptibilities are obtained from Eqs. (6.48) and (6.49),

$$\begin{aligned} \tilde{\Pi}_l(q, i\epsilon) &= \frac{\Theta(2 < |q| < 1 + e^l)}{4\tilde{c}_l q} \ln\left(\frac{i\epsilon + \tilde{\xi}_l(-q) - 2\tilde{c}_l|q|}{i\epsilon - \tilde{\xi}_l(q) + 2\tilde{c}_l|q|} \right) \\ &\quad - \frac{\Theta(1 + e^l < |q| < 2e^l)}{4\tilde{c}_l q} \ln\left(\frac{i\epsilon + \tilde{\xi}_l(-q) - 2e^l\tilde{c}_l|q|}{i\epsilon - \tilde{\xi}_l(q) + 2e^l\tilde{c}_l|q|} \right) , \end{aligned} \tag{8.64}$$

$$\tilde{\chi}_l(q, i\epsilon) = \frac{l}{2\tilde{v}_l} + \frac{\Theta(|q| < e^l - 1)}{4(\tilde{v}_l + \tilde{c}_l q)} \ln\left(\frac{\epsilon^2 + (\tilde{v}_l + \tilde{c}_l q)^2(|q| + 2)^2}{\epsilon^2 + (\tilde{v}_l + \tilde{c}_l q)^2(|q| + 2e^l)^2} \right) , \tag{8.65}$$

and

$$\begin{aligned} \tilde{\chi}_l'(q, i\epsilon) &= \frac{1}{4\tilde{v}_l} \ln\left(\frac{\tilde{v}_l^2 - \tilde{c}_l^2}{\tilde{v}_l^2 e^{-2l} - \tilde{c}_l^2} \right) + \frac{\Theta(|q| < e^l - 1)}{4\sqrt{\tilde{v}_l^2 + 2\tilde{c}_l(i\epsilon - \tilde{c}_l q^2/2)}} \\ &\quad \times \sum_{\alpha = \pm 1} \alpha \ln\left[\frac{\left[\tilde{v}_l - \alpha\sqrt{\tilde{v}_l^2 + 2\tilde{c}_l(i\epsilon - \tilde{c}_l q^2/2)}\,\right]^2 - \tilde{c}_l^2(|q| + 2)^2}{\left[\tilde{v}_l - \alpha\sqrt{\tilde{v}_l^2 + 2\tilde{c}_l(i\epsilon - \tilde{c}_l q^2/2)}\,\right]^2 - (\tilde{c}_l e^l)^2(2 - |q|e^{-l})^2} \right] , \end{aligned} \tag{8.66}$$

Similar to the linear model in case of $\tilde{\chi}_l$ and $\tilde{\chi}_l'$ we had to subtract the momentum- and frequency-independent part, corresponding to the first term on the r.h.s. of Eqs. (8.65) and (8.66), respectively. On the other hand, for Π_l the subtraction term just equals to zero. The first thing we should check is, that the limit $\tilde{c}_l \to 0$ recovers the corresponding expressions of the linear model, given by Eqs. (6.50) and (6.51). For convenience let us denote the former results here by $\tilde{\Pi}_l^{(lin)}(q, i\epsilon)$ and $\tilde{\chi}_l^{(lin)}(q, i\epsilon)$. It is then not difficult to show that

$$\tilde{\Pi}_l(q, i\epsilon) \overset{\tilde{c}_l \to 0}{\longrightarrow} \tilde{\Pi}_l^{(lin)}(q, i\epsilon) \,, \tag{8.67}$$

as well as

$$\left.\begin{matrix} \tilde{\chi}_l(q, i\epsilon) \\ \tilde{\chi}_l'(q, i\epsilon) \end{matrix}\right\} \overset{\tilde{c}_l \to 0}{\longrightarrow} \tilde{\chi}_l^{(lin)}(q, i\epsilon) \,. \tag{8.68}$$

Before we discuss the limit $l \to \infty$, i.e. the dimensionless susceptibilities at the fixed point, let us try to recover the perturbative expressions given in Eqs. (8.16), (8.17) and (8.18). To show the procedure we take the contribution of the BCS channel, i.e. $\tilde{\chi}_l'(q, i\epsilon)$. Like for linear dispersion, we have to skip the q- and ϵ-independent subtraction term of $\tilde{\chi}_l'(q, i\epsilon)$ before we transform back to the physical variables. Using $q = v_F p/\Lambda_0$ and $\epsilon = \omega/\Lambda_0$ together with Eq. (4.29) we obtain

$$\begin{aligned}\chi_\Lambda'(p, i\omega) &= \frac{\Theta(|v_F p| < \Lambda_0 - \Lambda)}{4\pi v_F \sqrt{\tilde{v}_l^2 + 2\frac{\tilde{c}_l}{\Lambda}[i\omega - \frac{\tilde{c}_l}{\Lambda}(v_F p)^2/2]}} \\ &\times \sum_{\alpha=\pm 1} \alpha \ln \left[\frac{\left[\tilde{v}_l - \alpha\sqrt{\tilde{v}_l^2 + 2\frac{\tilde{c}_l}{\Lambda}[i\omega - \frac{\tilde{c}_l}{\Lambda}(v_F p)^2/2]}\,\right]^2 - \left(\frac{\tilde{c}_l}{\Lambda}\right)^2 (2\Lambda + |v_F p|)^2}{\left[\tilde{v}_l - \alpha\sqrt{\tilde{v}_l^2 + 2\frac{\tilde{c}_l}{\Lambda}[i\omega - \frac{\tilde{c}_l}{\Lambda}(v_F p)^2/2]}\,\right]^2 - \left(\frac{\tilde{c}_l}{\Lambda}\right)^2 (2\Lambda_0 - |v_F p|)^2} \right] . \end{aligned} \tag{8.69}$$

Replacing $\tilde{v}_l \to 1$ and $\tilde{c}_l \to c_l$ such that $c_l/\Lambda = 2mv_F^2$ according to Eq. (8.19), it is straightforward to show that

$$\chi_\Lambda'(p, i\omega) \stackrel{\Lambda \to 0}{\longrightarrow} \chi_{\mathrm{PT}}'(p, i\omega) . \tag{8.70}$$

In the same way the perturbative results for the contributions of the zero-sound and the Peierls channel can exactly be recovered. Keeping in mind the discussion of Sec. 6.5 we thus confirm again that transforming back to the physical susceptibilities *before the limit* $l \to \infty$ *is taken* conserves the full structure of the correlation functions, including their non-universal features, here represented by the irrelevant parameter $1/m$.

Finally let us consider the dimensionless susceptibilities at the fixed point. Provided that $\tilde{c}_l \to 0$ and $\tilde{v} < \infty$ for $l \to \infty$ it can be shown from Eqs. (8.64), (8.65) and (8.66) that

$$\lim_{l\to\infty} \tilde{\Pi}_l(q, i\epsilon) = \Theta(2 < |q|)\, \frac{s_q}{2}\, \frac{|q| - 2}{i\epsilon - \tilde{v}q}, \tag{8.71}$$

and

$$\lim_{l\to\infty} \tilde{\chi}_l(q, i\epsilon) = \lim_{l\to\infty} \tilde{\chi}_l'(q, i\epsilon) = \frac{1}{4\tilde{v}} \ln\left(\frac{\epsilon^2 + \tilde{v}^2(2 + |q|)^2}{4\tilde{v}^2}\right) . \tag{8.72}$$

Except for the fact that the fixed-point value $\tilde{v}$ might differ from its analogue in the linear model this is precisely the result obtained for the fixed-point susceptibilities with linear energy dispersion, see for instance Eq. (6.150).

In Sec. 6.5 we have also emphasized that only for the zero-sound contribution $\tilde{\Pi}_l$

the scaling hypothesis can be used to derive an approximate expression for the physical susceptibility $\Pi(p, i\omega)$, since only $\tilde{\Pi}_\infty(q, i\epsilon)$ is a homogeneous function in the scaling regime. Explicitly we obtain from Eq. (8.71) for $|q|, |\epsilon| \gg 1$ and subsequent transformation to the physical variables

$$\Pi(p, i\omega) \approx \nu_0 \tilde{\Pi}_\infty\left(\tfrac{v_F p}{\Lambda}, \tfrac{i\omega}{\Lambda}\right) = \frac{\nu_0}{2} \frac{v_F p}{i\omega - v_F p}\,, \tag{8.73}$$

where to leading order we have set $\tilde{v} \approx 1$. This corresponds to the result of the linear model, see Eq. (6.152). On the other hand, first transforming back and taking the limit $l \to \infty$ afterwards yields for $|v_F p| \leq \Lambda_0$

$$\Pi(p, i\omega) = \frac{m}{2\pi p} \ln\left(\frac{i\omega + \xi(-p)}{i\omega - \xi(p)}\right)\,. \tag{8.74}$$

The results (8.73) and (8.74) confirm again what we have pointed out in Sec. 5 : Results obtained by using the scaling hypothesis are only valid in the limit $p, \omega \to 0$. Note that in this limit Eq. (8.74) indeed turns into the expression given by Eq. (8.73). The condition for the low-energy form to be adequate can be derived from Eq. (8.74) to be $p^2/2m \ll |v_F p|$, i.e. $|p| \ll 2mv_F$.

From an experimental point of view it would of course be desirable to fix the energy scale at which the asymptotic results for the correlation functions represent a correct description of the physical system. Here we can see explicitly that the answer depends very sensitively not only on the fixed-point value $\tilde{c}$ of the irrelevant coupling $\tilde{c}_l$ *but also on its asymptotic behavior as a function of the flow parameter* l. Note that in deriving the results (8.70) and (8.74) we have set $\tilde{c}_l = c_l = \lambda e^{-l}$, which corresponds to a non-self-consistent treatment of the coupling $\tilde{c}_l$. In this case the combination $\tilde{c}_l/\Lambda = \lambda = 1/(2mv_F^2)$ is a constant involving the initial value of the irrelevant coupling. However, in a self-consistent calculation the exponential decay of $\tilde{c}_l$ may be accelerated or slowed down due a the finite anomalous dimension η at the fixed point and due to finite contributions of $\partial_q^2 \dot{\Gamma}_l^{(2)}(Q)|_{Q=0}$, see Eq. (8.48). In case that the flow is found to be accelerated this implies $\tilde{c}_l/\Lambda \to 0$ when $l \to \infty$, which in turn means *that all non-universal features of the susceptibilities related to the coupling* $\tilde{c}_l$ *will be suppressed due to anomalous scaling.* This can again be seen from Eq. (8.69). Let us assume that $\tilde{c}_l$ decays slightly faster than exponentially in l. In this case $\tilde{c}_l/\Lambda \to 0$, and taking the limit $l \to \infty$ in Eq. (8.69) this time yields

$$\chi'_\Lambda(p, i\omega) \xrightarrow{\Lambda \to 0} \frac{\nu_0}{4\tilde{v}} \ln\left(\frac{\omega^2 + (v_F p)^2}{\omega^2 + (2\Lambda_0 - |v_F p|)^2}\right)\,, \tag{8.75}$$

which is independent of the mass terms and precisely recovers the result obtained for linear dispersion up to $\tilde{v}$ in the prefactor, see Eq. (6.143). In the following section where we study the two-loop flow of the couplings, we will find that the

decay of $\tilde{c}_l$ is indeed accelerated due to anomalous scaling. If we accept the above results for the susceptibilities as representative also for non-perturbative correlation functions, we have found strong evidence that non-universal features in the momentum (and frequency) dependence of the correlation functions are suppressed due to anomalous scaling.
Finally let us discuss the two possible cases when the exponential decay of $\tilde{c}_l$ is slowed down but still arrives at a zero fixed-point value, and, alternatively, when it approaches a non-zero limit. In both cases $\tilde{c}_l/\Lambda \to \infty$, resulting in a complete suppression of the *physical* susceptibilities. This can again be seen from Eq. (8.69): In the limit $l \to \infty$ the r.h.s. of the equation vanishes, and the same will be true for Π_Λ and χ_Λ. In contrast, the *dimensionless* susceptibilities behave completely different. Here, only the fixed-point *value* of $\tilde{c}_l$ is crucial but not the flow towards this point. For $\tilde{c}_l \to 0$ we have already shown that the dimensionless susceptibilities approach the expressions of the linear model, see Eqs. (8.71) and (8.72). On the other hand for $\tilde{c}_l \to \tilde{c} > 0$ the functions Π_l and χ_l' approach finite limits which are different from their linear analogues, while the Peierls contribution χ_l diverges, which can be seen from Eq. (8.65).
Of course it makes little sense to discuss these limits in more detail as long as we do not know the precise flow of $\tilde{c}_l$ at two-loop level. However, as an important result we state that the destination of the physical susceptibilities at the fixed point depends sensitively on the *flow* of the irrelevant coupling $\tilde{c}_l$, which may even drastically alter the physics when its decay is slowed down compared to the canonical exponential decay.

8.5 Self-Consistent Two-Loop Flow

A complete two-loop calculation that also includes the flow of the coupling $\tilde{g}_l$ at this level is very difficult to perform. We will thus proceed in determining the self-consistent two-loop flow of the two-point vertex and combine the resulting flow equations with the one-loop result for the coupling $\tilde{g}_l$. Afterwards we shall demonstrate that the two-loop corrections to the flow of $\tilde{g}_l$ cannot qualitatively change the results, i.e. that they cannot give rise to new fixed points.
The function $\dot{\Gamma}_l^{(2)}(q, i\epsilon)$ which determines the two-loop flow of the couplings Z_l, $\tilde{v}_l$ and $\tilde{c}_l$ is here (in contrast to Eq. (6.57)) determined by

$$\begin{aligned}\dot{\Gamma}_l^{(2)}(q, i\epsilon) &= -\frac{\tilde{g}_l}{2} + \dot{\Gamma}_l^{(2,\mathrm{ZS})}(q, i\epsilon) \\ &\quad + \dot{\Gamma}_l^{(2,\mathrm{P})}(q, i\epsilon) + \dot{\Gamma}_l^{(2,\mathrm{BCS})}(q, i\epsilon) + \mathcal{O}(\tilde{g}_l^3)\,, \end{aligned} \tag{8.76}$$

where we have neglected contributions of order $\sim \tilde{g}_l^2$ to the chemical-potential parameter $\tilde{\mu}_l$. Like in the linear model the zero-sound contribution $\dot{\Gamma}_l^{(2,\mathrm{ZS})}$ can easily be seen to vanish for $|q| < 1$, such that it does not contribute to the flow of the couplings. The contributions of the Peierls and the BCS channel are given by

$$\dot{\Gamma}_l^{(2,\mathrm{P})}(q,i\epsilon) = \tilde{g}_l^2 \int \frac{dq'}{2} \int \frac{d\epsilon'}{2\pi}\, \dot{G}_l(q',i\epsilon')\, \chi_l(q+q',i\epsilon-i\epsilon')\,, \tag{8.77}$$

and

$$\dot{\Gamma}_l^{(2,\mathrm{BCS})}(q,i\epsilon) = -\,\tilde{g}_l^2 \int \frac{dq'}{2} \int \frac{d\epsilon'}{2\pi}\, \dot{G}_l(q',i\epsilon')\, \chi_l'(q'-q,i\epsilon'+i\epsilon)\,. \tag{8.78}$$

The simplest way to proceed is to expand $\chi_l(q+q',i\epsilon-i\epsilon')$ and $\chi_l'(q'-q,i\epsilon'+i\epsilon)$ directly in powers of $\tilde{c}_l$ and to perform the integrations afterwards. Such a procedure is of course only justified if $\tilde{c}_l$ remains small during the whole flow. In case that $\tilde{c}_l$ approaches a fixed-point value which is not small compared to unity the expansion cannot be trusted anymore, and we would have to resort to other methods. However, since $\tilde{c}_l$ is initially small, a Taylor expansion will at least be justified at the beginning of the flow, and the tendency towards a large fixed-point value would also be reflected in a solution of the flow equations relying on an expansion in powers of $\tilde{c}_l$. We will thus proceed in this way.
The rest of the calculations leading to the set of flow equations is a very tedious matter. For instance, to determine the flow of $\tilde{c}_l$ up to order $\sim \tilde{c}_l^2$ we need to expand χ_l and χ_l' up to this order, then we have to perform the integrations, and finally we have to calculate the second order derivative with respect to q at $q = \epsilon = 0$ (or vice-versa). This can be seen from Eq. (8.48). Let us hence only display the results, starting with the flow of the quasi-particle residue,

$$\partial_l Z_l = -\,\eta_l\, Z_l\,, \tag{8.79}$$

where the anomalous dimension is given by

$$\boxed{\begin{aligned} \eta_l \;=\; & \Theta(e^l-2)\,\frac{\tilde{g}_l^2}{16\tilde{v}_l^3}\Big\{(2\tilde{v}_l-\tilde{c}_l)(1-2e^{-l}) \\ & +\frac{\tilde{c}_l^2}{32\tilde{v}_l}\big[512(e^l+\ln 2-l)-887-256e^{-l} \\ & \qquad -32e^{-2l}-8e^{-3l}\big]\Big\}+\mathcal{O}(\tilde{g}_l^3,\tilde{c}_l^3)\,. \end{aligned}} \tag{8.80}$$

For the flow of the velocity parameter we find

$$\begin{aligned}\partial_l \tilde{v}_l &= \Theta(e^l-2)\,\frac{\tilde{g}_l^2}{4\tilde{v}_l^2}\Big\{\,2\tilde{v}_l\,e^{-l}+\tilde{c}_l(l-\ln 2-e^{-l})\\ &\quad+\frac{\tilde{c}_l^2}{16\tilde{v}_l}\big[-48e^l+32(\ln 2-l)+93\\ &\qquad+24e^{-l}+4e^{-2l}+2e^{-3l}\big]\Big\}+\mathcal{O}(\tilde{g}_l^3,\tilde{c}_l^3)\,,\end{aligned} \tag{8.81}$$

and the flow of the curvature parameter is determined by

$$\begin{aligned}\partial_l \tilde{c}_l &= -\tilde{c}_l\left[1+\Theta(e^l-2)\,\frac{\tilde{g}_l^2}{32\tilde{v}_l^2}\left(\tfrac{21}{8}-4e^{-l}-2e^{-2l}-e^{-3l}\right)\right]\\ &\quad+\tilde{c}_l^2\,\Theta(e^l-2)\,\frac{\tilde{g}_l^2}{8\tilde{v}_l^3}\left[2-5e^{-l}-2e^{-2l}\right]+\mathcal{O}(\tilde{g}_l^3,\tilde{c}_l^3)\,.\end{aligned} \tag{8.82}$$

The first thing we can check from these equations is the limit of linear energy dispersion. By simply setting $\tilde{c}_l = 0$ in Eqs. (8.80) and (8.81) we immediately see that the corresponding flow equations of the linear model are recovered, see Eqs. (6.62) and (6.63). Furthermore it can be shown that the derivatives of $\tilde{v}_l$ and $\tilde{c}_l$ are not continuous at $l = \ln 2$, but the couplings themselves of course are. This is also true for the anomalous dimension η_l, and can be seen from Eq. (8.80) by inserting $l = \ln 2$ in the expression within the curly brackets. For instance the coefficient of the $\tilde{c}_l^2$-term then yields $2\cdot 512 - 887 - 256/2 - 32/4 - 8/8 = 0$.
Before we present a numerical integration of the flow equations let us discuss wether they open up the possibility of a new fixed point. To find the correct answer we still have to add the two-loop equation for the coupling $\tilde{g}_l$, which we do not know yet at this level. Fortunately it turns out that we can find a solution to the problem without knowing all the details of the flow. Let us first consider the one-loop result given in Eq. (8.58), which for consistency reasons we should also expand up to order $\sim \tilde{c}_l^2$. This yields

$$\partial_l \tilde{g}_l = -\,\Theta(e^l-2)\,\frac{\tilde{g}_l^2}{2\tilde{v}_l}\left(\frac{\tilde{c}_l}{\tilde{v}_l}\right)^2+\mathcal{O}(\tilde{g}_l^3,\tilde{c}_l^4)\,. \tag{8.83}$$

As we have already emphasized in the vicinity of a fixed point the flow of the couplings must stop, i.e. their l-derivatives must vanish. This is expected to happen for $l \gg 1$, such that for the determination of possible fixed points the asymptotics of the flow equations are relevant. As concerns the flow of $\tilde{g}_l$ we know from our two-loop solution of the linear model (which represents the leading order

of an expansion in $\tilde{c}_l$) that for large l the r.h.s. of the flow equation vanishes, see Eq. (6.101). This in turn means that the two-loop flow of the model including curvature must asymptotically be proportional to a power of $\tilde{c}_l$. Hence for large l in the vicinity of a fixed point the two-loop flow of $\tilde{g}_l$ will be given by an equation of the form

$$0 \simeq \frac{\tilde{g}_l^2}{\tilde{v}_l}\,\frac{\tilde{c}_l}{\tilde{v}_l}\Big[-\frac{\tilde{c}_l}{\tilde{v}_l}+\tilde{g}_l\Big(R_l+\frac{\tilde{c}_l}{\tilde{v}_l}S_l\Big)\Big]\,, \tag{8.84}$$

where "$\simeq$" like before means "asymptotically equal". The unknown functions R_l and S_l may implicitly depend on $\tilde{v}_l$ but not on $\tilde{g}_l$ or $\tilde{c}_l$, and they may also equal zero. Equivalently, the asymptotic forms of the flow equations for $\tilde{v}_l$ and $\tilde{c}_l$ are

$$0 \simeq \frac{\tilde{g}_l^2}{\tilde{v}_l}\,\frac{\tilde{c}_l}{\tilde{v}_l}\Big[l-3\,\frac{\tilde{c}_l}{\tilde{v}_l}\,e^l\Big]\,, \tag{8.85}$$

and

$$0 \simeq \tilde{c}_l\Big[-4-\frac{21}{64}\Big(\frac{\tilde{g}_l}{\tilde{v}_l}\Big)^2+\frac{\tilde{c}_l}{\tilde{v}_l}\Big(\frac{\tilde{g}_l}{\tilde{v}_l}\Big)^2\Big]\,, \tag{8.86}$$

respectively. From the last equation we immediately see that principally two solutions are possible. The first one is simply given by

$$\tilde{c}_l \to 0\,, \quad \text{for} \quad l\to\infty\,, \tag{8.87}$$

while a possible non-trivial solution would have the form

$$\frac{\tilde{c}_l}{\tilde{v}_l} \to \frac{21}{64}+4\Big(\frac{\tilde{v}_l}{\tilde{g}_l}\Big)^2\,, \quad \text{for} \quad l\to\infty\,. \tag{8.88}$$

Let us first discuss the implications of Eq. (8.87), which leads to the well-known Luttinger-liquid fixed-point manifold. Note that $\tilde{c}=\tilde{c}_\infty=0$ is consistent with Eq. (8.84) provided $\tilde{g}/\tilde{v}<\infty$. The simplest way to satisfy this condition is to assume $\tilde{g}_l\to\tilde{g}=\text{const}$ and $\tilde{v}_l\to\tilde{v}=\text{const}$, which in turn implies $\tilde{c}_l\to 0$ at least as $\tilde{c}_l\sim e^{-(1+x)l/2}$ due to Eq. (8.85), for some positive x. The anomalous dimension will then approach a finite fixed-point value, and the system represents a Luttinger liquid.

On the other hand, the assumption that $\tilde{c}_l/\tilde{v}_l$ in Eq. (8.88) approches a non-zero fixed-point value can be shown to lead to a contradiction with the flow equation (8.81) for $\tilde{v}_l$. For $\tilde{c}_l/\tilde{v}_l$ to remain finite when $l\to\infty$ the ratio $\tilde{v}_l/\tilde{g}_l$ must remain finite as well, i.e. $0\le\tilde{v}/\tilde{g}<\infty$. In case that $\tilde{v}/\tilde{g}<\infty$ but non-zero Eq. (8.85) implies that $\tilde{c}_l\sim e^{-(1+x)l}$, since $\tilde{c}_l/\tilde{v}_l$ is finite by assumption. Consequently, the couplings $\tilde{v}_l$ and $\tilde{g}_l$ also have to vanish like $\sim e^{-(1+x)l}$ for the ratios $\tilde{c}_l/\tilde{v}_l$ and $\tilde{v}_l/\tilde{g}_l$ to approach finite fixed-point values. Although these results are compatible with

Eq. (8.84) they lead to a contradiction with the original flow equation (8.81) for $\tilde{v}_l$. Inserting $\tilde{g}_l \sim e^{-(1+x)l}$ and $\tilde{c}_l \sim e^{-(1+x)l}$ in this equation it is easy to see that this cannot lead to an exponential decay for the flow of $\tilde{v}_l$. Instead, $\tilde{v}_l$ will approach a finite and non-zero fixed-point value, leading in turn to a diverging ratio $\tilde{v}_l/\tilde{g}_l$ – in contradiction with the assumption. Similarly it can be shown that the case $\tilde{c}/\tilde{v} = 21/64$, i.e. $\tilde{v}/\tilde{g} = 0$, leads to a contradiction.
We thus have shown that only the Luttinger-liquid fixed-point manifold is a regular solution of the flow equations. Note that our reasoning was independent of the explicit form of the functions R_l and S_l, such that a complete two-loop calculation four $\tilde{g}_l$ is not necessary to confirm this result. Since at the Luttinger-liquid fixed point the coupling $\tilde{c}_l$ flows to zero the corrections to the results of the linear model will remain small, in particular the corrections to the one-loop flow of $\tilde{g}_l$ will be negligible for $\tilde{g}_l \ll 1$. In Figs. 8.4 and 8.5 we show the flow of the couplings in the $(\tilde{g}_l, \tilde{c}_l)$ and the $(\tilde{g}_l, \tilde{c}_l)$ plane, obtained by numerical integration of Eqs. (8.81) and (8.82) combined with the one-loop flow of $\tilde{g}_l$, Eq. (8.83). Note that due to the fact that the flow equations depend explicitly on the flow parameter l, nothing forbids the phase-space trajectories to intersect. In Fig. 8.4 we have plotted the combined flow of $\tilde{g}_l$ and $\tilde{c}_l$ for $\tilde{g}_0 = 0.2$ and various initial values for $\tilde{c}_l$. The black dots in the figure mark the initial values of $\tilde{c}_l$ for the three trajectories presented by a solid line. Within the interval $0 \leq l \leq \ln 2$ the value of $\tilde{c}_l$ just decreases exponentially without affecting the value of $\tilde{g}_l$, the flow of which only starts at $l = \ln 2$. Thus the flow first follows the vertical line in Fig. 8.4. When $l = \ln 2$ is reached the common flow is abruptly deviated to the left until it reaches the fixed line $(\tilde{g}, 0)$. The solid curves correspond to the allowed initial values $\tilde{c}_0 = 1/2$, $\tilde{c}_0 = 3/8$ and $\tilde{c}_0 = 1/4$, while for the dotted trajectories $\tilde{c}_0 > 1/2$, which principally contradicts our assumption $c_0 = \lambda \leq 1/2$, see Eq. (8.3). The fixed-point value $\tilde{g}$ turns out to be slightly smaller than the initial value $\tilde{g}_0$, which can also be seen by the approximate non-self-consistent result for $\tilde{g}$ in Eq. (8.61).
The flow in the $(\tilde{g}_l, \tilde{v}_l)$ plane in Fig. 8.5 looks quite differently. This is due to the fact that the flow of $\tilde{v}_l$ always starts at $\tilde{v}_0 = 1$ and rests on this point as long as $l < \ln 2$. We have plotted the common flow of $\tilde{g}_l$ and $\tilde{v}_l$ for the two initial values $\tilde{c}_0 = 1/2$ (solid curves) and $\tilde{c}_0 = 1/3$ (dotted curves). For $l > \ln 2$ the flow starts at the initial values $(\tilde{g}_0, \tilde{v}_0)$ and runs into a fixed line which is represented by the thick solid (dotted) line. This fixed line as a function of $\tilde{g}$ is approximately given by a parabola, which can be understood by the fact that $\tilde{v} \approx 1 + C(\tilde{c}_0)\,\tilde{g}^2$. Here $C(\tilde{c}_0)$ is a constant of the order of unity but different for each initial value of $\tilde{c}_l$. From both figures it is evident that the fixed-point values of the couplings $\tilde{v}_l$ and $\tilde{g}_l$ differ only very slightly from their respective initial values. However, in both cases $\tilde{v}$ and $\tilde{g}$ do depend on the initial value of $\tilde{c}_l$. In Figs. 8.6 and 8.7 the behavior of $\tilde{v}_l$ and $\tilde{g}_l$ as a function of the logarithmic

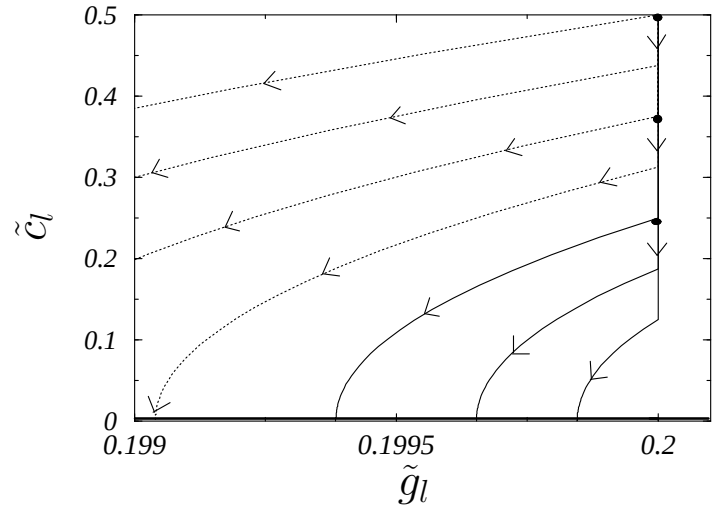

Figure 8.4: Flow of the couplings in the $(\tilde{g}_l, \tilde{c}_l)$ plane for $\tilde{g}_0 = 0.2$ and various initial values of $\tilde{c}_l$. The dotted curves correspond to initial values $\tilde{c}_0 > 1/2$ and the solid trajectories to the values $\tilde{c}_0 = 1/2$, $\tilde{c}_0 = 3/8$ and $\tilde{c}_0 = 1/4$, which are indicated by the black dots. For explanations see the text.

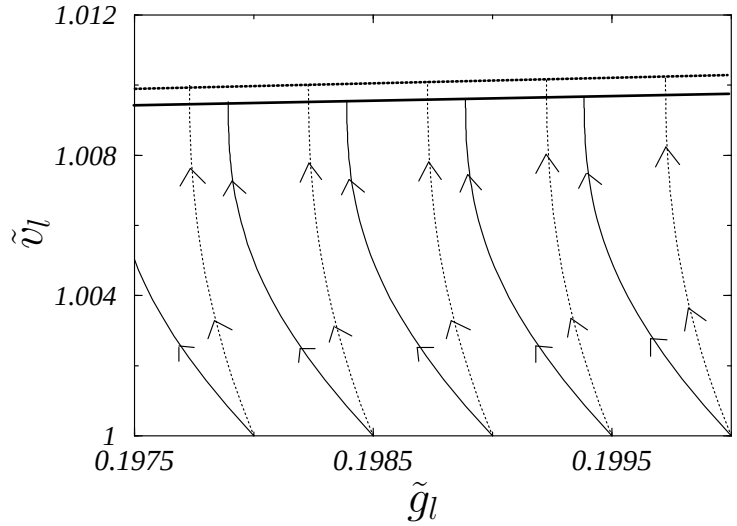

Figure 8.5: Flow of the couplings in the $(\tilde{g}_l, \tilde{v}_l)$ plane. The flow of $\tilde{v}_l$ always starts at $\tilde{v}_0 = 1$ and ends in a fixed line, the location of which depends on the initial value of $\tilde{c}_l$. The solid trajectories correspond to $\tilde{c}_0 = 1/2$ and the dotted ones to $\tilde{c}_0 = 1/3$. The thick solid and dotted lines represent the respective line of fixed points.

scale parameter l for various initial values c_0 is shown. Like above, the results are obtained by numerical integration of the self-consistent two-loop flow equations (8.81) and (8.82), combined with the one-loop result (8.83) for $\tilde{g}_l$. In both cases the fixed-point values are rapidly approached and differ only slightly from the corresponding result for linear dispersion, i.e. for $c_0 = 0$. In case of $\tilde{v}_l$ it can be seen in Fig. 8.6 that for large values of c_0 the fixed-point value is smaller than for linear dispersion, while for small values of c_0 it is larger. This is due to the fact that in the flow equation for $\tilde{v}_l$ the coefficient of the term linear in $\tilde{c}_l$ is positive, and negative for the term proportional to $\tilde{c}_l^2$, resulting in two competing effects. On the other hand, the fixed-point value of $\tilde{g}_l$ increases monotonically with decreasing c_0, which can analytically be understood from the non-self-consistent result in Eq. (8.59). In Fig. 8.7 the self-consistent calculation for $\tilde{g}_l$ is compared with the predictions of the non-self-consistent result, and it can be seen that the significance of self-consistency increases with the initial value c_0. Nonetheless, it does not qualitatively change the results.

Finally let us consider the fixed-point values of η_l and $\tilde{c}_l$. From Eq. (8.80) it can be seen that the fixed-point value of η_l depends crucially on the decay of the coupling $\tilde{c}_l$ and not only on its fixed-point value. Note that the term $\sim \tilde{c}_l^2 e^l$ only vanishes in the limit $l \to \infty$ if $\tilde{c}_l$ decays faster than $\tilde{c}_l \sim e^{-l/2}$. In a non-self-consistent calculation this condition is satisfied since then $\tilde{c}_l = c_l \sim e^{-l}$. In a self-consistent approach the decay of $\tilde{c}_l$ is even accelerated, which can be seen from the asymptotics of Eq. (8.80). For $l \gg 1$ we obtain

$$\partial \tilde{c}_l \simeq -\tilde{c}_l \left[1 + \frac{21}{32}\,\tilde{\eta}\right] + \mathcal{O}(\tilde{c}_l^2, \tilde{g}_l^3)\,, \tag{8.89}$$

where we have inserted $\tilde{\eta} = \tilde{g}^2/8$, which corresponds to the anomalous dimension of the linear model. For large l we hence find $\tilde{c}_l$ to decay exponentially as

$$\boxed{\tilde{c}_l \sim e^{-(1+\frac{21}{32}\,\tilde{\eta})\,l}\,.} \tag{8.90}$$

Inserting this result in Eq. (8.80) and taking the limit $l \to \infty$ we immediately get

$$\boxed{\eta = \tilde{\eta} = \frac{\tilde{g}_0^2}{8}\,,} \tag{8.91}$$

to leading order in $\tilde{g}_0$. We may hence confirm the assertion stated in Sec. 8.1 that the anomalous dimension is left unchanged by curvature at the two-loop level. However, due to the fact that the fixed-point value of $\tilde{g}_l$ itself depends on c_0, this will in general also be true for η in the next-to-leading orders. The flow towards the fixed-point value is of course changed by $\tilde{c}_l$, which is shown in Fig.

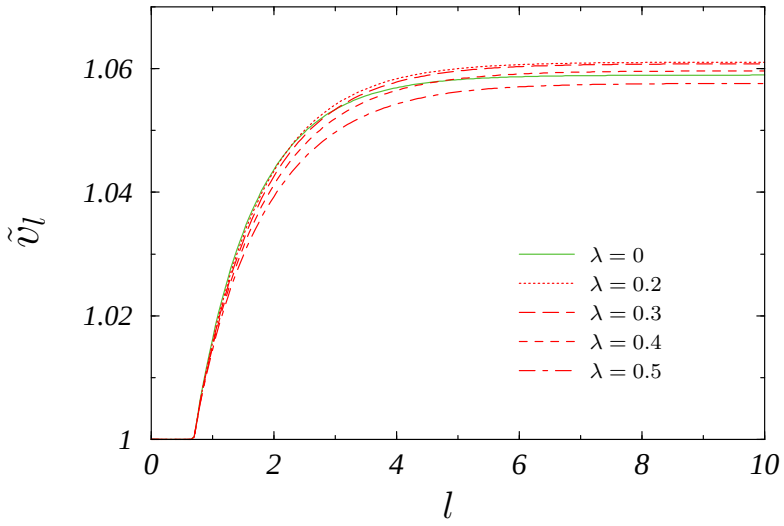

Figure 8.6: The coupling $\tilde{v}_l$ as a function of the logarithmic scale parameter l for various initial values of $c_0 = \lambda$. The solid curve with $\lambda = 0$ corresponds to the result for linear dispersion. Explanations see text.

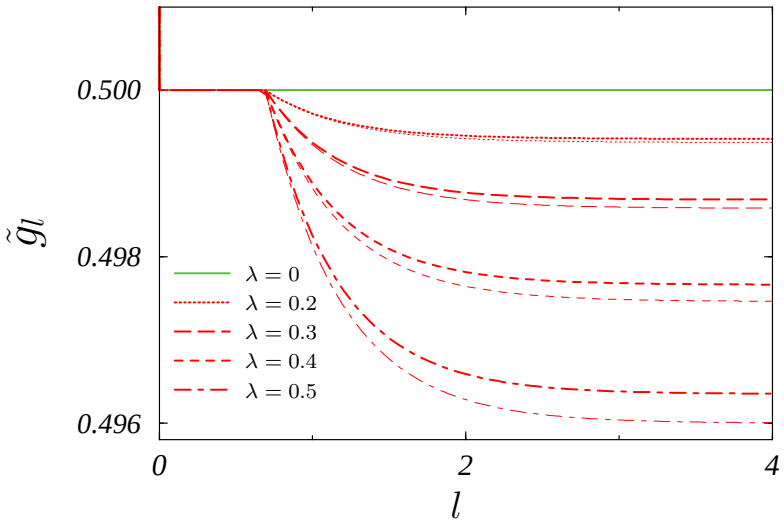

Figure 8.7: The momentum- and frequency-independent part of the four-point vertex, $\tilde{g}_l$, as a function of the logarithmic scale parameter l for various initial values of $c_0 = \lambda$. The thick curves are obtained by numerical integration of the flow equations (8.81), (8.82) and (8.83), while the thin lines follow from Eq. (8.59). The solid line corresponds to the one-loop result for linear dispersion.

8.8 for various initial values $\tilde{c}_0$. It turns out that the common fixed-point value $\eta = \tilde{\eta}$ is reached faster for finite $\tilde{c}_l$ than in the linear model with $c_0 = 0$. This is also true for the flow of Z_l, which is determined by the scale-averaged anomalous dimension $\bar{\eta}_l$, see Eq. (6.115). In Fig. 8.9 we compare the flow of Z_l for the linear model with our present results with finite c_0. In both cases Z_l approaches zero, and the decay is found to be slightly slowed down for $c_0 > 0$. The dashed curves in Fig. 8.9 have been obtained from Eq. (8.82) by replacing $\tilde{c}_l$ with c_l.
In summary we have found that the effects of a curved energy dispersion on the fixed-point values of the couplings are small compared to the leading order given by the model with strictly linear dispersion. In case of $\tilde{v}_l$ and $\tilde{g}_l$ we have found a dependence of $\tilde{v}$ and $\tilde{g}$ on the initial value c_0 of the dimensionless coupling $\tilde{c}_l$ in the next-to-leading orders. As suggested by Haldane [10] this further reduces the universality of the Luttinger-liquid parameters. In case of η_l and Z_l we have seen that the flow towards the fixed point is slightly accelerated compared to the linear model. The most important result is however given by Eq. (8.90). As we have shown in Sec. 8.4 the detailed momentum and frequency dependence of the *physical* susceptibilities at the fixed-point depends crucially on the behavior of the ratio $\tilde{c}_l/\Lambda$ for large l. In a non-self-consistent approach we simply have $\tilde{c}_l/\Lambda = c_0/\Lambda_0$, such that non-universal features in the momentum and frequency dependence related to c_0 are conserved at the fixed point. This is not true anymore if we take $\tilde{c}_l$ self-consistently into account using Eq. (8.90). In this case

$$\frac{\tilde{c}_l}{\Lambda} \sim \frac{c_0}{\Lambda_0}\, e^{-\frac{21}{32}\eta\, l} \quad \stackrel{l\to\infty}{\longrightarrow} \quad 0\,, \tag{8.92}$$

which has been shown to extend the validity of the results for the physical susceptibilities with linear dispersion to arbitrary frequencies and momenta. We expect that this scenario is not only characteristic of perturbative correlation functions such as susceptibilities, but also of non-perturbative ones like the spectral function. For the $k = k_F$ spectral function, which at perturbative level has been shown in Fig. 8.3, we hence expect that the small asymmetries related to the broken particle-hole symmetry will be suppressed in a non-perturbative calculation.

Finally, what can we expect in general from a non-perturbative RG calculation of the spectral function including curvature? Since an analytical expression cannot even be obtained within simple perturbation theory it is obvious that only numerical results can be achieved. Due to the fact that the curvature parameter $\tilde{c}_l$ vanishes at the fixed point, it seems clear that a calculation *using the scaling hypothesis* will at least recover the result of the $q = 0$ scaling function (7.66) for linear dispersion. The asymptotic behavior of the spectral function for $\omega \to 0$ and $|k| = k_F$ is hence expected to remain the same as in the linear model, except

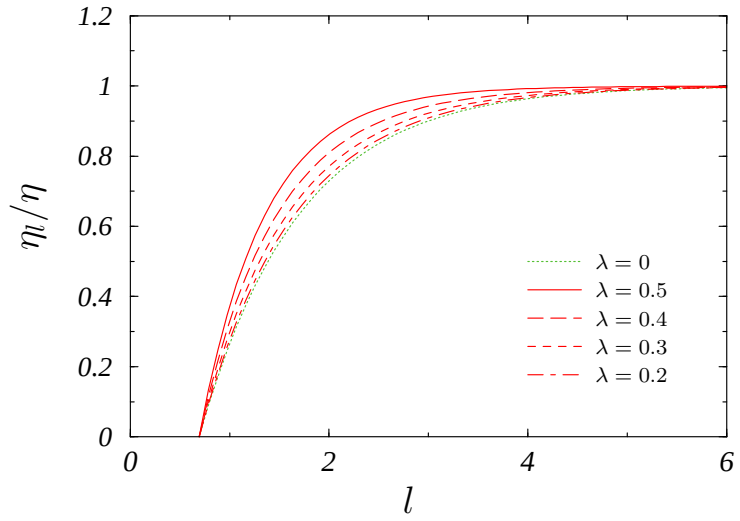

Figure 8.8: Comparison of the flow of the anomalous dimension η_l in units of the fixed-point value η for finite curvature (solid and dashed curves) with the predictions of the linear model (dotted curve). The flow the first set is predicted by Eq. (8.80) with $\tilde{v}_l = 1$ and $\tilde{c}_l = c_l = \lambda e^{-l}$, whole the dotted curve is determined by Eq. (6.115).

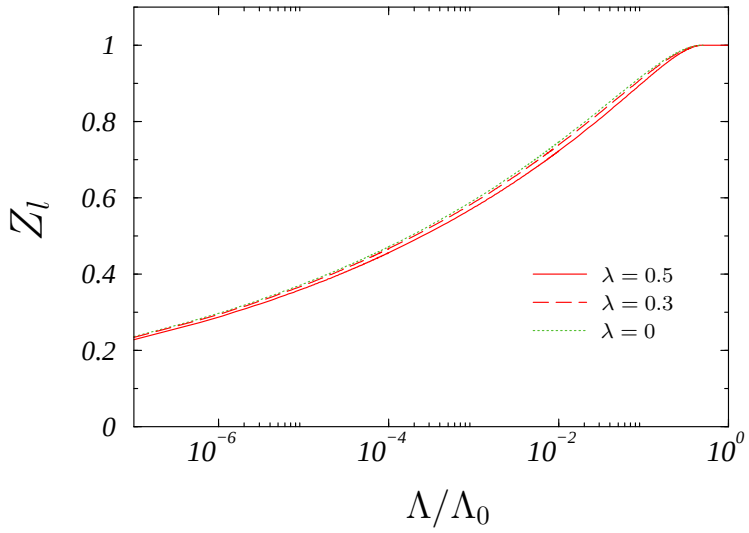

Figure 8.9: The decay of the quasi-particle residue Z_l as a function of the relative energy scale Λ/Λ_0. The dotted curve shows the result of the linear model with $\eta = 0.1$, while the solid and the dashed curves represent the corresponding flow obtained for finite curvature and the same value for η.

for the slightly altered algebraic exponent. In case that we transform back to the physical variables before the limit $l \to \infty$ is taken, we obtain a result which is valid for arbitrary momenta. According to the above discussion we have preliminary evidence that even in this case a self-consistent approach will lead to a suppression of the non-universal features at large frequencies which we have found in the perturbative spectral function for $|k| = k_F$. However, as concerns the momentum-resolved spectral function for $|k| \neq k_F$ we should be more careful with such predictions. Here, the detailed line-shape is more complicated, and depends crucially on the fixed-point value of the charge velocity v_c. In particular it will be important, if the spectral function in the low-energy limit depends exclusively on v_c (in the spinless case), or if a dependence on the bare Fermi velocity v_F is also left. Physically, this could be interpreted as a remainder of single-particle behavior besides the plasmon excitations. As we have shown in Sec. 7.3, yet within the TLM a dependence of the real-space and real-time Green function on v_F remains in the limit of large distances and time scales. Although we have not been able to calculate the effects on the spectral function, one must be aware of the fact that an additional velocity can lead to new singularities. This is for instance known from the TLM including the spin degree of freedom, where different charge and a spin velocities are responsible for two algebraic singularities in the line-shape of the spectral function instead of a single one [93]. On the other hand, single-particle behavior should rather be reflected in an additional δ-like feature. It is then important to recall the central result of Sec. 7.2: A vanishing of the quasi-particle residue Z_l obtained as a result of the RG coupling flow does *not* contradict the presence of a quasi-particle peak in the spectral function for momenta with $|k| \neq k_F$. The calculation of the momentum-resolved spectral function for a curved energy dispersion remains thus an interesting task, which can principally be tackled by means of our ERG formalism.

Chapter 9

Conclusion

In this thesis we derived the flow equations for the one-particle irreducible vertex functions of the Legendre effective action for interacting fermions within the framework of the exact renormalization group (ERG). We presented an explicit construction that allows for a proper scaling towards the true Fermi surface (FS) of the interacting system in arbitrary dimensions. In contrast to other authors [58,61,63] our method also includes the important rescaling steps of the RG. We discussed how the semi-group property of the renormalization group (RG), which is closely related to the concept of universality classes, is reflected within our formalism. It was shown that this general feature of the RG is expressed by the fact that the one-to-one correspondence between the physical and the dimensionless vertices gets lost at the fixed point. We also showed that in the scaling regime the dimensionless two-point vertex has the properties of a scaling function in the sense of dynamic critical phenomena, provided the fixed-point expression is a homogeneous function of the dimensionless variables. According to the scaling hypothesis [80] it is then possible to transform back to the physical vertex functions *after* having performed the fixed-point limit. In general, i.e. when the fixed-point vertex is not homogeneous, this procedure was demonstrated to fail, and no finite result for the physical vertex function can be achieved in this way. Under these circumstances we rather have to transform back to the physical vertices *before* the fixed-point limit is taken.
Like in the theory of dynamic critical phenomena the scaling function is characterized by an invariance under simultaneous scaling of all length and time scales and is assumed to be independent of most of the microscopic details of the initial Hamiltonian ("universality"). We raised the important question concerning the energy range for which the scaling form is adequate, and we showed that mathematically the dimensionless scaling function of non-Fermi liquids is only characteristic of momenta located directly on the FS and zero frequency within our formalism. While the scaling hypothesis assumes that the range of validity

of the fixed-point results for the coupling flow can be extended to momenta close to the FS and frequencies different from zero, we demonstrated with an explicit example that this is not necessarily true in fermionic systems.
The generic model for testing the usefulness of our formalism was the spinless g_2-model for fermions in one spatial dimension. We performed a complete self-consistent two-loop calculation for the flow of the marginal and relevant couplings related to the two- and the four-point vertex. It was shown that at two-loop level the rescaling step of the RG is essential to obtain a finite fixed-point value four the momentum- and frequency-independent part of the four-point vertex (the interaction strength). We also demonstrated explicitly that the introduction of the Dirac sea within our model leads to fixed-point values for the marginal couplings which are different from the model without Dirac sea. The fact that varying cut-off procedures lead to finite renormalizations of the fixed-point results reminds one of being careful with *quantitative* predictions of the RG.
As a next step we tackled the problem of calculating entire correlation functions by means of the one-particle irreducible ERG. While for the susceptibilities of our model we were able to exactly reproduce the results of perturbation theory, for the non-perturbative spectral function we could only give approximate expressions, which however coincide well with the weak-coupling result of the Tomonaga-Luttinger model (TLM) as obtained by means of the bosonization approach. For momenta equal to the Fermi points we even obtained exact agreement. Since our calculation made explicit use of the scaling hypothesis the results are only valid in the immediate vicinity of the Fermi points. To remedy this defect we presented an alternative calculation for the special case of momenta equal to the Fermi points. We again obtained the correct power-law singularity at zero frequency but different behavior for large frequencies, such that the sum rule for the spectral function could be checked and was found to be satisfied. Here it was even possible to calculate the complete flow of the spectral function starting from the scale $\Lambda = \Lambda_0$ until the fixed point at $\Lambda = 0$ is reached. A crossover from a Fermi-liquid-like spectral function for large values of Λ to the power-law behavior of the Luttinger-liquid at $\Lambda = 0$ was found. The sum rule for the spectral weight was again checked and found to be satisfied independently of scale: With decreasing Λ the spectral weight switches smoothly from the δ-function residue to the continuous part of the spectral function. Following a suggestion of Zanchi [58] who interprets the scale Λ as an effective temperature, we have discussed if such an interpretation also applies to the above crossover scenario. By simply replacing Λ with an effective temperature T_{eff} in our result for the spectral function we would get an undamped quasi-particle peak with residue $Z \sim (T_{\text{eff}})^{\eta}$ rather than a broadened power-law feature for finite T_{eff}. Here η is the anomalous dimension. Only in the quantum critical limit $T_{\text{eff}} \to 0$ the generic Luttinger-liquid behavior would be recovered. However, we came to the

conclusion that a direct identification of Λ with T_{eff} is too simple and cannot replace a true finite-temperature calculation. On the other hand, identifying Λ with a transverse hopping amplitude $t_\perp$ to neighboring chains (which appears in quasi-one-dimensional systems) below some finite energy scale predicts the above crossover scenario with $Z \sim (t_\perp^\star)^\eta$. Here, $t_\perp^\star$ is the assumed fixed-point value for the flow of $t_\perp(\Lambda)$ and our result for Z is in qualitative agreement with the result of Ref. [16] and the references therein.
Finally we proposed an approximation scheme that allows for taking the flow of irrelevant couplings systematically into account. As an example we studied the effect of a non-linear correction to the energy dispersion within the spinless g_2-model. We explained how a self-consistent consideration of the dimensionless curvature parameter may lead to new fixed points in coupling space. However, as our main result we simply found small renormalizations of the fixed-point values of the marginal couplings. We could thus confirm Haldane's suggestion [10] that the Luttinger-liquid parameters get renormalized in the next-to-leading orders. Though this shows that the Luttinger-liquid parameters do not only depend on the initial values of the marginal but also on those of irrelevant couplings, a new fixed point or instability could not be detected within our approach.
In a detailed study of the susceptibilities with finite curvature it was also shown that the fixed-point results of correlation functions may depend very sensitively on the *flow* of irrelevant couplings and not only on their fixed-point values. Depending on wether the flow is accelerated or slowed down with respect to the canonical exponential decay, it can happen that a physical susceptibility and its dimensionless analogue do not only differ by some non-universal features but are indeed completely different functions at the fixed-point. Such a scenario would of course drastically alter the physical properties compared to the model that neglects the contribution of the corresponding irrelevant couplings. In our case we found the flow of the curvature parameter to be *accelerated* due to a contribution of the finite anomalous dimension. As a consequence all terms quadratic in the momentum variable (measured relativ to the Fermi points) in the expressions for the physical susceptibilities get suppressed when the curvature parameter is taken into account selfconsistently. Anomalous scaling thus "flattens" the energy dispersion, such that the momentum range for which the linearization of the energy dispersion is a reliable approximation gets enlarged.

In summary we showed by applying our ERG equations to the problem of the g_2-TLM that they provide a powerful tool for describing systems of strongly-correlated fermions in a non-perturbative way. By a careful analysis of the Luttinger-liquid physics we clearly pointed out advantages and limitations of the formalism. Besides the more conventional task of determining the flow of only a finite number of coupling constants, we presented an approximation scheme

that even allows for the calculation of entire correlation functions. Our result for the momentum-resolved spectral function is rather promising, and it seems principally feasible to derive corresponding expressions for more complicated situations, for instance when the spin degree of freedom or backscattering is included. Furthermore the systematic inclusion of irrelevant couplings into the set of flow equations opens the door for the detection of fixed-points which are inaccessible by other methods like the field theoretic RG or conventional momentum-shell techniques.

Appendix A

The Flow Equation for $\mathbf{\Gamma^{(6)}_{\Lambda}}$

In this appendix we show how the different contributions to the flow of the six-point vertex may be obtained from Eq. (3.45). As the procedure is the same for all the various terms on the r.h.s. of this equation we pick out just one of them. To this end let us define

$$\dot{\Gamma}^{\Lambda}_{3}[\bar{\varphi},\varphi] = \zeta \int_K \int_{K'} \dot{G}_\Lambda(K)\,(\boldsymbol{\delta\Gamma}^{\Lambda}_{sub})^{22}_{KK'}\,G_\Lambda(K')\,(\boldsymbol{\delta\Gamma}^{\Lambda}_{sub})^{22}_{K'K}\,, \tag{A.1}$$

which corresponds to the third term on the r.h.s. of Eq. (3.45). Now using Eq. (2.24) and applying the functional derivatives to both sides of Eq. (3.45), for the l.h.s. we simply get

$$\begin{aligned} -\zeta \frac{\delta^6 \partial_\Lambda \Gamma^\Lambda[\bar{\varphi},\varphi]}{\delta\bar{\varphi}_{K_1'}\delta\bar{\varphi}_{K_2'}\delta\bar{\varphi}_{K_3'}\delta\varphi_{K_3}\delta\varphi_{K_2}\delta\varphi_{K_1}}\Big|_{\bar{\varphi}=\varphi=0} &= \partial_\Lambda \bar{\Gamma}^{(6)}_{\Lambda}(K_1',K_2',K_3';K_3,K_2,K_1) \\ &= \partial_\Lambda \Gamma^{(6)}_{\Lambda}(K_1',K_2',K_3';K_3,K_2,K_1) \\ &\quad \times \delta(K_1'+K_2'+K_3'-K_1-K_2-K_3)\,, \end{aligned} \tag{A.2}$$

while for the contribution of $\dot{\Gamma}^{\Lambda}_{3}$ to the r.h.s. we need the combination

$$\begin{aligned} & -\frac{\delta^6}{\delta\bar{\varphi}_{K_1'}\delta\bar{\varphi}_{K_2'}\delta\bar{\varphi}_{K_3'}\delta\varphi_{K_3}\delta\varphi_{K_2}\delta\varphi_{K_1}}\Big[(\boldsymbol{\delta\Gamma}^{\Lambda}_{sub})^{22}_{KK'}\,(\boldsymbol{\delta\Gamma}^{\Lambda}_{sub})^{22}_{K'K}\Big]\Big|_{\bar{\varphi}=\varphi=0} \\ = \; & -\frac{\delta^6}{\delta\bar{\varphi}_{K_1'}\delta\bar{\varphi}_{K_2'}\delta\bar{\varphi}_{K_3'}\delta\varphi_{K_3}\delta\varphi_{K_2}\delta\varphi_{K_1}} \\ \times & \Big[\Big(\frac{\delta^2\Gamma^\Lambda}{\delta\varphi_K\delta\bar{\varphi}_{K'}} - \Sigma_\Lambda(K)\,\delta(K-K')\Big)\Big(\frac{\delta^2\Gamma^\Lambda}{\delta\varphi_{K'}\delta\bar{\varphi}_K} - \Sigma_\Lambda(K')\,\delta(K-K')\Big)\Big]\Big|^{\bar{\varphi}=0}_{\varphi=0}. \end{aligned} \tag{A.3}$$

Here we have included the ζ-factor of Eq. (A.1) and used Eq. (3.49). From the $2^6 = 64$ terms produced by the product rule only 18 terms will survive. First of all this is due to the fact that according to the definition of the self-energy in Eq. (3.28) , the two contributions for which all derivatives act on just one of the two factors vanish. Furthermore, without symmetry breaking the particle-number has to be conserved, i.e. the number of $\bar\varphi$-derivatives acting on Γ^Λ must equal the number of φ-derivatives. Consequently, in Eq. (A.4) only two qualitatively different choices are possible: four derivatives (two $\bar\varphi$-derivatives and two φ-derivatives) acting on the first and the remaining two derivatives acting on the second factor, or vice versa. For each of the two cases there are nine possible orderings of the arguments which yield, by rearranging the order, different ζ-factors. We may proceed by just choosing one representative for each case, finding the other terms by demanding the whole expression to be anti-symmetric.

Case 1: We apply the $\bar\varphi_{K_3'}$- and the φ_{K_3}-derivative to the second factor in Eq. (A.3) and the rest to the first factor. Keeping in mind that second derivatives of $\Gamma^\Lambda[\bar\varphi,\varphi]$ lead to even functionals, the product rule yields for this particular choice

$$\begin{aligned}
\rightarrow\ & -\Big[\frac{\delta^6\Gamma^\Lambda[\bar\varphi,\varphi]}{\delta\bar\varphi_{K_1'}\delta\bar\varphi_{K_2'}\delta\bar\varphi_{K'}\delta\varphi_K\delta\varphi_{K_2}\delta\varphi_{K_1}}\,\frac{\delta^4\Gamma^\Lambda[\bar\varphi,\varphi]}{\delta\bar\varphi_{K_3'}\delta\bar\varphi_K\delta\varphi_{K'}\delta\varphi_{K_3}}\Big]_{\bar\varphi=\varphi=0}\\
=\ & \zeta\,\bar\Gamma^{(6)}_\Lambda(K_1',K_2',K';K,K_2,K_1)\,\bar\Gamma^{(4)}_\Lambda(K_3',K;K',K_3)\\
=\ & \zeta\,\Gamma^{(6)}_\Lambda(K_1',K_2',K';K,K_2,K_1)\,\Gamma^{(4)}_\Lambda(K_3',K;K',K_3)\\
\times\ & \delta(K_3'+K-K'-K_3)\,\delta(K_1'+K_2'+K_3'-K_1-K_2-K_3)\,. \qquad \text{(A.4)}
\end{aligned}$$

Case 2: We apply the $\bar\varphi_{K_3'}$- and the φ_{K_3}-derivative to the first and the remaining derivatives to the second factor, yielding in the same way as above

$$\begin{aligned}
\rightarrow\ & \zeta\,\bar\Gamma^{(4)}_\Lambda(K_3',K';K,K_3)\,\bar\Gamma^{(6)}_\Lambda(K_1',K_2',K;K',K_2,K_1)\\
=\ & \zeta\,\Gamma^{(6)}_\Lambda(K_1',K_2',K;K',K_2,K_1)\,\Gamma^{(4)}_\Lambda(K_3',K';K,K_3)\\
\times\ & \delta(K_3'+K'-K-K_3)\,\delta(K_1'+K_2'+K_3'-K_1-K_2-K_3)\,. \qquad \text{(A.5)}
\end{aligned}$$

Note that this is the same as in Eq. (A.4) with the role of K and K' interchanged. All other terms produced by the product rule are now obtained by demanding that the whole expression has to be anti-symmetric with respect to permutations of the outer labels within the two variable sets. From Eqs. (A.4) and (A.5) we see that both terms are already anti-symmetric with respect to the exchange of

K_1' and K_2' as well as the exchange of K_1 and K_2. Hence to anti-symmetrize the whole expression we just have to apply the operators $\mathcal{A}_{(1',2'),3'}$ and $\mathcal{A}_{3,(2,1)}$ defined in Eqs. (3.56) and (3.57). Note that this yields nine different terms, since for the labels K_3' and K_3 there are three choices each.
Finally observe that the second δ-function in Eqs. (A.4) and (A.5) is due to overall energy, momentum and σ conservation and also appears in Eq. (A.2). Inserting these results into Eq. (A.1) and using the first δ-function, one time to remove the K'- and one time to remove the K-integration, we get

$$-\zeta \left.\frac{\delta^6 \dot{\Gamma}_3^{\Lambda}[\bar{\varphi},\varphi]}{\delta\bar{\varphi}_{K_1'}\delta\bar{\varphi}_{K_2'}\delta\bar{\varphi}_{K_3'}\delta\varphi_{K_3}\delta\varphi_{K_2}\delta\varphi_{K_1}}\right|_{\bar{\varphi}=\varphi=0} = \tag{A.6}$$

$$\Bigg\{ 9\,\zeta\,\mathcal{A}_{(1',2'),3'}\mathcal{A}_{3,(2,1)} \int_K \Big[\Big(\dot{G}_\Lambda(K) G_\Lambda(K') + G_\Lambda(K)\dot{G}_\Lambda(K') \Big) \times \Gamma_\Lambda^{(4)}(K_3', K'; K, K_3)\, \Gamma_\Lambda^{(6)}(K_1', K_2', K; K', K_2, K_1) \Big]_{K'=K_3-K_3'+K} \Bigg\}$$

$$\times\, \delta(K_1' + K_2' + K_3' - K_1 - K_2 - K_3)\,. \tag{A.7}$$

This leads, after factoring out the overall δ-function, to the fourth term on the r.h.s. of the flow equation for the six-point vertex, Eq. (3.54). In the same way we may easily derive the other contributions to Eq. (3.54).

Appendix B

Scale-Averaged Couplings at the Fixed Point

In this appendix we proof a little Lemma concerning the fixed-point value of an arbitrary scale-averaged flow parameter x_l , which we define by

$$\bar{x}_l = \frac{1}{l} \int_0^l dt\, x_t \,. \tag{B.1}$$

The statement is that given $\lim_{l\to\infty} x_l = x < \infty$ as well as $|x_l| < \infty$ this implies

$$\lim_{l\to\infty} \bar{x}_l = x \,. \tag{B.2}$$

where $x \equiv \lim_{l\to\infty} x_l$. The fixed-point value of the scale average hence equals the fixed-point value of the coupling itself.

Proof:

$$\begin{aligned} \frac{1}{l} \int_0^l dt\, x_t &= \frac{1}{l} \int_0^l dt \,\big(x + x_t - x\big) \\ &= x + \frac{1}{l} \Big(\int_0^{\sqrt{l}} + \int_{\sqrt{l}}^l \Big) dt\, \Delta x_t \,, \end{aligned} \tag{B.3}$$

where $\Delta x_t = x_t - x$. According to a basic mathematical theorem [99] we may write

$$\frac{1}{l} \Big(\int_0^{\sqrt{l}} + \int_{\sqrt{l}}^l \Big) dt\, \Delta x_t = \Delta x_{\tau_l} \frac{1}{l} \int_0^{\sqrt{l}} dt + \Delta x_{\tilde{\tau}_l} \frac{1}{l} \int_{\sqrt{l}}^l dt$$

$$= \frac{1}{\sqrt{l}}\,\Delta x_{\tau_l} + \Big(1 - \frac{1}{\sqrt{l}}\Big)\Delta x_{\tilde{\tau}_l}\,, \tag{B.4}$$

for some $\tau_l \in [0, \sqrt{l}]$ and some $\tilde{\tau}_l \in [\sqrt{l}, l]$. Now in the limit $l \to \infty$ the first term on the r.h.s. of Eq. (B.4) must vanish since by assumption Δx_{τ_l} is bounded from above and below. The second term vanishes due to the fact that $\tilde{\tau}_l \to \infty$ when $l \to \infty$ and $\Delta x = 0$ by its definition. Thus, the only term that remains for $l \to \infty$ on the r.h.s. of Eq. (B.3) is x. $\square$

Appendix C

Analytic Continuation of the Two-Point Scaling Function

In this appendix we perform the analytic continuation of the inverse propagator $\tilde{r}_\infty(q, i\epsilon)$ determined by Eq. (7.58) and formally obtained by the replacement $i\epsilon \to \epsilon + i0^+$. This will basicly be identical with the problem of analytic continuation of the hypergeometric function $F_\eta(z)$ defined in Eq. (7.57) . Once we have found explicit expressions for $\mathrm{Re}\, F_\eta(x \pm i0^+)$ and $\mathrm{Im}\, F_\eta(x \pm i0^+)$ we can apply them to Eq. (7.58) and show how the approximate results (7.62) and (7.63) for the real and the imaginary part of the retarded two-point scaling function $\tilde{\Gamma}^{(2,sub)}_\infty(q, \epsilon + i0^+)$ can be derived.[1]
The key to a proper analytic continuation of the function $F_\eta(z) \equiv F_\eta(x + iy)$ to the real x-axis is given by the integral representation (7.57) , explicitly

$$\begin{aligned} F_\eta(x \pm i0^+) &= \eta \int_0^1 d\lambda \, \frac{\lambda^{\eta-1}}{1 - \lambda x \mp i0^+} \\ &= \eta \, \text{⨍}\!\!\!\!\!\!\int_0^1 d\lambda \, \frac{\lambda^{\eta-1}}{1-\lambda x} \pm i\pi\, \eta \int_0^1 d\lambda \, \lambda^{\eta-1} \, \delta(1-\lambda x) \,. \end{aligned} \tag{C.1}$$

Here, ⨍ denotes the Cauchy principle value of the given integral. It is then straightforward to show that

$$\mathrm{Im}\, F_\eta(x \pm i0^+) = \pm\, \eta\pi \, \Theta(1 < x) \, |x|^{-\eta} \,. \tag{C.2}$$

For the real part however, a derivation of an explicit expression is less obvious. In this case we use the definition of the Cauchy principle value and introduce

[1] Note that $\mathrm{Re}\, \tilde{r}_\infty(q, \epsilon + i0^+) = \epsilon - \tilde{v}q + \mathrm{Re}\, \tilde{\Gamma}^{(2,sub)}_\infty(q, \epsilon + i0^+)$ and $\mathrm{Im}\, \tilde{r}_\infty(q, \epsilon + i0^+) = \mathrm{Im}\, \tilde{\Gamma}^{(2,sub)}_\infty(q, \epsilon + i0^+)$, such that the problem of analytic continuation of $\tilde{\Gamma}^{(2,sub)}_\infty(q, i\epsilon)$ can be reduced to the analytic continuation of $\tilde{r}_\infty(q, i\epsilon)$ and vice versa.

a positive and small parameter δ to split up the path of integration where the integral kernel is singular. The limit $\delta \to 0$ will then be taken at the very end. Note that the pole in the integrand of the first term on the r.h.s. of Eq. (C.1) is only located within the integration interval if $x > 1$. For $x < 1$ the principle value integral just equals the usual integration, such that we may write

$$\mathrm{Re}\, F_\eta(x \pm i0^+) = \Theta(x<1)\, F_\eta(x) + \Theta(1<x) \lim_{\delta\to 0} F_\eta^{(\delta)}(x)\,, \tag{C.3}$$

with the definition

$$F_\eta^{(\delta)}(x) = \eta \left[\int_0^{|x|^{-1}-\delta} + \int_{|x|^{-1}+\delta}^{\infty} - \int_1^{\infty} \right] d\lambda\, \frac{\lambda^{\eta-1}}{1-\lambda|x|}\,. \tag{C.4}$$

The remaining integrations can be found in standard integration tables [100], and to leading η-order in the prefactors and for arbitrarily small δ we find

$$\begin{aligned} F_\eta^{(\delta)}(x) &= |x|^{-\eta} \Big[F_\eta(1-\delta) - \eta\, F_{1-\eta}(1-\delta) \Big] \\ &\quad + \eta\, |x|^{-1}\, F_{1-\eta}(|x|^{-1})\,. \end{aligned} \tag{C.5}$$

It is now important to notice that the functions $F_\eta(z)$ and $F_{1-\eta}(z)$ both diverge logarithmically at the branch point $z = 1$ of the hypergeometric function, but that the combination in Eq. (C.5) remains finite. To show this we need a general property of the hypergeometric function that can be found in Ref. [91],

$$\begin{aligned} F_b(z) &\equiv {}_2F_1(1,b;1+b;z) \\ &= b \sum_{n=0}^{\infty} \frac{(b)_n}{n!} \Big[\psi(1+n) - \psi(b+n) + \ln(1-z) \Big] (1-z)^n\,, \end{aligned} \tag{C.6}$$

valid for $|\arg(1-z)| < \pi$ and $|1-z| < 1$. Furthermore we have defined $(b)_n = b(b+1)\cdots(b+n-1)$ for $n > 1$, $(b)_0 = 1$ and $\psi(z)$ denotes the Digamma function. In our case we have $z = 1-\delta$, i.e. $1-z = \delta$, so that each term of the series (C.6) is either proportional to δ^n or $\delta^n \ln\delta$. Thus, in the limit $\delta \to 0$ the only term that survives is the one for $n = 0$, which on the other hand diverges logarithmically. Eq. (C.6) then leads to

$$F_\eta(1-\delta) \sim \eta\, [\psi(1) - \psi(\eta) + \ln\delta]\,, \tag{C.7}$$

as well as

$$F_{1-\eta}(1-\delta) \sim \psi(1) - \psi(1-\eta) + \ln\delta\,, \tag{C.8}$$

to leading order in the prefactor. In the relevant combination of Eq. (C.5) the $\ln\delta$ contributions cancel each other and the limit $\delta \to 0$ remains thus finite. Furthermore using the fact that [91]

$$\psi(1-\eta) - \psi(\eta) = \pi \, \cot(\pi\eta) \approx \frac{1}{\eta} \,, \tag{C.9}$$

we get

$$\lim_{\delta\to 0} F_\eta^{(\delta)}(x) = |x|^{-\eta} + \eta \, |x|^{-1} \, F_{1-\eta}(|x|^{-1}) \,. \tag{C.10}$$

Inserting this on the r.h.s. of Eq. (C.3) we finally obtain

$$\begin{aligned} \mathrm{Re}\, F_\eta(x \pm i0^+) &= \Theta(x<1)\, F_\eta(x) \\ &\quad + \Theta(1<x) \Big[\, |x|^{-\eta} + \eta \, |x|^{-1} \, F_{1-\eta}(|x|^{-1}) \, \Big] \,. \end{aligned} \tag{C.11}$$

In this particular form the expression for $\mathrm{Re}\, F_\eta(x \pm i0^+)$ applies to the third and the fourth term on the r.h.s. of Eq. (7.58), for which even in the scaling limit the argument x remains of the order of unity. For the first and the second term however $|x|$ becomes large in the scaling limit[2], and Eq. (C.11) may further be simplified. Applying the transformation formula (7.59) to the first term on the r.h.s. of Eq. (C.11) (note that only for this term the application is allowed) we get

$$\begin{aligned} \mathrm{Re}\, F_\eta(x \pm i0^+) &= \big[\, \Theta(-x) + \Theta(1<x) \, \big] \, \big[\, |x|^{-\eta} + \eta \, x^{-1} \, F_{1-\eta}(x^{-1}) \, \big] \\ &\quad + \Theta(0<x<1) \, F_\eta(|x|) \qquad (C.12) \\ &\approx |x|^{-\eta} \,, \qquad \text{for} \quad |x| \gg 1 \,. \qquad (C.13) \end{aligned}$$

Let us now derive the explicit expressions for $\mathrm{Im}\, \tilde{r}_\infty(q, \epsilon + i0^+)$ and $\mathrm{Re}\, \tilde{r}_\infty(q, \epsilon + i0^+)$ in the scaling limit. First of all we turn our attention to the system at criticality, when the infrared cutoff Λ can be reduced to zero and no finite low-energy scale $\Lambda_\star$ is present; see the discussion in below Eq. (7.78). In this case in the scaling limit we do not only have $|q|, |\epsilon| \gg 1$ but also $|\epsilon \pm \tilde{v} q| \gg 1$, unless precisely $\epsilon = \pm \tilde{v} q$. For the imaginary part of $\tilde{r}_\infty(q, \epsilon + i0^+)$ this leads after appropriate combination of the various terms in Eq. (7.58) directly to the result given in Eq. (7.62). Again, for the real part some more work is to do. Following the above discussion, in the scaling limit we apply Eq. (C.13) to the first two terms of Eq. (7.58) and Eq. (C.11) to the other contributions. This leads to

[2]For the moment we neglect the subtleties related to this limiting procedure, which have been discussed below Eq. (7.78),

$$
\begin{aligned}
&\mathrm{Re}\,\tilde{r}_\infty(q,\epsilon+i0^+)\\
&\quad\approx \Theta(\epsilon s_q<-3\tilde{v}|q|)\,\frac{\epsilon-\tilde{v}q}{2}\,\Big\{\,\Big|\frac{\epsilon s_q-\tilde{v}|q|}{4\tilde{v}}\Big|^{-\eta}+\Big|\frac{\epsilon s_q+\tilde{v}|q|}{2\tilde{v}}\Big|^{-\eta}\\
&\quad\quad+\eta\,|q|^{-\eta}\,\Big[\,F_\eta\Big(\frac{|\epsilon s_q-\tilde{v}|q||}{4\tilde{v}|q|}\Big)-F_\eta\Big(\frac{|\epsilon s_q+\tilde{v}|q||}{2\tilde{v}|q|}\Big)\,\Big]\,\Big\}\\
&\quad\quad+\Theta(-3\tilde{v}|q|<\epsilon s_q)\,\frac{\epsilon-\tilde{v}q}{2}\,\Big\{\,2\,\Big|\frac{\epsilon s_q-\tilde{v}|q|}{4\tilde{v}}\Big|^{-\eta}\\
&\quad\quad+\eta\,|q|^{-\eta}\,\Big[\,\tilde{F}_{1-\eta}\Big(\frac{4\tilde{v}|q|}{|\epsilon s_q-\tilde{v}|q||}\Big)-\tilde{F}_{1-\eta}\Big(\frac{2\tilde{v}|q|}{|\epsilon s_q+\tilde{v}|q||}\Big)\,\Big]\,\Big\}\,,
\end{aligned}
\tag{C.14}
$$

where in the last line we have defined $\tilde{F}_{1-\eta}(z)=z\,F_{1-\eta}(z)$. Following our general approximation strategy we should only keep the leading contributions to this equation. This would imply to neglect all terms proportional to η, i.e. all terms involving hypergeometric functions. Before we do so we have to make sure that the values of these functions remain small. This is not obvious at first sight, since at $\epsilon s_q=-3\tilde{v}|q|$ the arguments of all hypergeometric contributions are equal to one and each single term diverges. The nature of this singularity is logarithmic, which is obvious from the integral representation (7.57). However, approaching the branch point $z=1$ from the left, we find by the same methods presented in the evaluation of the principle value integral in Eq. (C.1) that the combinations $F_\eta(1-\delta_1)-F_\eta(1-\delta_2)$ and $\tilde{F}_{1-\eta}(1-\delta_1)-\tilde{F}_{1-\eta}(1-\delta_2)$ remain finite and small in the limit $\delta_1,\delta_2\to 0$. It is then consistent to neglect these terms. Keeping in mind that in the scaling regime $\mathrm{Re}\,\tilde{r}_\infty(q,\epsilon+i0^+)=\epsilon-\tilde{v}q+\tilde{\Gamma}^{(2)}_\infty(q,\epsilon+i0^+)$ we are finally led to Eq. (7.63).

Let us now turn our attention to the second relevant limiting procedure in the presence of a finite infrared cutoff $\Lambda_\star$, leading to the δ-like spectral function in Eq. (7.82). Following the discussion below this equation we then *first* take the limit $\epsilon\to\tilde{v}q$ and only then we consider the scaling limit $|q|,|\epsilon|\gg 1$. In this case it is advantageous to directly use Eq. (7.58). Due to the fact that the branch cut of the hypergeometric function $F_\eta(z)$ is located on the positive real axis extending from $z=1$ to infinity [91], it is easy to sea that for $\epsilon\to\tilde{v}q$ no finite imaginary part is obtained for the analytic continuation of $\tilde{r}_\infty(q,i\epsilon)$. On the other hand, in the vicinity of $\epsilon=\tilde{v}q$ the real part is to leading order given by

$$
\begin{aligned}
\mathrm{Re}\,\tilde{r}_\infty(q,\epsilon+i0^+) &\approx \frac{1}{2}(\epsilon-\tilde{v}q)\,\big[\,1+F_\eta(-|q|)+(1-F_\eta(-1))|q|^{-\eta}\,\big]\\
&\approx \frac{1}{2}(\epsilon-\tilde{v}q)\,[1+\mathrm{const}\,|q|^{-\eta}]\,.
\end{aligned}
\tag{C.15}
$$

In the first line we have used $F_\eta(0) = 1$ and in the second line the fact that to leading order $F_\eta(-|q|) \approx |q|^{-\eta}$ for $|q| \gg 1$, which directly follows from Eq. (7.59). The term in (C.15) involving the factor $|q|^{-\eta}$ will be subleading in the scaling limit, such that the dominant contribution to $\mathrm{Re}\,\tilde{r}_\infty(q, \epsilon + i0^+)$ is indeed given by Eq. (7.80).

Appendix D

Deutsche Zusammenfassung

D.1 Einleitung

Die Physik wechselwirkender Elektronen in einer Raumdimension gilt heute als Musterbeispiel für Nicht-Fermi-Flüssigkeitsverhalten. Aufgrund des starken Einflusses der Wechselwirkung bricht hier das sonst für metallische Systeme typische Quasiteilchen-Bild einer Landauschen Fermiflüssigkeit zusammen. Die elementaren Anregungen sind nicht mehr fermionischer sondern bosonischer Natur und beschreiben Ladungs- und Spindichte-Wellen, die sich mit unterschiedlichen Geschwindigkeiten ausbreiten; ein Phänomen, das als „Spin-Ladungs-Trennung“ oder auch „Fraktionierung des Elektrons“ bezeichnet wird. Im Jahr 1950 veröffentlichte S. Tomonaga [1] eine grundlegende Arbeit, in der die Prinzipien einer Abbildung von wechselwirkenden Fermionen in einer Raumdimension auf bosonische Freiheitsgrade dargestellt wird. Dieses als „Bosonisierung“ bezeichnete Verfahren erlaubte eine anschauliche Interpretation der niederenergetischen Anregungen solcher Systeme und wurde in der Folge durch Beiträge einer Vielzahl von Autoren [2–4, 6–9] in ein exakt lösbares Modell überführt. Dabei wurde im später so genannten Tomonaga-Luttinger-Modell (TLM) nur der Beitrag von Vorwärtsstreuung berücksichtigt. Für die charkteristischen Eigenschaften korrelierter Elektronen in einer Raumdimension prägte Haldane [10] 1981 den Begriff der „Luttingerflüssigkeit“ .
Die Physik niedrigdimensionaler Fermionensysteme ist aus vielerlei Gründen von Interesse. In den letzten Jahren ist es z.B. gelungen, Materialien herzustellen, die in Bezug auf die Ladungsträgerdynamik stark anisotrope Eigenschaften aufweisen. Der Ladungstransport ist hier effektiv auf zwei oder sogar nur eine Raumdimension beschränkt, so dass die theoretischen Vorhersagen der Luttingerflüssigkeits-Physik experimentell überprüfbar geworden sind. Zum Beispiel wurden mit Hilfe impulsauflösender Fotoemissions-Spektroskopie Anzeichen für Nicht-Fermi-

flüssigkeitsverhalten in den Bechgaard-Salzen [20], den blauen Bronzen $K_{0.3}Mo\,O_3$ und $Rb_{0.3}Mo\,O_3$ [21, 22] und der Lithium lila Bronze $Li_{0.9}Mo_6O_{17}$ [23], sowie anderen Verbindungen [25] entdeckt. Seine besondere Bedeutung erhält die Physik in reduzierten Raumdimensionen jedoch als möglicher Kandidat für die Erklärung der Hochtemperatur-Supraleitung in Schichtmaterialien wie den Kupraten. Wie erst kürzlich von Kivelson et al. [11] gezeigt wurde, ist die Ladungsträger-Dynamik hier im Grenzfall starker Kopplung effektiv auf eine Dimension beschränkt.
Natürlich stellen strikt eindimensionale Modelle eine theoretische Idealisierung dar. Zum besseren Verständnis der Eigenschaften quasi-eindimensionaler Materialien ist es dann wichtig, Modelle zu entwickeln, die einen eingeschränkten Transport senkrecht zur Richtung einer einzelnen Kette zulassen. Dies geschieht z.B. im Modell „gekoppelter Ketten“ [12–16]. Als weitere theoretische Vereinfachung beschreibt das TLM streng genommen nur die Physik genau am quantenkritischen Punkt, also bei verschwindender absoluter Temperatur. Die Frage, inwiefern thermische Fluktuationen die Struktur und die analytischen Eigenschaften der Korrelationsfunktionen beeinflussen, ist Gegenstand aktueller Forschung [17–19].
Unter den theoretischen Methoden, die zur Analyse eindimensionaler Fermionensysteme eingesetz wurden, ist es neben der exakten Bethe-Ansatz-Lösung des eindimensionalen Hubbard-Modells [5,31] vor allem die oben genannte Bosonisierungs-Technik gewesen, die die Natur der elementaren Anregungen des eindimensionalen Elektronengases enthüllt hat. Voraussetzung für die exakte Lösbarkeit dieses Modells sind jedoch zwei Annahmen, die in realistischen Systemen allenfalls näherungsweise erfüllt sind. Dies sind die Annahmen einer strikt linearen Energiedispersion sowie die Beschränkung ausschließlich auf Vorwärtsstreuprozesse. Obwohl z.B. auch der Einfluss von Rückwärtsstreuung prinzipiell mit Hilfe der Bosonisierung beschrieben werden kann, gibt es Methoden, die in solchen Fällen einfacher zu handhaben sind. Dazu gehört z.B. die Technik der Renormierungsgruppe (RG), die wir in einer speziellen Ausprägung in dieser Arbeit entwickelt und auf das Problem des eindimensionalen Elektronengases angewandt haben. Man unterscheidet in der Literatur im Wesentlichen zwischen zwei Formen der RG, die als feldtheoretische RG und als Wilsonsche RG bezeichnet werden. In der theoretischen Festkörperphysik hat sich vor allem letztere durchgesetzt, deren Grundzüge in den siebziger Jahren durch K.G. Wilson entwickelt wurden [34–36]. Wilson entwarf das Bild eines Phasenraum-Flusses in einem unendlichdimensionalen Raum von Kopplungskonstanten (Hamilton-Operatoren), dessen Fixpunkte stabile Zustände des physikalischen Systems beschreiben. Seine Methode basiert auf drei grundlegenden Schritten:

1. Ausintegration von hochenergetischen Freiheitsgraden in einer Impulsschale infinitesimaler Breite,

2. Reskalierung von Impulsen (und Frequenzen in Quantenproblemen) mit einem geeigneten Skalenfaktor, der die ursprüngliche Systemgröße wieder herstellt und

3. Reskalierung der Felder, um sicher zu stellen, dass der Fluss im Kopplungsraum einer Fixpunkt-Bedingung genügt.

Im vergangenen Jahrzehnt hat eine spezielle Weiterentwicklung der Wilsonschen RG besonderes Interesse hervorgerufen, die als exakte Renormierungsgruppe (ERG) bezeichnet wird. Obwohl deren Grundzüge bereits 1972 von Wegner und Houghton [38] formuliert wurden, wobei alle drei der oben genannten Schritte in den Formalismus mit einbezogen wurden, ist die Nützlichkeit der resultierenden Flussgleichungen in der Anwendung auf physikalische Problemstellungen erst in der jüngeren Vergangenheit durch eine größere Zahl von Autoren erkannt worden. Am Anfang dieser Entwicklung steht eine grundlegende Arbeit von Polchinski [39], die eine Vielzahl von Weiterentwicklungen unter anderem in Bereichen der statistischen Physik und Feldtheorie [40–47] sowie in der Festkörperphysik [48–52] nach sich zog. Als Beispiele seien hier Neuformulierungen der ursprünglichen Wilson-Kadanoff-RG [51, 53–55] genannt, Zugänge die Polchiskis Version benutzen [56–58], sowie eine spezielle Form, die sich Wick-geordneter Monome bedient [59–61]. Die vielleicht vielversprechenste Methode benutzt die Einteilchen-irreduziblen Vertexfunktionen des Legendre-Funktionals [44, 50, 52, 62, 63] und wurde unabhängig von Wetterich [40] und Morris [42] vorgeschlagen. Während alle Zugänge zur ERG auf eine formal exakte, unendliche Hierarchie von gekoppelten Differential- oder Rekursionsgleichungen führen, kann die Nützlichkeit des jeweiligen Formalismus aufgrund der zur Lösung der Gleichungen notwendigen Näherungen stark variieren. Zum Beispiel zeigt sich, dass die Lösungen der Polchinski-Gleichungen sehr empfindlich von der speziellen Implementierung der Cutoff-Funktion abhängen, die die Breite der ausintegrierten Impulsschale bestimmt. Diese unphysikalische Eigenschaft tritt in der Einteilchen-irreduziblen Version nicht auf, da die Cutoff-Funktionen hier stets innerhalb von Integralkernen auftreten, was die analytischen Eigenschaften der Flussgleichungen in Bezug auf die Cutoff-Abhängigkeit deutlich verbessert.
Trotz der großen Vielfalt von bereits vorhandenen RG-Methoden bestand aus verschiedenen Gründen die Notwendigkeit, den Morris-Wetterich-Formalismus weiter auszubauen. Tatsächlich hängt die Eignung der verschiedenen Zugänge stark von der jeweiligen physikalischen Fragestellung ab, so dass keine Version in allen Fällen gleichermaßen gut geeignet ist. Zum anderen stand eine Ausdehnung der Einteilchen-irreduziblen RG auf fermionische Systeme noch aus.[1] Ferner erschien

[1] Etwa zeitgleich zu unserer Arbeit [89] wurde eine Einteilchen-irreduzible Version für Fermionen von M. Salmhofer und C. Hohnerkamp [63] vorgeschlagen, die jedoch die wichtigen

es uns von entscheidender Bedeutung, das Reskalieren von Impulsen, Frequenzen und fermionischen Feldern in den Formalismus mit ein zu beziehen. Wie wir in dieser Arbeit mit der Anwendung auf das eindimensionale Elektronengas gezeigt haben, ist dieser Schritt in Zwei-Schleifen-Rechnungen unverzichtbar. Darüber hinaus eröffnet er die Möglichkeit, den Fluss ganzer Korrelationsfunktionen nicht perturbativ zu berechnen, ein Potential der RG, dem bisher nur in einer Arbeit von Ferraz [71] im Rahmen der feldtheoretischen Renormierung Rechnung getragen wurde.

D.2 Überblick über Methoden und Ergebnisse dieser Arbeit

Entwicklung des RG-Formalismus: Im ersten Teil dieser Arbeit wurden die Flussgleichungen für die Einteilchen-irreduziblen Vertexfunktionen sowohl in unreskalierter als auch in reskalierter Form hergeleitet. Obwohl die Notwendigkeit des Reskalierens schon früh betont wurde [36, 65, 66], verzichten viele Autoren auf diesen wichtigen Bestandteil einer vollständigen RG-Transformation [42, 49–54, 58, 61, 63]. Wie wir anhand theoretischer Überlegungen und durch Anwendung auf das Modell spinloser Fermionen in einer Raumdimension gezeigt haben, ist ein solches Vorgehen nur innerhalb von Ein-Schleifen-Näherungen zulässig. In Zwei-Schleifen-Rechnungen können in den unreskalierten Gleichungen Divergenzen im Fluss der Kopplungskonstanten auftreten, die durch den Beitrag eines stark reduzierten oder sogar verschwindenden Quasi-Teilchen-Gewichtes in den reskalierten Größen unterdrückt werden. Eine Interpretation der Divergenzen der unreskalierten Kopplungen als Instabilitäten des physikalischen Systems ist in diesem Fall unzulässig [67, 68]. Eine besondere Schwierigkeit der RG-Methode in der Anwendung auf fermionische Systeme besteht in der Bestimmung der Fermifläche des wechselwirkenden Systems. Diese kann als diejenige Untermannigfaltigkeit im Impulsraum beschrieben werden, auf der die Anregungsenergie des Vielteilchensystems verschwindet, und die für eine korrekte Implementierung des Formalismus prinzipiell *zu Beginn* der RG-Transformation bekannt sein muss. Wir haben in dieser Arbeit eine Methode vorgestellt, wie dieses konzeptionelle Problem gelöst werden kann, indem man die Fermifläche als Fixpunktmannigfaltigkeit der Flussgleichungen betrachtet, die wiederum selbstkonsistent bestimmt werden kann. Eine weitere, nicht nur die Notation betreffende Schwierigkeit ergibt sich durch die Einbeziehung des Reskalierens: Jede Vertexfunktion tritt in zwei Formen auf, die am Fixpunkt in subtiler Weise miteinander verbunden sind. Dies sind einerseits die dimensionsbehafteten, physikalischen Vertizes als Funktionen

Reskalierungsschritte nicht mit einschließt.

von Impulsen und Frequenzen, die in den unreskalierten Gleichungen auftreten, und andererseits die dimensionslosen, reskalierten Vertizes als Funktionen dimensionsloser Variablen. Solange der Flussparameter der RG endlich bleibt, besteht ein eineindeutiger Zusammenhang zwischen beiden Formen, der durch die Skalierungsgleichung (4.29) gegeben ist. Wie wir durch theoretische Überlegungen und auch anhand von Beispielen gezeigt haben, können die Eigenschaften beider Formen am Fixpunkt jedoch im Extremfall sehr verschieden sein. In solchen Fällen muss die Tatsache berücksichtigt werden, dass die Fixpunktresultate der Vertexfunktionen von Nicht-Fermiflüssigkeiten streng genommen nur für verschwindende Frequenzen und für Impulse direkt auf der Fermifläche Gültigkeit besitzen. Die Ausdehnung auf einen physikalisch sinnvollen Bereich, der die nähere Umgebung der Fermifläche mit einschließt, so wie es die Skalenhypothese von Halperin und Hohenberg [80, 81] im Kontext dynamischer kritischer Phänomene fordert, ist dann nicht möglich. Im Normalfall jedoch ist die Skalenhypothese anwendbar, und die dimensionslosen Vertexfunktionen haben am Fixpunkt die Eigenschaften physikalischer Skalenfunktionen. Die Frage, inwieweit die Skalenfunktionen von den mikroskopischen Details des ursprünglichen Hamilton-Operators abhängen, ist eng mit dem Konzept der Universalitätsklassen der RG verknüpft und war wiederholt Gegenstand dieser Arbeit. Insbesondere die Einbeziehung irrelevanter Kopplungen in den Satz von Flussgleichungen hat gezeigt, dass die Fixpunktwerte der marginalen Kopplungskonstanten von den Anfangswerten irrelevanter Kopplungen abhängen.

Anwendung auf das spinlose g_2-Modell: Um die Nützlichkeit der reskalierten RG-Gleichungen für fermionische Systeme zu testen und den Formalismus gewissermaßen zu kalibrieren, haben wir das einfachste Modell einer Nicht-Fermiflüssigkeit ausgewählt, für das sich neben numerischen auch analytische Ergebnisse formulieren lassen. Dies ist das weiter oben beschriebene, eindimensionale Elektronengas unter Vernachlässigung von Spin-Freiheitsgraden und Rückstreuprozessen. Zunächst wurde eine vollständige, selbstkonsistente Zwei-Schleifen-Rechnung für die marginalen und relevanten Kopplungskonstanten durchgeführt. Dabei haben wir im Detail die Rolle des Energieband-Cutoffs Λ studiert, der für die Konstruktion der RG eine zentrale Rolle spielt, und dessen Anfangswert Λ_0 in unserem Modell unter anderem auch die Reichweite der Wechselwirkung im Impulsraum simuliert. Es zeigte sich, dass die Fixpunktwerte der verschiedenen Kopplungen zwar unabhängig vom expliziten numerischen Wert von Λ_0 sind. Jedoch hängen sie für schwache Kopplung in den Korrekturen zur führenden Ordnung davon ab, ob der Cutoff zu Beginn endlich oder unendlich ist. Wie wir gezeigt haben, entspricht ein anfänglich unendlicher Band-Cutoff im Wesentlichen der Einführung des Dirac-Sees. Somit konnte eine Vermutung von Schulz und Shastry [92], wonach der Wert für die anomale Dimension durch die Einführung

des Dirac-Sees beeinflusst wird, innerhalb unseres Modells bestätigt werden. Dieses Ergebnis mahnt auch zur Vorsicht bei quantitativen Vorhersagen der RG, da physikalisch sinnvolle Aussagen nicht von mathematischen Konstruktionen wie dem Dirac-See abhängen dürfen. In führender Ordnung ist das Resultat für die anomale Dimension jedoch in beiden Fällen identisch mit dem Bosonisierungsergebnis des TLM für schwache Kopplung. Ferner zeigte unsere Rechnung, dass auf Zwei-Schleifen-Niveau der Beitrag der Reskalierungsterme zur Flussgleichung des impuls- und frequenzunabhängigen Anteils des Vierpunkt-Vertex (der Wechselwirkungskonstanten) nicht vernachlässigt werden darf: Während die unreskalierte Kopplung bei einem endlichen Wert des Flussparameters divergiert, sorgt der Beitrag vom Reskalieren dafür, dass die zugeordnete dimensionslose Wechselwirkungskonstante endlich bleibt.

In einem sehr viel weiter reichenden Schritt haben wir dann ein Näherungsverfahren vorgeschlagen, mit dessen Hilfe die vollständige Berechnung von Korrelationsfunktionen innerhalb der RG möglich wird. Zunächst wurde in diesem Zusammenhang die Spetralfunktion des Modells in Störungstheorie zweiter Ordnung berechnet, ein Ergebnis, das mit Hilfe unseres RG-Formalismus *exakt* reproduziert werden kann. Auf diesem Level war es daher möglich, den Fluss bestimmter Kopplungskonstanten, so wie er in den konventionellen RG-Zugängen ermittelt wird, mit dem Fluss der dazu gehörenden Korrelationsfunktion direkt zu vergleichen. Hier zeigte sich explizit, dass z.B. der Fluss des Quasiteilchen-Residuums ausschließlich die Eigenschaften der Spektralfunktion für Impulse direkt auf der Fermifläche (hier: den Fermipunkten) beschreibt. Eine Ausdehnung des Fixpunkt-Resultats auf Impulse k nahe den Fermipunkten $\pm k_F$ erwies sich hingegen als unzulässig. Ob eine solche Einschränkung auch für die nicht perturbative Spektralfunktion gilt, konnte innerhalb unseres Formalismus nicht zweifelsfrei geklärt werden. Jedoch gelang es unter Verwendung der Halperinschen Skalenhypothese, ein nicht triviales Ergebnis für die impulsaufgelöste Spektralfunktion aus der Flussgleichung für den Zweipunkt-Vertex abzuleiten, das erstaunlich gut mit dem Bosonisierungsresultat für schwache Kopplung übereinstimmt. Während für Impulse $|k| = k_F$ exakte Übereinstimmung erzielt werden konnte, ergab sich für $|k| \neq k_F$ eine kleine Abweichung in den algebraischen Potenzen der Singularitäten der Spektralfunktion. Für den Spezialfall $|k| = k_F$ konnte dann mit Hilfe einer anderen Methode, die von der Skalenhypothese keinen Gebrauch macht, sogar der Fluss der Spektralfunktion über den gesamten Bereich des Flussparameters von dessen Anfangswert $\Lambda = \Lambda_0$ bis hin zum Fixpunkt bei $\Lambda = 0$ berechnet werden. Es zeigte sich, dass die Spektralfunktion während des Flusses aus einer Deltafunktion und einen kontinuierlichen Anteil besteht, für deren spektrale Gewichte die Summenregel unabhängig vom jeweiligen Wert des Flussparameters Λ erfüllt ist. Erst am Fixpunkt verschwindet der Deltafunktionsanteil vollständig, so dass lediglich die bekannte algebraische Singularität des Bosonisierungsergeb-

nisses übrig bleibt. Einem Vorschlag von Zanchi et al. [72] und Honerkamp et al. [73, 74] folgend, die dem Flussparameter Λ die Bedeutung einer effektiven Temperatur beimessen, wurde diskutiert, ob das oben beschriebene Crossover-Szenario der Spektralfunktion als Funktion der Temperatur physikalisch relevant ist. Obwohl einige Aspekte der Cutoff-Abhängigkeit unseres Modells denen einer Temperaturabhängigkeit ähnlich sind, ist unserer Meinung nach eine direkte Identifizierung fragwürdig und kann eine explizite Rechnung bei endlicher Temperatur nicht ersetzen.
Als letzte Anwendung unseres Formalismus auf Fermionen in einer Raumdimension wurde der Einfluss einer nicht linearen Energiedispersion untersucht. Bisher gibt es nur wenige Arbeiten, die sich quantitativ mit dem Einfluss einer gekrümmten Energiedispersion in eindimensionalen Systemen auseinander setzen. Neben der wichtigen Arbeit von Haldane [10], in der das Konzept der Luttingerflüssigkeiten begründet wurde, sind dies unseres Wissens vor allem eigene Arbeiten im Rahmen der Bosonisierungstechnik [97, 101]. Innerhalb des RG-Formalismus bedeutet die Berücksichtigung von Krümmung die Einbeziehung einer *irrelevanten* Kopplungskonstante in den Satz von Flussgleichungen. Wie weiter oben erwähnt wurde, eignet sich die Einteilchen-irreduzible ERG in ihrer reskalierten Form besonders gut für diese Aufgabe. In einem ersten Schritt wurde zunächst die Spektralfunktion des Modells mit endlicher Krümmung in Störungstheorie zweiter Ordnung für den Spezialfall $|k| = k_F$ berechnet. Der Kurvenverlauf zeigt einige nicht universelle Eigenschaften bei Frequenzen von der Größenordnung des Ultraviolett-Cutoffs Λ_0 , was auf das Fehlen der im linearen Modell vorhandenen perfekten Teilchen-Loch-Symmetrie zurück zu führen ist. Für hinreichend kleine Frequenzen ergibt sich jedoch dieselbe logarithmische Singularität wie zuvor, so dass seitens der Störungstheorie keine wesentliche Änderung der Luttingerflüssigkeitsphysik zu erwarten ist. Für den nicht perturbativen Zugang wurden dann die Flussgleichungen für die marginalen und relevanten Kopplungen, die auch im linearen Modell auftreten, zusammen mit der Gleichung für den irrelevanten Krümmungsparameter aufgestellt. In einer selbstkonsistenten Zwei-Schleifen-Rechnung für den Zweipunkt-Vertex, kombiniert mit einer Ein-Schleifen-Rechnung für den Vierpunkt-Vertex, konnte gezeigt werden, dass der wesentliche Einfluss einer endlichen Krümmung in einer betragsmäßig kleinen Renormierung der Fixpunktwerte der marginalen und relevanten Kopplungen liegt. Neue Fixpunkte neben der Fixpunktmannigfaltigkeit der Luttingerflüssigkeit konnten auch als mögliche Lösung einer vollständigen, selbstkonsistenten Zwei-Schleifen-Rechnung, die den Vierpunkt-Vertex auf diesem Niveau mit einschließt, ausgeschlossen werden. Dieses der physikalischen Intuition entsprechende Ergebnis zeigt dennoch, dass irrelevante Kopplungen die Universalität des generischen linearen Modells weiter verringern können, wie schon von Haldane [10] vermutet wurde. Inbesondere bleibt der Wert für die anomale Dimension

auf Zwei-Schleifen-Niveau unverändert. Die endliche Renormierung des impuls- und frequenzunabhängigen Anteils des Vierpunkt-Vertex durch die Krümmung deutet jedoch darauf hin, dass auch die anomale Dimension jenseits des Zwei-Schleifen-Niveaus renormiert wird. Dies steht in Einklang mit einem früheren Ergebnis, welches im Kontext der Bosonisierung hergeleitet wurde [97]. Als weiteres wichtiges Resultat der RG-Rechnung zeigte ein detailliertes Studium der Suszeptibilitäten des Vierpunkt-Vertex, dass die Eigenschaften der physikalischen Vertexfuntionen und ihrer dimensionslosen Analoga sehr empfindlich vom *Fluss* irrelevanter Kopplungen abhängen können. In unserem Modell ergab sich aufgrund der endlichen anomalen Dimension eine leichte Beschleunigung des kanonisch exponentiellen Abfalls des Krümmungsparameters als Funktion des logarithmischen Flussparameters. Dies führt zu einer Unterdrückung der nicht universellen Impulsabhängigkeiten in den physikalischen Suszeptibilitäten und dehnt somit den Gültigkeitsbereich der linearen Näherung im Impulsraum aus. Es scheint nahe liegend, dass ein ähnliches Verhalten auch in nicht perturbativen Korrelationsfunktionen wie der Spektralfunktion auftritt. In dem hypothetischen Fall einer leichten Verzögerung des exponentiellen Abfalls des Krümmungsparameters würden sich in unserem Modell sogar drastische Unterschiede in den Eigenschaften der physikalischen und der dimensionslosen Vertizes ergeben, die sich nicht mehr nur auf die Unterdrückung nicht universeller Eigenschaften beschränken. Dies belegt auf subtile Weise, dass irrelevante Kopplungen die Physik des Systems entscheidend verändern können.

Insgesamt haben wir mit dieser Arbeit einen RG-Formalismus bereitgestellt, der, wie in der Anwendung auf das spinlose g_2-Modell gezeigt wurde, sogar zur Berechnung nicht perturbativer Korrelationsfunktionen geeignet ist. Diese Möglichkeit geht weit über die üblichen Anwendungen der RG hinaus, die lediglich den Fluss einer endlichen Anzahl von Kopplungskonstanten beschreibt. Entscheidend hierfür erwies sich die Einbeziehung der Reskalierungsschritte, die auch eine systematische Berücksichtigung irrelevanter Kopplungen im Rahmen des konventionellen Kopplungsflusses ermöglichte. Unser Ergebnis für die Spektralfunktion des Tomonaga-Luttinger-Modells gibt in diesem Zusammenhang Anlass zu der Hoffnung, dass sich mit Hilfe der exakten Renormierungsgruppe in Zukunft auch gute Näherungen für Spektralfunktionen komplexerer Modelle berechnen lassen. Der in dieser Arbeit entwickelte Formalismus stellt somit ein viel versprechendes Werkzeug zur Berechnung experimentell messbarer physikalischer Größen dar.

Bibliography

[1] S. Tomonaga, *Remarks on Bloch's Method of Sound Waves applied to Many-Fermion Problems*, Prog. Theo. Phys. **5**, 54 (1950).

[2] J.M. Luttinger, *An Exactly Solvable Model of a Many-Fermion System*, J. Math. Phys. **4**, 1154 (1963).

[3] D.C. Mattis and E.H. Lieb, *Exact Solution of a Many-Fermion System and Its Associated Boson Field*, J. Math. Phys. **6**, 304 (1965).

[4] H. Gutfreud and M. Schick, *Momentum Distribution in the Tomonaga Model*, Phys. Rev **168**, 418 (1968).

[5] E.H. Lieb and F.Y. Wu, *Absence of Mott transition in an exact solution of the short-range, one-band model in one dimension*, Phys. Rev. Lett. **25**, 1445 (1968).

[6] A. Luther and I. Peschel, *Single-particle states, Kohn anomaly, and pairing fluctuations in one dimension*, Phys. Rev. B **9**, 2911 (1974).

[7] A. Luther and V.J. Emry, *Backward Scattering in the One-Dimensional Electron Gas*, Phys. Rev. Lett. **33**, 589 (1974).

[8] A. Theumann, *Preservation of Sum Rules for the 1p-Green Function in Luttinger Model*, Phys. Lett. A **59**, 99 (1976).

[9] J. Sólyom, *The Fermi gas model of one-dimensional conductors*, Adv. Phys. **28**, 201 (1979).

[10] F. D. M. Haldane, *'Luttinger-liquid theory' of one-dimensional quantum fluids: I. Properties of the Luttinger model and their extension to the general 1D interacting spinless Fermi gas*, J. Phys. C **14**, 2585 (1981).

[11] S. Kivelson, E. Fradkin and T.H. Geballe, *Quasi-1D dynamics and the Nematic phase of the 2D Emery model*, cond-mat./0302163.

[12] A.M. Finkel'stein and A.I. Larkin, *Two coupled chains with Tomonaga-Luttinger interactions*, Phys. Rev. B **47**, 10461 (1992).

[13] M. Fabrizio, *Role of transverse hopping in a two-coupled-chains model*, Phys. Rev. B **48**, 15838 (1993).

[14] D.G. Clarke, S.P. Strong and P.W. Anderson, *Incoherence of Single Particle Hopping between Luttinger Liquids*, Phys. Rev. Lett. **72**, 3218 (1994).

[15] N. Shannon, Y. Li and N. d'Ambrumenil, *Spin-Charge Separation, Anomalous Scaling and the Coherence of Hopping in exactly solved Two Chain Models*, Phys. Rev. B **55**, 12963 (1997)

[16] E. Arrigoni, *Crossover form Luttinger- to Fermi-liquid behavior in strongly anisotropic systems in large dimensions*, Phys. Rev. Lett. **83**, 128 (1999).

[17] D. Orgad, *Spectral Functions for the Tomonaga-Luttinger and Luther-Emery Liquids*, Phil. Mag. B **81**, 375 (2001).

[18] D. Orgad, S. A. Kivelson, E. W. Carlson, V. J. Emery, J. X. Zhou and Z. X. Shen, *Evidence of Electron Fractionalization from Photoemission Spectra in the High Temperature Superconductors*, Phys. Rev. Lett. **86**, 4362 (2001).

[19] S. Sachdev, *Quantum Phase Transitions*, (Cambridge University Press, Cambridge, 1999).

[20] B. Dardel, D. Malterre, M. Grioni, P. Weibel, Y. Bear and F. Lévi, *Possible Observation of a Luttinger-Liquid Behaviour from Photoemission Spectroscopy of One-Dimensional Organic Conductors*,
Europhys. Lett. **24**, 687 (1993).

[21] B. Dardel, D. Malterre, M. Grioni, P. Weibel, Y. Bear and F. Lévi, *Unusual Photoemission Spectral Function of Quasi-One-Dimensional Metals*,
Phys. Rev. Lett.**67**, 3144 (1991).

[22] B. Dardel, D. Malterre, M. Grioni, P. Weibel, Y. Bear, C. Schlenker and Y. Pétroff, *Temperature Dependence of the Spectral Function through the Peierls Transition in Quasi-One-Dimensional Compounds*,
Europhys. Lett. **19**, 525 (1992).

[23] J.D. Denlinger, G.-H. Gweon, J.W. Allen, C.G. Olson, J. Marcus, C. Schlenker and L.-S. Hsu, *Non-Fermi-Liquid Single Particle Line Shape of the Quasi-One-Dimensional Non-CDW Metal* $Li_{0.9}Mo_6O_{17}$ *: Comparison to the Luttinger Liquid*,
Phys. Rev. Lett. **82**, 2540 (1999).

[24] G.-H. Gweon, J.W. Allen and J.D. Denlinger, *Generalized Spectral Signatures of Electron Fractionalization in Quasi-One and -Two Dimensional Molybdenum Bronzes and Superconducting Cuprates*,
cond-mat/0303122, (unpublished).

[25] J.W. Allen, *Quasi-particles and their absence in photoemession spectroscopy*, Solid State Comm. **123**, 469 (2002).

[26] T.W. Ebbesen, *Carbon Nanotubes*, Phys. Today **49**, No. 6, 26 (1996).

[27] C. Kane, L. Balents and P.A. Fisher, *Coulomb Interactions and Mesoscopic Effects in Carbon Nanotubes*, Phys. Rev. Lett **79**, 5086 (1997).

[28] R. Tarkiainen et al., *Multiwalled carbon nanotube: Luttinger versus Fermi liquid*, Phys. Rev. B **64**, 195412 (2001).

[29] X.G. Wen, *Electrodynamic Properties of Gapless Edge Excitations in the Fractional Quantum Hall States*, Phys. Rev. Lett **64**, 2206 (1990).

[30] R. Claessen, M. Sing, U. Schwingenschlögl, P. Blaha, M. Dressel and C.S. Jacobsen, *Spectroscopic Signatures of Spin-Charge Separation in the Quasi-One-Dimensional Conductor TTF-TCNQ*,
Phys. Rev. Lett **88**, 096402 (2002).

[31] H.A. Bethe, *Zur Theorie der Metalle. I. Eigenwerte und Eigenfuktionen der linearen Atomkette*, Z. Phys. **71**, 205 (1931).

[32] J. v.Delft and H. Schoeller, *Bosonization for Beginners - Refermionization for Experts*, Annalen Phys. **7**, 225 (1998).

[33] J. Zinn-Justin, *Quantum Field Theory and Critical Phenomena*, (Clarendon Press, Oxford, 1989).

[34] K. G. Wilson, *Renormalization Group and Critical Phenomena. I. Renormalization Group and the Kadanoff Scaling Picture*, Phys. Rev. B **4**, 3174 (1971).

[35] K. G. Wilson, *Renormalization Group and Critical Phenomena. II. Phase-Space cell Analysis of Critical Behavior*, Phys. Rev. B **4**, 3184 (1971).

[36] K. G. Wilson and J. G. Kogut, Phys. Reports **12C**, 75 (1974).

[37] L. Kadanoff et al., *Static Phenomena Near Critical Points: Theory and Experiment*, Rev. Mod. Phys. 39, 395 (1967).

[38] F. J. Wegner and A. Houghton, *Renormalization Group Equation for Critical Phenomena*, Phys. Rev. A **8**, 401 (1973).

[39] J. Polchinski, *Renormalization and Effective Lagrangians*, Nucl. Phys. B **231**, 269 (1984).

[40] C. Wetterich, *Exact evolution equation for the effective potential*, Phys. Lett. B **301**, 90 (1993).

[41] L. Balents and D.S. Fisher, *Large-N expansion of $(4-\epsilon)$-dimensional orientated manifolds in random media*, Phys. Rev. B **48**, 035106 (2003).

[42] T. R. Morris, *The Exact Renormalization Group and Approximate Solutions*, Int. J. Mod. Phys. A **9**, 2411 (1994).

[43] T.R. Morris, *The derivative expansion of the renormalization group*, Nucl. Phys. B **42**, 811 (1995).

[44] U. Ellwanger, *The running gauge coupling in the exact renormalization group approach*, Z. Phys. C **76**, 721 (1997).

[45] T.R. Morris, *A gauge invariant exact renormalization group. (I)*, Nucl. Phys. B **573**, 97 (2000).

[46] P. Kopietz, *Two-loop β-function from the exact renormalization group*, Nucl. Phys. B **595**, 493 (2001).

[47] P. Chauve, P. Le Doussal and K.J. Wiese, *Renormalization of Pinned Elestic Systems: How Does It Work Beyond One Loop?*, Phys. Rev. Lett. **86**, 1785 (2001).

[48] P. Carta, *Third-order renormalization group applied to the attractive one-dimensional Fermi gas*, Phys. Rev. B **62**, 10687 (2000).

[49] C. Honerkamp, M. Salmhofer and T.M. Rice, *Flow to strong coupling in the two-dimensional Hubbard model*, Eur. Phys. J. B **27**, 127 (2002).

[50] C. Honerkamp and M. Salmhofer, *Flow of the quasi-particle weight in the N-patch renormalization group scheme*, cond-mat/0212066 (unpublished).

[51] G.Y. Chitov and C. Bourbonnais, *Wilson-Kadanoff Renormalization Group in Higher Orders: One-Dimensional g-ology as an Example*, cond-mat/0212493 (unpublished).

[52] V. Meden and U. Schollwöck, *Persistent currents in mesoscopic rings: A numerical and renormalization group study*, Phys. Rev. B **67**, 5949 (2003).

[53] D. Zanchi and H.J. Schulz, *Instabilities of weakly correlated electronic gas on a two dimensional lattice*, Z. Phys. B **103**, 339 (1997).

[54] B. Binz, D. Beariswyl and B. Douçot, *Wilson's renormalization group applied to 2D lattice electrons in the presence of van Hove singularities*, Eur. Phys. J. B **25**, 69 (2002).

[55] C. Bourbonnais, B. Guay and R. Wortis, in *Theoretical methods for strongly correlated electrons*, edited by A.M. Tremblay, D. Sénéchal, A. Ruckenstein and C. Bourbonnais, (Springer, Heidelberg, 2003).

[56] J. Comellas, Y. Kubishin and E. Moreno, *Exact renormalization group study of fermionic theories*, Nucl. Phys. B **490**, 653 (1997).

[57] J. Comellas, *Polchinski equation, reparametrization invariance and the derivative expansion*, Nucl. Phys. B **509**, 662 (1998).

[58] D. Zanchi and H. J. Schulz, *Weakly correlated electrons on a square lattice: Renormalization-group theory*, Phys. Rev. B **61**, 13609 (2000).

[59] M. Salmhofer, *Continuous Renormalization for Fermions and Fermi Liquid Theory*, Commun. Math. Phys. **194**, 249 (1998).

[60] M. Salmhofer, *Renormalization*, (Springer, Berlin, 1998).

[61] C.J. Halboth and W. Metzner, *Renormalization-group analysis of the two-dimensional Hubbard model*, Phys. Rev. B **61**, 7364 (2000).

[62] J.F. Nicoll, T.S. Chang and H.E. Stanley, *Exact and approximate differential renormalization-group generators*, Phys. Rev. A **13**, 1251 (1976).

[63] M. Salmhofer and C. Honerkamp, *Fermionic Renormalization Group Flows*, Prog. Theor. Phys. **105**, 1 (2001).

[64] C. Bagnuls and C. Bervillier, *Exact Renormalization Group Equations. An Introductary Review.*, Phys. Rept. **348**, 91 (2002)

[65] T. L. Bell and K. G. Wilson, *Nonlinear renormalization groups*, Phys. Rev. B **74**, 3935 (1974).

[66] M. E. Fisher, *Renormalization group theory: Its basis and formulation in statistical physics*, Rev. Mod. Phys. **70**, 653 (1998).

[67] T. Busche, L. Bartosch and P. Kopietz, *Dynamic scaling in the vicinity of the Luttinger liquid fixed point*, J. Phys. Cond. Mat. **14**, 8513 (2002).

[68] D. Zanchi, *Angle-resolved loss of Landau quasiparticles in 2D Hubbard model*, Europhys. Lett. **55**, 376 (2001).

[69] R. Shankar, *Renormalization-group approach to interacting fermions*, Rev. Mod. Phys. **66**, 129 (1994).

[70] C. Honerkamp, M. Salmhofer, N. Furukawa and T. M. Rice, *Breakdown of the Landau-Fermi liquid in two dimensions due to umklapp scattering*, Phys. Rev. B **63**, 035109 (2001)

[71] A. Ferraz, *Non-Fermi Liquid in a Truncated Two-Dimensional Fermi Surface*, cond-mat/0104576 (unpublished).

[72] D. Zanchi and H.J. Schulz, *Weakly correlated electrons on a square lattice: Renormalization-group theory*, Phys. Rev. B **61**, 16609 (2000).

[73] C. Honerkamp and M. Salmhofer, *Temperature-flow renormalization group and the competition between superconductivity and ferromagnetism*, Phys. Rev. B **64**, 184516 (2001).

[74] C. Honerkamp and M. Salmhofer, *Magnetic and Superconducting Instabilities of the Hubbard Model at the Van Hove Filling*, Phys. Rev. Lett. **87**, 187004 (2001).

[75] J. M. Luttinger, *Fermi Surface and Some Simple Equilibrium Properties of a System of Interacting Fermions*, Phys. Rev. **119**, 1153 (1960).

[76] M. Yamanaka, M. Oshikawa and I. Affleck, *Nonperturbative Approach to Luttinger's Theorem in One Dimension*, Phys. Rev. Lett. **79**, 1110 (1997).

[77] K.B. Blagoev and K.S. Bedell, *Luttinger Theorem in One Dimensional Metals*, Phys. Rev. Lett. **79**, 1106 (1997).

[78] D. Pines and P. Nozière, *The Theory of Quantum Liquids*, (Addison-Wesley, New York, 1988).

[79] J. M. Luttinger, *Analytic Properties of Single-Particle Propagators for Many-Fermion Systems*, Phys. Rev. **121**, 942 (1960).

[80] B. I. Halperin and P. C. Hohenberg, *Generalization of Scaling Laws to Dynamical Properties of a System Near its Critical Point*, Phys. Rev. Lett. **19**, 700 (1967).

[81] B. I. Halperin and P. C. Hohenberg, *Scaling Laws for Dynamic Critical Phenomena*, Phys. Rev. **177**, 952 (1969).

[82] V. Meden, *Nonuniversality of the one-particle Green's function of a Luttinger liquid*, Phys. Rev. B **60**, 4571 (1999).

[83] Ph.D. thesis, *Spektrale Eigenschaften niedrigdimensionaler Elektronensysteme*, Universität Göttingen, 1996.

[84] J. W. Negele and H. Orland, *Quantum many-particle systems*, (Addison-Wesley, Redwood City, 1988).

[85] F. A. Berezin, *The Method of Second Quantization*, (Academic Press, New York, 1966)

[86] A. L. Fetter and J. D. Walecka, *Quantum Theory of Many-Particle Systems*, (McGraw-Hill, New York, 1971)

[87] M. Le Ballac, *Quantum and Statistical Field Theory*, (Clarendon Press, Oxford, 1991).

[88] V. N. Popov, *Functional Integrals in Quantum Field Theory and Statistical Physics*, (Reidel, Dordrecht, 1983)

[89] P. Kopietz and T. Busche, *Exact renormalization group flow equations for nonrelativistic fermions: Scaling towards the Fermi surface*, Phys. Rev. B **64**, 155101 (2001).

[90] S. Ledowski and P. Kopietz, *Exact integral equation for the renormalized Fermi surface*, cond-mat/0208517 (unpublished).

[91] M. Abramowitz and I. Stegun, *Handbook of Mathmatical Functions*, (Dover, New York, 1965).

[92] H.J. Schulz and B.S. Shastry, *A New Class of Exactly Solvable Interacting Fermion Models in One Dimension*, Phys. Rev. Lett. **80**, 1924 (1998).

[93] V. Meden and K. Schönhammer, *Spectral functions for the Tomonaga-Luttinger Model*, Phys. Rev. B **46**, 15753 (1992).

[94] J. Voit, *One-dimensional Fermi liquids*, Rep. Prog. Phys. **58**, 977 (1995).

[95] C.M. Varma et al., *Phenomenology of the Normal State of Cu-O High-Temperature Superconductors*, Phys. Rev. Lett. **63**, 1996 (1989).

[96] C. Sire et al., *Theory of the Marginal-Fermi-Liquid Spectrum and Pairing in a Local Copper Oxide Model*, Phys. Rev. Lett. **72**, 2478 (1994).

[97] T. Busche and P. Kopietz, *How does a quadratic term in the energy dispersion modify the single-particle Green's function of the Tomonaga-Luttinger model?*, Int. J. Mod. Phys. B **14**, 1481 (2000).

[98] T. Busche, *Effekte nichtlinearer Energiedispersion auf die Einteilchen-Greenfunktion wechselwirkender Fermionen in einer Raumdimension*, Diplomarbeit, (Universität Göttingen, 1999, unpublished).

[99] T. Broecker, *Analysis I*, (BI Wissenschaftsverlag, Mannheim, 1992).

[100] I.S. Gradshteyn and I.M. Ryzhik, *Tables of Integrals, Series and Products*, (Academic Press, New York, 1965).

[101] P. Kopietz, *Bosonization of Interacting Fermions in Arbitrary Dimensions*, (Springer, Berlin, 1997).

[102] E. Schmidt, personal conversation.

Danksagung

Natürlich überwiegt am Ende einer Doktorarbeit die Freude darüber, es endlich geschafft zu haben, und man ist geneigt, die Strapazen der vergangenen Monate großzügig zu vergessen. Wenn ich aber an den Endorphinen vorbei zurück blicke, fällt mir sehr wohl wieder ein, wieviel Mühe mich diese Zeit gekostet hat. Um so wichtiger war es deshalb, dass ich von verschiedenen Seiten direkte oder indirekte Unterstützung erfahren habe, und ich möchte mich an dieser Stelle bei den betreffenden Personen ganz herzlich dafür bedanken.
Zunächst gilt mein Dank meinem Betreuer Prof. Dr. Peter Kopietz für das sehr interessante Thema dieser Arbeit.
Ganz besonders bedanken möchte ich mich bei Ivan Spremo, Lorenz Bartosch und Marcus Kollar aus meiner Arbeitsgruppe für viele hilfreiche Diskussionen, vor allem aber für die aufmunternden Worte, die ich bisweilen nötig gebraucht habe. Außerdem waren Ivan, Markus und Lorenz zusammen mit Florian Schütz mit dem Korrekturlesen dieser Arbeit betraut, und auch hier schulde ich ihnen Dank für die Mühe, sowie für zahlreiche wichtige Anmerkungen und Verbesserungsvorschläge. Ivan, dem besten und gewissenhaftesten Systemadministrator seit Alexander Schinner, danke ich darüber hinaus für Tips und Hilfestellungen rund um Linux, sowie für viele nette Abende in Gesellschaft der schönen Zlatorog aus Laško.
Je länger man in den Prozess des Zusammenschreibens eingebunden ist, desto mehr läuft man Gefahr, in unerwarteten Momenten in die Klauen des Verwaltungsapparates zu geraten. Vor den nicht zu unterschätzenden Folgen dieser Bedrohung hat mich auf liebenswürdige Art immer wieder Frau Edda Vogel bewahrt: Vielen Dank dafür!
Wenn man unter großer Anspannung steht, ist es besonders wichtig, von einem sicheren Fundament aus zu agieren. Meiner Familie und insbesondere meinen Eltern Siegrun und Eckhard Schmidt danke ich dafür, dass sie mir diesen stillen Rückhalt immer geboten hat. Bei meinem Bruder Robert und seiner Freundin Angela möchte ich mich außerdem ganz herzlich für die finanzielle Unterstützung in den letzten Monaten bedanken – „Geld allein macht zwar nicht glücklich, aber es beruhigt ungemein!“ [102].

Und schließlich Marina: Amtlich nicht bestätigten Umfragen zufolge ist ein Doktorarbeit schreibender Physiker nicht unbedingt das, wovon Frauen heimlich träumen. Ich danke Dir sehr dafür, dass Du dieses ungnädige Urteil der Statistik wohlwollend ausgelegt hast, und gelobe für die Zukunft Besserung. Denn zumindest das Doktorarbeit Schreiben hat ja nun ein Ende.